TARGETING MTOR AND METABOLIC PATHWAYS FOR ANTI-TUMOUR THERAPY IN A *TSC2*$^{+/-}$ MOUSE MODEL

Ashley Jones

2019

Thesis submitted to Cardiff University in fulfilment of the requirements for the degree of Doctor of Philosophy

Contents

Acknowledgments

Firstly, I would like to thank my supervisor Dr Ming Hong Shen for his patience, understanding and dedication throughout my PhD. He has guided and supported me, especially during my final year, and I really appreciate all the help and advice he has given me. I would also like to thank Prof Julian Sampson for his expertise throughout my project.

I would like to thank all previous and existing members of the MHS lab group. Dr Jian Yang for her help, guidance and teaching of many experimental techniques in the lab and Dr Paulina Samsel for teaching me procedures important for working in the animal facility. I especially would like to thank Dr Kalin Narov, one of the cleverest people I know, for his assistance and support throughout my PhD, for his help during animal procedures, and, in particular, for keeping my time during my PhD enjoyable and interesting with his unbelievable depth of funny and fascinating scientific and historical facts. It was a pleasure to work with this group.

I would also like to thank Derek Scarborough for helping me prepare my kidney sections for analysis

Last but not least, I would like to thank my family and Akvilė for their understanding and financial/emotional support. This would not have been possible without them.

I would also like to thank the Tuberous sclerosis association for funding my project.

Summary

Tuberous sclerosis (TSC) is a genetic tumour syndrome characterised by the formation of tumours in multiple organs, including the kidneys. TSC is caused by mutations in the *TSC1* or *TSC2* gene leading to aberrant activation of the mTOR signalling pathway. The mTOR signalling pathway regulates numerous biological processes such as cell growth, proliferation, metabolism and epithelial-to-mesenchymal transition (EMT). The mTOR inhibitor rapamycin (rapalogs) is effective for TSC-associated tumours. However, not all TSC-associated tumours respond to rapalogs and tumours usually regrow after treatment withdrawal. Therefore, this study aims to test alternative therapeutic approaches for treating TSC-associated renal tumours and to investigate mechanisms of tumorigenesis in *Tsc2*$^{+/-}$ mice.

Firstly, this study presented a new model of EMT activation during tumour progression from cysts through papillary adenomas to solid carcinomas in the kidneys of *Tsc2*$^{+/-}$ mice. Effect on EMT and anti-tumour efficacy of the ATP-competitive inhibitor of mTOR, AZD2014, was compared with rapamycin in these mice. Both AZD2014 and rapamycin inhibited EMT and significantly reduced tumour burden as indicated by number and size of tumours. Nevertheless, AZD2014 was not superior to rapamycin for these tumours, suggesting that the anti-tumour efficacy was probably achieved mainly through inhibition of mTORC1.

Secondly, this study revealed that renal tumours of *Tsc2*$^{+/-}$ mice are metabolically active with the increased expression of enzymes associated with glycolysis and glutaminolysis. The dual inhibition of glycolysis and glutaminolysis with 3-BrPA and CB-839 significantly reduced renal tumour burden in these mice. However, this combination treatment was not as effective as rapamycin alone. These results suggest that dual inhibition of glycolysis and glutaminolysis is unlikely to offer better therapy than rapalogs for treating TSC-associated tumours.

Finally, this study sought to investigate the role of the glycolytic enzyme, *Pkm2*, in renal tumourigenesis of *Tsc2*$^{+/-}$ mice using doxycycline-induced gene deletion. *Pkm2* was successfully deleted in the epithelial cells of renal tubules and *Pkm2* loss did not have significant effect on renal tumourigenesis. However, increased expression of *Pkm1* was observed following *Pkm2* deletion in renal tumour cells which may functionally compensate for *Pkm2* loss to promote tumourigenesis.

Declaration

This work has not previously been accepted in substance for any degree and is not concurrently submitted in candidature for any degree.

Signed……. (Candidate) Date ……..

STATEMENT 1

This thesis is being submitted in partial of the requirements for the degree of ……. (Insert MCh, MD, MPhil, PhD etc., as appropriate)

Signed……. (Candidate) Date ……..

STATEMENT 2

This thesis is the result of my own independent work/investigation, except where otherwise stated.

Other sources are acknowledged by explicit references.

Signed……. (Candidate) Date ……..

STATEMENT 3

I hereby give consent for my thesis, if accepted, to be available for photocopying and for inter-library loan, and for the title and summary to be made available to outside organisations.

Signed……. (Candidate) Date ……..

STATEMENT 4: PREVIOUSLY APPROVED BAR ON ACCESS

I hereby give consent for my thesis, if accepted, to be available for photocopying and for inter-library loans **after expiry of a bar on access previously approved by the Graduate Development Committee.**

Signed……. (Candidate) Date ……

Abbreviations

2-DG	2-Deoxyglucose
3-BrPA	3-Bromopyruvate
3PG	3-phosphoglycerate
4E-BP1	eIF4E binding protein 1
5' TOP	5' tract oligopyrimidine
ADHD	Attention Deficit Hyperactivity Disorder
AKT1S1	Akt substrate 1
AMBRA1	autophagy/beclin1 regulator 1(AMBRA1)
AML	Angiomyolipomas
AMPK	AMP-activated protein kinase
ASD	Autism Spectrum Disorder
AST	Aspartate aminotransferase
ATP	Adenosine triphosphate
AVV	Adeno-associated virus
CAD	Carbamoyl-phosphate synthetase 2, aspartate transcarbamoylase and dihydroorotase
CaMKKB	Ca^{2+}/CaM-dependent protein kinase β
CDK1	Cyclin-dependent kinase 1
cDNA	Complementary DNA
CNS	Central nervous system
CREB2	cAMP-responsive element binding 2
CT	Computed tomography
DEPTOR	DEP domain containing mTOR-interacting protein
DNA	Deoxyribonucleic acid

EGFR	Epidermal growth factor receptor
eIF4B	Eukaryotic translation initiation factor 4B
eIF4E	Eukaryotic translation initiation factor 4E
EMT	Epithelial-to-Mesenchymal Transition
ERK	Extracellular signal-regulated kinase
F6P	Fructose-6-phosphate
FDA	Food and Drug Administration
FLCN	Folliculin
FRB domain	FKBP-rapamycin-binding domain
G3P	Glyceraldehyde-3-phosphate
GAP	GTP-activating protein
GAPDH	Glyceraldehyde-3-phosphate dehydrogenase
GDH	Glutamate dehydrogenase
GDP	Guanosine diphosphate
GEF	Guanine nucleotide exchange factor
GLS1/2	Glutaminase 1/2
GLUTs	Glucose transporters
GRB10	Growth factor receptor-bound protein 10
GTP	Guanosine triphosphate
HIF1	Hypoxia-inducible factor 1
HIF2	Hypoxia-inducible factor 2
HKII	Hexokinase II
hnRNPS	Heterogenous nuclear ribonucleoproteins
HRE	hypoxic response elements
IAP	Intracisternal A particle
IGF-1	Insulin-like growth factor 1

IGFR	Insulin-like growth factor receptor
IHC	Immunohistochemistry
IL-2	Interleukin-2
IRS1/2	Insulin substrate receptor 1/2
kDa	KiloDaltons
LAM	Lymphangioleiomyomatosis
LDHA	Lactate dehydrogenase-A
LKB1	Liver kinase B1
LOH	Loss of heterozygosity
MCT	Monocarboxylate transporter
MEFs	Mouse embryonic fibroblasts
MET	Mesenchymal-to-epithelial transition
MLC2v	Modified myosin light chain 2v promotor
mLST8	Mammalian lethal with sec-13 protein 8
MMPH	Multifocal micronodular pneumocyte hyperplasia
MRI	Magnetic Resonance Imaging
mRNA	Messenger RNA
mSIN1	Mammalian stress-activated map kinase-interacting protein 1
MS-IHC	Multiple sequential IHC
mTOR	Mammalian target of rapamycin
mTORC1	mTOR complex 1
mTORC2	mTOR complex 2
NADPH	Nicotinamide adenine dinucleotide phosphate
NMI	No mutation identified
NMR	Nuclear magnetic resonance
PDGFRα/β	Platelet derived growth factor receptor α/β

PDK	Pyruvate dehydrogenase kinase
PEP	Phosphoenolpyruvate
PH	Pleckstrin homology
PHGDH	Phosphoglycerate dehydrogenase
PI3K	Phosphoinositide 3-kinase
PIKK	Phosphatidylinositol 3-kinase-related kinase
PIP2	Phosphatidylinositol-4,5-bisphosphate
PIP3	Phosphatidylinositol-3,4,5-trisphosphate
PKC-α	Protein kinase C-α
PKD	Polycystic kidney disease
PKM1/2	Pyruvate kinase M1/2
PPAR-Y	Peroxisome proliferator-activated receptor γ
PPP	Pentose phosphate pathway
PRAS40	Proline-rich Akt substrate 40 kD
Protor1/2	Protein observed with rictor 1/2 (protor1/2)
PSAT1	Phosphoserine aminotransferase 1
PTEN	Phosphatase and tensin homolog deleted on chromosome 10
RAPTOR	Regulatory associated protein of mTOR
RCC	Renal cell carcinoma
REDD1	Regulated in DNA damage and development 1
RICTOR	Rapamycin-insensitive companion of mTOR
RNA	Ribonucleic acid
ROS	Reactive Oxygen Species
rRNA	Ribosomal RNA
RSK1	Ribosomal S6 Kinase 1
RTK	Receptor tyrosine kinase

S6K1	Ribosomal protein S6 kinase 1
SEGA	Subependymal Giant Cell Astrocytoma
SENs	Subependymal nodules
SESN1-3	Sestrins1-3
SGK1	Serum- and glucocorticoid-induced protein kinase 1
SREBP1/2	Sterol regulatory element-binding protein 1 and 2
STAT3	Signal transducer and activator of transcription 3
TANDs	TSC-associated neuropsychiatric disorders
TBC1D7	TBC domain family member 7
TCA	Tricarboxylic acid cycle
TFEB	Transcription factor EB
TGFβ	Transforming growth factor β
TIF-1A	Tripartite motif-containing protein-24
TRAF6	TNF receptor-associated factor 6, E3 ubiquitin protein ligase
tRNA	Transfer RNA
TSC	Tuberous Sclerosis
TSC1	Tuberous Sclerosis 1
TSC2	Tuberous Sclerosis 2
UDP-GlcNAc	Uridine diphosphate N-actylglucosamine
ULK1	Unc-51 like autophagy activating kinase 1
VEGFR	Vascular endothelial growth factor receptor
VHL	Von Hippel-Lindau

1 CHAPTER ONE

General Introduction

1.1 Molecular genetics of tuberous sclerosis

Tuberous sclerosis (TSC) is an autosomal dominant tumour syndrome characterised by tumour formation in multiple organs including the brain, kidney, heart, skin, eyes and lungs. The current estimated prevalence of TSC is 1:6000 to 1:12,500 live births.

1.1.1 History of TSC

The first manifestations of TSC were described in 1835 by Pierre Francois Olive Rayer (Rayer 1835) . Rayer published an atlas illustrating skin diseases, revealing a young man with facial erythematous papules. These papules closely resembled facial angiofibromas, found in TSC patients. Later in 1862, Friedrich Daniel von Recklingghausen identified several cardiac tumours or “myomata” and a “great number of scleroses” within the brain of a deceased new-born (von Recklinghausen 1862). This was the first report of cardiac rhabdomyomas and cortical tubers, often seen in new-borns with TSC. It was not until 1879 when the term “tuberous sclerosis” was first used by Desire-Magloire Bourneville. Bourneville observed white nodular tumours in the brain of a deceased 15-year-old girl who suffered from seizures and facial angiofibromas. He coined the term “Tuberous sclerosis of the cerebral convolutions” to describe his pathological findings (Bourneville 1880). A year later, a second patient who suffered from seizures was examined by Bourneville and showed similar cerebral features (Bourneville and Brissaud 1881) (Figure 1.1).

At the end of the 19th century, Balzar and Menetrier recognised patients with adenoma sebaceum facial lesions correlated with frequent seizures and mental retardation (Balzer and Menetrier 1885). This led to Heinrich Vogt in 1908 to propose a clinical triad of seizures, mental handicap and adenoma sebaceum for the diagnosis of cerebral TSC (Vogt 1908). Further studies at the beginning and middle of the 20th century started to

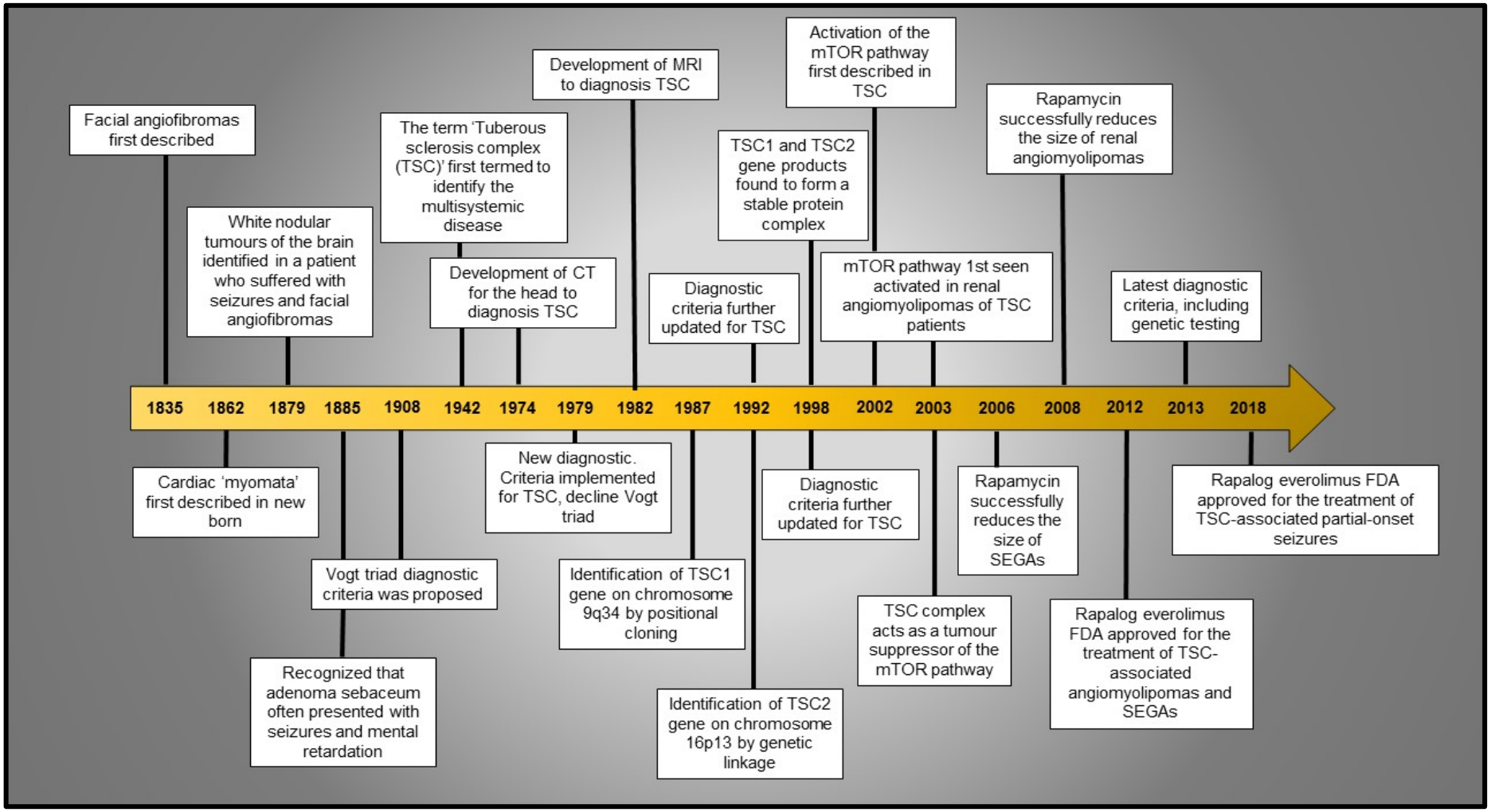

Figure 1.1 Significant events in the history of Tuberous Sclerosis. Adapted from (Kwiatkowski *et al.* 2010)

reveal the correlation of renal, skin, cardiac and retinal lesions with cerebral TSC. In 1942, Moolten coined the term “Tuberous sclerosis complex” to recognise and define the disease as a multi-systemic disorder, affecting many organs of the body (Moolten 1942) (Figure 1.1).

The new era of non-invasive imaging technologies in the 1970s enabled more accurate and robust methods of TSC diagnosis. Imaging techniques developed included computed tomography (CT) of the head (1974), echocardiography, renal ultrasound and magnetic resonance imaging (MRI) (1982). This led to the expansion of the diagnostic criteria from Vogt’s triad by the identification of new clinical manifestations (Lagos and Gomez 1967). This also allowed the diagnosis of patients who presented with no clinical symptoms, increasing the prevalence of TSC. An early report estimated that only 29% of TSC patients fulfilled Vogt clinical triad, with 6% of patients having none of the triad features (Dalsgaard-Nielsen 1935). Therefore, a new, updated diagnostic criteria for TSC was published in 1979 based on new imaging techniques (Gomez 1979). Further advancement in experimental techniques towards the end of the 20th century led to the identification of *TSC1* and *TSC2* as the TSC causing genes (Figure 1.1).

1.1.2 Clinical features of TSC

TSC has an almost complete penetrance with an extensive variety of clinical features. TSC affects nearly all organs of the body, causing a wide range of clinical symptoms. Organ systems primarily affected include the brain, kidney, skin, lungs, heart and eyes (Figure 1.2) (Rosser *et al.* 2006; Curatolo *et al.* 2015; De Waele *et al.* 2015).

1.1.2.1 Neurological features

The central nervous system (CNS) is affected in up to 90% of TSC patients. CNS abnormalities are the leading cause of morbidity and mortality in these individuals. Neurological manifestations include an array of brain lesions causing epilepsy and other neuropsychiatric disorders (Curatolo et al. 2015).

Neurological brain lesions associated with TSC include cortical tubers, subependymal nodules (SENs) and subependymal giant cell astrocytomas (SEGAs) (Figure 1.2A) (Grajkowska *et al.* 2010; Northrup *et al.* 2013). Cortical tubers are focal malformations in cortical development resulting in loss of normal cortical architecture and organisation of

the cerebral cortex (Ruppe *et al.* 2014). Tubers vary in size and number and consist of abnormal neurons, giant cells and mis-shaped astrocytes (Curatolo et al. 2015). SENs are benign growths primarily occurring on the ependymal layer of the lateral and third ventricles within the brain. They occur in up to 80% of TSC patients and can be detected prenatally (Northrup et al. 2013). They usually begin asymptomatic but can continue to grow, degenerate and calcify (Hosoya *et al.* 1999). SENs that grow greater than 5mm have a risk of developing into SEGAs (Figure 1.2A) (Kim *et al.* 2001). SEGAs are found in 5-15% of TSC patients and are slow-growing brain tumours (Grajkowska et al. 2010). They are the greatest risk of morbidity and mortality in children and adolescences (Adriaensen *et al.* 2009). Although usually benign in nature, their location with respect to surrounding structures and ability to grow can be life-threatening. SEGAs can cause narrowing or blocking of the foremen of Monro preventing cerebral spinal fluid circulation through the ventricles and to the brain ventricular system. This can lead to an increased intracranial pressure, obstructive hydrocephalus and death (Shepherd *et al.* 1991; Grajkowska et al. 2010).

TSC brain lesions cause a wide range of neuropsychiatric disorders (TANDs) with varying degrees of penetrance and severity, known as TANDs. These neurological manifestations include intellectual, behavioural, neuropsychological, psychosocial and psychiatric disorders (de Vries *et al.* 2015). Epileptic seizures can occur in 85-90% of individuals and 80% of cases happen before 3 years old (Chu-Shore *et al.* 2010). These seizures include focal seizures and infantile spasms. Seizures are associated with neurodevelopment delay and cognitive problems throughout life. Autism spectrum disorder is also strongly associated with TSC patients, developing in 40-50% of individuals, as well as attention deficit hyperactivity disorder (ADHD) in 30-40% of individuals (D'Agati *et al.* 2009; Curatolo *et al.* 2010). Behavioural changes are frequently seen in TSC patients, including aggressive behaviour, mood swings, self-harm and sleep difficulties (Prather and de Vries 2004; Eden *et al.* 2014). Depression and anxiety are diagnosed in adolescences and adults at a higher percentage than the general population (Leclezio and de Vries 2015). Moreover, around 50% of patients have various degrees of intellectual disability. Of those who have normal or above average intellectual ability, individuals may still exhibit neurological deficits, such as attentional and memory deficits. A recent study has shown that 30% of school-children with TSC of normal intellectual ability still have academic difficulties (de Vries *et al.* 2009)

1.1.2.2 Renal features

Renal manifestations affect 80-90% of TSC patients and are one of the leading causes of morbidity and mortality. Renal lesions associated with TSC include angiomyolipomas (Figure 1.2B) (AMLs), renal cysts, oncocytomas and renal cell carcinomas. Renal lesion number and size increase with age and are the main cause of mortality in patients over 30 years of age (Northrup et al. 2013; Pirson 2013; De Waele et al. 2015).

Angiomyolipomas (AMLs)

AMLs affect up to 85% of TSC individuals and are derived from the renal parenchyma (Rakowski *et al.* 2006). Tumours consist of abnormal blood vessels, smooth muscle and adipose tissue (Figure 1.2B) (De Waele et al. 2015). AMLs often appear multiple and bilateral. They have been shown to develop in infancy (Ewalt *et al.* 1998), grow rapidly during childhood and continue to grow more slowly into adulthood (O'Callaghan *et al.* 2004; Rakowski et al. 2006). They are the most common cause of morbidity in adults with TSC. The size and location of AMLs highly affect patients' prognosis. Large and numerous AMLs interfere with normal kidney function by destruction of renal tissue, leading to chronic kidney failure (Clarke *et al.* 1999). Furthermore, due to their abnormal vasculature, AMLs can develop micro- and macro- aneurysms (Adler *et al.* 1984). TSC patients with AMLs larger than 4cm are at risk of spontaneous retroperitoneal haemorrhage which can be life threatening (Bissler *et al.* 2002; Yamakado *et al.* 2002). AML-associated aneurysm rupture risk is around 25-50% in TSC adults (Kessler *et al.* 1998).

Renal cysts

Renal cysts develop in 30-45% of TSC patients (Rakowski et al. 2006). They may be detected prenatally and are derived from kidney nephrons. Microcysts cluster within the renal cortex before spreading to the renal medulla (Bernstein and Robbins 1991). They can range from small, undetectable cysts to large, multiple cysts. Early onset polycystic kidney disease (PKD) can develop from gene deletions in the *TSC2* and adjacent *PDK1* genes on chromosome 16p13, leading to TSC2/PDK1 contiguous gene deletion syndrome. This syndrome has been found to occur in 2-5% of TSC patients (Sampson

et al. 1997). Renal cysts, however, can also occur in TSC1-related disease (Rakowski et al. 2006). Renal cysts can cause hypertension and renal failure (Miller *et al.* 1989).

Oncocytomas and renal cell carcinoma (RCC)

Oncocytomas and RCC develop in around 2-4% of TSC patients (Al-Saleem *et al.* 1998; Siracusano *et al.* 1998; Yang *et al.* 2014). They typically arise more frequently at a younger age in TSC patients than the general population (Henske 2005). Oncocytomas originate from the collecting duct of the nephron (Zerban *et al.* 1987) whereas RCC derive from the lining of renal cysts (Robertson *et al.* 1996). The average age of RCC development is 28-50 (Al-Saleem et al. 1998). However, RCC can be diagnosed in children (Robertson et al. 1996). TSC-associated RCC can develop with various types of histology, such as clear cell, papillary, chromphobe or unclassified RCC (Yang et al. 2014).

1.1.2.3 Dermatological features

Skin or dental manifestations are detected in the majority of TSC patients (Northrup et al. 2013; Ebrahimi-Fakhari *et al.* 2017). These include Hypomelanotic macules, angiofibromas (Figure 1.2C), fibrous cephalic plaques, shagreen patches, ungual fibromas and confetti skin lesions. These lesions do not necessarily cause any serious clinical complications but may cause psychological problems for patients (Muzykewicz *et al.* 2007). Hypomelanotic macules are found in 90% of patients and occur in the 1st years of life. They are used as a major clinical diagnostic feature if larger than 5mm (Table 1.1). Smaller and more numerous macules are classed as confetti lesions (Northrup et al. 2013; Ebrahimi-Fakhari et al. 2017). Facial angiofibromas occur in 75% of TSC individuals and develop in infancy. They increase in size and number during adulthood and may be mistaken for acne (Figure 1.2C) (Teng *et al.* 2014). Hamartomas nodules consist of connective and vascular tissue and found bilaterally over centro-facial areas. Shagreen patches are unique to TSC and are large plaques with an uneven surface, usually found on the trunk. They are observed in about 50% of patients (Northrup et al. 2013; Ebrahimi-Fakhari et al. 2017). Fibrous cephalic plaques mainly occur on the forehead and are found in 25% of TSC patients. Histologically, these are very similar to angiofibromas. Ungual fibromas do not develop until adolescence or even adulthood and are found in 20% of patients. They can occur adjacent to or underneath

nails and increase in size throughout life (Northrup et al. 2013; Ebrahimi-Fakhari et al. 2017)

1.1.2.4 Lung manifestations

Lymphangioleiomyomatosis (LAM) is the most common lung manifestation in TSC patients and nearly exclusively affects women (Figure 1.2D) (Castro *et al.* 1995; Henske and McCormack 2012). LAM probably develops from the abnormal proliferation of smooth muscle cells and cystic changes within the lung parenchyma (De Waele et al. 2015). This leads to a gradual destruction of lung tissue, causing progressive dyspnea, hemoptysis and respiratory failure (Castro et al. 1995; Henske and McCormack 2012). One hypothesis is that LAM is the result of metastatic spread of smooth muscle cells from benign AMLs (Astrinidis and Henske 2004). Up to 80% of women with TSC have LAM by the age of 40 (Cudzilo *et al.* 2013). LAM is very rare in men with TSC and male sufferers typically have less severe symptoms (Aubry *et al.* 2000; Adriaensen *et al.* 2011). It is suggested that LAM is hormonally linked. This could partly explain why it exclusively affects woman and gets worse during pregnancy (Costello *et al.* 2000). Lung transplantation is often required at end stage disease (Eugene 1998). Other lung manifestations in TSC patients include multifocal micronodular pneumocyte hyperplasia (MMPH) in 40-85% of individuals and clear cell tumours of the lungs (Franz *et al.* 2001).

1.1.2.5 Cardiac tumours

Cardiac rhabdomyomas are often the first identifiable manifestations of TSC. They can be recognised prenatally, after only 22-28 weeks of gestation (Figure 1.2E) (Holley *et al.* 1995). Around 96% of new-borns with cardiac rhabdomyomas are diagnosed with TSC (Bader *et al.* 2003). These hamartomas are predominantly located in the ventricles and composed of irregular cardiac myocytes. They can affect up to 50% of TSC patients (Becker 2000; Freedom *et al.* 2000; Bader et al. 2003). Although usually asymptomatic, larger lesions can obstruct blood outflow and cause congestive heart failure (Nir *et al.* 1995; Freedom et al. 2000). Rhabdomyomas found in the heart septum can interrupt conduction pathways, causing an array of dysrhythmias such as supraventricular tachycardia and Wolff-Parkinson-White syndrome (Freedom et al. 2000; Bader et al. 2003). Interestingly, cardiac rhabdomyomas have been reported to naturally regress and disappear during the first years of life (Nir et al. 1995).

1.1.2.6 Ophthalmologic lesions

Retinal and non-retinal lesions can be observed in the eyes of TSC patients (Rowley *et al.* 2001). Retinal hamartomas can be found in 30-50% of TSC individuals, usually bilateral and occur at any age (Robertson 1991; Rowley et al. 2001; Franz 2004). There are 3 morphological types of retinal lesions. Non-calcified, flat and smooth surfaced hamartomas are the most common lesions and are located in the posterior retinal pole (Robertson 1991). Retinal lesions are usually asymptomatic unless they affect the macula or optic nerve, leading to vision loss or blindness (Figure 1.2F) (Franz 2004). Non-retinal problems include eyelid angiofibromas, cataracts, iris depigmentation and colobomas (Rowley et al. 2001)

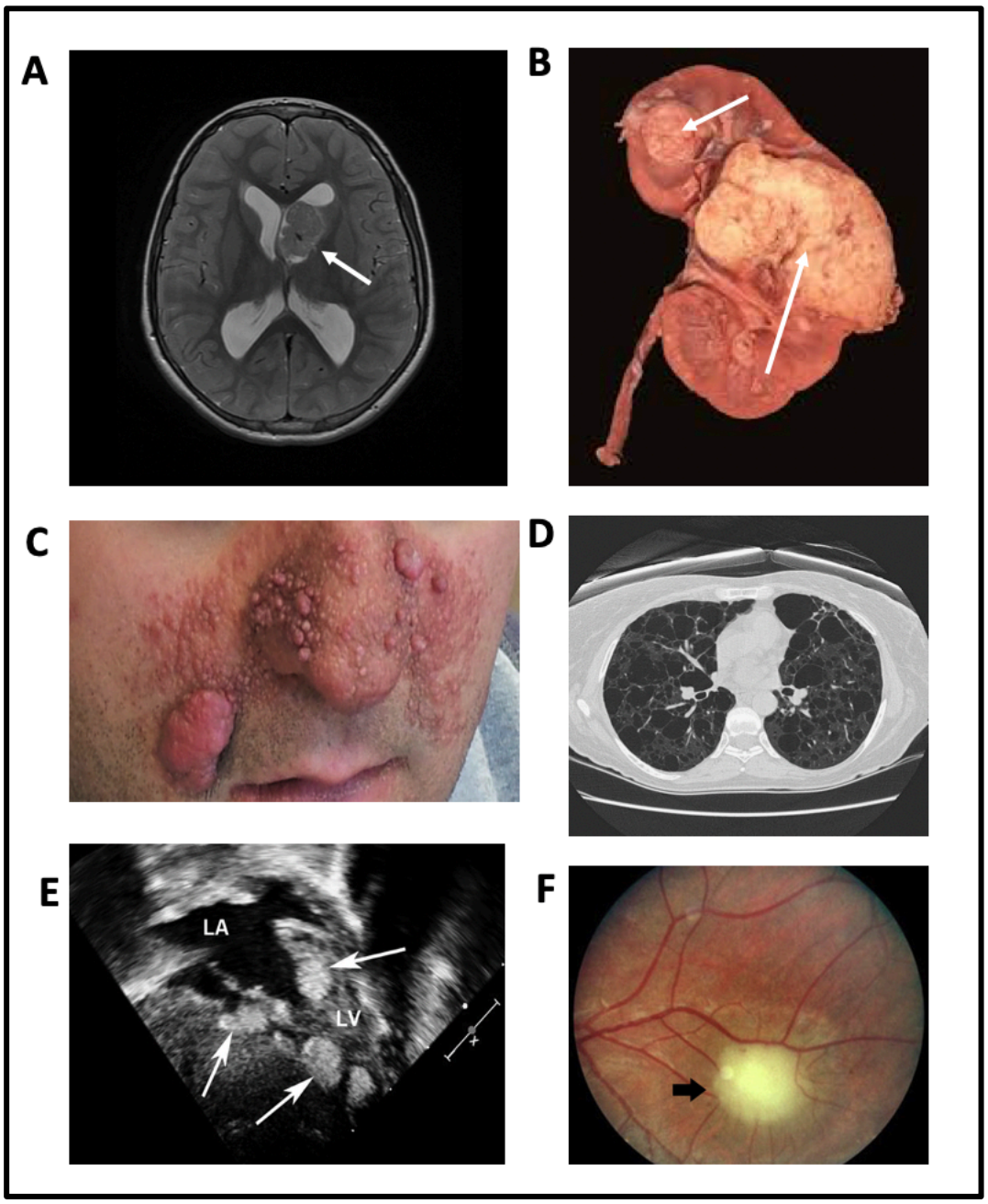

Figure 1.2 Clinical manifestations of TSC. (A) Brain MRI highlighting SEGA (white arrow). **(B)** Angiomyolipoma of a human kidney (white arrows). **(C)** Facial angiofibromas of a male with TSC. **(D)** Chest CT scan of a patient with LAM. **(E)** Fetal echocardiogram showing cardiac rhabdomyomas (White arrows; LA: Left Atrium; LV: Left Ventricle). **(F)** Retinal harmatoma in the eye of a TSC patient (Northrup et al. 2013)

1.1.3 Diagnostic criteria of TSC

TSC is diagnosed with a specific clinical criterion. The diagnostic criteria have been changed and updated numerous times since Vogt's triad in 1908 (Gomez 1979; Roach *et al.* 1992; Roach *et al.* 1998; Roach and Sparagana 2004; Northrup et al. 2013). A 2012 international consensus group has recently further updated the recommendations for TSC diagnostic criteria (Northrup et al. 2013). This criterion predicts a patient's TSC diagnosis as "definite" or "possible", on the detection of major or minor clinical symptoms, summarised in Table 1.1. Patients with two major features or one major feature and 2 minor features are classed as "definite" TSC diagnosis. Patients with one major feature and one minor feature, or 2 or more minor features are classed as "possible" TSC diagnosis. The new updated diagnostic criteria have reduced the number of minor features it accepts for diagnosis and includes genetic testing as a major criterion.

A positive identification of a pathogenic mutation, even in the absence of clinical features, can confirm TSC diagnoses. A clear pathogenic mutation is described as a mutation that inactivates *TSC1* or *TSC2* function. Genetic testing, however, is not an absolute requirement for diagnosis. This is because a mutation in *TSC1* or *TSC2* is not identified in 10-15% of clinically diagnosed TSC patients. Therefore, a normal result does not exclude TSC (Northrup et al. 2013).

Table 1.1 Clinical diagnostic criteria of TSC

Major clinical features	Minor clinical features
Hypomelanotic macules (>2), at least 5mm diameter	'Confetti' skin lesions
Angiofibromas (>2) or fibrous cephalic plaque	Dental enamel pits (>3)
Ungual fibromas (>1)	Intraoral fibromas (>1)
Shagreen patch	Retinal achromic patch
Multiple retinal hamartomas	Multiple renal cysts
Cortical dysplasia's	Non-renal hamartomas
Subependymal nodules	
Subependymal giant cell astrocytoma	
Cardiac rhabdomyoma	
Angiomyolipomas (>1)	

1.1.4 Identification and cellular functions of *TSC* genes

Our understanding of TSC has improved dramatically over the past 30 years. With the development of new molecular genetic techniques, two genes responsible for TSC, *TSC1* and *TSC2*, have been isolated, characterised and their cellular functions revealed.

1.1.4.1 *TSC1* gene

The first TSC-causing gene was identified by genetic linkage studies in 1987. Fryer *et al* studied 19 multigenerational TSC families using 26 polymorphic markers. It was reported that linkage was found between a TSC-causing gene and the ABO blood group gene on chromosome 9q34. This locus was named *TSC1* (Fryer et al. 1987; Northrup et al. 1987). A follow-up study confirmed this linkage by testing a DNA polymorphism in the *v-abl* gene, a gene proximal to the ABO blood group gene (Connor *et al.* 1987). However, it was noted that some families showed no evidence of linkage between TSC and polymorphic markers on chromosome 9q34. Continued genetic linkage studies by independent groups indicated the possibility of another TSC-causing gene locus within the genome, indicating genetic heterogeneity (Sampson *et al.* 1989; Janssen *et al.* 1990; Northrup *et al.* 1992; Sampson *et al.* 1992).

The *TSC1* gene locus was found to be a gene-rich region with over 30 genes. Positional cloning of the *TSC1* gene within the locus was performed by comprehensive sequencing of a cosmid contig and mutational screening of exons by heteroduplex analysis of a group of 20 unrelated familial and 40 sporadic TSC cases (van Slegtenhorst *et al.* 1997). This analysis revealed mobility shifts associated with truncating mutations within the 62nd exon screened. These mutations were found in 10 of 60 patient samples screened. The complete *TSC1* sequence was then determined by genomic and cDNA clone sequence comparison (van Slegtenhorst et al. 1997). *TSC1* gene is located on chromosome 9q34.13 and contains 23 exons (Figure 1.3A). The full-length 8.6kb transcript consists of a 221bp 5' untranslated region (exons 1 and 2), 3492bp coding region (exons 3-22) and a 4.5kb 3' untranslated region (exon 23). The coding region is translated into a 130 kilodalton (kDa) protein containing 1164 amino acids named hamartin or TSC1 (to be referred to as TSC1 throughout this thesis) (van Slegtenhorst et al. 1997; Gomez *et al.* 1999; Cheadle *et al.* 2000) (Figure 1.3B). TSC1 is a hydrophilic protein with a single

transmembrane domain localised to the centrosome of a cell (van Slegtenhorst et al. 1997).

1.1.4.2 *TSC2* gene

By genetic linkage analysis, the *TSC2* gene was approximately localised to chromosome 16p13 (1.5Mb) in 1992, using a polymorphic marker close to the *ADPKD1* locus (Kandt *et al.* 1992). The isolation of the *TSC2* gene was then reported in 1993 (European chromosome 16 Tuberous sclerosis consortium, 1993; Kwiatkowski *et al.* 1993). Positional cloning of *TSC2* gene was relatively rapid due to previous work by groups investigating alpha-globin and *PDK1* genes for disorders of haemoglobin and polycystic kidney disease, respectively. Both genes lie in the same region as the *TSC2* locus on the short arm of chromosome 16 and served as fixed landmarks for *TSC2* positional information (Gomez et al. 1999).

A cosmid contig of 300kb in the candidate region of *TSC2* was constructed from the 1.4Mb locus when 1.1Mb was excluded through comparison of chromosome 16p13 translocation breakpoints between two patients, one with and one without TSC (Consortium 1993; Consortium 1994). Probes generated from the contig were used to examine DNA in a panel of 255 unrelated TSC patients for rearrangements by pulse field electrophoresis and Southern Blotting. Five TSC patients showed genomic deletions of 30-100kb within the same 120kb genomic segment. From this 120kb segment, 4 genes were isolated and only 1 gene showed to be disrupted in all 5 patients. Using conventional gel electrophoresis for higher resolution, 4 smaller intragenic deletions were found in patients with TSC. This confirmed the identification of the *TSC2* gene on chromosome 16p13.3 (Consortium 1993; Gomez et al. 1999) (Figure 13.A). *TSC2* contains 42 exons, with 41 coding exons and 1 non-coding exon, spreading over 44kb of genomic DNA (Kobayashi *et al.* 1997b). The coding region of the gene produces a 5.5kb transcript and is translated into a 198 kDA protein product containing 1807 amino acids named tuberin or TSC2 (to be referred to as TSC2 throughout this thesis) (Consortium 1993) (Figure 1.3B).

1.1.4.3 Cellular functions of TSC proteins and their regulation

TSC1 and TSC2 directly interact with each other to form a stable TSC1-TSC2 protein complex (Plank *et al.* 1998; Van Slegtenhorst *et al.* 1998). The TSC1-TSC2 complex is responsible for the functional activity of the proteins. TSC proteins directly associate with each other through their binding domains to maintain complex stability (Figure 1.3B). TSC2 is stabilised by TSC1, preventing its ubiquitination and degradation by association with HERC1 ubiquitin ligase (Benvenuto *et al.* 2000; Chong-Kopera *et al.* 2006). Equally, TSC1 is stabilised by TSC2, preventing TSC1 self-aggregation and homomeric protein formation (Nellist *et al.* 1999). The protein complex is further stabilised by a recently identified protein unit called Tre2-Bub2-Cdc16 1 domain family member 7 (TBC1D7) (Dibble *et al.* 2012). This subunit is critical for TSC1-TSC2 activity. TSC1-TSC2 can be phosphorylated in response to growth factors to further regulate their association, critical for their downstream activity.

The TSC protein complex acts as a tumour suppressor to regulate cell cycle, proliferation and cell growth through the mTOR signalling pathway (Inoki *et al.* 2003a). TSC2 contains a domain at its C-terminus which shares homology with Rap1GAP, a GTPase activating protein (GAP) (Maheshwar *et al.* 1997). This domain has a high activity against the small G-protein Rheb, a critical regulator of the mTOR pathway. GTP bound Rheb is a potent activator of mTOR signalling. TSC2 can exert optimal GAP activity towards Rheb-GTP, converting it to its inactive GDP form and inhibit mTOR signalling (Inoki et al. 2003a; Tee *et al.* 2003; Zhang *et al.* 2003b).

The TSC complex is considered upstream of mTORC1. Many upstream cellular pathways converge on the TSC1-TSC2 complex to regulate mTORC1 signalling. Both TSC1 and TSC2 are phosphorylated by upstream kinases to regulate their stability, localisation and GAP activity. Phosphorylation of TSC2 by ribosomal S6 kinase 1 (RSK1) at Ser1798 (Roux *et al.* 2004), extracellular signal-regulated kinase (ERK) at Ser540 and Ser664 (Ma *et al.* 2005), and Akt at Ser939, Ser981, Ser1130, Ser1132 and Thr1462 (Inoki *et al.* 2002; Potter *et al.* 2002; Huang and Manning 2008, 2009), inhibits its GAP activity through increasing TSC1-TSC2 dissociation and driving mTORC1 signalling (Figure 1.3B). Conversely, phosphorylation of TSC2 by AMP kinase (AMPK) at Thr1271 and Ser1387 (Inoki *et al.* 2003b) and GSK3 at Ser1337 and Ser1341 (Inoki *et al.* 2006) activates its GAP activity on Rheb, therefore inhibiting mTORC1 signalling (Figure 1.3B).

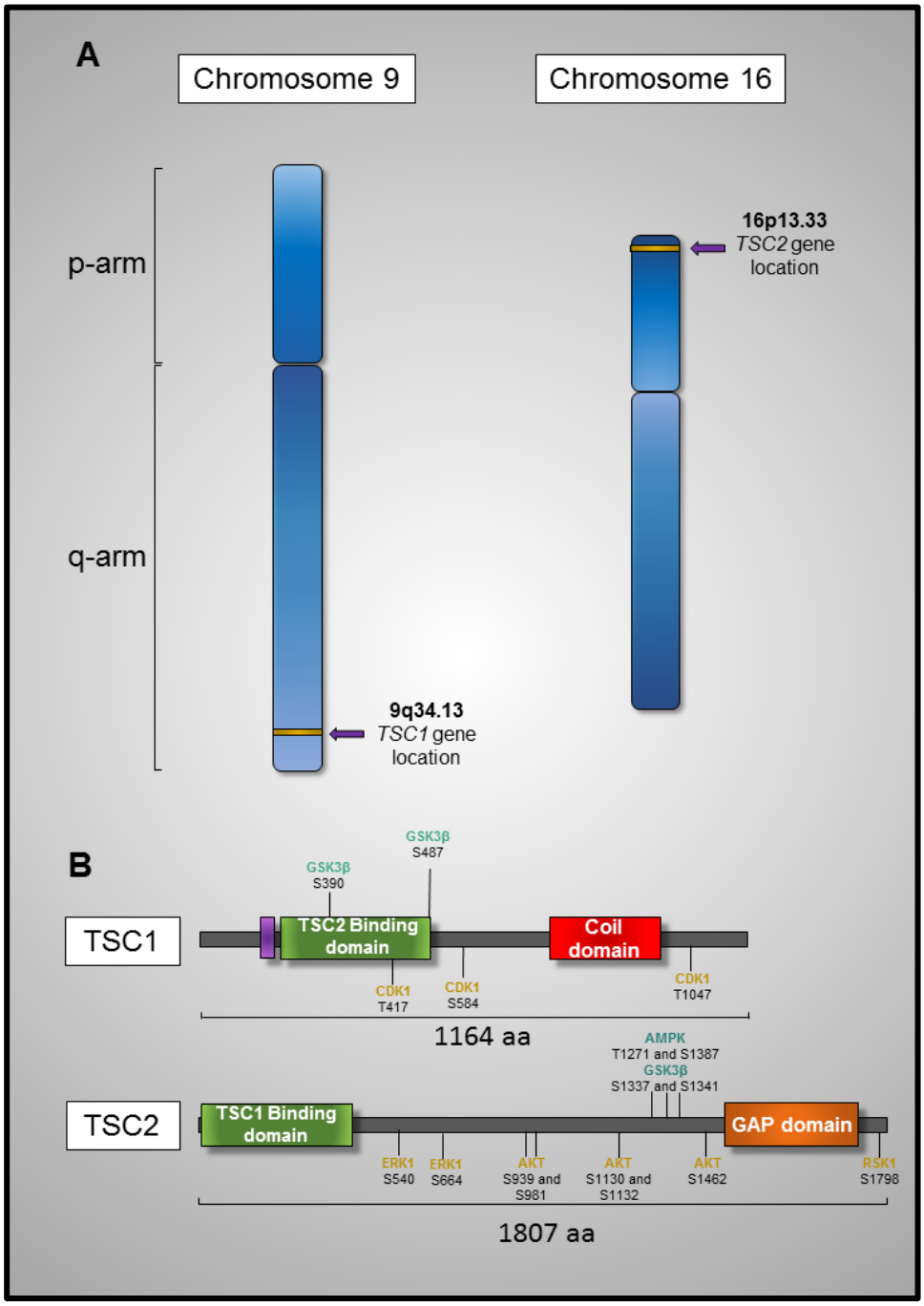

Figure 1.3 Genomic location of human *TSC1* and *TSC2* genes and protein structures. (A) *TSC1* gene is located at chromosome 9q34.13. *TSC2* gene is located at chromosome 16p13.33. **(B)** TSC1 spans 1164 aa and contains a transmebrane domain (purple box), TSC2 binding domain and a coil domain. TSC1 is phophorlyated and inactivated by CDK1 at T417, S584 and T1047. TSC1 is phosphorylated and activated by GSK3β at S390 and S487. TSC2 spans 1807 aa and contains a TSC1 binding domain and a GAP doamin. TSC2 is phosphorlyated and inactivated by ERK1 at S540 and S664, Akt at S939, S981, S1130, S1132 and S1462 and RSK1 at S1798. TSC2 is phosphorlayted and activated by AMPK at T1271 and S1387 and GSK3β at S1337 and S1341. aa: amino acids

TSC1 is also regulated by phosphorylation. Phosphorylation by CDK1 at Thr417, Ser584 and Thr1047 can cause complex dissociation and increased mTORC1 signalling (Figure 1.3B) (Astrinidis *et al.* 2003). Phosphorylation of TSC1 by GSK3β at Ser487 and Thr390 enhances complex stability and TSC2 GAP activity (Figure 1.3B) (Mak *et al.* 2005; Huang and Manning 2008).

1.1.5 Roles of TSC gene mutations in disease development

Mutations in *TSC1* and *TSC2* genes are responsible for the development TSC. The phenotype and severity of the disease are determined by many factors such as mutation location within the gene, types of mutation such as missense, nonsense, small and large deletions, genes mutated (*TSC1* or *TSC2*), frequency of mosaicism and organs involved.

1.1.5.1 *TSC* gene mutations

Over 1500 gene mutations have been identified in *TSC1* and *TSC2*, leading to functional inactivation and disease development (Maheshwar et al. 1997; Sampson et al. 1997; van Slegtenhorst et al. 1997; Cheadle et al. 2000; Kwiatkowski et al. 2010). The *TSC2* gene is mutated in around 64% of TSC cases, compared to *TSC1* in around 26% of TSC cases (Cheadle et al. 2000; Kwiatkowski et al. 2010). Around 10% of TSC patients have no mutation identified (NMI) in either *TSC1* or *TSC2* (Kwiatkowski et al. 2010). *TSC2* gene mutations are suggested to be more frequent due to a larger genomic size, gene complexity and higher number of mutation prone splice sites. Furthermore, mutations in *TSC1* produce a mild phenotype, leading to potential misdiagnosis of TSC (Dabora *et al.* 2001; Sancak *et al.* 2005; Au *et al.* 2007). *TSC* gene mutations consist of “small mutations” affecting just a single exon, and “genomic mutations” affecting one or more exons.

The type of small mutations, the TSC genes involved, their location within the gene and their mutation frequency vary considerably between TSC patients. The *TSC1* gene has 453 small mutations identified. The most frequent mutations found are deletion and nonsense mutations (37.1% and 35.5% of small deletions, respectively). Other mutations include splice and insertion mutations (14.8% and 9.5%) and rare missense mutations (3.1%). The majority of mutations in the *TSC1* gene are located in exon 15, 17 and 18.

Mutations are rarely seen in exons 3 and 22 and no mutations have been observed in exon 23 (Gomez et al. 1999). *TSC2* has 1162 small mutations identified. The most common are deletion, nonsense and missense mutations, occurring at around equal frequency (22-27% of small deletions). Insertion and splice mutations are less frequent (16.2% and 8.5%). Exons 16, 33 and 40 contain the highest frequency of mutations within the *TSC2* gene whereas mutations within exons 2, 25, 31 and 41 are rare. Mutations in exons related to the GAP domain of *TSC2* are frequent and can cause a severe phenotype (Gomez et al. 1999; Cheadle et al. 2000; Kwiatkowski et al. 2010). Most of the small mutations in both *TSC1* and *TSC2* lead to a truncated and non-functional protein.

Genomic deletions/rearrangements, although rare in *TSC1* (0.5% of all TSC patients), are more common in *TSC2* (6% of all TSC patients) (Kozlowski *et al.* 2007). Over 130 genomic deletions or rearrangements have been reported in *TSC2* compared to 9 in *TSC1* (Longa *et al.* 2001; Kozlowski et al. 2007). It has been reported that 73% of large *TSC2* deletions extend greater than the gene itself (Kozlowski et al. 2007). Large genomic deletions towards 3' end of the gene can extend to the adjacent *PKD1* gene and cause *TSC2/PDK1* contiguous gene deletion syndrome (Sampson et al. 1997).

1.1.5.2 Hamartoma development in TSC patients

Hamartoma development is a consequence of *TSC1* or *TSC2* mutations. The loss of mTOR regulation leads to its aberrant activation and increased cell growth and proliferation. Knudsons two-hit hypothesis has been the suggested model for the initiation of TSC hamartoma development (Knudson 1971; Henske *et al.* 1996; Au *et al.* 1999). This hypothesis proposes that 2 'hits' are necessary, one in each allele of tumour suppressor genes, for full gene inactivation and tumorigenesis. Following an inherited germline mutation in one allele of *TSC1* or *TSC2*, a second hit on the corresponding normal functioning allele is required for hamartoma development. Second hit mutations typically occur in somatic cells by large genomic deletion. This results in complete loss of TSC1 or TSC2 protein within cells with a second hit. This loss of heterozygosity (LOH) can be screened using genetic markers. LOH for *TSC1* and *TSC2* has been observed in up to 60% of AMLs in TSC patients (Henske et al. 1996; Au et al. 1999). Facial angiofibromas have shown LOH of *TSC1* and *TSC2* due to a second hit from UV-induced DNA damage from sun exposure (Tyburczy *et al.* 2014). LOH has also been observed

in TSC-associated SEGAs, rhabdomyomas, LAMs and RCCs (Smolarek *et al.* 1998; Chan *et al.* 2004; Kotulska *et al.* 2009). TSC-associated lesions can also develop without LOH (Tucker and Friedman 2002). Cortical tuber development in TSC patients has previously been shown to have no evidence of LOH (Niida *et al.* 2001). Alternatively, epigenetic changes may also lead to inactivation of the second allele of *TSC1* or *TSC2* (Jiang *et al.* 2005; Chakraborty *et al.* 2008; Lu *et al.* 2008). In addition, some TSC-associated lesions may result from *TSC1* or *TSC2* haploinsufficiency (Henske et al. 1996). Haploinsufficiency occurs when one copy of the wild type allele is not sufficient to produce the wild type phenotype (to suppress tumourigenesis). However, *TSC* haploinsufficiency may only manifest through further pathological changes within a cell. Phosphorylation and inactivation of TSC2 by oncogenic activation of ERK and Akt have been seen in TSC brain lesions with no evidence of LOH (Han *et al.* 2004). Therefore, pathogenic kinase activation could promote lesion development by enhancing TSC haploinsufficiency. Other TSC-associated lesions have been observed without LOH, including early renal cysts and rhabdomyomas (Wilson *et al.* 2005).

1.1.5.3 Mosaicism

Mosaicism describes the presence of two or more different populations of cells with different genotypes within the same individual. Mosaicism can occur when *TSC* gene mutations develop during embryogenesis after fertilisation. This can lead to a mutation only evident in a small fraction of somatic cells, rather than a whole organism. In TSC, both somatic mosaicism and germline mosaicism are common (Verhoef *et al.* 1999). Somatic mosaicism occurs due to *in utero* mutations. TSC patients with large genomic mutations have a relatively high frequency of mosaicism (15-25%) (Kozlowski et al. 2007). The frequency of mosaicism in patients with small mutations is relatively low (Sancak et al. 2005). Germline mosaicism occurs when a mutation arises in the germ cells (sperm/eggs) of an individual and all other cells are normal. This mutation can be passed to the next generation without the parent showing any clinical symptoms of TSC (Verhoef et al. 1999).

In somatic mosaicism, early mutations during embryogenesis can lead to a high frequency of mosaicism. A high frequency of mosaicism tends to have higher disease severity due to the mutation present in a high proportion of cells and tissues (Gomez et al. 1999; Verhoef et al. 1999). A patient with 30% mosaicism of a mutation in the *TSC1*

gene was shown to have very severe TSC manifestations (Kwiatkowska *et al.* 1999). Patients with around 13-15% of mosaicism show only mild TSC clinical features (Jones *et al.* 2001). Patients with low mosaic frequency, thus a low proportion of cells with the mutated *TSC* gene show a low disease severity. However, disease severity and phenotype may depend on tissues and organs affected and the chance of second 'hit'. TSC patients with mosaicism also present with less severe symptoms than sporadic TSC cases (Sampson et al. 1997; Dabora et al. 2001; Sancak et al. 2005).

1.1.5.4 *TSC* gene mutations in cancer

Cancer develops from the accumulation of numerous genetic and epigenetic changes resulting in deregulation of cellular pathways. One of the pathways most frequently affected in many cancers is the PI3K/PTEN/Akt/mTOR signalling pathway. mTOR signalling is aberrantly activated in over 50% of cancers and the TSC complex is an essential negative regulator of mTOR by modulating its upstream signalling (Laplante and Sabatini 2012; Dibble and Cantley 2015; Ilagan and Manning 2016; Conciatori *et al.* 2018). The TSC complex also integrates signals from other oncogenic pathways to control mTOR signalling, such as the Ras/MAPK/ERK pathway(Conciatori et al. 2018). Mutations in *TSC1* and/or *TSC2* themselves have been observed in sporadic adult malignancies. Genomic single copy loss of chromosome 9q, where the *TSC1* gene resides, is a common change in bladder cancer patients (Adachi *et al.* 2003; Knowles *et al.* 2003; Pymar *et al.* 2008). Small inactivating mutations in the second allele of *TSC1* have been observed in 14% of bladder cancers, leading to LOH and complete loss of *TSC1* gene product (Knowles et al. 2003; Pymar et al. 2008). *TSC1* LOH and *TSC2* LOH have been observed in lung adenocarcinoma and pancreatic cancer, respectively (Chung *et al.* 1998; Takamochi *et al.* 2001). Methylation of gene promotor regions and therefore reduced expression of *TSC1* and *TSC2* have been reported in oral squamous cell carcinoma, breast cancer, and endometrial cancer. (Jiang et al. 2005; Chakraborty et al. 2008; Lu et al. 2008). Loss of *Tsc2* has also been seen in RCC, causing the increased expression of HIF2α and tumorigenesis (Liu *et al.* 2003). It is still unknown whether these genetic/epigenetic changes are drivers of tumorigenesis or secondary pathological changes.

1.2 mTOR signalling pathway

The mammalian target of rapamycin (mTOR), also known as the mechanistic target of rapamycin or FK506-binding protein 12-rapamycin-associated protein 1 (FRAP1), is a highly conserved serine/threonine kinase of the phosphoinositide 3-kinase-related kinase (PIKK) family. This pathway has evolved to allow cells to transition from anabolic to catabolic processes by integrating a variety of upstream signals, allowing them to survive and grow in nutrient-variable environments. In early 1990s, genetic screens in budding yeast identified TOR1 and TOR2 as effectors of the immunosuppressive molecule, rapamycin (Cafferkey *et al.* 1993). Further biochemical advances in mammals lead to the identification of mTOR as the mammalian target of rapamycin (Brown *et al.* 1994; Sabatini *et al.* 1994). mTOR can form two functionally distinct multi-protein complexes with different sensitivities to rapamycin: mTOR complex 1 (mTORC1) and mTOR complex 2 (mTORC2), that differ in their protein composition, upstream inputs and downstream effectors. mTOR contains various HEAT repeats and a FRAP-ATM TTRAP (FAT) domain. These domains facilitate the interactions of mTOR with mTORC1 and mTORC2 components (Figure 1.4A and B) (Sengupta *et al.* 2010)

1.2.1 mTORC1

mTORC1 is the most studied of the 2 complexes and can respond to a range of upstream signals including nutrients, growth factors, amino acids, energy levels, oxygen levels and cell stress. mTORC1 is rapamycin sensitive and is composed of 6 known components: mTOR, regulatory associated protein of mTOR (RAPTOR), mammalian lethal with sec-13 protein 8 (mLST8), DEP domain containing mTOR-interacting protein (DEPTOR) , proline-rich Akt substrate 40 kDa (PRAS40) and the Tti1/Tel2 complex (Kaizuka *et al.* 2010). RAPTOR is a mTORC1 specific component and acts as a scaffold protein, important in regulating its assembly, localisation and interaction with its substrates (Hara *et al.* 2002; Dunlop *et al.* 2009) (Figure 1.4A). PRAS40 and DEPTOR are inhibitors of mTOR, important in regulating feedback mechanisms. Upon mTORC1 activation, phosphorylation of PRAS40 and DEPTOR by mTOR weakens their association and inhibitory effects on the complex, thus promoting mTORC1 signalling (Fonseca *et al.* 2007; Peterson *et al.* 2009).Roles of the mLST8 protein are not clear as its deletion has no effect on mTORC1 function (Kim *et al.* 2003).

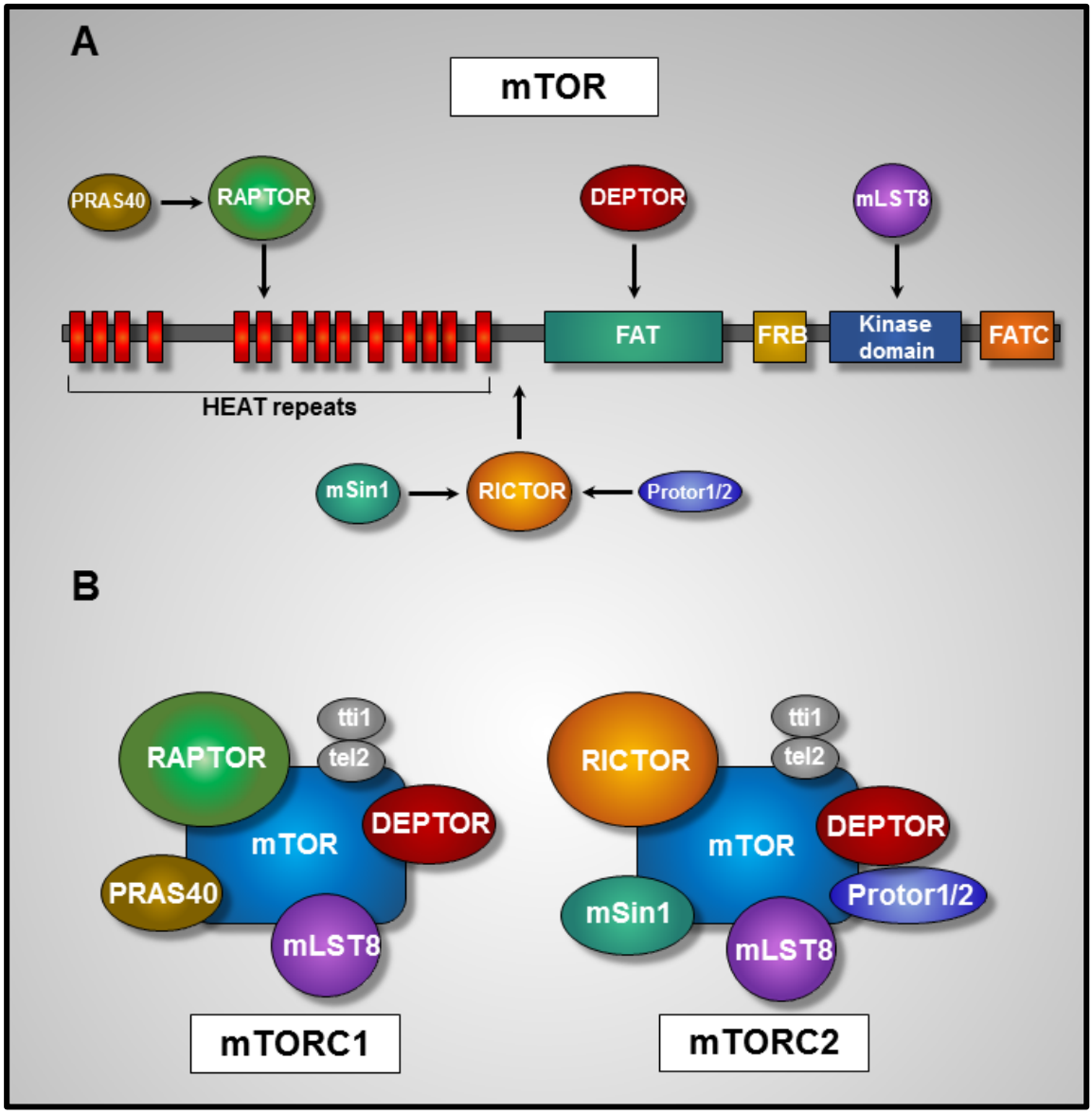

Figure 1.4 mTOR protein structure and complexes. (A) The N-terminus of the mTOR protein structure contains HEAT repeats, followed by a FAT domain, FRB domain, a highly conserved kinase domain and a FATC domain. The individual domains of mTOR allow the interactions of various proteins to regulate mTOR activity. **(B)** mTOR complexes. mTOR can assemble into two functionally distinct complexes, mTORC1 and mTORC2. mTORC1 contains mLST8, RAPTOR, DEPTOR, PRAS40, tti1 and tel2. mTORC2 contains mLST8, RICTOR, DEPTOR, mSIN1, Protor1/1, tti1 and tel2. Differences in their protein composition result in their differing functions. Adapted from (Laplante and Sabatini 2012).

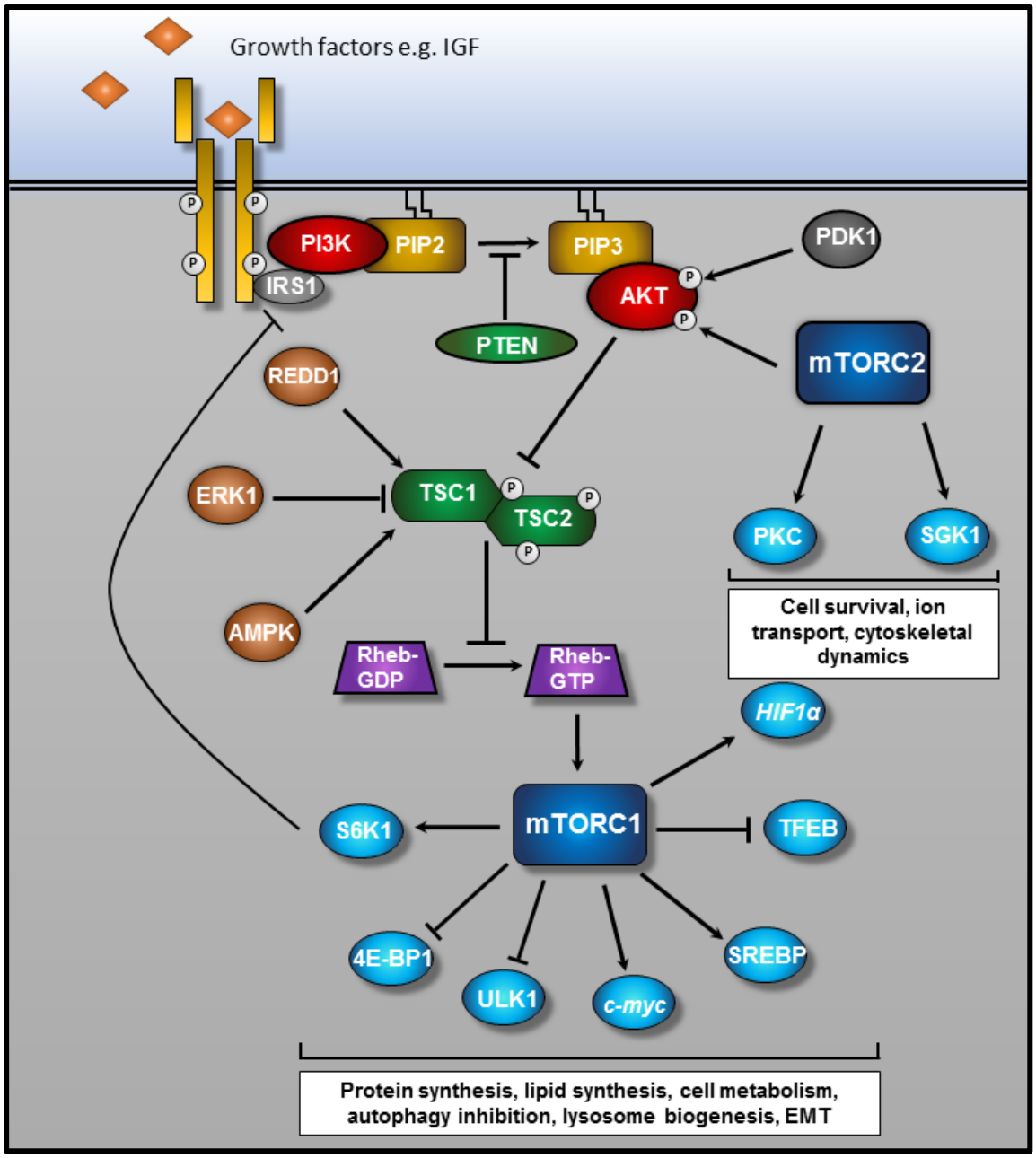

Figure 1.5 mTOR signalling pathway. The main inputs regulating mTORC1 signalling include growth factors, amino acids, stress, oxygen levels and energy status. When activated by Rheb-GTP, mTORC1 promotes protein synthesis, cell metabolism, lipogenesis and EMT and inhibits autophagy and lysosome biogenesis. mTORC2 is insensitive to nutrients but can be activated by growth factors and PI3K signalling by unknown mechanisms. mTORC2 regulates cytoskeletal organisation and cell survival/metabolism through the activation of members of the AGC family, such as Akt, SGK1 and PKC. Adapted from (Laplante and Sabatini 2012).

1.2.1.1 Upstream regulators of mTORC1

mTORC1 is a master regulator of many cellular processes as it can integrate a wide range of upstream signals to balance anabolic and catabolic processes within the cell (Figure 1.5). These signals regulate mTORC1 primarily through the direct modification of mTORC1 components or through the regulation of Rheb GTPase. Rheb is a small GTPase located on endomembrane surfaces and, when GTP bound, can directly interact and activate mTOR kinase activity (Tee et al. 2003). As previously discussed, the TSC1/TSC2/TBC1D7 complex acts as a GTPase activating protein (GAP) to hydrolysis Rheb-GTP into its inactive GDP-bound state, thus inhibiting mTORC1 (Inoki et al. 2003a; Tee et al. 2003). Many of the upstream regulators of mTORC1 converge on the TSC1/TSC2/TBC1D7 complex to regulate its GAP activity on Rheb, thus influencing mTORC1 activity (Huang and Manning 2009). Upstream inputs of mTORC1 include growth factors, nutrient sensors, amino acids, energy levels and oxygen levels (Figure 1.5).

1.2.1.1.1 Hormones and Growth factors

Hormones such as insulin and growth factors such as insulin-like growth factor 1 (IGF-1) can activate mTORC1 through phosphoinositide 3-kinase (PI3K) and Ras signalling (Figure 1.5). Upon ligand binding, receptor tyrosine kinases, such as epidermal growth factor receptor (EGFR) and insulin-like growth factor receptor (IGFR), undergo trans-autophosphorlyation to allow recruitment of adaptor protein insulin receptor substrate 1 (IRS1). Activated IRS1 phosphorylates and activates class I PI3Ks. PI3K catalyses the conversion of phosphatidylinositol-4,5-bisphosphate (PIP2) to phosphatidylinositol-3,4,5-trisphosphate (PIP3) at the cytoplasmic face of the membrane. This conversion can be reversed by phosphatase and tensin homolog deleted on chromosome 10 (PTEN). PIP3 recruits pleckstrin homology (PH) domain containing proteins to the membrane, such as PDK1 and Akt to allow their interaction (Vanhaesebroeck *et al.* 2012; Dibble and Cantley 2015; Thorpe *et al.* 2015). Binding to PIP3 induces a conformational change in Akt allowing its phosphorylation by PDK1 at Thr 308 (Mora *et al.* 2004). Akt is further phosphorylated at Ser473 by mTORC2 for full activation (Sarbassov *et al.* 2005b). Phosphorylation of Ser473 alone is not sufficient to induce Akt activity, but it can promote the stabilisation of the active conformational state of Akt and increase its phosphorylation

rate at Thr308 by 10-fold (Pearce *et al.* 2010). Fully activated Akt can phosphorylate TSC2 at multiple sites (Ser939, Ser981, Ser1130, Ser1132, Thr1462), inhibiting its GAP function on Rheb. Phosphorylation of all 5 sites is needed for full inhibition of the TSC complex and activation of mTORC1 (Inoki et al. 2002; Potter et al. 2002). Phosphorylation and inhibition of AMPK by Akt also enhances mTORC1 signalling. Akt can regulate mTOR activity independently of TSC by directly phosphorylating and inhibiting PRAS40 at Thr246 (Haar *et al.* 2007; Sancak *et al.* 2007). The mTOR component of mTORC1 can directly phosphorylate PRAS40 on S183 and S221, causing its dissociation and relieving its inhibitory effect on the complex (Wang *et al.* 2008).

Growth factor signalling through RTKs can also activate mTORC1 signalling through the Ras/ERK/RSK pathway. RTKs can recruit the Grb2/SOS complex to activate the Ras signalling cascade. Ras activates the Raf/Mek1 signalling cascade which phosphorylates and activates ERK1/2. ERK1/2 can inhibit TSC2 GAP activity directly by phosphorylation at Ser540 and Ser664 or indirectly through activation of p-90-RSK1 (Ma et al. 2005). P-90-RSK1 can phosphorylate and inhibit TSC2 at Ser1798 (Roux et al. 2004). In addition, p-90-RSK1 can phosphorylate RAPTOR at multiple sites to directly increase mTOR kinase activity within the complex.

1.2.1.1.2 Amino acids

Amino acid availability, along with growth factor signalling is vital for mTORC1 activation (Figure 1.6). Amino acids, particularly leucine, arginine and glutamine, are crucial for the localisation of mTORC1 to the lysosome membrane, where Rheb-GTPase resides. mTORC1 activation only occurs in the presence of amino acids, irrespective of other signals. Amino acid sensing by mTORC1 is still not fully understood but involves Rag GTPases (Kim *et al.* 2008; Sancak *et al.* 2008). There are 4 Rag GTPases in mammals forming heterodimers of RagA/B with RagC/D. These heterodimers are anchored to the lysosomal membrane by a complex known as the ragulator, shown to be essential for mTORC1 signalling. Each heterodimer has opposing GTP loading states, where RagC/D is GTP loaded, and RagA/B is GDP loaded. Upon amino acid sensing, the GTP loading states are switched, so that RagA/B is GTP-loaded and RagC/D is GDP loaded (Sancak *et al.* 2010). This allows the recruitment and interaction with RAPTOR, and mTORC1 localisation (Sancak et al. 2008). The ragulator acts as a guanosine exchanging factor (GEF) upon amino acid sensing, converting RagA/B to their GTP-loaded state (Bar-Peled *et al.* 2012). In addition, folliculin (FLCN) acts as a GAP to RagC/D, converting

them to their GDP-loaded state (Tsun *et al.* 2013). These processes support the conversion Rag GTPases to their active state (Figure 1.6).

Rheb resides on all endomembranes whereas the Rag GTPases and ragulator are only found on the lysosomal membrane. This suggests that the lysosome must play an important role in amino acid sensing of mTORC1. Recent studies have suggested that the ragulator interacts with V-ATPases on the lysosomal surface and senses amino acids through an inside-out model (Zoncu *et al.* 2011). Amino acids accumulate in the lumen of the lysosome and signal through V-ATPases, inducing a conformational change in the ragulator, initiating its GEF activity and GTP loading of RagA/B (Figure 1.6). Furthermore, V-ATPases and the ragulator have been shown to interact with various amino acid transporters, such as SLC38A9, important for arginine sensing of mTORC1 (Jung *et al.* 2015) (Figure 1.6). Moreover, Glutamine has been observed to induce GTP-loading of RagA/B through glutaminolysis. α-ketoglutarate, produced by glutaminolysis, is thought to mediate GTP-loading of RagA/B and mTORC1 activation, but the mechanisms are yet to be determined (Duran *et al.* 2012). RagA/B loading state can also be regulated upstream by leucine. Sestrins (SESN1-3) are the main leucine sensors for mTORC1, regulating RagA/B GTP-loading via GATOR1/2 (Figure 1.6). GATOR1 has GAP activity on RagA/B, reverting it to its inactive GDP-loaded state, and GATOR2 is an inhibitor of GATOR1 (Bar-Peled *et al.* 2013). In the presence of leucine, sestrins relive their inhibitory effect on GATOR2 leading to the inhibition of GATOR1, allowing the active conformation of Rag A/B (Chantranupong *et al.* 2014). Furthermore, arginine can be sensed by mTORC1 (Figure 1.6). Arginine can bind and inhibit CASTOR1, an inhibitor of GATOR2. This allows GATOR2 inhibition of GATOR1 and sequential activation of mTORC1 (Chantranupong *et al.* 2016). Arginine can also inhibit TSC1/2 GAP activity through an unknown mechanism, thus leading to mTORC1 activation by Rheb (Carroll *et al.* 2016). Further signalling of Rag GTPases and the importance of mTOR and lysosome localisation for its activation is reviewed here (Tee and Johnson 2017).

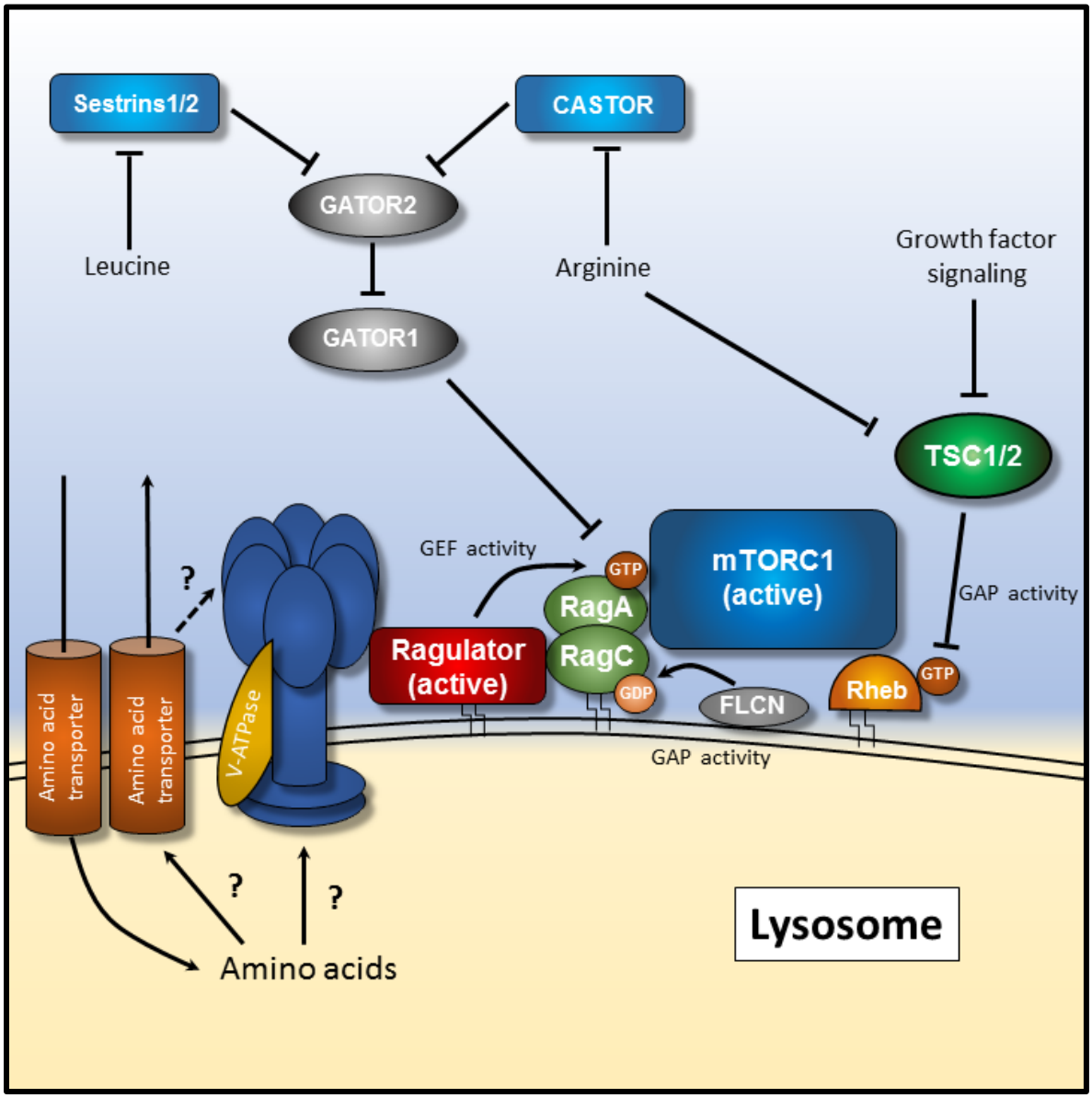

Figure 1.6 mTORC1 amino acid sensing pathway. Amino acid availability regulates the localisation of mTORC1 to the surface of the lysosome, where Rheb-ATP resides. Amino acid availability is necessary for activation of mTORC1. Upon amino acid sensing, GATOR1 can be inhibited by arginine and leucine (through GATOR2). The ragulator and v-ATPase also undergo conformational change activating the GEF activity of the ragulator on RagA/B. How v-ATPase and the ragulator sense amino acids is still not fully understood. GEF activity loads RagA-GTP whilst folliculin GAP activity promotes Rag-C hydrolysis. The now active dimer of RagA-GTP and RagC-GDP recruits mTORC1 to the lysosome surface to interact with Rheb. Rheb is GTP-loaded through growth factor signalling. Adapted from (Bar-Peled and Sabatini 2014)

1.2.1.1.3 Cellular stress

Many cellular stress pathways can signal through the TSC complex and regulate mTOR signalling. Inhibition of mTOR signalling can occur when a cell is ATP-deficient, to transition from anabolic to catabolic processes, and direct a cell to ATP producing pathways. AMP-dependant protein kinase (AMPK) is activated under low ATP conditions by liver kinase B1 (LKB1) (Ballif *et al.* 2005) or Ca^{2+}/CaM-dependent protein kinase β (CaMKKβ) (Hawley *et al.* 2005) by phosphorylation of its α-subunit at Thr172. AMPK can inhibit mTOR directly by phosphorylating RAPTOR at Ser722 and Ser792, leading to 14-3-3 binding and allosteric inhibition (Gwinn *et al.* 2008). AMPK can also phosphorylate TSC2 at Ser1387 and Thr1271, increasing its GAP activity and decrease in mTOR activation (Inoki et al. 2003b) (Figure 1.5). Hypoxic conditions can also lead to mTORC1 suppression. The expression of regulated in DNA damage and development 1 (REDD1) is increased through stabilisation of HIF1α, enabling it to activate the TSC complex through a yet unknown mechanism (Brugarolas *et al.* 2004; DeYoung *et al.* 2008) (Figure 1.5). This allows a cell to conserve more ATP for vital homeostatic processes. Furthermore, DNA damage can signal through mTORC1, primarily through p-53-dependent transcription. p-53 induces the expression of *Tsc2* and *Pten*. Both genes are involved in the suppression of mTORC1 (Feng *et al.* 2005)

1.2.1.2 Downstream effectors

In response to upstream signals, activation of mTOR involves the synthesis of macromolecules such as proteins, lipids and nucleic acids. It also regulates many cellular pathways, such cell metabolism, autophagy, epithelial to mesenchymal transition (EMT) and lysosome biogenesis. These processes are vital for cellular growth and proliferation (Figure 1.5).

1.2.1.2.1 Protein synthesis

A high protein output is required for cellular growth and division. Upon activation, mTORC1 directly phosphorylates translational regulator ribosomal protein S6 kinase 1 (S6K1) and eukaryotic translation initiation factor 4E (eIF4E)-binding protein 1 (4E-BP1) (Figure 1.5). The phosphorylation of S6K1 at 2 sites is needed for its full activation.

mTORC1 phosphorylates one of these sites at Thr389 (Martin and Blenis 2002). S6K1 has a wide range of downstream effectors to enhance protein translation. S6K1 primarily enhances protein synthesis by activating ribosomal protein S6, a vital component of the 40S ribosomal subunit for protein translation. Secondary to this, S6K1 can phosphorylate eukaryotic translation initiation factor 4B (eIF4B) at Ser422. eIF4B, together with eIF4A, aid the unwinding of secondary structures in the 5' untranslated region of mRNA (Sarbassov *et al.* 2005a; Ma and Blenis 2009). eIF4A activity is prevented by PDCD4 and can block mRNA unwinding. S6K1 can also phosphorylate PDCD4 to target it for degradation (Dorello *et al.* 2006). Furthermore, mTORC1 is important in the translation of 5' tract oligopyrimidine (TOP) mRNA. 5' TOP mRNA encodes important protein components for translational machinery. It was originally thought that S6K1 was responsible for this translation. However, it has been observed that S6K1 is not required for 5'TOP translation (Tang *et al.* 2001). The mechanism by which mTORC1 drives 5'TOP translation is currently not known.

mTORC1 phosphorylation of 4E-BP1 releases its binding of cap-binding protein eIF4E. This enables eIF4E to form a multiunit complex with eIF4F and other elongation factors for cap-dependent translation. Phosphorylation of 4E-BP1 at Thr37 and Thr46 by mTORC1 primes it for subsequent phosphorylation at Thr65 and Thr70 to allow its release from eIF4E. Under low growth factors levels, 4E-BP1 binds eIF4E to inhibit protein translation initiation (Ma and Blenis 2009)

mTORC1 can indirectly increase protein synthesis through various mechanisms. mTORC1 can activate tripartite motif-containing protein-24 (TIF-1A), involved in the expression of ribosomal RNA (rRNA) for ribosome biogenesis (Mayer *et al.* 2003). mTORC1 can also inhibit Maf1, to allow the expression of 5S rRNA and transfer RNA (tRNA) transcription (Shor *et al.* 2010). Furthermore, mTORC1 enhances the synthesis of pyrimidines through the phosphorylation of carbamoyl-phosphate synthetase 2, aspartate transcarbamoylase and dihydroorotase (CAD). mTORC1 mediated translation has been fully reviewed previously (Ma and Blenis 2009).

1.2.1.2.2 Lipid synthesis

Lipids synthesis is vital for the generation of membranes in proliferating cells. mTORC1 can signal through sterol regulatory element-binding protein 1 and 2 (SREBP1/2) transcription factors to express genes associated with fatty acid and cholesterol

synthesis (Figure 1.5). SREBP1/2 normally reside as inactive precursors on the endoplasmic reticulum. mTORC1 can cleave inactive SREBPs to render them active through multiple mechanisms, including through S6K1 (Duvel *et al.* 2010). The release of SREBPs from the endoplasmic retinaculum allow their translocation to the nucleus. Moreover, mTORC1 can phosphorylate and inhibit Lipin1, an inhibitor of SREBPs (Peterson *et al.* 2011). Peroxisome proliferator-activated receptor γ (PPAR-γ) is a major regulator of adipogenesis and its expression and activity is also increased by mTORC1 (Kim and Chen 2004).

1.2.1.2.3 Autophagy

Autophagy is the catabolic process within cells resulting in lysosomal degradation of damaged organelles and macromolecules. It is activated under nutrient starved conditions to recycle molecules and produce energy to resume cell homeostasis. mTORC1, as a major cellular nutrient sensor, is a regulator of autophagy. (Ravikumar *et al.* 2010). mTORC1 strongly inhibits autophagy by regulating the function of unc-51 like autophagy activating kinase 1 (ULK1) protein complexes necessary for autophagy induction (Figure 1.5). mTORC1 phosphorylates ULK1 at Ser758. This inhibits autophagy by preventing the interaction and phosphorylation of ULK1 by AMP-dependant protein kinase (AMPK), a potent activator of autophagy and required for protein complex initiation (Ganley *et al.* 2009). mTORC1 also inhibits ULK1 indirectly by phosphorylating and inhibiting autophagy/beclin1 regulator 1(AMBRA1) at Ser52. Active AMBRA1 allows Lys-63-linked ubiquitination of ULK1 by TNF receptor-associated factor 6, E3 ubiquitin protein ligase (TRAF6). This ubiquitination is responsible for ULK1 stabilisation, activation and thus autophagy initiation (Nazio *et al.* 2013).

mTORC1 can regulate autophagy at a transcriptional level by controlling the localisation of transcription factor EB (TFEB) (Figure 1.5). This transcription factor plays an important role in the transcription of lysosomal and autophagy genes. mTORC1 enhances the cytoplasmic localisation of TFEB through phosphorylation at Ser142 and Ser211, causing it to bind to Rag GTPases on the lysosome surface. The cytoplasmic sequestration of TFEB prevents transcription of these genes (Martina *et al.* 2012).

1.2.1.2.4 Epithelial-mesenchymal transition (EMT)

EMT is a complex molecular program whereby polarised epithelial cells convert into non-polarised mesenchymal cells, capable of locomotion. EMT involves complex changes in gene expression, enabling the individual characterisation of epithelial and mesenchymal cells. In some types of cancer, individual tumour cells can express both epithelial and mesenchymal genes. This partial EMT is suggested to play an important role in tumour progression and metastasis by giving cells a greater plasticity (Lecharpentier *et al.* 2011; Jolly *et al.* 2016b; Nieto *et al.* 2016). It is believed to enhance reverse process of EMT (mesenchymal-epithelial transition (MET)) for metastatic colonisation at a secondary site (Lecharpentier et al. 2011). The expression or repression of genes associated with EMT can be regulated by mTOR signalling. It has previously been observed that mTORC1 and mTORC2 both contribute to cell motility (Liu *et al.* 2006; Gulhati *et al.* 2011). Furthermore, EMT progression has been reported to correlate with an increase in cell size and phosphorylation of S6 and 4E-BP1. Activation of the mTOR pathway can regulate cytoskeletal remodelling, through Rho-like GTPases. Rho-like GTPases, comprising of Rho, Rac and cdc42 subfamilies, are important regulators of actin remodelling and cell locomotion. mTOR inhibitor, rapamycin, can increase the levels of cyclin-dependant kinase inhibitor p27, an inhibitor of RhoA activation (Moss *et al.* 2010) and silencing of mTORC2 can prevent cell spreading and actin reorganisation in fibroblasts (Jacinto *et al.* 2004; Sarbassov *et al.* 2004). mTORC1 and mTORC2 inhibition in a mouse model of advanced colorectal cancer has been also shown to attenuate cell migration and invasion by preventing cytoskeletal reorganisation associated with decreased RhoA and Rac1. This inhibition also increased MET (Gulhati et al. 2011). The inhibition of cell migration and invasion by rapamycin through decreased levels of RhoA and Rac1 has also been demonstrated in other cancer models (Liu *et al.* 2010; Zong *et al.* 2014).

1.2.1.3 Feedback loops

mTORC1 can regulate upstream signalling via various feedback loops. The best characterised feedback loop involves mTORC1 suppression of PI3K/Akt signalling. There are several rapamycin sensitive phosphorylation sites on IRS1 and IRS2 which can be phosphorylated by both mTORC1 and S6K1 (O'Reilly *et al.* 2006). The activation of mTORC1 and subsequent activation of S6K1, therefore, can phosphorylate and inhibit

IRS1 to reduce signalling through PI3K (O'Reilly et al. 2006). This has been best observed in *Tsc2* null mouse embryonic fibroblasts (MEFs) which show a decrease in Akt phosphorylation at T308 and are insensitive to insulin. Furthermore, a mouse model with *S6k1* deletion are insensitive to insulin and resistant to obesity due to loss of S6K1-dependent feedback through IRS1 (Um *et al.* 2004). Decreased Akt signalling through mTORC1 activation can also impact TSC2 and PRAS40 activity on mTOR. Loss of Akt phosphorylation leads to inhibition of mTORC1 via reduced phosphorylation of TSC2 and PRAS40 (Fonseca et al. 2007; Huang and Manning 2009). This enables cells to finely tune the level of mTORC1 signalling.

Consistent with findings in *Tsc2* null MEFs, phosphorylation of Akt at S473 was attenuated in liver tumours of *Tsc2*$^{+/-}$ mice and in human TSC-associated renal AMLs (Manning *et al.* 2005; Huang *et al.* 2009). These observations suggest that feedback inhibition of PI3K/Akt signalling may contribute to the low malignant potential of TSC-associated tumours. In contrast to findings in *Tsc2* null MEFs and liver tumours of *Tsc2*$^{+/-}$ mice, a recent study has demonstrated that feedback suppression of Akt was lost in renal lesions including cysts, papillary adenomas and solid carcinomas (as evidenced by increased phosphorylation of Akt and its substrates such as eNOS at S1177, MDM2 at S166, GSK3α at S21 and GSK3β at S9 (Yang *et al.* 2015)). The disruption in feedback mechanisms in these tumours may be due to changes in expression, phosphorylation or stability of numerous pathway components

In addition to IRS proteins mitigating feedback loops, growth factor receptor-bound protein 10 (Grb10), a negative regulator of PI3K signalling, has also been shown to accumulate and repress PI3K/Akt signalling upon its activation by mTORC1 in *Tsc1* and *Tsc2* MEF cells (Yu *et al.* 2011). Moreover, S6K1 activation can reduce the expression of RTKs such as platelet derived growth factor receptor α and β (PDGFRα/β) in *Tsc1* or *Tsc2* null MEFs (Zhang *et al.* 2007) and EGFR to further reduce PI3K signalling in pancreatic tumours of a xenograft mouse model (Wei *et al.* 2015). Taken together, mTORC1-mediated feedback loops appear to be more complicated than initially thought and warrant further investigations.

1.2.2 mTORC2

mTORC2 is the rapamycin-insensitive complex of mTOR, consisting of mTOR, mLST8, DEPTOR, Tti/Tel2, as well as the mTORC2 specific components rapamycin-insensitive

companion of mTOR (RICTOR) (Sarbassov et al. 2004), mammalian stress-activated map kinase-interacting protein 1 (mSIN1) (Jacinto *et al.* 2006) and protein observed with rictor 1/2 (protor1/2) (Pearce *et al.* 2007) (Figure 1.4B). RICTOR, like RAPTOR in mTORC1, is a scaffold protein responsible for mTORC2 assembly and the interaction with its specific substrates (Sarbassov et al. 2004). mSin1 is also a scaffold protein, important for its interaction with downstream substrate, serum- and glucocorticoid-induced protein kinase 1 (SGK1). Protor 1/2 are responsible for SGK1 interaction (Pearce *et al.* 2011). Like mTORC1, mLST8 function is still unknown in mTORC2. However, it has been shown to be essential for mTORC2 activity.

As previously mentioned, mTORC2 is insensitive to the mTOR inhibitor, rapamycin. Consistent studies demonstrate no inhibition of its downstream effectors after acute treatment. It has been observed that the rapamycin-FKBP12 complex necessary for inhibition is unable to bind mTORC2. However, there is evidence of long-term rapamycin treatment inhibiting mTORC2 (Phung *et al.* 2006; Sarbassov *et al.* 2006). As the rapamycin-FKBP12 complex is unable to bind intact mTORC2, there must be another mechanism preventing its signalling. It is suggested that the rapamycin-FKBP12 complex can bind newly synthesised mTOR, thus preventing the assembly of mTORC2 (Sarbassov et al. 2006)

1.2.2.1 Upstream regulation and downstream effectors

Compared to mTORC1, less is understood about how mTORC2 is regulated. mTORC2 is insensitive to nutrients but can be stimulated by growth factors and PI3K signalling although the mechanisms are unknown. Ribosomes may be involved as mTORC2 binds them in a PI3K-dependent manner (Zinzalla *et al.* 2011). This suggests an upstream regulatory mechanism linking both mTORC1 and mTORC2. mTORC2 phosphorylation of Akt at Ser473 can enhance mTORC1 activity whilst mTORC1 signalling can induce ribosomal synthesis (Willems *et al.* 2012). More investigation is needed to fully understand upstream regulation of mTORC2.

mTORC2 has different substrates from mTORC1 that can control cell growth and proliferation (Jacinto et al. 2004; Sarbassov et al. 2005b). Members of the AGC subfamily, such as Akt, SGK1 and protein kinase C-α (PKCα) are known substrates of mTORC2 (Figure 1.5). mTORC2 is responsible for the phosphorylation of Akt at Ser473, priming it for its full activation by PDK1 at T308. However, phosphorylation of Akt at

T308 can occur independently of S473 phosphorylation (Sarbassov et al. 2005b; Pearce et al. 2010). Dephosphorylation of Ser473 can occur by PHLPP phosphatases (PHLPP1 and 2) (Brognard *et al.* 2007). mTORC2 is also responsible for the phosphorylation of Ser450 on Akt for its stability (Oh and Jacinto 2011). Akt is involved in many downstream signalling pathways associated with cell survival, glucose uptake, cell cycle progression and apoptosis. SGK1 activation by mTORC2 is necessary for controlling ion transport and cell growth (Garcia-Martinez and Alessi 2008). mTORC2 can also regulate cytoskeletal dynamics, primarily through its activation of PKC (Jacinto et al. 2004; Ikenoue *et al.* 2008) and controls cell shape and structure through Rho-GTPases (Figure 1.5) (Figure 1.5) (Jacinto et al. 2004; Chen *et al.* 2015). Recently, mTORC2 has been found to play a role in regulating EMT (Liao *et al.* 2014; Gupta *et al.* 2016; Sakre *et al.* 2017).

1.2.3 mTOR hyperactivation in cancer and tumour syndromes

Deregulation of the mTOR pathway is frequently implicated in tumorigenesis (Laplante and Sabatini 2012). Cancer cells utilise processes downstream of mTOR to accumulate biomass for cell growth and proliferation. These processes include increased protein translation and lipid synthesis for dividing cells. mTOR is also involved in metabolic transformation, angiogenesis and metastasis of tumour cells (Guertin and Sabatini 2007; Laplante and Sabatini 2012). Although mutations in mTOR are uncommon, mutations in upstream components are frequent. Components of the mTOR pathway include many proto-oncogenes and tumour-suppressor genes, of which mutations can lead to mTOR hyperactivation and insensitivity to nutrients and other upstream regulators. Proto-oncogenes include PI3K, Akt, Rheb, S6K1, eIF4E and cyclin D1 (Dibble and Cantley 2015). Gene amplification of growth factor receptors that are upstream of PI3K are also common. Activating mutations of proto-oncogenes can lead to sporadic cancer. Amplification of *PI3KCA* gene leads to constitutively activate mTOR signalling, implicated in many cancer subsets (Samuels *et al.* 2004). Loss of tumour suppressor genes also results in tumorigenesis. Tumour suppressor genes associated with the mTOR pathway include *PTEN, TSC1/2, LKB1, REDD1, TP53* and *BLCN1* (Laplante and Sabatini 2012). The development of tumour syndromes such as TSC and Cowden disease is a result from loss of the tumour suppressor proteins TSC1 or TSC2 and PTEN, respectively (Krymskaya and Goncharova 2009). *PTEN* is the second most commonly mutated gene in human cancers, following *TP53* (Milella *et al.* 2015). As discussed in

1.1.5.4, TSC gene mutations have been observed in some types of cancer, such as bladder and lung cancer (Takamochi et al. 2001; Knowles et al. 2003) Frequent mutations within the PI3K/Akt/TSC1-TSC2/mTOR pathway have been reported in renal and head and neck cancers (Giudice and Squarize 2013). Frequent mutations in the RAS/RAF/MAPK pathway have also been observed in many cancers (Molina and Adjei 2006). Members of this pathway can directly inhibit TSC1/2 and thus activate mTOR. The current understanding of the mTOR pathway has been mainly achieved through the study of rare genetic diseases, such as TSC (Tee et al. 2003; Huang and Manning 2009).

1.3 mTOR and cancer metabolism

mTOR is a master regulator of cellular metabolism. Increased mTOR signalling leads to a metabolic transformation in cancer cells to give them a proliferative advantage. Metabolic reprogramming ensures cancer cells to acquire the nutrients needed to fulfil their bioenergetic, biosynthetic and redox needs for rapid proliferation (Vander Heiden *et al.* 2009). mTOR activation results in the oncogenic expression of genes involved in glycolysis and glutaminolysis, for the metabolism of glucose and glutamine, respectively (Cantor and Sabatini 2012; Altman *et al.* 2016; Nagarajan *et al.* 2016). This can render cancer cells addicted to these nutrients and an increase flux in these pathways.

1.3.1 Glycolysis

Glucose is the most abundant nutrient in the plasma and is central for normal metabolic function. The glycolysis pathway comprises of several committed and non-committed reactions to produce pyruvate (Figure 1.7). In oxygen rich conditions, pyruvate is converted into acetyl CoA and fed into the tricarboxylic acid cycle (TCA) for macromolecule and ATP biosynthesis. Cancer cells undergo metabolic transformation to favour aerobic glycolysis. Glucose is consumed at an elevated rate and secreted as lactate, even under normal oxygen conditions, rather than completely oxidised through oxidative phosphorylation (Warburg 1956). This phenomenon was first observed by Otto Warburg in the late 1920s and is known as the “Warburg effect” (Warburg 1927). A high flux of aerobic glycolysis provides cells a proliferative advantage by producing sufficient amounts of ATP, macromolecules and reducing agents (Hay 2016). The Warburg effect is a traditional metabolic phenotype observed in cancer cells.

1.3.1.1 Energy production

Proliferating cancer cells require high amounts of energy in the form of ATP. Glycolysis is naturally an ineffective way of generating ATP. For every 1 molecule of glucose, only 2 molecules of ATP are produced, compared to 38 molecules through oxidative phosphorylation. However, glycolysis has a higher rate of ATP production, up to 100 times faster. When glucose levels are not rate limiting, an increase flux through glycolysis generates higher levels of ATP quicker than oxidative phosphorylation (Warburg 1956; Pfeiffer *et al.* 2001). A recent study has shown that when the demand of ATP by a cell is

increased, aerobic glycolysis is increased whilst oxidative phosphorylation stays constant (Epstein *et al.* 2014). This provides evidence of aerobic glycolysis being utilised for rapid ATP production when cellular bioenergetic demands change. Cancer cells have an abnormally high rate of glucose uptake for maximum ATP production to meet their bioenergetic needs (Figure 1.7)

1.3.1.2 Macromolecule synthesis

Cancer cells increase their biomass through the synthesis of macromolecules in preparation for cell division. The abnormal rate of glucose uptake and increased flux through glycolysis results in an accumulation of intermediate glycolytic substrates which are shunted into various biosynthetic pathways (Figure 1.7)(DeBerardinis *et al.* 2008; Vander Heiden et al. 2009; Cairns *et al.* 2011). This accumulation is facilitated by the attenuation of the final step of glycolysis by pyruvate kinase M2 (PKM2) (to be discussed later). Upon entering the cell via glucose transporters (many of which are programmed to be highly expressed in cancer for maximum glucose uptake (Szablewski 2013)), glucose is immediately converted to glucose-6-phosphate (G6P) by hexokinases. This is an important committed step of glycolysis to trap glucose within the cell. Five hexokinases exist, all encoded by separate genes (Wilson 2003). Hexokinase I is ubiquitously expressed in most tissues. Hexokinase II is highly expressed in cancer cells and not normal adult cells to accelerate the high flux of glucose through biosynthetic pathways (Mathupala *et al.* 2001; Patra *et al.* 2013). G6P is a convergence point for many interconnected biosynthesis pathways, including the pentose phosphate pathway (PPP), glycogen synthesis and the hexosamine pathway (Figure 1.7)(Hay 2016). Entry into these pathways is further enhanced by oncogenic signalling pathways.

The PPP comprises of two individual branches: the oxidative and non-oxidative branches. The oxidative branch is responsible for the synthesis of reduced nicotinamide adenine dinucleotide phosphate (NADPH) and ribonucleotides. Enhanced glucose uptake produces increased levels of NADPH for maintaining redox balance during macromolecule biosynthesis, particularly lipid biosynthesis (Patra and Hay 2014). NADPH is also necessary to sustain the reduced form of the antioxidant glutathione to combat the increased exposure to reactive oxygen species (ROS) during rapid proliferation. The non-oxidative branch is required for the generation of pentose phosphates for ribonucleotides synthesis, involving the recruitment of further glycolytic intermediates, such as fructose-6-phosphate (F6P) and glyceraldehyde-3-phosphate

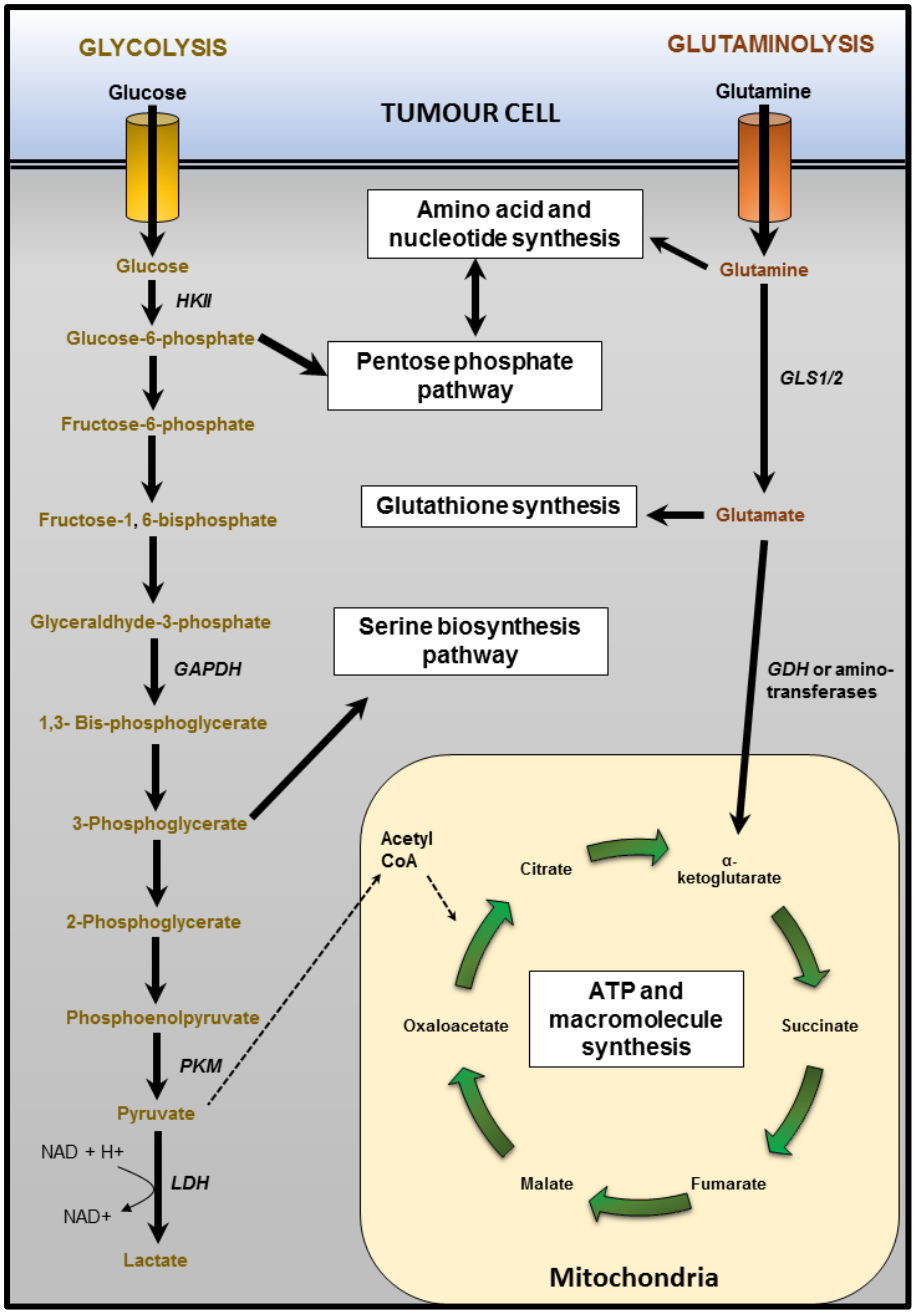

Figure 1.7 Glycolysis and glutaminolysis in cancer cells. Cancer cells reprogram their metabolism to favour aerobic glycolysis. The uptake of both glucose and glutamine is increased through the increased expression of transporters. Glucose is converted to lactate to produce reduced NADH required to maintain high glycolytic flux, thus depleting the Krebs cycle, important for ATP and macromolecular synthesis. Glutamine is converted to α-ketoglutarate through glutaminolysis to replenish the Krebs cycle through anaplerosis. This metabolic transformation ensures cancer cells acquire the ATP and macromolecules required for rapid growth and proliferation. Glycolytic and glutaminolytic intermediates can also be shunted into branching synthetic pathways throughout glycolysis and glutaminolysis. Some of these pathways require both glucose and glutamine for biosynthesis. Thick black arrows indicate increased flux. Thin dotted black arrows indicate decreased flux. Some enzymes that are overexpressed in cancer cells are shown. Adapted from (Cantor and Sabatini 2012)

(G3P) (Patra and Hay 2014; Hay 2016). Ribonucleotides are essential for DNA and RNA synthesis in proliferating cells. G6P is also shunted into the hexosamine pathway, in conjunction with acetyl-CoA, glutamine and UTP, for the generation of uridine diphosphate N-actylglucosamine (UDP-GlcNAc). This molecule is important in the glycosylation and post-translational modification of proteins (Love and Hanover 2005).

In addition to G6P, the glycolytic intermediate 3-phosphoglycerate (3PG) can accumulate and be utilised in the serine biosynthesis pathway (Figure 1.7). Serine produced in this pathway is used for the generation of non-essential amino acids, glutathione (in conjunction with glutamine metabolism) and nucleic acids in the folate cycle (Yang and Vousden 2016). Phosphoglycerate dehydrogenase (PHGDH) expression is amplified in breast cancer and melanoma cells and is necessary for their proliferation (Mullarky *et al.* 2011; Possemato *et al.* 2011). Increased channelling into the serine biosynthesis pathway can be enhanced by the low activity of PKM2 (Gui *et al.* 2013).

1.3.1.3 Pyruvate Kinase M2 (PKM2)

PKM2 is an isoenzyme that catalyses the final ATP-generating step of glycolysis, the conversion of phosphoenolpyruvate (PEP) to pyruvate (Figure 1.7. It is one of 4 isoenzymes that exist of pyruvate kinase: PKM1 and PKM2, encoded from the *Pkm* gene by alternative splicing; PKL and PKR, encoded from the *Pklr* gene by alternate promoters (Noguchi *et al.* 1986; Noguchi *et al.* 1987). PKM1 is expressed in muscle and brain tissue whereas PKM2 is expressed in highly proliferating cells, such as adult stem cells and embryonic cells (Mazurek *et al.* 2005; Wong *et al.* 2015). PKM2 is also expressed in a large subset of cancers, such as colon carcinoma and RCC, due to its ability to provide cells a proliferative advantage over PKM1 (Brinck *et al.* 1994; Christofk *et al.* 2008).

Pyruvate kinases are active when in a tetrameric conformation. PKM1 is constantly in an active tetrameric conformation, whereas PKM2 is allosterically regulated between a high active tetrameric conformation and low active dimeric conformation (Mazurek et al. 2005; Gui et al. 2013; Wong et al. 2015). PKM2 in its low active dimeric state attenuates the final step of glycolysis. This facilitates the upstream accumulation and diversion of glycolytic metabolites into biosynthetic pathways, as described above, for anabolic growth and sustained proliferation (Cairns et al. 2011; Hay 2016). Dimeric PKM2 also enhances the Warburg effect through the conversion of pyruvate to lactate (Wong et al.

2015). The ability to finely regulate PKM2 activity is important to meet the physiological requirements of a cancer cell. The high active tetramer formation enhances ATP synthesis and cellular energy levels by driving the production of pyruvate whereas the low activity dimer formation can enhance macromolecular biosynthesis and anabolic growth of a cell (Gui et al. 2013).

Metabolite concentrations of glycolytic intermediates can finely regulate the conformational state of PKM2 and its function (Luo *et al.* 2011; Garcia-Cao *et al.* 2012; Gui *et al*. 2013). The metabolites serine and fructose-1,6-bisphosphate (FBP) are potent activators of PKM2 activity by increasing the tetrameric form of PKM2. This provides feedback regulation of macromolecule biosynthesis (Gui et al. 2013). Reactive oxygen species (ROS) are negative regulators of PKM2 to enhance intermediate shunting into the PPP pathway for redox homeostasis (Anastasiou *et al.* 2011). PKM2 expression and activity are also regulated by oncogenic pathways such as the mTOR signalling (to be discussed in detail in 1.3.3.3).

The role of PKM2 in cancer, however, is still a subject of debate. Increased PKM2 expression has been reported in advanced cancers and shown to be associated with a poor prognosis. *Pkm2* deletion in mouse models of leukaemia also delayed the onset of leukemogenesis (Wang *et al.* 2014) . Expression of PKM2 in lung cancer cell lines and xenograft models of lung cancer conferred a proliferative advantage for tumour growth and is required for aerobic glycolysis (Christofk et al. 2008). Moreover, PKM2 acts as a protein kinase and a transcriptional coactivator of genes involved in cell proliferation, migration and apoptosis (Wong et al. 2015). Some recent studies, however, suggest that *Pkm2* is not required for tumourigenesis and, in contrast, loss of *Pkm2* promotes tumour formation in some types of cells/tissues. *Pkm2* conditional deletion accelerated tumour growth in a *Brca1*-loss-driven mouse model of breast cancer (Israelsen *et al.* 2013). Germline deletion of *Pkm2* promoted metabolic stress and tumour formation in a mouse model of hepatocellular carcinoma (Dayton *et al.* 2016). Furthermore, *Pkm2* is not required for tumourigenesis in a colon cancer model initiated by conditional deletion of *Apc* (Lau *et al.* 2017). It would be interesting to see whether *Pkm2* is required for development of TSC-associated tumours

1.3.1.4 Lactate secretion

The secretion of lactate plays an integral role in tumour progression. Lactate secretion is required to maintain an elevated flux through glycolysis. The glycolysis pathway requires NAD^+ as a cofactor for the regular function of some of its enzymes, such as glyceraldehyde-3-phosphate dehydrogenase (GAPDH) and PHGDH. NAD^+ levels are quickly depleted by its conversion to NADH from the high glycolytic flux. The increased expression of lactate dehydrogenase-A (LDHA), as seen in cancer cells, catalyses the conversion of pyruvate to lactate, a reaction regenerating NAD^+ to maintain glycolytic flow (Figure 1.7)(Hirschhaeuser *et al.* 2011; Hay 2016). Furthermore, lactate may support tumour growth through its secretion into the microenvironment through monocarboxylate transporters (MCTs). Acidification of the tumour microenvironment has been shown to enhance tumour invasion (Gatenby *et al.* 2006). Lactate has also been shown to be taken up by stromal cells, converted back to pyruvate and used as an energy substrate by nearby tumour cells to replenish the TCA intermediates and fuel further ATP synthesis (Sonveaux *et al.* 2008; Feron 2009).

1.3.2 Glutaminolysis

Glutamine, like glucose, is a vital nutrient for cancer cells. It is the most abundant amino acid in the plasma and its uptake is increased dramatically in tumours (Eagle 1955; Kovacevic and McGivan 1983). Glutamine is considered a non-essential amino acid and is maintained at high levels in the blood. Cancer cells utilise glutamine for cell bioenergetics, biosynthesis and redox balance (Figure 1.7) (DeBerardinis *et al.* 2007). Glutamine is an essential nitrogen donor and couples with glycolysis for the biosynthesis of nucleotides, hexosamines and amino acids. Its uses also extend to its carbon backbone as a major biosynthetic precursor (DeBerardinis and Cheng 2010; Altman et al. 2016; Hosios *et al.* 2016). Glutamine metabolism, along with the Warburg effect, is a traditional metabolic characteristic seen in proliferating tumour cells (Kovacevic and McGivan 1983).

Glutamine can be used as a biosynthetic precursor. Upon entering the cell via glutamine transporters, glutamine can immediately be required for nucleotide synthesis or UDP-GlcNAc synthesis (Figure 1.7)(DeBerardinis et al. 2007). Glutamine can also be transported to the mitochondria and converted to glutamate by mitochondrial

glutaminases. Glutaminases exist as multiple tissue-specific forms, encoded by 2 mammalian genes: kidney-type glutaminase (GLS1) and liver-type glutaminase (GLS2) (Curthoys and Watford 1995). GLS1 can be further spliced into glutaminase C (GAC) or kidney type glutaminase (KGA) (Elgadi *et al.* 1999). Both GLS1 and GLS2 differ in their tissue expression and regulation. GLS1 expression has consistently been increased in many experimental tumour models in rats and mice (Knox *et al.* 1969; van den Heuvel *et al.* 2012; Gross *et al.* 2014). This increase correlates with tumour growth and GLS1 inhibition has been shown to attenuate tumour progression (Gao *et al.* 2009). GLS1 has also shown evidence of positively regulating glucose uptake in prostate cancer cells, indicating feedback mechanisms between glucose and glutamine metabolism (Pan *et al.* 2015). Interestingly, it has recently been suggested that GLS2 may have tumour suppressor functions in some cancer subsets and is a target of p53 (Zhang *et al.* 2013; Liu *et al.* 2014a).

Glutamate produced by glutaminases has the potential to enter many significant biosynthesis pathways. It can be utilised for glutathione synthesis, a source of an amino group for non-essential amino acid synthesis or converted to α-ketoglutarate (Figure 1.7) (DeBerardinis et al. 2007). Conversion to α -ketoglutarate is performed by either glutamate dehydrogenase (GDH) or aminotransferases, such as phosphoserine aminotransferase 1 (PSAT1), part of the serine biosynthesis pathway (Moreadith and Lehninger 1984). GDH can be regulated by the mTOR pathway and is allosterically regulated by leucine and ATP levels (Li *et al.* 2012; Csibi *et al.* 2013).

1.3.2.1 Anaplerosis of the TCA cycle

Cancer metabolism by aerobic glycolysis and secretion as lactate results in depletion of TCA cycle intermediates. The TCA cycle produces many substrates that can act as precursors for biosynthetic pathways. It is also crucial for ATP synthesis through the generation of NADH and $FADH_2$ for oxidative phosphorylation. Glutamine-derived α-ketoglutarate provides an alternative source of carbon to replenish the TCA cycle through a process called anaplerosis (Figure 1.7)(DeBerardinis et al. 2007; DeBerardinis and Cheng 2010; Mayers and Vander Heiden 2015; Altman et al. 2016). A study in glioma cells of both rats and humans using nuclear magnetic resonance (NMR) spectroscopy to follow ^{13}C-labeleled substrates showed the glutamine carbon backbone as a major anaplerotic precursor for the TCA cycle (Portais *et al.* 1996; DeBerardinis et al. 2007). Glutamine deprivation has also shown a significant reduction in TCA cycle intermediates

fumarate and malate. This indicates that the carbon backbone of glutamine is essential for the maintenance TCA cycle intermediates and synthesis of macromolecules (Yuneva *et al.* 2007). Glutamine-derived α-ketoglutarate is used by the TCA cycle to produce metabolites such as citrate via the process of reductive carboxylation for fatty acid synthesis (Wise *et al.* 2011). In addition, glutamine-derived malate can be converted to pyruvate by the malic enzyme and produce NADPH necessary for redox stability (DeBerardinis et al. 2007). Pyruvate can be further converted to acetyl-CoA and recycled back into the TCA cycle or is converted to lactate by LDHA for NAD^+ regeneration (Moreadith and Lehninger 1984). The glutamine carbon backbone can also be incorporated into glucose by gluconeogenesis in glucose deprived conditions, providing more evidence of feedback mechanisms between the two metabolic routes. Furthermore, glutamine-derived oxaloacetate can be transaminated with excess glutamate by aspartate aminotransferase (AST) to produce aspartate for nucleotide biosynthesis and additional α-ketoglutarate (Patel *et al.* 2016).

1.3.3 Metabolic transformation driven by mTOR

mTOR hyperactivation induces metabolic reprogramming of cancer cells, as described previously, via many mechanisms (Duvel et al. 2010; Zha *et al.* 2014). mTORC1 has been shown to enhance glutamine metabolism and anaplerosis by activating GDH. This is achieved by suppressing SIRT4, an inhibitor of GDH, through the degradation of cAMP-responsive element binding 2 (CREB2) (Csibi et al. 2013). SIRT levels are decreased in many cancers exhibiting mutations in the mTOR pathway (Csibi et al. 2013). mTORC2 also regulates metabolic rewiring through Akt phosphorylation. mTORC2 phosphorylates Akt at S473 and T450 leading to full activation of Akt and a variety of signalling mechanisms to meet the changing bioenergetic needs of a cancer cell (Elstrom *et al.* 2004). Akt1 stimulates the generation and translocation of glucose transporters and the phosphorylation and activation of many key glycolytic enzymes, such as hexokinases (Robey and Hay 2009). Moreover, Akt activation activates mTORC1 signalling through the inhibition of TSC2 and FOXO3a (Inoki et al. 2002; Khatri *et al.* 2010). mTORC1 enhances metabolic flux through glycolysis and glutaminolysis by elevating the expression of transcription factor families such as hypoxia-inducible factor 1 (HIF1) and MYC.

1.3.3.1 Hypoxia-inducible factor transcription factors

The HIF transcription factors are responsible for gene expression changes during hypoxic conditions to ensure cell survival. The HIF complex are heterodimers comprised of HIF1α and HIF1β subunits. HIF1β is constitutively expressed whereas HIF1α is regulated by cellular oxygen concentrations. In high oxygen conditions, proline residues on HIF1α are hydroxylated by prolyl hydroxylase enzymes. This results in the recruitment of the tumour suppressor, von Hippel-Lindau (VHL), an E3 ubiquitin ligase, for subsequent ubiquitin-mediated degradation of HIF1α (Brahimi-Horn *et al.* 2007). In hypoxic conditions, HIF1α is stabilised and binds to HIF1β and other cofactors for the transcription of many genes associated with glycolysis containing hypoxic response elements (HRE) (Lu *et al.* 2005). However, oncogenic activation of mTOR or mutations within the VHL protein, as seen in Von Hippel-Lindau syndrome, stabilises and activates HIF1α in normoxic conditions, and results in overexpression of metabolic genes (Inoki *et al.* 2005; Guertin and Sabatini 2007; Gossage *et al.* 2015). mTORC1 promotes HIF1α mRNA transcription via signal transducer and activator of transcription 3 (STAT3) and translation via eIF4F and S6K1 and is rapamycin sensitive (Duvel *et a*l. 2010; Laplante and Sabatini 2013; Dodd *et al.* 2015). A recent study using *Tsc2* null MEFs found that HIF1α transcription was increased 7-fold in hypoxic conditions and was also rapamycin sensitive (Dodd *et al*. 2015). This may result in a significant increase in glycolysis in these mTOR-driven tumours.

Oncogenic activation of mTOR and HIF1 complex provides growth and survival advantages for a cancer cell by modulating energy metabolism and switching to aerobic glycolysis. Genes involved in these changes include LDHA, MCT1 and pyruvate dehydrogenase kinase (PDK) to prevent pyruvate entry into the TCA cycle for rapid ATP production (Kim *et al.* 2006; Hirschhaeuser et al. 2011). HIF1 complex also induces the expression of glycolytic transporters and enymes to enhance glucose uptake and utilisation, such as glucose transport 1 (GLUT1), GLUT3, hexokinase II (HKII) and enzymes involved with intermediate shunting to biosynthetic pathways (Duvel et al. 2010).

1.3.3.2 MYC transcription factors

The MYC family of proteins are a group of transcription factors able to bind gene promotors containing enhancer box (E-Box) sequences. They strongly regulate many genes associated with cell metabolism and the Warburg effect. The amplification of MYC genes are frequently seen in cancers (Stine *et al.* 2015). mTORC1 signalling is an essential regulator of MYC expression. mTORC1 is required for STAT3 dependent transcription of *c-myc* and its cap-dependent translation (Laplante and Sabatini 2013; Csibi *et al.* 2014). mTORC1 can also indirectly affect MYC stability through the autophagy protein AMBRA1. AMBRA1 promotes dephosphorylation of MYC by protein phosphatases, leading to its destabilisation and degradation. mTORC1 signalling inactivates AMBRA1 to reduce MYC degradation (Cianfanelli *et al.* 2015). Furthermore, mTORC2 has been recently found to increase MYC levels through the acetylation of FoxO1 and FoxO3. This mechanism releases MYC from its suppressive miR-34c-dependent network and the increased MYC levels correlates with a reduced survival time in glioblastoma patients (Masui *et al.* 2013).

MYC collaborates with HIF1 to regulate the expression of key enzymes involved in glycolysis such as LDHA and induce the metabolic transformation of cancer cells (Shim *et al.* 1997; Dang *et al.* 2008). MYC transcription factors also regulate the expression of key enzymes involved in the glutaminolysis pathway (DeBerardinis et al. 2007). MYC-transformed cells have been shown to become addicted to glutamine that is required for cell survival (Yuneva et al. 2007). Another study using a conditional transgenic mouse model showed that MYC overexpression drives the initiation of renal cell carcinoma through upregulation of glutamine metabolism (Shroff *et al.* 2015). MYC is involved in the expression of glutamine transporters, GLS and GDH (Wise *et al.* 2008). MYC induces GLS expression by suppressing miR-23a and miR-23b, transcriptional repressors of GLS expression (Gao et al. 2009). These pathways couple with HIF1 complex for anaplerosis of the TCA cycle.

1.3.3.3 mTOR regulation of PKM2

PKM2 is suggested to be required for mTOR-mediated aerobic glycolysis. Expression of *PKM2* correlates with mTOR activation and is sensitive to mTOR inhibition (Iqbal and Bamezai 2012). Consistently, increased PTEN expression inhibits PKM2 expression (Garcia-Cao et al. 2012). PKM2 knockdown in *Tsc2*$^{-/-}$ MEFs is enough to decrease

glucose consumption and lactate production (Sun *et al.* 2011). mTOR signalling controls PKM2 expression through its regulation of HIF1 and MYC (Figure 1.8)(Sun et al. 2011). The PKM gene contains a HIF Response Element (HRE), making it a target of HIF1 dependent transcription (Sun et al. 2011). In addition, MYC has been recognised to promote specific mRNA splicing of PKM2. In their pre-mRNA, PKM1 contains exon 9 and excludes exon 10, whereas PKM2 includes exon 10 and excludes exon 9 (Figure 1.7). MYC enhances the splicing and expression of PKM2 by increasing the expression of heterogenous nuclear ribonucleoproteins (hnRNPs). These proteins bind exon 9 to prevent its inclusion into the mRNA, leading to exon 10 inclusion to favour PKM2 expression (Figure 1.8)(David *et al.* 2010). MYC co-operates with HIF1 dependent transcription of PKM for PKM2 expression (Sun et al. 2011). Interestingly, PKM2 has been observed to increase mTOR signalling through a positive feedback loop in RCC and breast cancer cell lines. This is achieved by the PKM2 dependent phosphorylation and inhibition of Akt substrate 1 (AKT1S1), an inhibitor of mTOR (He *et al.* 2016). PKM2 can also be phosphorylated by ERK1/2 for its nuclear translocation to act as a cofactor for *c-myc* expression (Yang *et al.* 2012).

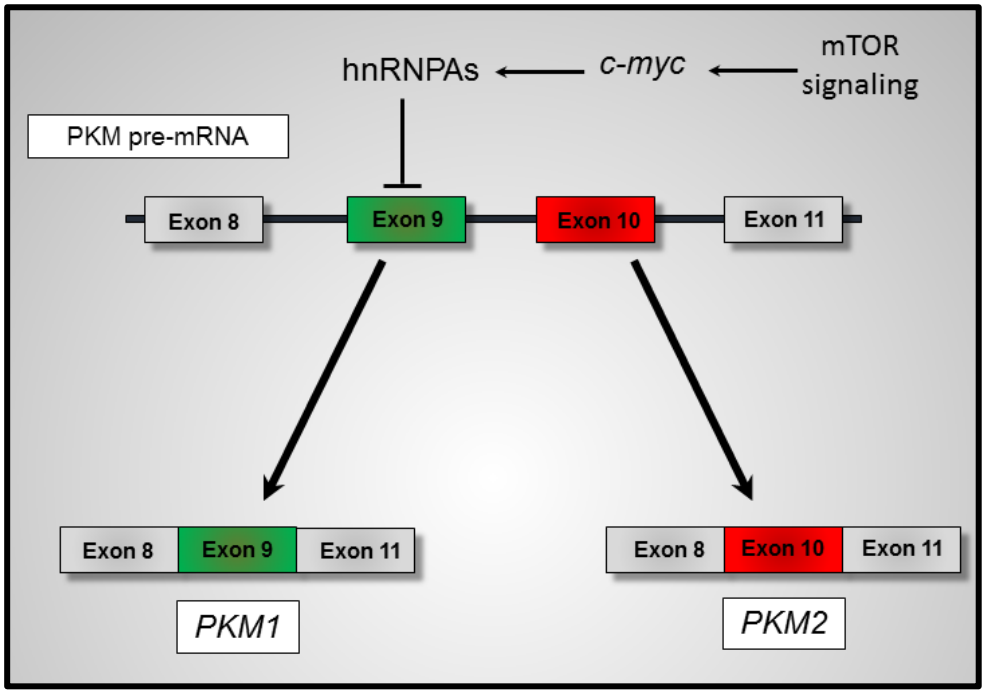

Figure 1.8 Alternative splicing of *PKM1* and *PKM2* controlled by mTOR signalling. The *PKM* gene contains 11 exons and produces 2 protein products by alternative splicing. Alternative splicing can be finely controlled by *c-myc* expression. *PKM* pre-mRNA is produced through HIF1α dependent transcription. *c-myc* expression, partly controlled by mTOR signalling, upregulates hnRNPs which can bind and inhibit exon 9, causing its exclusion from the mRNA, and expression of *PKM2*.

1.4 Animal models of TSC

TSC animal models have been developed to understand mechanisms underlying disease development and to test various treatment strategies for TSC-associated tumours. Models derived from *Drosophilia*, rat and mouse were fundamental in these investigations and are described below.

1.4.1 Use of *Drosophila* in understanding functions of TSC genes.

Drosophila was a powerful model used to help understand the function of TSC genes as tumour suppressors. *Tsc1* and *Tsc2* orthologue genes were first reported in *Drosophila* and further studies identified mutations in either *Tsc2* or *Tsc1* leading to increases in cell size (Ito and Rubin 1999; Tapon *et al.* 2001). Genetic studies of *Tsc1* and *Tsc2* in *Drosophila* led to the identification of a TSC1-TSC2 complex which interacted with Rheb GTPase to regulate TOR signalling (Zhang *et al.* 2000; Gao *et al.* 2002; Garami *et al.* 2003; Zhang et al. 2003b). S6K activation was found in Drosophila larvae and eggs deficient of the TSC complex (Radimerski *et al.* 2002). Other studies using *Drosophila* include the identification of TORC1 as an inhibitor of autophagy (Scott *et al.* 2007), the relationship between the TSC complex and Scylla/Charbdis (Drosophila homologue of REDD/RTP801) in response to hypoxic conditions (Reiling and Hafen 2004) and the discovery of Rag GTPases for amino-acid mediated TORC1 activation (Sancak et al. 2008).

1.4.2 Rat model of TSC-associated tumours: the Eker Rat

The Eker rat was first described in 1954 (Eker 1954), and was used as an animal model for hereditary RCC (Eker *et al.* 1981; Everitt *et al.* 1992).The Eker rat was predisposed to develop kidney lesions such as cysts, cyst with papillary projections and solid carcinomas. These lesions were observed as early as 2 months of age. By 12 months of age, these lesions exhibit complete penetrance in Eker rats. Kidney lesions mostly developed in the outer cortex (Eker et al. 1981). Further analysis found that the majority of cystic and solid carcinomas developed from collecting duct and proximal tubular epithelial cells, respectively (Wolf *et al.* 1995). Eker rats also develop brain hamartomas similar to human TSC patients (Yeung *et al.* 1997). Other primary tumours observed in Eker rats include pituitary adenomas (55% at 2 years old), uterine leiomyomas and

leiomyosarcomas (47-62% 14 months-2 years old) and splenic haemangiomas (23-68% 14 months-2 years old) (Hino *et al.* 1994).

Genetic linkage analysis was performed years later after the identification of the Eker rat to determine the disease-causing genes. The gene was localised to rat chromosome 10p12, a region homologue to human chromosome 16p13.3, encoding TSC2 (Yeung *et al.* 1993; Hino et al. 1994). At this region, a mutation occurred resulting from the insertion of a 6.3 kb intracisternal A particle (IAP) on one allele (*Tsc2*$^{ek/+}$)(Kobayashi *et al.* 1995). This insertion resulted in a disruption of codon 1272 in the rat *Tsc2* gene. This leads to a disrupted transcript and approximately a 30% deletion of the 5' end, containing the TSC2 catalytic domain (Yeung *et al.* 1994).To confirm *Tsc2* as the disease causing gene, a wild-type *Tsc2* gene was introduced into the Eker rat. The introduced wild-type *Tsc2* gene was found to suppress the Eker rat phenotype efficiently (Orimoto *et al.* 1996; Kobayashi *et al.* 1997a).

1.4.3 Mouse models of TSC-associated tumours

Mouse models of TSC have been developed. They can be classified as conventional and conditional models. These models are particularly useful for investigating mechanisms underlying development of TSC-associated tumours and for testing agents and strategies of prevention and therapy of these tumours.

1.4.3.1 Conventional mouse models of TSC

The first *Tsc2* mouse models were developed in 1999 by 2 independent groups (Kobayashi *et al.* 1999; Onda *et al.* 1999). A gene targeting construct was created by inserting a neomycin cassette into exon 2 of a *Tsc2* genomic DNA clone. The DNA was electroporated into J1 embryonic stem cells. Clones that successfully underwent homologous recombination of the gene construct were selected and injected into a blastocyst and transferred to pseudopregnant female mice. Offspring were then interbred to produce *Tsc2* null homozygotes. *Tsc2*$^{-/-}$ mice were embryonically lethal and no viable offspring were observed past E12.5. *In utero* death was caused by a severely hypoplastic liver, delay in development, circulatory failure and delay in neural tube closure. The survival of *Tsc2*$^{+/-}$ mice was normal and similar to *Tsc2*$^{+/+}$ littermates. The development of benign renal tumours in *Tsc2*$^{+/-}$ mice, however, began during the first year of life, with full penetrance at 18 months of age (Figure 1.9C and D). These renal tumours included

cysts, papillary adenomas and solid carcinomas. Liver haemangiomas were observed in 50% of *Tsc2*$^{+/-}$ mice at around 18 months (Figure 1.9E). Lung tumours were observed in 33% (Figure 1.9F) and angiosarcomas in 7% at 18 months (Figure 1.9A and B)(Onda et al. 1999). The development of renal cell carcinoma was also observed in 5-10% of heterozygotes at 18 months of age.

Mouse models by constitutively deleting *Tsc1* alleles in germline were also developed using a similar approach to that used for generating *Tsc2* mouse models. *Tsc1* models have a less severe phenotype than *Tsc2* models (Kobayashi *et al.* 2001; Kwiatkowski *et al.* 2002; Wilson et al. 2005). As with *Tsc2*$^{-/-}$ mice, *Tsc1*$^{-/-}$ mice were embryonically lethal but viable cells survive up to a day later than *Tsc2*$^{-/-}$ mice (Kwiatkowski et al. 2002). Moreover, the number of viable cells that survived between E11 and E12.5 was greater in *Tsc1*$^{-/-}$ than *Tsc2*$^{-/-}$ mice (30% vs 13%) (Kobayashi et al. 2001). Death of embryos was due to delay in development and delay in neural closure (Kobayashi et al. 2001; Kwiatkowski et al. 2002; Wilson et al. 2005). Tumours found in *Tsc1*$^{+/-}$ mice include renal cystadenomas and liver haemangiomas, similar to *Tsc2*$^{+/-}$. However, the incidence and progression of renal tumours was higher in *Tsc2*$^{+/-}$ mice (Kobayashi et al. 2001; Kwiatkowski et al. 2002). A study by Wilson et al demonstrated strain-dependent disease severity of *Tsc1* mouse models. There was an increase in mortality among *Tsc1*$^{+/-}$ mice (27%) on a C57BL/6 background compared to other backgrounds. Forty four percent of C3H mice developed macroscopically visible renal lesions while only 8% in C57BL/6 and 13% in BALB/c mice had macroscopically visible renal lesions at 3-6 months of age. All backgrounds had visible microscopic lesions at 15-18 months of age. Kobayashi et al (2001) failed to observe any macroscopic visible lesions in their *Tsc1* model by 9-12 months. Renal cell carcinoma was also strain dependant in *Tsc1*$^{+/-}$ mice, with 80% of BALB/c mice developing RCC by 18 months and C3H and C57BL/6 rarely developing RCC by 18 months (Wilson et al. 2005).

Similar to observations in human TSC-associated tumours, a second (somatic) hit of *Tsc1* or *Tsc2* was observed in tumours of *Tsc1*$^{+/-}$ or *Tsc2*$^{+/-}$ mice. About 24% of renal tumours and 50% of liver haemamgiomas were identified with LOH in *Tsc2*$^{+/-}$ mice. These observations suggested that alternative mechanisms of *Tsc2* inactivation may be common in these tumours (Onda *et a*l. 1999). Loss of the wild-type allele was detected in 42% (5/12) renal lesions, two out of five hepatic haemangiomas, one out of two uterine lesions and one out of one lung lesion (a kidney metastasis) in *Tsc1*$^{+/-}$ mice (Wilson et al. 2005). Oncogenic pathways, particularly mTORC1 and mTORC2 signalling, are

aberrantly activated in renal tumours including cysts, papillary adenomas and solid carcinomas in *Tsc1*$^{+/-}$ or *Tsc2*$^{+/-}$ mice.

1.4.3.2 Conditional mouse models of TSC

The Cre/loxP system has been used to generate mouse models through specifically deleting *Tsc1* or *Tsc2* in particular tissues or cell types (Stricklett *et al.* 1999; Meikle *et al.* 2005; Reith *et al.* 2013) Tissue- and age-specific deletion of *Tsc1* or *Tsc2* can be achieved through spatial and temporal control by tissue-specific promotor-driven and tetracycline- or tamoxifen-inducible expression of Cre (Traykova-Brauch *et al.* 2008; Rao and Monks 2009; Espana-Agusti *et al.* 2016). This method is useful to produce heterozygous or homozygous deletions in specific tissues to avoid embryonic lethality. Deleting a gene of interest in a particular tissue could also minimise or reduce adverse effects.

Tsc1$^{lox/lox}$ mice were produced by homologues recombination (Kwiatkowski et al. 2002). A targeting vector containing a *loxp*-flanked neomycin resistance-thymidine kinase gene cassette preceding exon 17 and a third *loxp* site downstream of exon 18 was produced and electroporated into embryonic stem cells from mice on a 129/S4/Sv background. Correctly targeted cells were collected and injected into C57BL/6J blastocysts. Mice were backcrossed for germline transfer in multiple backgrounds and the resulting heterozygotes were bred to produce homozygotes on a mixed background. *Tsc2*$^{lox/lox}$ mice were generated by a similar procedure, but *loxp* sites flanked exon 3 of the *Tsc2* gene (Pollizzi *et al.* 2009a). Exon 3 encodes a strip of amino acids near the N-terminus of the protein. Mice homozygous for *Tsc1*$^{lox/lox}$ or *Tsc2*$^{lox/lox}$ were viable, fertile and normal in size. Breeding these mice with mice containing tissue-specific Cre recombinase and inducible systems can result in deletions of *floxed* exons described in above models in specific tissues at specific ages and associated disease phenotypes can be assessed.

Tsc1$^{lox/lox}$ or *Tsc2*$^{lox/lox}$ mice have been used to investigate gene roles in some of the most affected tissues in TSC patients. These include the kidneys, skin, heart and brain (Uhlmann *et al.* 2002; Meikle et al. 2005; Ehninger *et al.* 2008; Tsai *et al.* 2012; Prabhakar *et al.* 2013; Reith et al. 2013; Leech *et al.* 2015; Rozas *et al.* 2015). Conditional tissue specific deletions leading to conditions other than TSC-associated tumourigenesis will not be discussed here. A conditional knockout allele of *Tsc1* with modified myosin light chain 2v promotor *(MLC2v)-creKI* in ventricular myocytes presented phenotypes resembling TSC-associated rhabdomyomas. These mice showed no difference in

development compared to *Tsc1*$^{flox/flox}$ mice at 3 months but survived no longer than 8 months. No abnormalities in the kidneys or liver were observed, a typical phenotype of *Tsc1*$^{+/-}$ mice (Meikle et al. 2005). Conditional deletion of *Tsc1* or *Tsc2* was also reported in Purkinje cells of the brain in two separate studies, leading to an increased repetitive behaviours and other behavioural defects associated Autism Spectrum Disorder (ASD) but no tumour-related phenotypes (Tsai et al. 2012; Reith et al. 2013). A TSC-associated brain lesion model was reported after injecting an adeno-associated virus (AAV) combined with Cre-recombinase into the cerebral ventricles of *Tsc1*$^{lox/lox}$ mice. These mice developed brain lesions similiar to cortical tubers, SENs, leading to hydrocephalus (Prabhakar et al. 2013). More recently, a conditional knockout allele of *Tsc1* with a *Darpp32-Cre* allele resulted in accelerated formation of kidney cystadenomas and paw angiosacromas. Full penetrance in all mice was seen within 6 weeks. Paw angiosacromas are easily observable, suggesting a non-invasive technique for analysing drug efficacy against TSC-related tumours (Leech et al. 2015).

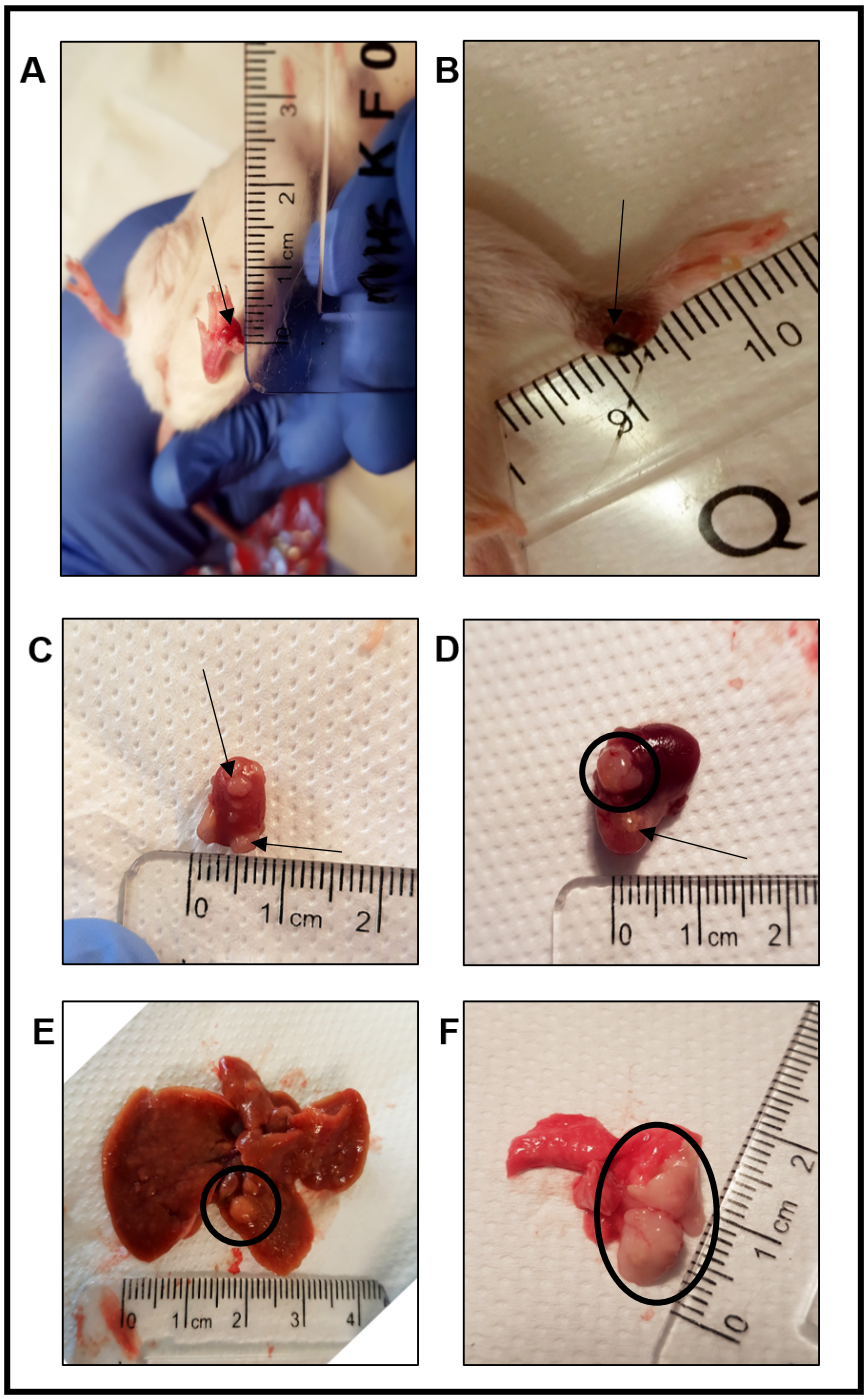

Figure 1.9 Macroscopic tumour development in *Tsc2*$^{+/-}$ mice. Mice dissected at 18 months of age display tumours varying in location, size and aggressiveness. **(A and B)** External paw angiosacromas (arrows). **(C and D)** Renal tumours varying in size and location (Black arrows and circle). **(E)** Large liver tumour (within black circle) and rough surface of liver containing many little tumours. **(F)** TSC-associated lung tumour (pale colour; black circle)

1.5 Molecularly targeted tumour therapy

1.5.1 Targeting mTOR

Constitutive activation of the mTOR signalling pathway has been observed in many cancers and tumour syndromes including TSC. mTOR inhibitors have been developed and used to treat various types of cancer and TSC-associated tumours. These inhibitors include allosteric inhibitors rapamycin and its derivatives (Rapalogs), and ATP-competitive inhibitors, targeting the catalytic site of mTOR.

1.5.1.1 Rapamycin and rapalogs

Rapamycin is a macrolide produced by the soil bacterium *Streptomyces hygroscopicus.* This bacterium was first isolated from a soil sample collected on Easter island (Rapa Nui) in 1965. Rapamycin was later isolated from the bacterium in 1970s (Vezina *et al.* 1975). Rapamycin was discovered to have a wide range of anti-fungal, anti-tumour and immunosuppressive properties (Martel *et al.* 1977; Sehgal 1998). It is a potent allosteric inhibitor of mTORC1 by forming a gain-of-function complex with the intracellular FK506-binding protein (FKBP12). The complex directly binds the FRB domain of mTOR and inhibits mTOR (Li *et al.* 2014). The rapamycin-FKBP12 complex is generally unable to bind and inhibit mTORC2 but it shows evidence of mTORC2 inhibition after prolonged treatment (Sarbassov et al. 2006).

Rapamycin is an effective immunosuppressant and was approved in 1999 for the prevention of graft rejection in kidney transplants. It strongly suppresses interleukin-2 (IL-2) stimulated T-cell proliferation, which is required for prevention of allograft rejection. It was approved in 2002 as an anti-restenosis drug following balloon angioplasty due to its ability to inhibit the growth of vascular smooth muscle (Benjamin *et al.* 2011). As mTOR is a key driver of cell growth and proliferation in many cancers and tumour syndromes, rapamycin has been studied as an anti-cancer drug (Eng *et al.* 1984). Rapamycin acts as a cytostatic and can arrest cells in G1 phase of the cell cycle in pancreatic, breast and prostate cancer, amongst other cancer subtypes (Seufferlein and Rozengurt 1996; Grewe *et al.* 1999; Yu *et al.* 2001). However, due to its poor water solubility and stability, synthetic rapamycin analogues have been developed to improve its pharmacokinetic properties and efficacy. These include temsirolimus (CCI-779) (Rini

2008), everolimus (RAD001) (Gabardi and Baroletti 2008) and ridaforolimus (AP23573) (Mita *et al.* 2008). These rapalogs have been analysed in a variety of cancer cells *in vitro*, *in vivo* and, in some cases, in clinical trials (Wander *et al.* 2011).

1.5.1.1.1 Pre-clinical treatment with rapamycin and rapalogs in TSC-associated tumours

TSC-associated tumours have hyper-activation of mTORC1. Several pre-clinical studies have shown that rapamycin and rapalogs are effective for treating TSC-associated tumours in rat and mouse. Two month rapamycin treatment resulted in the significant reduction in tumour size without any evidence of non-tumour toxicity, as seen by serial non-invasive ultrasound imaging in the Eker rat. However, further analysis confirmed drug resistance in a small proportion of tumours after prolonged therapy (Kenerson *et al.* 2005). The rapalog CCI-779 reduced the severity of kidney cystadenomas (62-92% reduction in tumour number) without any significant toxicity in *Tsc2*$^{+/-}$ mice (Lee *et al.* 2005). The rapalog everolimus was highly effective for renal cystadenomas (up to 99% reduction) in *Tsc2*$^{+/-}$ mice (Guo and Kwiatkowski 2013). Everolimus suppressed cell proliferation, as indicated by decreased number of tumour cells positive for Ki67. However, tumour growth reversal occurred by 8 weeks after treatment stopped. This provided further evidence of the cytostatic effect of rapalogs (Pollizzi *et al.* 2009b). Topical rapamycin also reduces the growth of subcutaneous TSC-associated tumours in nude mice (Rauktys *et al.* 2008). Long term rapamycin has been successful at blocking the development of renal tumours in *Tsc2*$^{+/-}$ mice (Yang et al. 2015).

1.5.1.1.2 Clinical trials

Clinical trials have been performed to evaluate the efficacy of rapamycin and its raplogs for TSC-associated tumours in patients (Franz *et al.* 2006; Bissler *et al.* 2008; Tabernero *et al.* 2008; Krueger *et al.* 2013; Franz and Capal 2016). A 24-month, non-randomised open-label trial assessed the effect of sirolimus on angiomyolipomas and lymphangioleiomyomatosis in TSC patients. In this study, the volume of angiomyolipomas regressed up to 50% after 1-year treatment but tumour regrowth began upon treatment cessation. Patients with LAM had an increase in lung function, as seen by increases in lung capacity and FEV1, after 1 year treatment but improvements also began to reverse after treatment stopped (Bissler et al. 2008). Similar results have

been reported in a study to treat TSC-associated angiomyolipomas using everolimus (42% tumour response rate but regrowth after treatment stopped) (Bissler *et al.* 2013). Furthermore, everolimus has shown clinical efficacy in TSC-associated renal carcinoma (Kim *et al.* 2014). Further clinical studies have been carried out to test the efficacy of everolimus on SEGAs in patients with TSC. Everolimus treatment caused both regression and/or stabilisation of SEGAs in TSC patients but interruption of treatment again resulted in regrowth of SEGAs (Franz et al. 2006). These studies have led to Food and Drug Administration (FDA) approval of everolimus for the treatment of TSC-associated renal AML, SEGAs and TSC-associated partial-onset seizures (Hasskarl 2018).

1.5.1.1.3 Mechanisms of rapamycin/rapalogs limited activity

Rapamycin/rapalogs have shown promise in treating TSC-associated tumours and RCC. However, as mentioned above, tumours can regrow upon withdrawal of rapamycin/rapalogs and drug resistance can develop in treating TSC-associated tumours (Benjamin et al. 2011).These limited activities of rapamycin/rapalogs possibly involve different mechanisms. First, rapamycin/rapalogs are cytostatic rather than cytotoxic and thus, drug withdrawal is likely to cause tumour growth (Franz et al. 2006; Bissler et al. 2008; Pollizzi et al. 2009b). Second, rapamycin/rapalogs do not normally inhibit mTORC2, promoting tumour cell survival through Akt signalling (O'Reilly et al. 2006; Tabernero et al. 2008). Third, rapamycin/rapalogs are only partial inhibitors of 4E-BP1 (Feldman *et al.* 2009; Thoreen *et al.* 2009). Long-term treatment has shown a gradual increase in phosphorylated 4E-BP1 and development of resistance (Benjamin, 2011). Fourth, inhibition of mTORC1 by rapamycin/rapalogs leads to suppression of negative feedback loops, resulting in activation of PI3K/Akt signaling (Harrington *et al.* 2004). Finally, mutations of mTOR or FKBP12 may prevent rapamycin/rapalog binding to mTOR and mutations in other proteins associated with the mTOR pathway may confer resistance (Huang and Houghton 2001).

To overcome its limited efficacy as a monotherapy, combination of rapamycin/rapalogs with other agents has been tested for treating TSC-associated tumours (Rao *et al.* 2005; Pollizzi et al. 2009b; Cirstea *et al.* 2010; Yang *et al.* 2017). Everolimus has been used in combination with the vascular endothelial growth factor receptor (VEGFR) inhibitor, sorafenib, for treating renal tumours in a *Tsc2*$^{+/-}$ mouse model. Combinational treatment

signifiifanctly reduced tumour number and size of solid renal tumours, whereas everolimus and sorafenib alone did not (Yang et al. 2017). The Pi3K/mTOR inhibitor, NVP-BEZ235 has also been used in combination with rapamycin in *Tsc2*$^{+/-}$ mice, and shows to be as effective at suppressing tumour development, but does not completey elminate tumour burden in these mice. Furthermore, recovery of tumour growth was observed when treatment was discontinued (Pollizzi et al. 2009b). However, combination of rapamycin/rapalogs with other agents remains to be examined for treating TSC-associated in clinical settings.

1.5.1.2 ATP-competitive inhibitors of mTOR

ATP-competitive inhibitors of mTOR are small synthetic molecules developed that target the kinase activity of mTOR. They bind the ATP-binding site of mTOR and thus block the phosphorylation and signalling of both mTORC1 and mTORC2. These inhibitors often overlap with PI3K inhibition due to the similarity between the kinase domains of mTOR and PI3Ks. However, the efforts of developing these mTOR inhibitors are focused on improving their selectivity to target mTOR. ATP-competitive inhibitors of mTOR are expected to overcome the limitations linked with rapamycin and have consistently shown greater anti-proliferative effects in pre-clinical studies (Feldman et al. 2009; Thoreen et al. 2009; Yu *et al.* 2009). Examples of ATP-competitive inhibitors of mTOR are shown in Table 1.2.

ATP-competitive inhibitors have exhibited effective IC_{50} inhibition of mTOR, inhibition of both mTORC1 and mTORC2, and anti-proliferative efficacy. Compared to rapamycin, ATP-competitive inhibitors are more efficient at inhibiting 4E-BP1 and have greater anti-tumour efficacy in a wide range of cancer cells *in vitro* and xenograft models *in vivo* (Schenone *et al.* 2011). However, the suppression of feedback loops have been reported to affect the efficiency of ATP-competitive inhibitors of mTOR. The increased signalling in RTK-PI3K-PDK1 through mTOR inhibition (as discuss previously) can enhance the phosphorylation of Akt at T308, which can be sufficient enough to accelerate tumour cell survival (O'Reilly et al. 2006; Peterson et al. 2009). Further investigation is warranted to further assess the role of feedback loops during treatment with these inhibitors. The development of ATP-competitive inhibitors (3rd generation inhibitors) that improve the dual inhibition of mTOR and PI3K, are currently under development and may help overcome some of these problems (Rodrik-Outmezguine *et al.* 2016).

AZD-2014 is a novel ATP-competitive inhibitor of mTOR, developed in 2013 from the optimisation of AZD-8055 (Pike *et al.* 2013). It is a potent inhibitor of mTOR (IC_{50} 0.0028uM) and is highly selective to the PIKK family. AZD2014 has been investigated in pre-clinical studies to evaluate its anti-tumour efficacy. AZD2014 significantly suppresses both mTORC1 and mTORC2 signalling and inhibited proliferation and growth of cancer cells in a variety of cultured cancer cell lines and various tumours of xenograft models (Huo *et al.* 2014; Kahn *et al.* 2014; Guichard *et al.* 2015; Leung *et al.* 2015; Zheng *et al.* 2015; Li and Cui 2016; Yu *et al.* 2016). AZD2014 also appeared to have superior anti-tumour efficacy to rapalogs in these pre-clincal investigations (Zheng et al. 2015). TSC-associated tumours consistently show aberrant activation of mTORC1 and mTORC2 and can have only partial response to rapalogs. It would be worthwhile to test whether ATP-competitive inhibitors of mTOR, particularly AZD2014, can improve therapy for these tumours.

Table 1.2 ATP-competitive inhibitors of mTOR under investigation

Compound name	Developer	Targets	Clinical trial phase	Tumour type under investigation	Notable References
AZD8055	AstraZeneca	mTORC1/2	Discontinued	Advanced solid tumours, lymphoma	Chresta *et al.* 2010
OSI027	OSI Pharma	mTORC1/2	Discontinued	Advanced solid tumours, lymphoma	Schenone *et al.* 2011
GSK2126458	GlaxoSmithKline	mTORC1/2	Phase I	Advanced solid tumours, lymphoma	Knight *et al.* 2010; Narov *et al.* 2017
AZD2014	AstraZeneca	mTORC1/2	Phase I/II	Advanced solid tumours, breast cancer, renal cell carcinoma	Pike *et al.* 2013; Basu *et al.* 2015; Liao *et al.* 2014
CC-223	Celgene	mTORC1/2	Phase I/II	Breast cancer, glioblastoma, hematologic malignancies, liver cancer, NSCLC, neuroendocrine tumours	Varga *et al.* 2013; Shih *et al.* 2012
INK128	Intellikine	mTORC1/2	Phase I/II	Advanced solid tumours, hematologic malignancies	Jessen *et al.* 2009
Ku-0063794	AstraZeneca	mTORC1/2	Not active		Garcia-Martinez et al. 2009
Torin2	Dana-Farber Cancer Institute and Whitehead Institute	mTORC1/2	Not active		Liu *et al.* 2013

1.5.2 Targeting tumour metabolism

The reprogramming of cell metabolism within tumours provides an alternative opportunity for therapy of mTOR-driven tumours. Aberrant activation of mTOR drives the expression of genes associated with glycolysis and glutaminolysis that can be utilised by targeted therapy. This strategy may be used to specifically kill tumour cells that are addicted to glucose and glutamine (Altman et al. 2016; Hay 2016; Martinez-Outschoorn *et al.* 2017).

1.5.2.1 Inhibition of glycolysis

Aerobic glycolysis, (Warburg effect) is a fundamental characteristic of tumour cells (Pelicano *et al.* 2006). The growth and proliferative advantage attained through increased glycolytic flux renders these cells addicted to glucose. Many different strategies for utilising and targeting the increased flux through glycolysis have been investigated for anti-tumour therapy. Aerobic glycolysis can be inhibited by targeting GLUTs and glycolytic enzymes as listed in Table 1.3 (Nagarajan et al. 2016; Martinez-Outschoorn et al. 2017). Although glucose metabolism is increased in tumour cells, the same enzymes and transporters are also utilised in normal cells. Inhibition of glycolysis therefore may result in adverse effects on these normal cells. However, identifying those transporters and enzymes that are preferentially used by cancer cells may provide potential therapeutic targets.

3-Bromopyruvate (3-BrPA) is an alkylating agent and a structural analog of pyruvate. (Lis *et al.* 2016). It is highly effective at killing cells with a high ATP demand through its potent inhibition of tumour-specific HKII (Sun *et al.* 2015). Other 3-BrPA targets include glycolytic enzyme GAPDH and the mitochondrial enzyme succinate dehydrogenase. 3-BrPA anti-tumour efficacy has been investigated in a wide range of *in vitro* and *in vivo* cancer models (Ko *et al.* 2001; Ko *et al.* 2004; El Sayed *et al.* 2012; Sun et al. 2015; Lis et al. 2016). 3-BrPA anticancer activity through ATP depletion has been demonstrated in prostate, RCC, gastric and multiple myeloma cell lines (Chen *et al.* 2009; Majkowska-Skrobek *et al.* 2014; Nilsson *et al.* 2015; Valenti *et al.* 2015; Xian *et al.* 2015). *In vivo* anti-tumour efficacy of 3-BrPA has also been reported in animal models as a single therapy or in combination with rapamycin (Ko et al. 2004; Zhang *et al.* 2015).

Activation of mTORC1 causes addiction of *Tsc1 or Tsc2 null* MEFs to glucose. Targeting glycolysis in TSC-tumours, therefore, may provide an alternative approach for treatment other than mTOR inhibitors. Glycolytic inhibition with 2-deoxyglucose (2-DG) has previously shown significant decrease in tumour growth in *Tsc2* null xenograft models, suggesting glucose deprivation as an effective treatment for mTOR-driven tumours (Jiang *et al.* 2011). 3-BrPA represents an alternative inhibitor of glycolysis due to its reported low toxicity, to be tested for TSC-associated tumours.

Table 1.3 Strategies targeting glycolysis for cancer treatment

Compound name	Metabolic target	Clinical trial phase	Tumour type under investigation	Notable References
WZB117	GLUT1	Pre-clinical	Lung cancer and breast cancer	Shibuya *et al.* 2015
Phloretin	GLUT1	Pre-clinical	Colon cancer and leukemia	Malavolta *et al*, 2018
Ritonavir	GLUT4	Not active	Multiple myeloma	Mishra *et al*. 2015
2-Deoxyglucose	Hexokinase II	Phase I/II/III	Leukemia, cervical cancer, hepatocarcinoma, breast cancer, small lung cancer, lymphoma, and prostate cancer	Maschek *et al.* 2004; Dwarakanath *et al.* 2009
3-Bromopyruvate	Hexokinase II	Pre-clinical	Leukemia, multiple myeloma, and colon cancer	Ko *et al*, 2004; Zhang *et al*. 2015; Buijs *et al*, 2009
Lonidamine	Hexokinase II	Discontinued	Leukemia, lymphoma and breast cancer	Papaldo *et al.* 2003
TLN-232	PKM2	Pre-clinical and Phase II	Metastatic melanoma and RCC	Vander- Heiden *et al*. 2010
Dichloroacetate (DCA)	PDK1	Pre-clinical	Colon cancer, lung cancer, squamous cell carcinoma, and prostate cancer	Stacpoole. 2017
Oxamate	LDHA	Pre-clinical	Breast cancer	Thornburg *et al.* 2008

1.5.2.2 Inhibition of glutaminolysis

Tumour cells are dependent on glutamine for survival (Kovacevic and McGivan 1983; DeBerardinis et al. 2007). Glutaminolysis provides an alternate route to refuel the depleted Krebs cycle from aerobic glycolysis, via anaplerosis, for the synthesis of important macromolecules for tumour growth and proliferation. Many different classes of compounds have been developed to target glutaminolysis for anti-tumour therapy, some of which are listed in Table 1.4 (Hensley *et al.* 2013; Altman et al. 2016). Most of these compounds are still in the early stages of research or have been limited by their adverse effects. GLS inhibitors such as CB-839, however, have shown promise in early preclinical trials of cancer and have entered clinical trials (Gross et al. 2014; Guo *et al.* 2016).

CB-839 is an allosteric, highly potent and selective inhibitor of GLS. It has been investigated in a variety of different cancer cell lines and xenografts models for its anti-tumour efficacy. CB-839 has displayed impressive anti-proliferative effects in pre-clinical trials as a single agent or in combination with other chemotherapeutic agent in solid and haematological cancer cell lines, with minimal toxicity (Gross et al. 2014; Jacque *et al.* 2015; Tanaka *et al.* 2015; Guo et al. 2016; Lampa *et al.* 2017). CB-839 has also shown a substantial reduction in tumour growth in animal models of breast cancer, lung cancer and RCC (Gross et al. 2014; Momcilovic *et al.* 2017).

Activation of mTORC1 is associated with glutamine addiction (Choo *et al.* 2010) and increased glutaminolysis in *Tsc2* deficient MEFs (Csibi et al. 2013). However, further investigation is necessary to determine whether *TSC* null tumours also have increased glutamine uptake and glutaminolysis *in vivo*. Blocking of glutamine anaplerosis in combination with glycolytic inhibition causes significant cell death in $Tsc2^{-/-}$ but not $Tsc2^{+/+}$ MEF cells (Csibi et al. 2013). However, it remains to be examined whether inhibition of glutaminolysis in combination with glycolysis inhibition, can potently induce cell death in TSC-associated tumours *in vivo.*

Table 1.4 Strategies targeting glutaminolysis for cancer treatment

Compound name	Metabolic target	Clinical trial phase	Tumour type under investigation	Notable References
Acivicin	Glutamine mimic	Phase II (Discontinued)	Many cancers and high-grade astrocytomas	Eisenhauer *et al.* 1987; Maroun *et al.* 1986
BPTES	GLS Inhibitor	Pre-clinical	Pancreatic and ovarian cancers	Robinson *et al.* 2007; Shukla *et al.* 2012; Hartwick *et al.* 2012
CB-839	GLS inhibitor	Phase I/II	Advanced solid tumours and haematological cancers	Gross *et al.* 2014; Momcliovic *et al.* 2017
968	GLS inhibitor	Pre-clinical	Lung cancer	Lukey *et al.* 2014; Han *et al.* 2017
Benzylserine	SLC1A5 inhibitor	Pre-clinical	Multiple myeloma	Grewer *et al.* 2004
EGCG	GDH inhibitor	Phase I/II/III	Advanced solid tumours	Li *et al.* 2006 Shankar *et al.* 2013; Maruyama *et al.* 2014 Schramm 2013
Aminooxyacetate	Aminotransferase inhibitor	Approved for tinnitus	Breast cancer and neuroblastomas	Thornburg *et al.* 2008; Wise et al. 2008
L-Asparaginase	Glutamine depletion	Approved for ALL;	Acute lymphoid leukemia	Oettgen *et al.* 1967; Willems *et al.* 2013

1.6 Aims

Rapamycin and rapalogs are currently used for treating TSC-associated tumours. However, partial tumour response to rapamycin/rapalogs, development of drug resistance, and tumour regrowth upon drug withdrawal warrants new therapeutic strategies to treat TSC-associated tumours. These strategies could also be translated into other cancers and tumours with hyperactivated mTOR signalling. In this project, both mTOR and cellular metabolism were targeted with therapeutic agents to assess their efficacy on renal tumours in *Tsc2*$^{+/-}$ mice. The potential roles of *Pkm2* in the tumourigenesis of the kidneys in these mice was also examined.

The aims of this project are:

- To compare the anti-tumour efficacy of the ATP-competitive dual inhibitor of mTORC1 and mTORC2, AZD2014, with that of rapamycin for the treatment of renal tumours in *Tsc2*$^{+/-}$ mice. AZD2014 has previously demonstrated to be superior to rapamycin in pre-clinical studies for treating renal cell carcinoma and, therefore, is expected to be better than rapamycin for treating TSC-associated renal tumours. This project focused on comparison of AZD2014 and rapamycin for their anti-tumour efficacy by estimation of tumour number and size, and molecular mechanisms of drug action by analysis of Western blot and Immunohistochemistry.
- To compare the anti-tumour efficacy of the dual inhibition of glycolysis and glutaminolysis with that of rapamycin for the treatment of renal tumours in *Tsc2*$^{+/-}$ mice. Inhibition of glycolysis or glutaminolysis has been tested widely for tumour therapy in *in vitro* and *in vivo* studies but results have not been very promising. Dual inhibition of glycolysis and glutaminolysis may be a better strategy for tumour therapy. However, this strategy has not been tested *in vivo,* although one *in vitro* study suggested dual inhibition of glycolysis and glutaminolysis could be effective for treating ovarian cancer cells. Therefore, this project was to test the anti-tumour efficacy of dual inhibition of glycolysis and glutaminolysis for renal tumours in *Tsc2*$^{+/-}$ mice in comparison with rapamycin by estimation of tumour number and size, and to analyse molecular mechanisms of drug action by analysis of Western blot and Immunohistochemistry.

- To investigate the effect of conditional deletion of *Pkm2* on tumourigenesis in the kidneys of *Tsc2*$^{+/-}$ mice. It is still a matter of debate whether *Pkm2* plays a role in tumourigenesis of different tumour types, and *Pkm2* was highly expressed in TSC-associated tumours. This project proposed to examine the possible contribution of *Pkm2* on tumourigenesis in the kidneys of *Tsc2*$^{+/-}$ mice by estimation of tumour number and size. The effect of *Pkm2* deletion on mTOR signalling was also to be analysed using Western blot and Immunohistochemistry.

2 CHAPTER TWO

Materials and Methods

2.1 Materials

2.1.1 Cell lines

Immortalised *TP53*$^{-/-}$*Tsc2*$^{+/+}$ and *TP53*$^{-/-}$*Tsc2*$^{-/-}$ MEFs were described previously (Zhang *et al.* 2003a). The Tsc2-KT12 and KT17 tumour cells were prepared from solid tumours of the kidneys in *Tsc2*$^{+/-}$ mice as described previously (Yang *et al.* 2013).

2.1.2 Animals

The *Tsc2*$^{+/-}$ mouse model was provided by Dr David J. Kwaitkowski (Onda et al. 1999). Wild type BALB/c mice were supplied by Charles River, UK. Genetically engineered mice B6;129S-*Pkm*$^{tm1.1Mgvh}$/J (C57BLK/6 background); Tg(tetO-cre)1Jaw/J (C57BL/6 background) and B6.Cg-Tg(Pax8-rtTA2S*M2)1Koes/J (C57BL/6 background) were purchased from Jackson Laboratories, Maine, USA.

2.1.3 Reagents, chemicals and enzymes

2.1.3.1 General laboratory reagents, chemicals and enzymes

β- Mercaptoethanol (Sigma, UK, cat no: M3148)

Agarose powder (Eurogentec, UK, cat no: EP-0010-05)

Bovine Serum Albumin (BSA) (Sigma, UK, cat no: A7906-50G)

Dimethyl sulfoxide (DMSO) (Sigma, UK, cat no: D8418)

Dithiothreitol (DTT) (Sigma, UK, cat no:43816-10mL)

ECL blocking agent (GE Healthcare, UK, cat no: RPN418)

Eosin (0.5%, aqueous) (Sigma, UK, cat no: HT110280)

Ethanol (Thermo Fisher Scientific, UK, cat no: E/06500F/17)

Ethidium bromide (Sigma, UK, cat no: E7637) Gel-loading dye (6x) and 100bp DNA ladder (New England Biolabs, UK, cat no: B7025)

Gill No 1 Haematoxylin (Sigma, UK, cat no: GHS132)

Glacial Acetic Acid (Sigma, UK, cat no: PHR1748)

Glycerol (Sigma, UK, cat no: G6279)

0.5 EDTA (Promega, UK, cat no: V423B)

ImmPACT™ NovaRED™ Peroxidase substrate kit (Vector laboratories, UK, cat no: SK-4800)

Isopentane (Fisher Scientific, UK, cat no: P/1030/17)

Isopropanol (Fisher Scientific, UK, cat no: P/7490/17)

Hydrochloric acid (HCL) (Sigma, UK, cat no: 320331)

Hydrogen peroxide (30%) (VWR, UK, cat no: 23615.261)

MagicMark XP western protein standards (Thermo Fisher Scientific, UK, cat no: LC5602)

Membrane blocking agent (GE Healthcare, UK, cat code: RPN2125)

Methanol (Thermo Fisher Scientific, UK, cat no: M/3900/17)

Methylated spirits (Fisher Scientific, UK, cat no: M/4450/17)

PCR Taq master mix (2x) (New England Biolabs, UK, cat no: M0270L)

Protein block (Abcam, UK, cat no: 64226)

Polyethylene glycol 400 (PEG-400) (Sigma, UK, cat no: 1546445)

Sodium chloride (Thermo Fisher Scientific, UK, cat no: S/3160/60)

Sodium Dodecyl Sulfate 10% (SDS) (Sigma, UK, cat no: 5030)

Trizma® Base (Sigma, UK, cat no: 154563)

Tris-HCl (pH 7.5) (Sigma, UK, cat no: 154563)

Tri-sodium citrate dihydrate (Thermo Fisher Scientific, UK, cat no: S/3320/60)

Tween-20 (Sigma, UK, cat no: P4780)

Tween-80 (Sigma, UK, cat no: P1754)

VectaMount Permenant Mounting Medium (Vector Laboratories, UK, cat no: H-5000)

Xylene (VWR, UK, cat no: 28975.360)

2.1.3.2 Cell culture chemicals reagents

Crystal violet (Sigma, UK, cat no: C0775-25G)

Dulbecco's Modified Eagle Medium (DMEM) (Invitrogen Life Technologies, UK, cat no: 41966-029)

Fetal Bovine Serum (FBS) 10% (Invitrogen Life Technologies, UK, cat no: 10270-106)

Minimum essential medium non-essential amino acids (MEM NEAAs) 100X (Invitrogen Life Technologies, UK, cat no: 11140-035)

Penicillin/Streptomycin (Pen/Strep) (Invitrogen Life Technologies, UK, cat no: 15140-122)

2.1.3.3 Chemical agents for treatment

3-Bromopyruvic acid (3-BrPA) (10g) (Sigma, UK, cat no: 16490-10G)

AZD-2014 (1g) (MedKoo Biosciences, USA, cat no: 204520)

CB-839 (8x230mL) (Calithera Biosciences, California, USA, Batch: 36220-80C).

Doxycycline (Sigma, UK , cat no: D9891-100G)

Rapamycin (1g) (LC Laboratories, USA, cat no: R-5000)

Vehicle solution (aq. 25% HPBCD/10mM Citrate/ pH2) (8x230mL) (Calithera Biosciences, California, USA, Batch: 36220-79V)

2.1.4 Buffers and solutions

50x TAE Buffer

For 1L: 242g Trizma® Base (MW=121.1) was dissolved in 600mL of ddH_20 then 100mL 0.5 M EDTA and 57.1mL Glacial Acetic Acid was added. Volume was brought to 1L with ddH_20.

1x TAE Buffer

For 1L: 20mL 50X TAE buffer was added to 980mL ddH_20

10x Tris Buffered Saline (TBS)

For 2L: 160g NaCL and 48.4g Trizma® Base were dissolved in 1500mL ddH_20. pH was adjusted to 7.6 with Hydrochloric acid (HCl) (approximately 30mL for 2L). Buffer was finally autoclaved for 20 minutes,

1x TBS-T

For 1L: 100mL 10X TBS was added to 900mL ddH_20 followed by 1mL Tween-80

10mM Sodium Citrate Buffer

For 1L: 2.94 g Tri-sodium citrate dihydrate was dissolved in dH_2O (pH adjusted to 6.0 with 1N HCl)

Tissue Lysis Buffer

For 50mL: 5mL 100mM Tris HCl (pH 8.5), 0.5mL EDTA, 1mL 10% SDS and 2mL 5M NaCl were mixed in a 50mL Falcon tube. Total volume was made up to 50mL with ddH_20. Five µL Proteinase K (Qiagen) was added to the lysis buffer before use at a ratio of 1:200.

TE Buffer

For 50mL: 500µL 10mM Tris-HCL and 200µL 0.5mM EDTA were mixed. Total volume was made up to 50mL with ddH_20.

1x MES SDS Running Buffer (SDS-PAGE)

For 1L: 950mL ddH_20 was added to 50mL 20x NuPAGE® MES SDS Running Buffer (Invitrogen Life Technologies)

1x Transfer Buffer

For 1L: 850mL ddH_20 and 100mL methanol were added to 50mL 20x NuPAGE Transfer (Invitrogen Life Technologies)

IHC stripping solution

For 200ml: 50g 5% SDS, 1mL 0.5% β- Mercaptoethanol and 10mL 50mM Tris HCL were mixed and made up to a total volume of 200mL with ddH_2O.

NuPAGE LDS buffer

0.5mL was provided by Invitrogen Life Technologies

ECL Advanced Western Blotting detection solutions

For 2mL: 1mL of Solution A was mixed with 1mL of solution B.

Formaldehyde Raymond Lamb tissue fixative (100%)

For 1L at 20%: 200mL formaldehyde was added to 800mL ddH_2O

2.1.5 PCR Primers

PCR Primers for *Pax8.rtTA*, *TetOCre*, *Pkm2* and *Tsc2* were synthesised by Eurogentec as shown in Table 2.1

Gene	Primer sequence		Annealing temperature (°C)	Amplicon size
Tsc2	Forward Reverse Reverse	CAAACCCACCTCCTCAAGCTTC AATGCGGCCTCAACAATCG AGACTGCCTTGGGAAAAGCG	56	WT: 86 Mutant: 105
*Pax8rtTA2 S*M2*	Forward Reverse	CCATGTCTAGACTGGACAAGA CTCCAGGCCACATATGATTAG	60	Transgene: 595 Control:
TetO-Cre	Forward Reverse Internal Positive Control Forward Internal Positive Control Reverse	GCGGTCTGGCAGTAAAAACTATC GTGAAACAGCATTGCTGTCACTT CTAGGCCACAGAATTGAAAGATCT GTAGGTGGAAATTCTAGCATCATCC	51.7	Transgene: 100 Control: 324
PKM2	Forward Reverse	CCTTCAGGAAGACAGCCAAG AGTGCTGCCTGGAATCCTCT	60	WT: 578 Mutant: 680

Table 2.1 Primer sequences and annealing temperatures used for PCR of genes

2.1.6 Antibodies

2.1.6.1 Primary antibodies

B-Actin (Cell Signalling, USA, cat no: 4970)

Phospho-S6 Ribosomal Protein (Ser235/236) (Cell Signalling, USA, cat no: 4858)

Phospho-Akt (Ser473) (Cell Signalling, USA, cat no: 3787)

Phospho-Akt (Thr450) (Cell Signalling, USA, cat no: 9267)

Phospho-Akt (Thr308) (Cell Signalling, USA, cat no: 2965)

Anti-PKC alpha (phospho T638) (Abcam, UK, cat no: ab32502)

PKC alpha (Phospho S657) (Santa Cruz, USA, cat no: sc-208)

Anti mTOR (phosphor S2481) (Abcam, UK, cat no: ab137133)

Phospho-p44/42 MAPK (Erk1/2) (Thr202/Tyr204) (Cell Signalling, USA, cat no: 4370)

RAF-1 (p-S259) (Abcam, UK, cat no: ab173539)

4E-BP1 (Cell Signalling, USA, cat no: 9644)

Phospho-4E-BP1 (Thr37/46) (Cell Signalling, USA, cat no: 2855)

Anti-phospho-FRAP1 (pSer2448) (Sigma, UK, cat no: SAB4300178-100UG)

Phospho-p70 S6 Kinase (Thr389) (Cell Signalling, USA, cat no: 9205)

Anti-phospho-MDM2 (pSer166) (Sigma, UK, cat no: SAB4503937-100UG)

Vimentin (Cell signalling, USA, cat no: 5741)

E-Cadherin (Cell signalling, USA, cat no: 3195)

Anti-Fibronectin (Abcam, UK, cat no: ab2413)

Anti-Glutaminase (Abcam, UK, cat no: ab156876)

Anti-Carbonic Anhydrase (Abcam, UK, cat no: ab184006)

Hexokinase II (Cell signalling, USA, cat no: 2867)

GAPDH (Cell signalling, USA, cat no: 2118)

Glutamate dehydrogenase (GDH) (Cell signalling, USA, cat no: 12793)

MCT1 (Insight Biotechnology, UK, cat no: C00668H)

Ki67 (Abcam, UK, cat no: 15580)

Active Caspase-3 (Abcam, UK, cat no: 2302)

2.1.6.2 Secondary antibodies

Secondary horseradish peroxidise-conjugated antibody against rabbit for western blotting was purchased from Cell Signalling Technology, USA, cat no: 7074. SignalStain® Boost IHC Detection Reagent (HRP, Rabbit) for IHC was supplied by Cell Signalling Technologies, USA, cat no: 8114.

2.1.7 Kits

All Prep DNA/RNA/Protein Mini kit was supplied by Qiagen, UK

2.1.8 Equipment

Thermal cycler for PCR was obtained from Bio-Rad, UK. TissueRuptor and TissueRuptor disposposable probes were purchased from Qiagen, UK. The Invitrogen NuPage Novex gel system was purchased from Invitrogen Life Sciences, UK. Cytomation wax pens were supplied by DAKO, UK.

2.1.9 Miscellaneous

PCR 0.2mL strips were bought from VWR, UK. Soft-Ject® 0.5mL insulin U-100 fixed needles (30G) for animal treatment were supplied by Henke Sass Wolf, Germany. 24 x 40mm coverslips for H&E and IHC were obtained by Thermo Fisher Scientific, UK. NuPAGE 4-12% Bis-Tris mini gels (12, 15 and 17 well) were ordered from Invitrogen Life Technologies, UK. Hybond ECL Nitrocellulose Membranes was provided by GE Healthcare, UK and 3MM Whatman filter paper was bought from Thermo Fisher Scientific, UK.

2.2 Methods

2.2.1 Cell culture and treatment

For MTT assay, $4x10^3$ cells per well were grown in a microtiter plate overnight in triplicate for each treatment group in DMEM containing 10% FBS, 50 units/ml penicillin and 50 µg/ml streptomycin at 37°C in a humidified 5% CO_2 incubator. Cells were then treated with DMSO, AZD2014 or rapamycin at designated concentrations for 48 hours and MTT assay was performed. For colony formation assay, 250 cells were plated in a 10cm dish in triplicate and grown overnight for each treatment group as for MTT assay. Cells were then treated for 48 hours with DMSO, AZD2014 or rapamycin at designated concentrations and left for additional 7 days in fresh medium without AZD2014 and rapamycin. Cell colonies stained with crystal violate were counted. For protein preparation, 10^5 cells were grown on one well of 6 well plates overnight in triplicate for

each treatment group in serum-free DMEM and treated for 24 hours with DMSO, AZD2014 or rapamycin at indicated concentrations in DMEM containing 10% FBS

2.2.2 Animal husbandry and breeding

All animal procedures were performed in accordance with the UK Home Office guidelines and approved by the Ethical Review Group of Cardiff University (PPL No. 30/3073; PIL No. I042529CA). Mice were kept under standard laboratory conditions in the JBIOS animal research facility, University Hospital Wales, Cardiff, in filter topped cages and provided with a standard rodent diet and de-chlorinated water. All cages were held in a 19-23°C, 55+/- 10% humidity room and provided with a 12-hour light/dark cycle (7am-7pm) each day. All litters were weaned 4 weeks after birth and males and females were transferred to separate cages. Identification of mice was performed by ear punches, which were collected for subsequent genotyping.

To test treatment efficacy, *Tsc2*$^{+/-}$ were backcrossed on the balb/c strain at least 10 times to produce *Tsc2*$^{+/-}$ balb/c mice and randomly allocated into different treatment groups with balanced sex, age and littermates. To test the roles of *Pkm2* in renal tumourigenesis, B6.Cg-Tg(Pax8-rtTA2S*M2)1Koes/J (Traykova-Brauch et al. 2008), B6;129S-*Pkm*$^{tm1.1Mgvh}$/J (Israelsen et al. 2013), Tg(tetO-cre)1Jaw/J (Gossen and Vujard 1992) and *Tsc2*$^{+/-}$ (Onda et al. 1999) mice were bred through multiple-rounds of breeding to produce *Pax8.rtTA+/Pkm2*$^{lox/lox}$*/TetO.Cre+/Tsc2*$^{+/-}$ mice. These mice are expected to induce the kidney-specific deletion of *Pkm2* after doxycycline treatment.

2.2.3 Genotyping

2.2.3.1 DNA extraction

Ear punches collected from mice were used for DNA extraction. These samples were placed into 1.5mL eppendorfs and stored in -20°C. For DNA extraction, 0.2mL of tissue lysis buffer plus proteinase K (see 2.1.4) was added to each eppendorf containing ear punch. Eppendorfs were incubated in a 55°C water bath overnight (16-18 hours). Following incubation, eppendorfs were allowed to cool for 5-10 minutes before adding 0.2mL isopropanol to each tube. Samples were mixed thoroughly and then centrifuged at 13,500rpm for 10 minutes at room temperature. The supernatant was discarded and

0.1mL 70% ethanol was added to each tube. Samples were centrifuged for a further 5 minutes at room temperature. Supernatant was removed carefully using a pipette and tubes were allowed to air-dry at room temperature for approximately 10 minutes. After drying, 100μL TE buffer was added to each sample and incubated in the 55°C water bath for 90 minutes. Following incubation, samples containing DNA were vortexed and centrifuged. DNA samples were used for PCR or stored at -20°C.

2.2.3.2 Polymerase chain reaction

The PCR reaction was set up in 0.2mL PCR tubes and each tube contained 9μL PCR reaction mixture and 1μL of the genomic DNA prepared from ear punches. The 9μL PCR reaction mixture contained 5μL Taq 2X Master mix 1μL primer mix and 3μL nuclease free water. Primers used for genotyping for specific genes are shown in Table 2.1.

PCR was performed using a Bio-Rad T100 thermal cycler. The PCR protocol for genotyping was as follows:

1. 95°C for 3 minutes
2. 94°C for 30 seconds
3. **X** °C for 30 seconds (For specific primer annealing temperature, see Table 2.1)
4. 72°C for 30 seconds
5. Repeat steps 2-4 34x
6. 72°C for 5 minutes
7. 12°C for ∞

PCR tubes were centrifuged for 5 seconds and immediately used for gel electrophoresis or stored at -20°C.

2.2.3.3 Agarose gel electrophoresis

Agarose gels were prepared using 1X TAE buffer and agarose powder. Three or 1.5% agarose gels were used for electrophoresis. Agarose powder was dissolved through heating in a microwave for approximately 2-minutes. Ethidium bromide (0.05μL/mL) was added and mixed before gel setting in a gel mould, to aid visualisation of DNA bands under UV light. Two μL of Gel loading dye (6X) was added to each PCR sample and mixed thoroughly. Gel was submerged in 1X TAE buffer and PCR samples were added

into separate gel wells, including a well for a 1Kb DNA fragment ladder. Gel electrophoresis was run at 100V for approximately 1 hour. PCR products were then visualised using a BioDoc-IT® Imaging System through its UV exposure and compared to the DNA fragment ladder to confirm DNA product size. Gel images were saved electronically and printed using a Digital UP-895MD Graphic Printer.

2.2.4 Animal treatment

Animals were treated with therapeutic agents for renal tumours or with doxycycline to induce cre expression.

2.2.4.1 AZD2014

AZD2014 was thoroughly dissolved in dimethyl sulfoxide (DMSO) at a concentration of 80mg/mL. Solution was then aliquoted and stored in -80°C. On day of treatment, an AZD2014 aliquot was thawed and diluted with a vehicle solution of 5% PEG-400 and 0.5% Tween-80 (sterile), to give a concentration of 5mg/mL. Mice were treated at 20mg/kg AZD2014 via intra-peritoneal injection (IP), once a day 5 days a week for two months.

2.2.4.2 Rapamycin

Rapamycin was prepared at 50mg/mL in DMSO. Rapamycin was aliquoted, stored and prepared as described for AZD-2014 but with a final concentration of 1mg/mL. Mice were treated at 5mg/kg Rapamycin via IP, once a day 5 days a week.

2.2.4.3 3-Bromopyruvate (3-BrPA)

3-BrPA was thoroughly dissolved in saline at concentration of 10mg/mL. 3-BrPA solution was aliquoted and stored at -80°C. On day of treatment, a 3-BrPA aliquot was thawed and diluted with saline to give a final concentration of 0.4mg/mL. Mice were treated at 2mg/kg via IP, once a day 5 days a week.

2.2.4.4 CB-839

CB-839 (20mg/mL) and its vehicle (aq. 25% HPBCD/10mM Citrate/ pH2) were prepared by Calithera in 230mL bottles. Bottles were vortexed, aliquoted and stored at -80°C. Mice were treated with CB-839 at 200mg/kg via gavage twice a day, 7 days a week.

2.2.4.5 Combination treatments

Combination treatments in this study include: 3-BrPA + Rapamycin, CB-839 + Rapamycin and 3-BrPA + CB-839. Each combination treatment was given at the same dosage through the same route as a single treatment.

2.2.4.6 Doxycycline

Doxycycline at a concentration of 2mg/mL was prepared in drinking water, supplemented with 5% sucrose. Drink bottles with doxycycline were changed with fresh solutions every Monday, Wednesday and Friday for 10 days.

2.2.5 Animal dissection

On the final treatment day of all studies, mice were treated as normal and transferred to a procedure room for necropsy analysis and tissue harvesting.

2.2.5.1 Necropsy analysis, dissection and tissue harvesting

Mice were killed by cervical dislocation. Mice were fully examined for external lesions, lumps or traumas and recorded before dissection. During dissection, all organs were examined for lesions and any lesions recorded. Small pieces of the kidney, liver, spleen, heart, lungs, small intestine, brain and muscle, and the remaining liver, spleen, heart, lungs, small intestine and brain were quickly snap frozen in isopentane for use in molecular analysis. Isopentane was placed in a beaker chilled by liquid nitrogen. Both kidneys, a section of the large lobe of the liver and half the brain were quickly transferred and fixed in buffered formalin saline (ph 7.0) for 24 hours before being processed. Snap frozen tissues were transferred to cryotubes and stored at -80°C.

2.2.6 Histology

2.2.6.1 Tissue fixation, embedding and sectioning

Kidneys fixed in buffered formalin saline were processed and sectioned for H&E analysis and immunohistochemistry. Kidneys were transferred to a LEICA TP1050 tissue processor for dehydration, cleaning and embedding. This process involved dehydration in 70, 95 and 100% ethanol at 1-hour intervals each. Kidneys were then cleaned in 2 rounds of xylene for 45 minutes and 1 hour. Kidneys were then immersed in molten paraffin wax (60°C) for 1 hour x 2 and 1.5 hours. Each kidney was finally embedded in a mould filled with molten paraffin wax and allowed to set and harden on a cold plate.

Embedded kidneys were then sectioned using a LEICA RM2235 microtome. Six coronal sections of 5μm were prepared at a 200μm interval from both kidneys of each mouse to investigate treatment efficiency. Ten coronal sections of 5μm were prepared at a 200μm interval from both kidneys of each mouse to test the roles of *Pkm2* in tumourigenesis. Sections from all studies were placed in a 45°C water bath and collect onto 25 x 75 1.00mm polysine slides. Three pairs of kidneys were collected per slide. Slides were allowed to dry on a hot plate and left in a 45°C oven overnight. Tissue, fixation and sectioning was kindly performed by Derek Scarborough.

2.2.6.2 Haematoxylin and eosin (H&E) staining

For H&E staining, kidney sections were deparaffinised in xylene for 3x3 minutes then rehydrated in 100%, 70%, 50% ethanol and tap water for 2 minutes each. Sections were stained with Gill No 1 haematoxylin for 2 minutes followed by a wash in tap water for 2x30 seconds Sections were then stained with 0.5% Aqueous eosin for 4 minutes followed by further washing in tap water for 30 seconds. Slides were dehydrated and cleaned in 50% ethanol for 30 seconds, 70% ethanol for 30 seconds, 100% ethanol for 2x1 minute and xylene for 2x2 minutes. VectaMount Permanent Mounting Medium was used to mount slides with a cover slip and slides were left to dry at room temperature overnight.

2.2.6.3 Slide scanning

Haematoxylin and Eosin (H&E) stained slides were scanned at 20x magnification using the ScanScope® CS microscope slide scanner (Aperio Technologies, UK) to produce virtual slides.

2.2.6.4 Tumour burden assessment

Virtual H&E slides were used for lesion identification and quantification using the Aperio ImageScope™ software (http://www.aperio.com/?gclid=CNXN-8by4aUCFclNfAods3eg1w). All lesions were located, characterised, measured and recorded. Individual renal lesions were photographed at their maximum size with a reference scale. Images were then exported to the ImageJ software for tumour quantification (http://rsbweb.nih.gov/ij). Each renal lesion was characterised by cystic, papillary adenomas, solid carcinomas, micro-cyst, micro-papillary or micro-solid. Each renal lesion maximum cross-sectional area and fluid filled cross-sectional area was measured to assess lesion size and cellular area. Total lesion number, lesion size and lesion cellular area of each individual mouse was calculated. Tumour burden analysis was conducted blindly in terms of treatment.

2.2.7 Immunohistochemistry (IHC)

For IHC, kidney sections were placed in an EasyDip™ Slide Staining Rack (Simport) (up to 10 slides) and were deparaffinised in xylene for 3x3 minutes then rehydrated in 100% ethanol, 70% ethanol, 50% ethanol and water, each for 2 minutes. Pre-staining treatment was performed by placing the rack in glass beaker containing 400mL 10mM sodium citrate buffer (pH 6.0) and autoclaving for 20 minutes. The rack of slides was allowed to cool for 20 minutes before rinsing in ddH_2O for 2x2 minutes. Slides were incubated in 100mL 3% hydrogen peroxide for 10 minutes and then washed with ddH_2O and TBST buffer for 2 minutes each. Slides were removed from the rack, circled with a cytomation wax pen and placed on a Slide Staining Tray System (Azer Scientific). Four drops of Protein block (3% horse serum) were applied to each slide and incubated for 10 minutes at room temperature to block non-specific background staining and then washed with TBST for 2 minutes. Slides were incubated overnight at 4°C or 60 minutes at room temperature with 150μL of the appropriately diluted primary antibody. Slides were then

washed in TBST 3x3 minutes and 3 drops of SignalStain® Boost IHC Detection Reagent (HRP, Rabbit) were applied to each slide and incubated for 30 minutes at room temperature. The slides were then further washed with TBST 3x3 minutes. Slides were stained with 150μL ImmPACT™ NovaRED™ for 10 minutes and washed with ddH_2O for 2x2 minutes (ImmPACT™ NovaRED™ solution is prepared before use according to the manufactuers protocol). Following washing, slides were counter-stained with 100% haematoxylin for 3 minutes and rinsed with tap water and ddH_2O for 2x2 minutes. Sections were dehydrated and cleaned in 50% ethanol for 15 seconds, 70% ethanol for 15 seconds, 100% ethanol for 40 seconds and xylene for 2x2 minutes. VectaMount Permanent Mounting Medium was used to mount slides with a cover slip and slides were left to dry at room temperature overnight. IHC slides were converted to virtual slides as explained in 2.2.6.3.

2.2.7.1 Multiple sequential IHC (MS-IHC)

MS-IHC was performed to co-localise multiple antigens in the same cells. A crucial step of MS-IHC was to completely strip previous primary antibodies to ensure efficiency and specificity of subsequent primary antibody-antigen reactions (Figure 2.1). The protocol used for stripping primary antibodies was modified from (Kim *et al.* 2012). For MS-IHC, previous IHC-stained slides were incubated in xylene for 10 minutes to remove coverslips, and then incubated at 50°C in IHC stripping solution (see 2.1.4) for 60 minutes to strip primary antibodies, and finally the protocol was followed for IHC as described above.

2.2.8 Protein, RNA, DNA extraction and purification

The AllPrep® DNA/RNA/Protein Mini Kit (Qiagen) was used for extraction of proteins and nucleic acid from frozen animal tissues. Approximately 10-30mg of animal tissue was rapidly transferred to 600mL RLT (mixed with β-mercaptoethanol at a ratio of 100:1 (1000μL RLT + 10μL β-mercaptoethanol)) in a 2mL round-bottom tube and quickly homogenised using a TissueRuptor (30 seconds operation). Samples were centrifuged for 3 mins at 12,000rpm and transferred to an ALLPrep DNA spin column placed in a 2mL collection tube. The ALLPrep DNA column was centrifuged for 30 seconds at 12,000rpm. The ALLPrep DNA column containing the sample DNA was stored at 4°C for later DNA purification. Four hundred and thirty microliters of 100% ethanol was

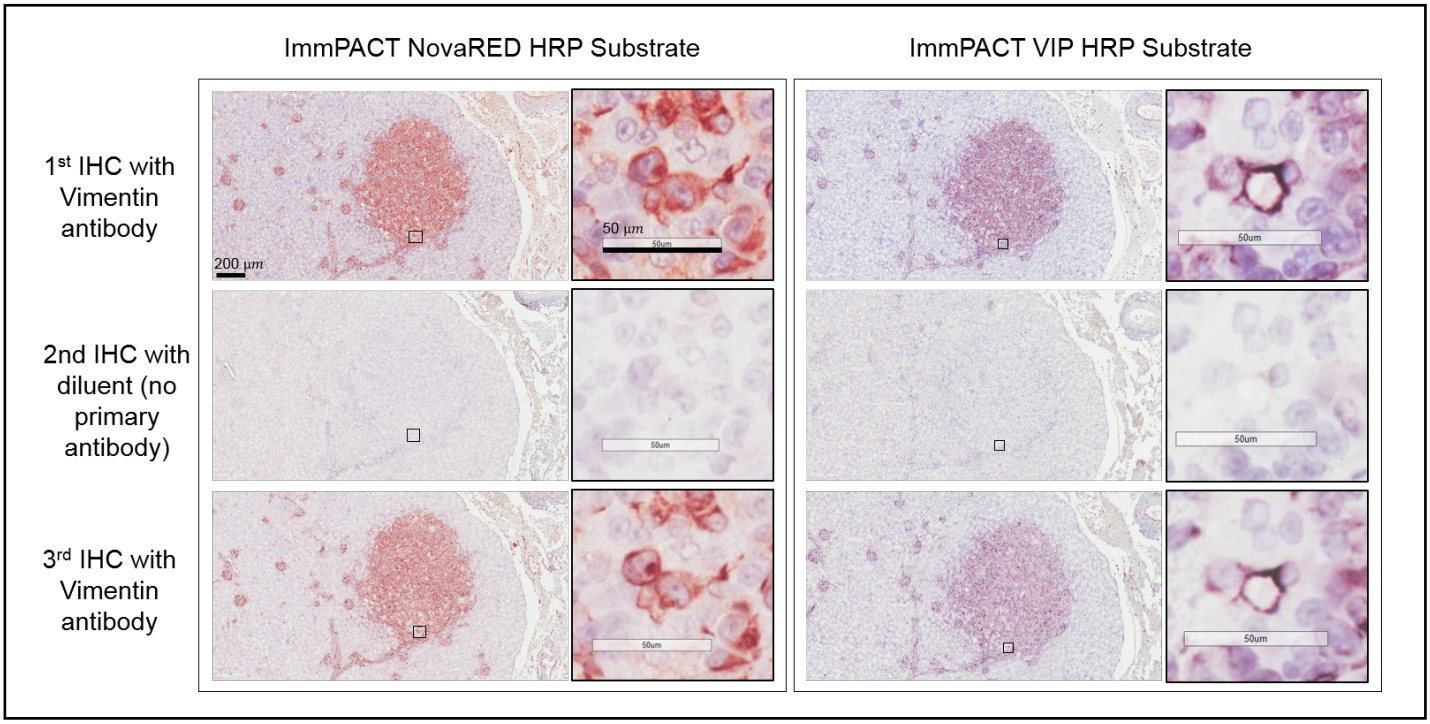

Figure 2.1 Multiple sequential IHC (MS-IHC). Multiple sequential IHC was used to detect the expression of more than one protein on the same kidney sections. Two adjacent kidney sections prepared from a *Tsc2*$^{+/-}$ mouse of 14 months old were used to stain Vimentin. Vimentin antibody was then completely stripped and stained with control (diluent) to reveal no specific staining, as seen in 2nd round IHC. Sections were then re-stained with Vimentin in 3rd IHC, with similar staining as seen in 1st IHC.

transferred to the flow-through and readily mixed. Seven hundred microliters of the mixture was transferred to an RNeasy spin column placed in a 2mL collection tube and centrifuged for 15 seconds at 12,000rpm. If mixture exceeded 700μL, successive centrifugations were performed in the same RNeasy spin column. The RNeasy spin column was then placed in a new 2mL collection tube and stored at 4°C for later RNA purification.

2.2.8.1 Protein purification

One volume (830μL) of Buffer APP was added to the flow-through and mixed vigorously. The mixture was left to incubate for 10 minutes for protein to precipitate. The mixture was then centrifuged for 10 minutes at 13,000rpm. The supernatants were removed to reveal the protein pellet and cleaned with 500μL of 70% ethanol. Samples were centrifuged for a further 5 minutes at 13,000rpm and the supernatant was removed using a pipette, being careful not to disturb the pellet. Protein pellets were left to dry at room temperature and up to 200μL of ALO Buffer (volume determined on pellet size) was added to each sample for resuspension. DTT was added to ALO Buffer before resuspension (50μL DDT + 100μL ALO Buffer). Following resuspension, samples were incubated at 95°C for 5 minutes and left to cool at room temperature. Samples were centrifuged for 1 minute at 13,000rpm, aliquoted and stored at -80°C or used for western analysis immediately.

2.2.8.2 RNA purification

Seven hundred μL of RW1 wash buffer was added to RNeasy spin columns. Columns were centrifuged for 15 seconds at 12,000rpm. The supernatant was discarded, and the columns were washed with 500μl RPE wash buffer for 15 seconds at 12,000rpm, twice. Following the 2nd wash, the samples were centrifuged for 2 minutes at 12,000rpm to collect any residual wash buffer. The RNeasy spin columns were then placed in new 1.5mL collection tubes and the RNA was eluted by adding 50μL RNase-free water to the spin column and centrifuging for 1 minute at 12,000rpm. Samples were aliquoted, with 1 aliquot to be used for quantification and the other stored at -80°C. RNA concentration was quantified using the ND8000 8-sample NanoDrop Spectrophotometer in ng/μL.

2.2.8.3 DNA purification

Five hundred μL AW1 wash buffer was added to each DNA spin column. Columns were centrifuged for 15 seconds at 12,000rpm. The supernatant was discarded and a further 500μL of AW2 wash buffer was added to the columns. Columns were centrifuged again for 15 seconds at 12,000rpm and the supernatant discarded. Columns was centrifuged for a further 2 minutes at 12,000rpm to remove any residual wash buffer. The ALLPrep DNA spin columns were placed in new 1.5μL collection tubes and the DNA was eluted using 100μL preheated 70°C EB buffer. Columns were left to incubate for 2 minutes in the EB buffer before centrifuging for 1 minute at 12,000rpm. DNA elutes were then stored at -20°C.

2.2.9 Western blot analysis

Electrophoresis was performed using the Invitrogen Novex gel system. NuPage Novex 4-12% Bis-Tris gels of 12, 15 or 17 wells were used for the separation of small and medium sized proteins. Protein samples and RNase free water of varying volumes were added to NuPage LDS Sample Buffer (2.5μL) to bring a total volume of 10μL. Samples were then incubated at 70°C for 10 minutes, left to cool at room temperature and centrifuged for 1 minute at 13,000rpm. Samples were loaded into the wells of the NuPage 4-12% Bis-Tris gel and run with 1X NuPage MES SDS Running Buffer at a constant 200V for 35 minutes. Following electrophoresis, Proteins were transferred to a Hybond ECL Nitrocellulose membrane within a 1X NuPage Transfer Buffer at a constant 30V for 1 hour. Blotting pads, 3 MM Whatman filter paper and ECL membrane were pre-treated in 1X NuPage Transfer Buffer.

The ECL membrane was then blocked after protein transfer in 10mL 1X TBST with 3% Advance Blocking Agent for 1 hour at room temperature on an orbital shaker. The membrane was then rinsed with 1X TBST. The primary antibody to be used for investigation was diluted with 10mL 1X TBST with 3% Advance Blocking Agent (according to the manufacturers protocol) and left to incubate with the membrane for 1 hour at room temperature on an orbital shaker. Membrane was then washed with 1X TBST for 10 minutes and washed again in 1X TBST for 3x3 minutes. Membrane was then incubated with secondary antibody conjugated with horse radish peroxidase (HRP) in 10mL 1X TBST with 3% Advance Blocking Agent (1:10,000 dilution) for 1 hour at room

temperature. The membrane was then washed with 1X TBST for 10 minutes and washed again in 1X TBST for 3x3 minutes. For detection, 2mL ECL Advanced Western Blotting detection solution was used to cover the membrane and kept in darkness for 5 minutes at room temperature. Following incubation with detection mixture, the membrane was drained and placed in a clear plastic sleeve and transferred in darkness to a BioSpectrum Imaging System for visualisation. Membrane was exposed for 60 minutes with 1-minute image exposures (60 images) to collect maximum chemiluminescent signal. A Digital UP-895MD Graphic Printer was used to print exposure photo and scanned images were electronically saved. Densitometry data was analysed using ImageJ software.

2.2.10 Statistics

2.2.10.1 Power analysis

Data from previous studies were used to determine sample sizes. The mean number of renal lesions was estimated at 60 (SD=13) in the *Tsc2*$^{+/-}$ mice at the age of 12 months. Assuming that at about 30% reduction in tumour number will be detected in mice treated with therapeutic agents or with specific deletion of *Pkm2* in the kidneys in comparison with vehicle treated mice, at least 8 mice in each group will be used. This sample size allows a statistical power of 0.8 with an α error of 0.05.

2.2.10.2 Statistical tests

The Mann-Whitney U test was used to compare lesion number, size and cellular area between treatment groups and for proliferation analysis. Two-tailed Fishers exact test was used for the comparison of vimentin expression in cystic/papillary adenomas and solid carcinomas, and FSP1 expression in cystic/papillary adenomas and solid carcinomas. Two tailed unpaired Student's t-Test was used for the comparison of relative intensity of Western analysis between vehicle and treatment groups. $P < 0.05$ was considered to be statistically significant.

3 CHAPTER THREE

Comparison of AZD2014 with Rapamycin for their Effect on Tumour Burden and Tumour-associated EMT in the Kidneys of a *Tsc2*$^{+/-}$ Mouse Model

3.1 Introduction

Mutations in *Tsc1* or *Tsc2* genes result in aberrant activation of mTOR signalling and tumorigenesis in TSC patients. Rapamycin and its derivatives (rapalogs; for convenience, rapalogs will include rapamycin and its derivatives, unless otherwise specified) are potent inhibitors of mTORC1 signalling. Rapalogs have shown good efficacy in pre-clinical and clinical trials for treating TSC-associated tumours (Bissler et al. 2008; Davies *et al.* 2011; Bissler et al. 2013). However, the response to rapalogs is only partial and tumour regrowth is apparent upon treatment cessation. TSC-associated tumours have also shown evidence of resistance after long-term rapamycin treatment (Benjamin et al. 2011). It is suggested that the limited activity of rapalogs is due to lack of inhibition on mTORC2 and loss of negative feedback regulation, leading to increased PI3K/Akt signalling (Harrington et al. 2004; O'Reilly et al. 2006; Tabernero et al. 2008). Akt activation promotes survival and growth of tumour cells. Partial inhibition of rapalogs on 4E-BP1 phosphorylation is also suggested to contribute to their limited therapeutic efficacy (Feldman et al. 2009; Thoreen et al. 2009).

ATP-competitive inhibitors of mTOR have been developed to overcome the limitations of rapalogs (Benjamin et al. 2011). AZD2014 is a novel ATP-competitive inhibitor of mTOR and has shown significant anti-tumour efficacy in many cancer cell lines and xenograft models of cancer (Pike et al. 2013; Guichard et al. 2015; Zheng et al. 2015). It effectively inhibits both mTORC1 and mTORC2, and also dramatically suppresses epithelial to mesenchymal transition (EMT) in hepatocellular cell lines (Liao et al. 2014). EMT is suggested to promote tumour progression, metastasis and resistance to chemotherapy in many types of cancer and tumour syndromes, including RCC (Nieto et al. 2016; Piva *et al.* 2016). The mTOR signalling pathway is an important regulator of EMT and its overactivation drives tumour progression (Guertin and Sabatini 2007; Gulhati et al. 2011). EMT has

been reported in TSC-associated AML and LAM, and the mesenchymal marker vimentin has been detected in TSC-associated RCC (Barnes *et al.* 2010; Yang et al. 2014; Bi *et al.* 2017).

In this study, the EMT status of TSC-associated tumours from both human and mouse were examined. The therapeutic efficacy of AZD2014 was tested in comparison with rapamycin on cultured TSC-associated tumour cells, and on renal tumours in *Tsc2*$^{+/-}$ mice. The effects of AZD2014 and rapamycin on mTOR signalling and EMT were also compared on tumour cells *in vitro* and *in vivo*.

3.2 Results

3.2.1 mTOR signalling and partial EMT in renal tumours of *Tsc2*$^{+/-}$ mice and TSC patients

Tsc2$^{+/-}$ mice spontaneously develop different types of renal lesions including cysts, papillary adenomas and solid carcinomas (Onda et al. 1999) (Figure 3.1). Non-treated *Tsc2*$^{+/-}$ mice at 16 months of age were culled to investigate mTOR signalling and EMT in renal lesions by IHC (Figure 3.2). As expected, mTORC1 and mTORC2 were activated in all cysts papillary adenomas and solid carcinomas, as seen by the increased phosphorylation of S6 at 235/236 and Akt at S473 (Figure 3.2A). The expression of epithelial marker E-cadherin was consistently expressed in all cystic and papillary adenoma cells. However, expression of E-cadherin was slightly reduced, variable or absent in solid carcinoma cells. Expression of mesenchymal markers vimentin, FSP1 and α-SMA in cystic lesions was minimal. In more advanced papillary adenomas and solid carcinomas, expression of mesenchymal markers increased significantly (Figure 3.2A and B). As seen in Figure 3.2A, epithelial and mesenchymal markers appeared to be co-expressed in tumour cells of TSC-associated renal lesions when IHC was applied to consecutive kidney sections. indicative of partial EMT. To confirm this observation, multiple sequential IHC (MS-IHC) was performed to detect multiple antigens on the same kidney sections (Figure 3.3; Methods 2.2.7.1 for details). The same kidney sections were subjected to 3 rounds of staining with E-cadherin, vimentin and FSP1 with complete stripping of each antibody per round. Many hybrid epithelial-mesenchymal tumour cells were observed as evidenced by co-expression of E-cadherin, vimentin and FSP1 (Figure 3.3; red circles). These results suggest that partial EMT is associated with tumour progression in the kidneys of *Tsc2*$^{+/-}$ mice.

Renal AML and RCC of TSC patients were also examined for mTOR signalling and EMT using MS-IHC (Figure 3.4A and B). Activation of mTORC1 and mTORC2 was observed in these tumours as indicated by the increased phosphorylation of S6 at S235/236, Akt at S473 and PKC at T638 (Figure 3.4A). Furthermore, these tumours showed consistent expression of vimentin and FSP1, and variable expression of E-cadherin. Interestingly, the co-expression of E-cadherin and vimentin or E-cadherin and FSP1 was frequently seen in many individual tumour cells (Figure 3.4B). These data revealed the existence of hybrid epithelial and mesenchymal cells (partial EMT) in human TSC-associated

tumours. These results together with the findings made in *Tsc2*$^{+/-}$ mice suggest that partial EMT in TSC-associated renal tumours is a common feature shared by human and mouse and increases as tumours progress from cysts to papillary adenomas and solid carcinomas.

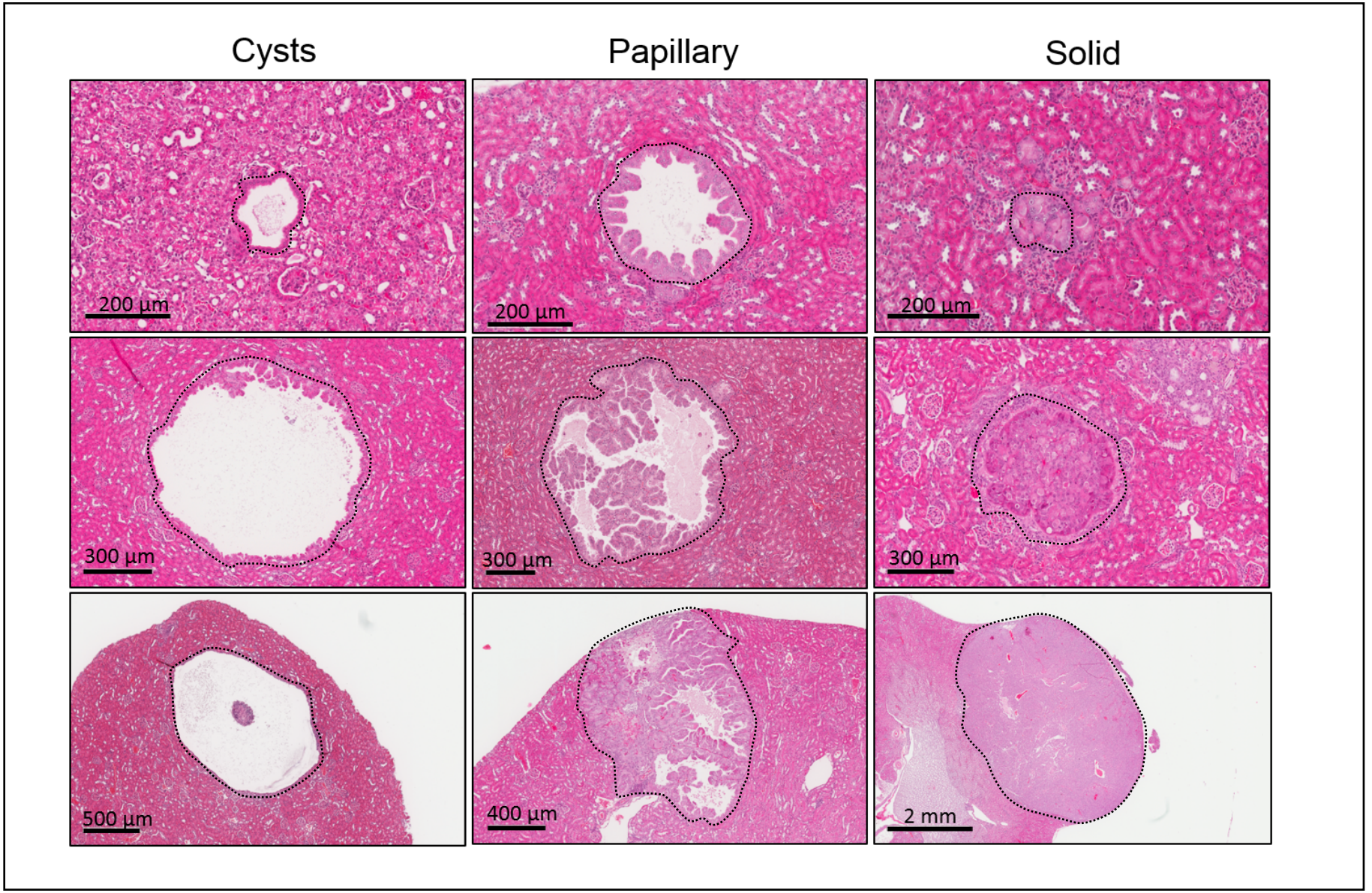

Figure 3.1 H&E staining of renal lesions in *Tsc2*$^{+/-}$ mice. *Tsc2*$^{+/-}$ mice develop microscopic lesions from 2 months and macroscopic lesions from 12 months of age. Renal lesions can be identified and characterised by H&E staining. Renal lesions found in *Tsc2*$^{+/-}$ mice include cysts (left), papillary adenomas (middle) and solid carcinomas (right). Lesions grow and become more aggressive through aging. Solid black lines indicate scale bars.

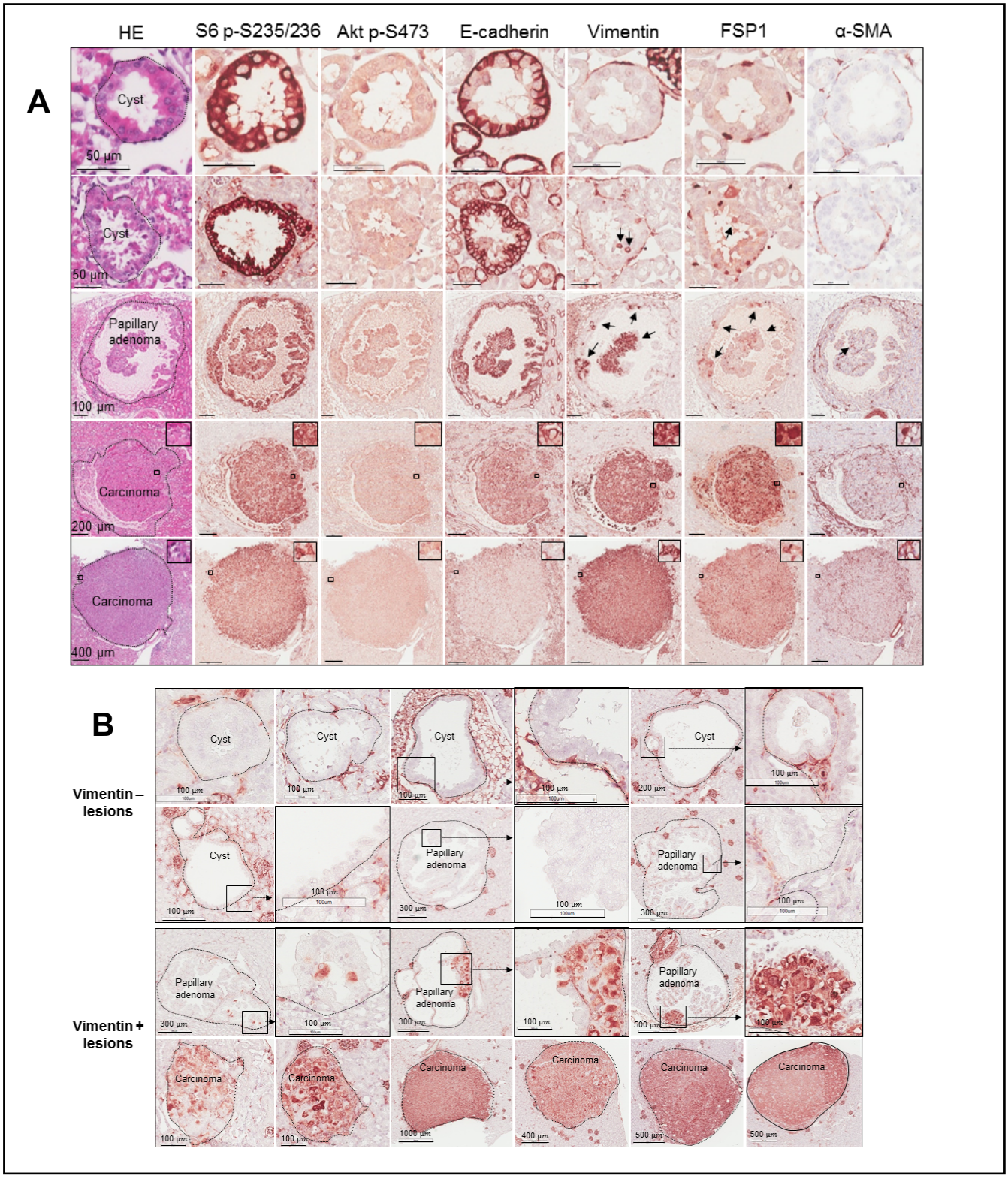

Figure 3.2 mTOR signalling and partial EMT in renal lesions of *Tsc2*$^{+/-}$ mice. Kidneys from *Tsc2*$^{+/-}$ mice were dissected at 16 months old for investigation by IHC. Sections contained cysts, papillary adenomas and solid carcinomas (**A)** Activation of mTOR signalling and EMT in renal lesions of *Tsc2*$^{+/-}$ mice by IHC. Phosphorylation of S6 at S235/236 and Akt at S473 were used as markers for mTORC1 and mTORC2 signalling, respectively. Protein levels of E-cadherin (epithelial marker), vimentin (mesenchymal marker), FSP1 (mesenchymal marker) and α-SMA (mesenchymal marker) were used as markers for EMT activation. Black arrows indicate individual tumour cells stained by vimentin, FSP1 or α-SMA. Solid black lines represent scale bars. (**B)** Detection of vimentin in renal lesions of *Tsc2*$^{+/-}$ mice by IHC. Sections were stained with mesenchymal marker vimentin to show protein levels in cysts, papillary adenomas and solid carcinomas. Solid black lines represent scale bar.

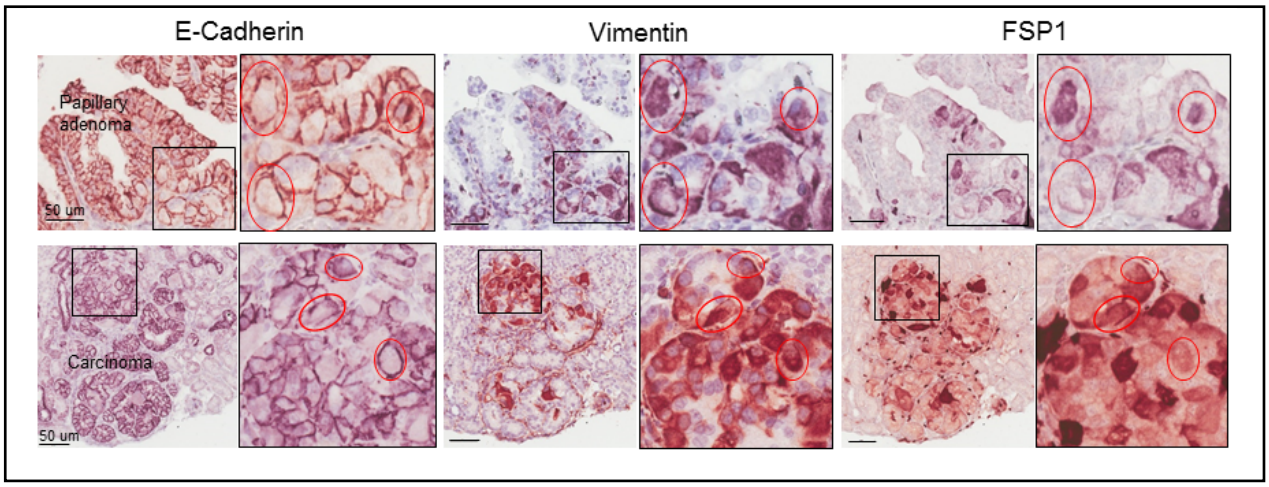

Figure 3.3 Co-expression of EMT markers in renal lesions of *Tsc2*$^{+/-}$ mice by MS-IHC. The same kidney section from non-treated *Tsc2*$^{+/-}$ mice were subjected to 3 rounds of IHC to detect co-expression of EMT proteins. Markers used for EMT assessment were E-cadherin, vimentin and FSP1. Individual cells co-expressing EMT markers in red circles. Black boxes indicate higher power views of adjacent image. Solid black lines indicate scale bars.

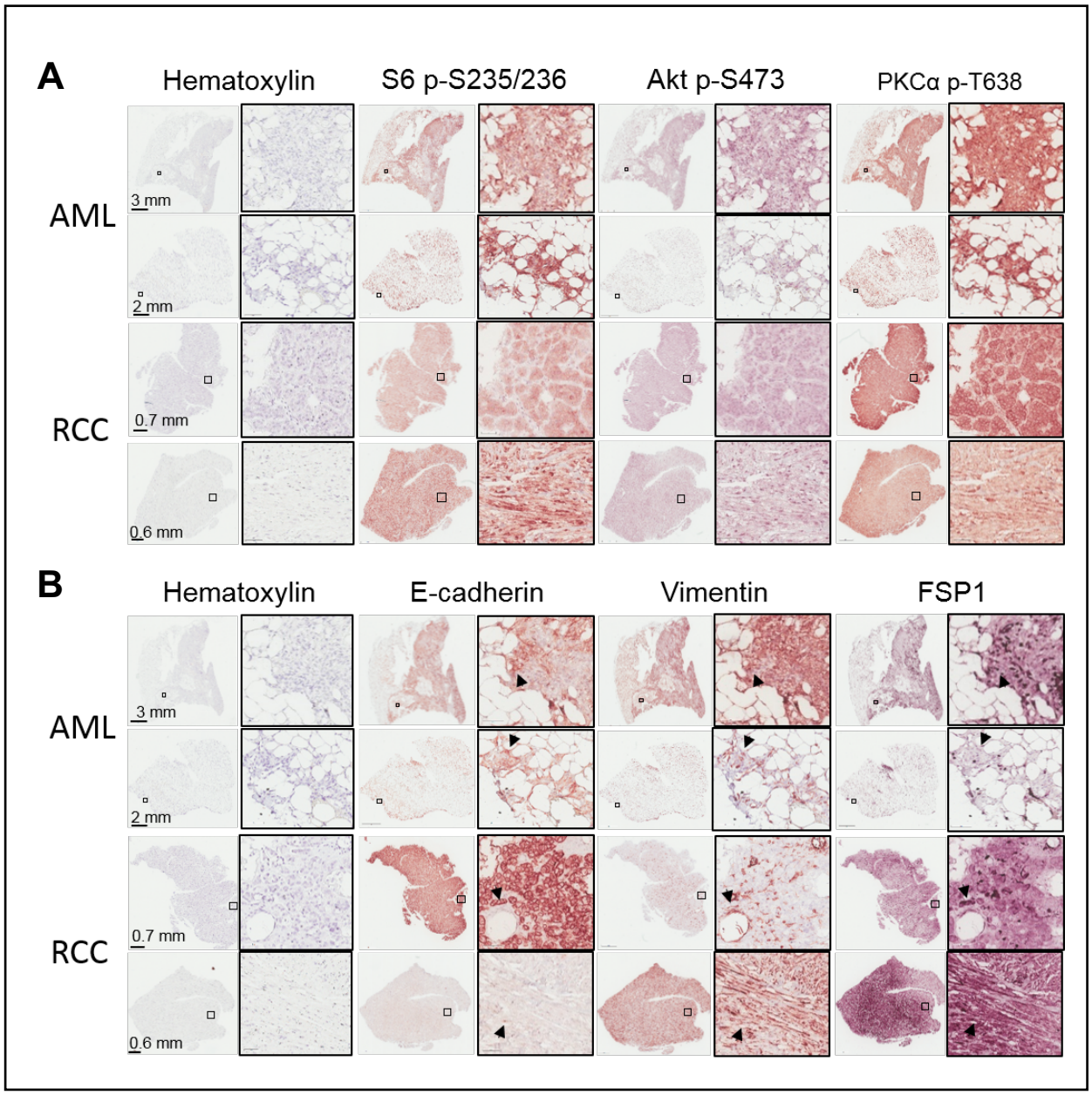

Figure 3.4 mTOR activation and partial EMT in TSC-associated tumours from TSC patients. mTOR activation and partial EMT was analysed by MS-IHC. **(A)** mTOR signalling in TSC-associated tumours from TSC patients. Sections of patient derived TSC-associated tumours were subjected to 3 rounds of IHC with complete stripping between each round. Phosphorylation of S6 at S235/236 was used as a marker for mTORC1 signalling. Phosphorylation of Akt at S473 and PKC at T638 were used as markers for mTORC2 signalling. No antibody (haematoxylin) was used as an IHC control. Black boxes indicate higher power views of adjacent image. AML: Angiomyolipoma; RCC: Renal cell carcinoma **(B)** Co-expression of EMT markers in TSC-associated tumours from TSC patients. Sections of patient derived TSC-associated tumours were subjected to 3 rounds of IHC to assess the co-expression of EMT markers E-cadherin, vimentin and FSP1. No antibody (haematoxylin) was used as an IHC control. Black boxes indicate higher power views of adjacent image. Black arrows point to individual tumour cells with the co-expression of E-cadherin and vimentin or FSP1. Solid black lines indicate scale bars. AML: Angiomyolipoma; RCC: Renal cell carcinoma

3.2.2 Effect of AZD2014 and rapamycin on survival, proliferation and EMT of *Tsc2*$^{-/-}$ MEFs and TSC2-associated renal tumour cells

Using MTT and colony formation assays, the effect of AZD2014 and rapamycin was first compared on the survival and proliferation of *Tsc2*$^{-/-}$ MEFs and TSC2-associated renal tumour cells derived from *Tsc2*$^{+/-}$ mice (Figure 3.5). It was found that both AZD2014 and rapamycin effectively reduced survival and suppressed proliferation of *Tsc2*$^{-/-}$ MEF cells and TSC2-associated tumour cells in a dose-dependent manner (Figure 3.5A and B). Importantly, *Tsc2*$^{-/-}$ MEFs and TSC-associated tumour cells were much more sensitive to AZD2014 and rapamycin treatment than *Tsc2*$^{+/+}$ MEFs.

The effect of AZD2014 and rapamycin on mTOR signalling and EMT were then evaluated by western blot in TSC2-associated kidney tumour cells (Figure 3.5C and D). AZD2014 and rapamycin dramatically inhibited mTORC1 in a dose-dependent manner, as indicated by markedly reduced phosphorylation of S6 at S235/236 and 4E-BP1 at T37/T46. Low concentrations of rapamycin were very potent at inhibiting mTORC1 in TSC2-associated tumour cells compared to only high concentrations with AZD2014 (Figure 3.5C). AZD2014 showed a dose-dependent inhibitory effect whilst rapamycin exhibited a variable inhibitory effect on mTORC2 as indicated by reduced phosphorylation of mTOR at S2481 and Akt at S473 in TSC2-associated tumour cells (Figure 3.5C). Vimentin levels were also reduced in TSC2-associated tumour cells treated with AZD2014 or rapamycin (Figure 3.5D). In TSC2-KT12 tumour cells, E-cadherin expression was induced by low doses of AZD2014 and rapamycin while in TSC2-KT17 tumour cells, E-cadherin expression was reduced by either treatment (Figure 3.5D).

These data suggest that AZD2014 may be useful for treating TSC-associated tumours.

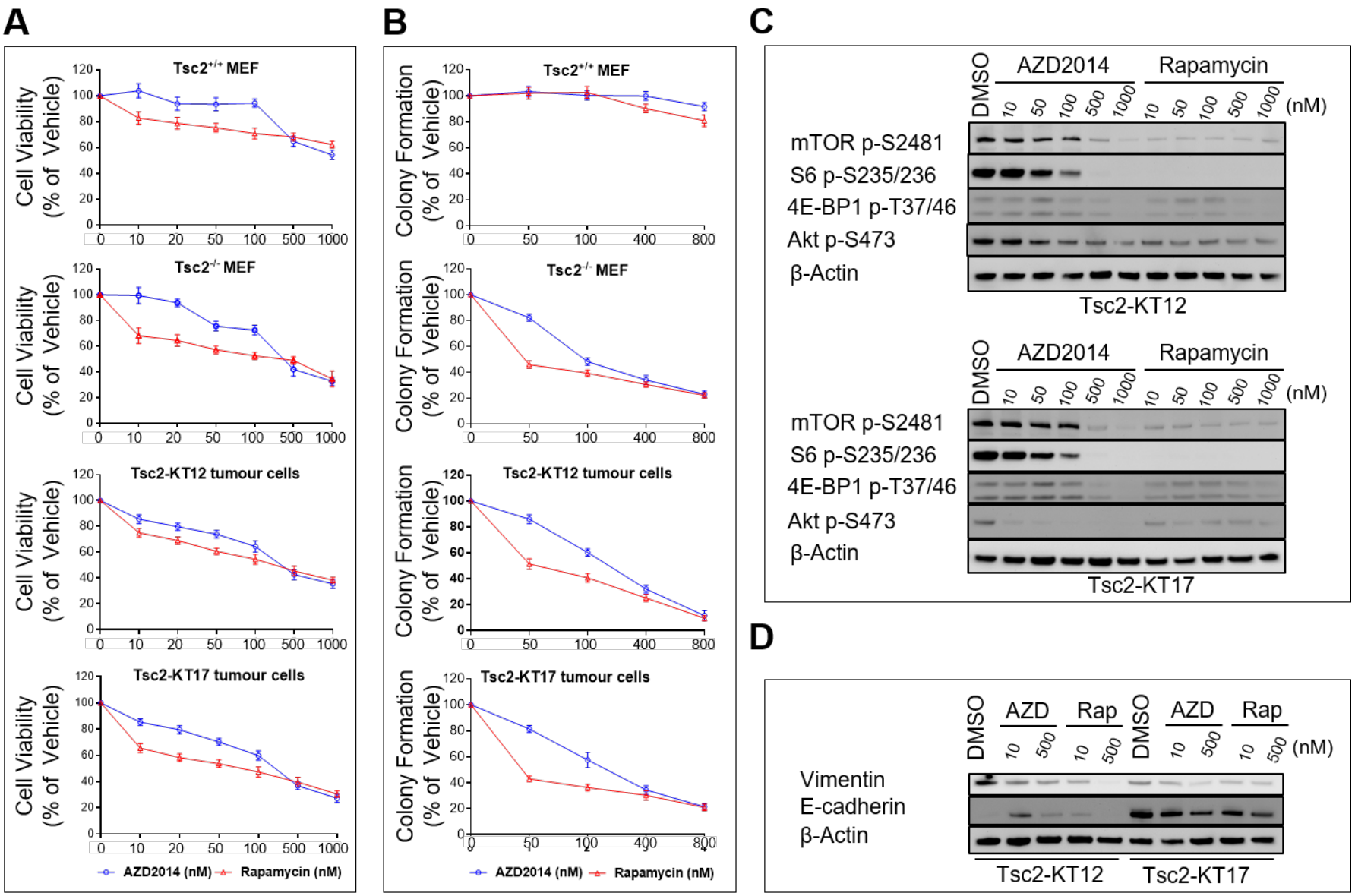
A
B
C
D
Cell Viability (% of Vehicle)
Colony Formation (% of Vehicle)
Tsc2+/+ MEF
Tsc2-/- MEF
Tsc2-KT12 tumour cells
Tsc2-KT17 tumour cells
AZD2014 (nM)
Rapamycin (nM)
DMSO
AZD2014
Rapamycin
(nM)
mTOR p-S2481
S6 p-S235/236
4E-BP1 p-T37/46
Akt p-S473
β-Actin
Tsc2-KT12
Tsc2-KT17
AZD
Rap
Vimentin
E-cadherin

Figure 3.5 Effect of AZD2014 and rapamycin on survival, proliferation and mTOR signalling/EMT in cultured *Tsc2*$^{-/-}$ MEFs and TSC2-associated tumour cells. (A) *Tsc2*$^{-/-}$ MEFs, TSC2-KT12 and TSC2-KT17 tumour cells were treated for 48 hours with AZD2014 and rapamycin at indicated concentration in DMEM containing 10% FBS. An MTT assay was used to assess cell viability. **(B)** *Tsc2*$^{-/-}$ MEFs, TSC2-KT12 and TSC2-KT17 tumour cells were treated as in **(A).** Cells were left to grow for 7 days without AZD2014 and rapamycin in DMEM containing 10% FBS and stained with crystal violate for colony formation assay. **(C)** TSC2-KT12 and TSC2-KT17 tumour cells derived from *Tsc2*$^{+/-}$ mice were grown overnight in serum-free DMEM and treated for 24 hours with DMSO, AZD2014 or rapamycin at indicated concentrations in DMEM containing 10% FBS. Protein samples from treated cells were prepared for western blot analysis to determine mTOR activation. Phosphorylation of S6 at S235/236, 4E-BP1 at T37/46, mTOR at S2481 and Akt at S473 was examined in *Tsc2*-associated tumour cells by western analysis. β-actin was used as a loading control **(D)** TSC2-KT12 and TSC2-KT17 tumour cells were treated as in **(C)** Expression of vimentin (mesenchymal marker) and E-Cadherin (epithelial marker) in *Tsc2*-associated tumour cells by western analysis. β-actin was used as a loading control.

3.2.3 Therapeutic efficacy of AZD2014 and rapamycin for renal tumours in *Tsc2*$^{+/-}$ mice

To test the efficacy for treating TSC2-associated renal tumours, the maximum tolerated dosage (MTD) of AZD2014 was first established in *Tsc2*$^{+/-}$ mice in a two-week pilot study. All *Tsc2*$^{+/-}$ mice used here were bred on the balb/c background and genotyped through PCR (as described in materials and methods, 2.2.3) (Figure 3.6). Mice were treated once a day by intraperitoneal injection at increasing dosages every 2 days until toxicity was observed. Rapid weight loss was observed at 25mg/kg. Therefore, it was determined that the lower dosage of 20 mg/kg body weight once a day five times a week was the maximum dosage tolerable in these mice via intraperitoneal injection.

A total of 24 *Tsc2*$^{+/-}$ mice were obtained and randomly allocated into three groups (n=8 each) (Table 3.1). These mice were treated from the age of 14 months with vehicle, AZD2014 (20 mg/kg) or rapamycin (5mg/kg) for two months. All animals survived until termination of treatment and no animals showed significant weight loss or other observable clinical signs. After treatment, animals were killed, and kidneys were collected for tumour burden assessment by histological analysis. To evaluate tumour burden, renal lesions were characterised, counted and measured for their whole area and cellular area (as described in methods 2.2.6.4). The lesion type, total lesion number, total lesion area and total lesion cellular area were documented for each animal and compared between treatment groups (Figure 3.7). Tumour burden was compared by analysing all lesions (cystic/papillary/solid), cystic/papillary adenomas only and solid carcinomas, only. AZD2014 and rapamycin both significantly reduced total lesion number (P=0.0012; P=0.0002), total lesion size (P=0.0047; P=0.0047) and total lesion cellular area (P=0.0047; P=0.0002) of all lesions (Figure 3.7, Table 3.2). Similarly, AZD2014 and rapamycin both significantly reduced total number (P=0.0017; P=0.0002) and cellular area (P=0.0002; P=0.0148) of cystic/papillary adenomas. Only AZD2014 significantly reduced the total size of cystic/papillary adenomas (P=0.0019) and not rapamycin (P=0.5737) (Figure 3.7, Table 3.3). Further, both AZD2014 and rapamycin significantly reduced total number (P=0.0003; P=0.0003), size (P=0.0095; P=0.0002) and cellular area (P=0.0095; P=0.0002) of solid carcinomas (Figure 3.7, Table 3.4). No other significant difference in anti-tumour efficacy was found between AZD2014 and rapamycin. These results suggest that both AZD2014 and rapamycin effectively stop tumour progression in the kidneys of *Tsc2*$^{+/-}$ mice.

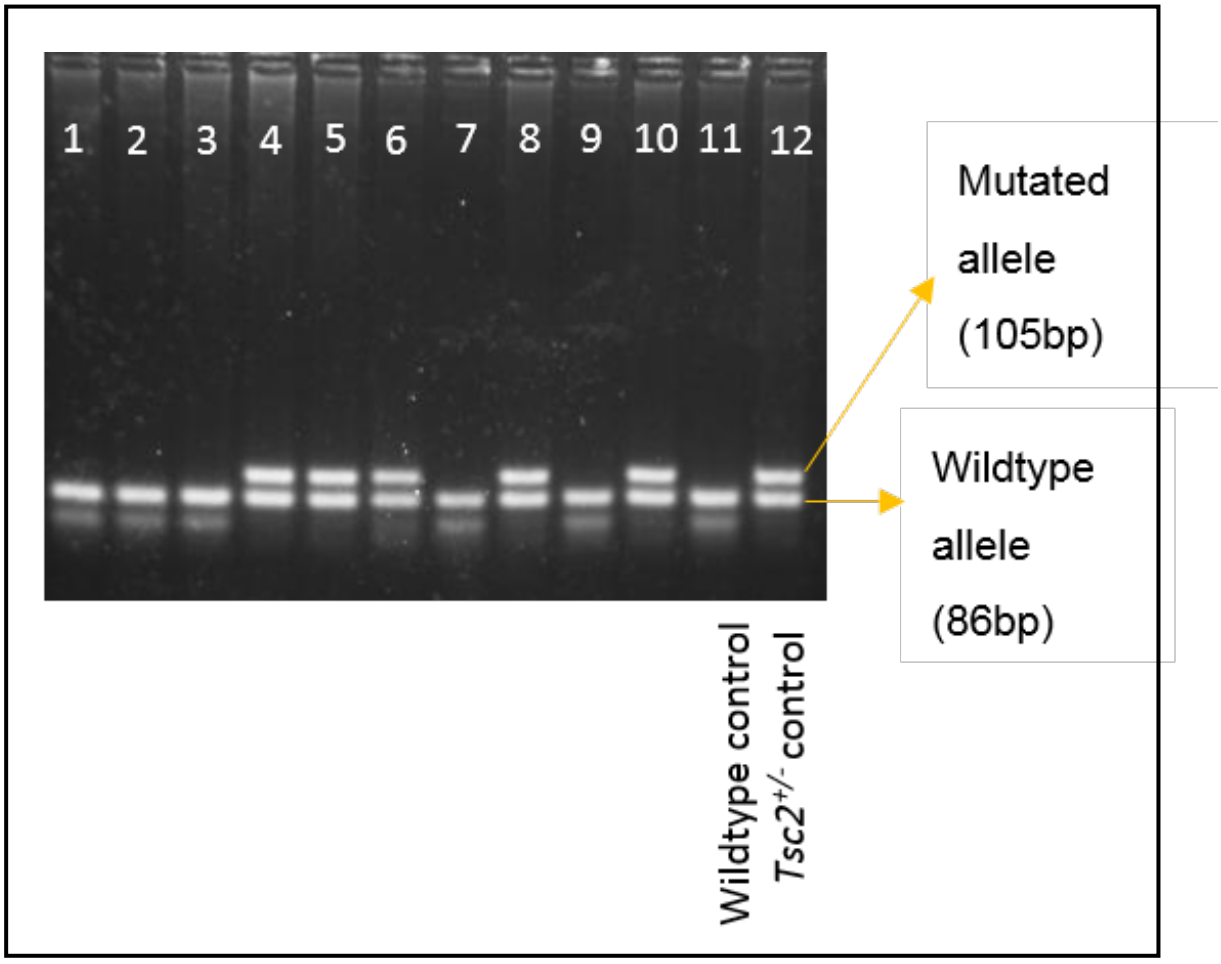

Figure 3.6 *Tsc2*$^{+/-}$ mouse genotyping. DNA was extracted from mouse ear punches and used for identification by PCR. Primers for *Tsc2* PCR are shown in Table 2.1 (Materials and Methods). PCR products were run on 3% agarose gel and visualised on an UV gel doc. The mutated *Tsc2* allele was 105bp and the wildtype *Tsc2* allele was 86bp. Lanes 4, 5, 6, 8 and 10 indicate mice heterozygous for *Tsc2.*

Table 3.1 Treatment summary

Treatment Group	Number of *Tsc2*$^{+/-}$ mice	Number of males	Number of females	Treatment start age (months)	Treatment end age (months)	Dosage*	Number of animals killed due to sickness before end of treatment**
Vehicle	8	4	4	14	16	10ul/g	0
AZD2014	8	3	5	14	16	20mg/kg	0
Rapamycin	8	3	5	14	16	5mg/kg	0

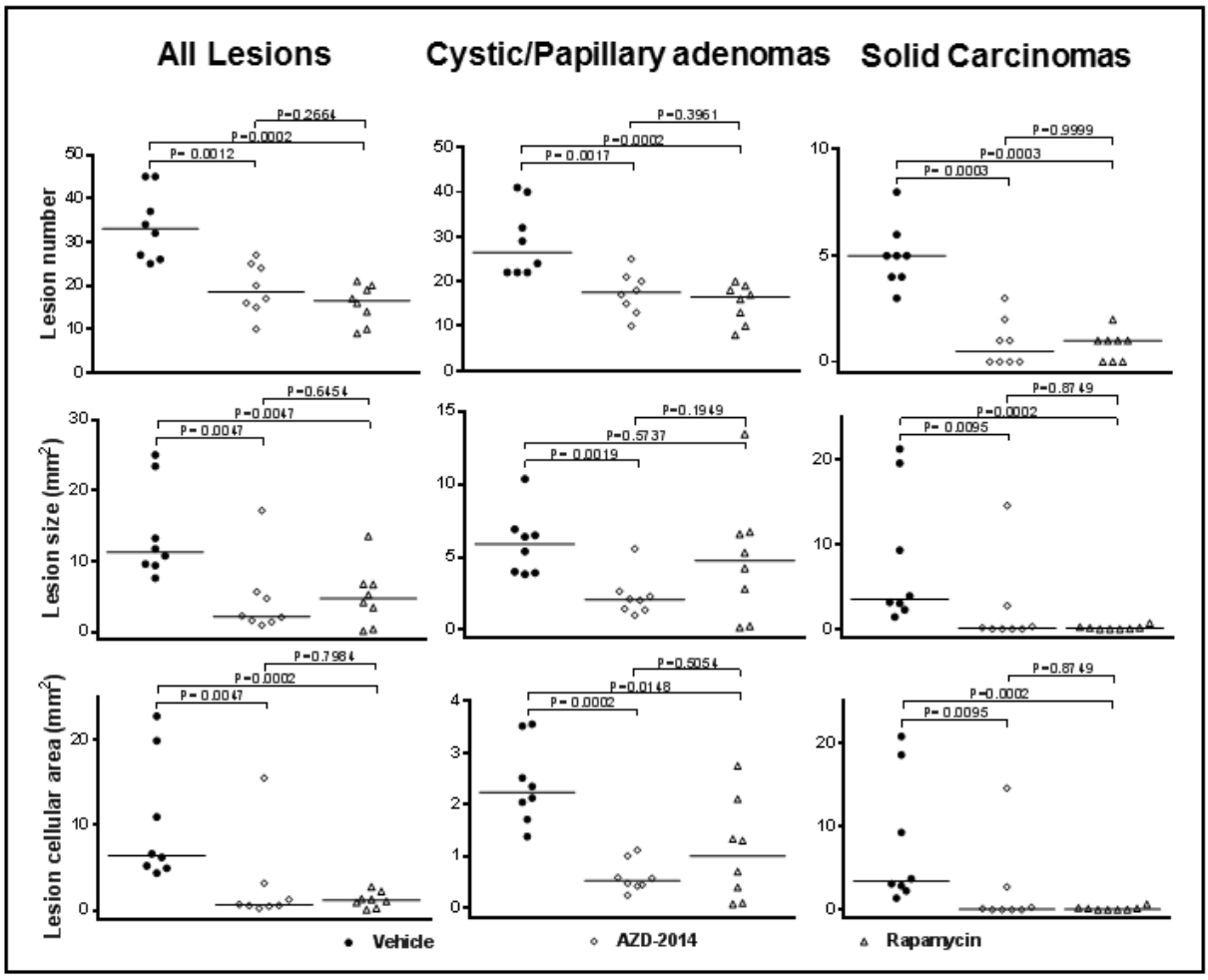

Figure 3.7 Anti-tumour efficacy of AZD2014 and rapamycin in renal lesions of *Tsc2*$^{+/-}$ mice. Twenty-four *Tsc2*$^{+/-}$ mice were randomly allocated to 3 treatment groups: AZD2014, rapamycin or vehicle (n=8). Mice were treated at 14 months of age for 2 months. On treatment end date, mice were culled and kidneys collected for histological analysis. Kidneys were fixed, processed, sectioned and stained with H&E to assess tumour burden. Kidney tumours were located, counted, characterised and measured for comparison of treatment efficacy. **Left panel:** Comparison of total lesion number, size and cellular area of all types of lesion (cyst, papillary and solid). **Middle panel:** Comparison of total cystic/papillary adenoma number, size, and cellular area. **Right panel:** Comparison of total solid carcinoma number, size and cellular area. Horizontal bars represent the median. P<0.05 is considered significant.

Table 3.2 Comparison of all lesions in *Tsc2*$^{+/-}$ mice by histological analysis (Mann Whitney test)

I. Lesion number (all lesions-cystic, papillary and solid)

Treatment*	Number of mice	Median (Number of lesions)	Range (Number of lesions)	P (Compared with Vehicle)	P (Compared with Rapamycin)
Vehicle	8	33	25-45	-	-
AZD-2014	8	18.5	10-27	0.0012	0.2664
Rapamycin	8	16.5	9-21	0.0002	-

II. Lesion size (mm^2) (all lesions-cystic, papillary and solid)

Treatment*	Number of mice	Median (mm^2)	Range (mm^2)	P (Compared with Vehicle)	P (Compared with Rapamycin)
Vehicle	8	11.285	7.641-25.042	-	-
AZD-2014	8	2.211	1.002-17.196	0.0047	0.6454
Rapamycin	8	4.77	0.167-13.580	0.0047	-

III. Lesion cellular area (mm^2) (all lesions-cystic, papillary and solid)

Treatment*	Number of mice	Median (mm^2)	Range (mm^2)	P (Compared with Vehicle)	P (Compared with Rapamycin)
Vehicle	8	6.429	4.386-22.793	-	-
AZD-2014	8	0.643	0.243-15.553	0.0047	0.7984
Rapamycin	8	1.185	0.073-2.235	0.0002	-

* Treatment was started from 14 months old and continued for two months.

Table 3.3 Comparison of all cystic/papillary adenomas in *Tsc2*$^{+/-}$ mice by histological analysis (Mann Whitney test)

I. Lesion number (cystic/papillary lesions)

Treatment*	Number of mice	Median (Number of lesions)	Range (Number of lesions)	P (Compared with Vehicle)	P (Compared with Rapamycin)
Vehicle	8	26.5	22-41	-	-
AZD-2014	8	17.5	10-25	0.0017	0.3961
Rapamycin	8	16.5	8-20	0.0002	-

II. Lesion size (mm^2) (cystic/papillary lesions)

Treatment*	Number of mice	Median (mm^2)	Range (mm^2)	P (Compared with Vehicle)	P (Compared with Rapamycin)
Vehicle	8	5.885	3.821-10.352	-	-
AZD-2014	8	2.076	1.002-5.565	0.0019	0.1949
Rapamycin	8	4.77	0.167-13.308	0.5737	-

III. Lesion cellular area (mm^2) (cystic/papillary lesions)

Treatment*	Number of mice	Median (mm^2)	Range (mm^2)	P (Compared with Vehicle)	P (Compared with Rapamycin)
Vehicle	8	2.238	1.379-3.552	-	-
AZD-2014	8	0.523	0.243-1.116	0.0002	0.5054
Rapamycin	8	1	0.073-2.750	0.0148	-

* Treatment was started from 14 months old and continued for two months.

Table 3.4 Comparison of solid carcinomas in *Tsc2*$^{+/-}$ mice by histological analysis (Mann Whitney test)

I. Lesion number (mm^2) (solid tumours)

Treatment*	Number of mice	Median (Number of lesions)	Range (Number of lesions)	P (Compared with Vehicle)	P (Compared with Rapamycin)
Vehicle	8	5	3-8	-	-
AZD-2014	8	0.5	0-3	0.0003	0.9999
Rapamycin	8	1	0-2	0.0003	-

II. Lesion size (mm^2) (solid tumours)

Treatment*	Number of mice	Median (mm^2)	Range (mm^2)	P (Compared with Vehicle)	P (Compared with Rapamycin)
Vehicle	8	3.518	1.425-21.221	-	-
AZD-2014	8	0.071	0.000-14.547	0.0095	0.8749
Rapamycin	8	0.076	0.000-0.676	0.0002	-

III. Lesion cellular area (mm^2) (solid tumours)

Treatment*	Number of mice	Median (mm^2)	Range (mm^2)	P (Compared with Vehicle)	P (Compared with Rapamycin)
Vehicle	8	3.414	1.400-20.747	-	-
AZD-2014	8	0.069	0.000-14.547	0.0095	0.8749
Rapamycin	8	0.076	0.000-0.676	0.0002	-

* Treatment was started from 14 months old and continued for two months.

3.2.4 Effect of AZD2014 and rapamycin on mTOR signalling, proliferation and apoptosis in renal tumours of *Tsc2*$^{+/-}$ mice

Western blotting and IHC were performed to determine the effect of AZD2014 and rapamycin on mTOR signalling, proliferation and apoptosis (Figure 3.8). Tissues were harvested from normal kidney, normal liver and solid carcinomas after treatment and proteins prepared for Western analysis. Phosphorylation of mTOR at S2448, S6 at S235/236 and 4E-BP1 at T37/46 were used as readouts of mTORC1 signalling. Phosphorylation of mTOR at S2481, Akt at S473 and T450, PKCα at T638 and Akt substrate MDM2 at S166 were used as readouts of mTORC2 signalling. As expected, AZD2014 significantly decreased phosphorylation of all mTORC1 and mTORC2 markers in all renal tumours, and in normal liver and kidney tissue (Figure 3.8A). AZD2014 also reduced phosphorylation of Akt at T308 in solid tumours (Figure 3.8A). Rapamycin significantly decreased phosphorylation of all mTORC1 markers in all renal tumours, and in normal liver and kidney tissue (Figure 3.8A). Furthermore, rapamycin decreased phosphorylation of mTOR at S2481, PKCα at T638 and MDM2 at S166 in solid tumours and of mTOR at S2481, and Akt at S473 and T450 in normal kidney tissues but effects of rapamycin on phosphorylation of Akt at T308 and S473 appeared to be variable in solid tumours (Figure 3.8A).

Kidney sections of treated 16-month-old *Tsc2*$^{+/-}$ mice were prepared for IHC. As shown in Figure 3.8B, AZD2014 clearly reduced phosphorylation of S6 at S235/236 and Akt at S473 in all AZD2014 treated tumours. Rapamycin also strongly inhibited phosphorylation of S6 at S235/236 but did not consistently inhibit Akt at S473 in solid tumours. In contrast, rapamycin increased phosphorylation of Akt at S473 in some cystic lesions (Figure 3.8B). These results are consistent with those by Western analysis.

Ki67 was used as a marker for proliferation and active caspase-3 was used as a marker for apoptosis in IHC. Both AZD2014 and rapamycin strikingly inhibited proliferation of tumour cells in the kidneys of *Tsc2*$^{+/-}$ mice but no significant changes in apoptosis were detected with either drug given individually (Figure 3.9).

In summary, AZD2014 strongly inhibited mTORC1 and mTORC2, whereas rapamycin significantly inhibited mTORC1 but had only partial inhibitory effect on mTORC2 in renal tumours of *Tsc2*$^{+/-}$. Both AZD2014 and rapamycin also reduced cell proliferation but did not induce apoptosis in renal tumours of *Tsc2*$^{+/-}$.

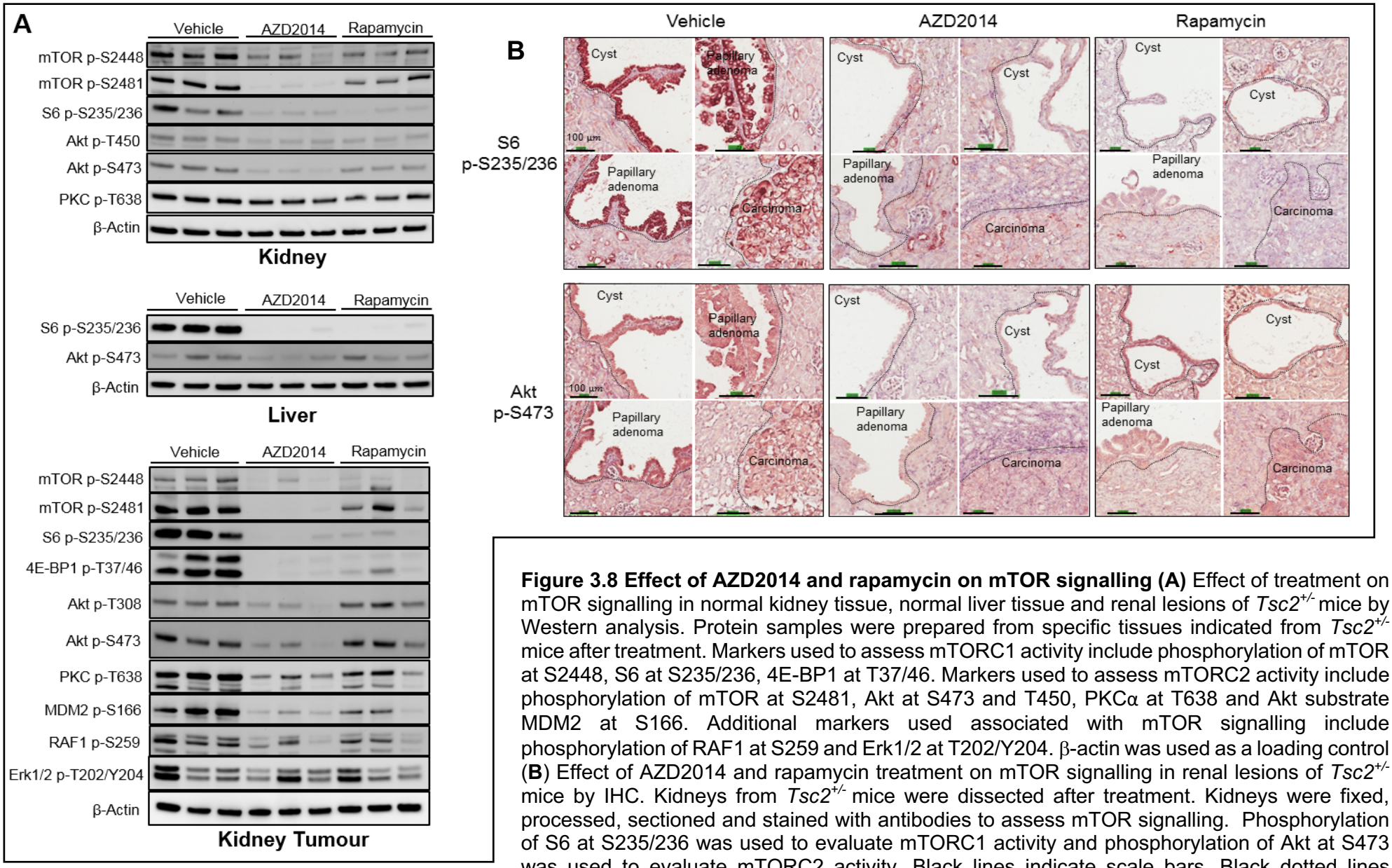

Figure 3.8 Effect of AZD2014 and rapamycin on mTOR signalling (A) Effect of treatment on mTOR signalling in normal kidney tissue, normal liver tissue and renal lesions of *Tsc2*$^{+/-}$ mice by Western analysis. Protein samples were prepared from specific tissues indicated from *Tsc2*$^{+/-}$ mice after treatment. Markers used to assess mTORC1 activity include phosphorylation of mTOR at S2448, S6 at S235/236, 4E-BP1 at T37/46. Markers used to assess mTORC2 activity include phosphorylation of mTOR at S2481, Akt at S473 and T450, PKCα at T638 and Akt substrate MDM2 at S166. Additional markers used associated with mTOR signalling include phosphorylation of RAF1 at S259 and Erk1/2 at T202/Y204. β-actin was used as a loading control (**B**) Effect of AZD2014 and rapamycin treatment on mTOR signalling in renal lesions of *Tsc2*$^{+/-}$ mice by IHC. Kidneys from *Tsc2*$^{+/-}$ mice were dissected after treatment. Kidneys were fixed, processed, sectioned and stained with antibodies to assess mTOR signalling. Phosphorylation of S6 at S235/236 was used to evaluate mTORC1 activity and phosphorylation of Akt at S473 was used to evaluate mTORC2 activity. Black lines indicate scale bars. Black dotted lines indicate lesion/normal tissue boundary.

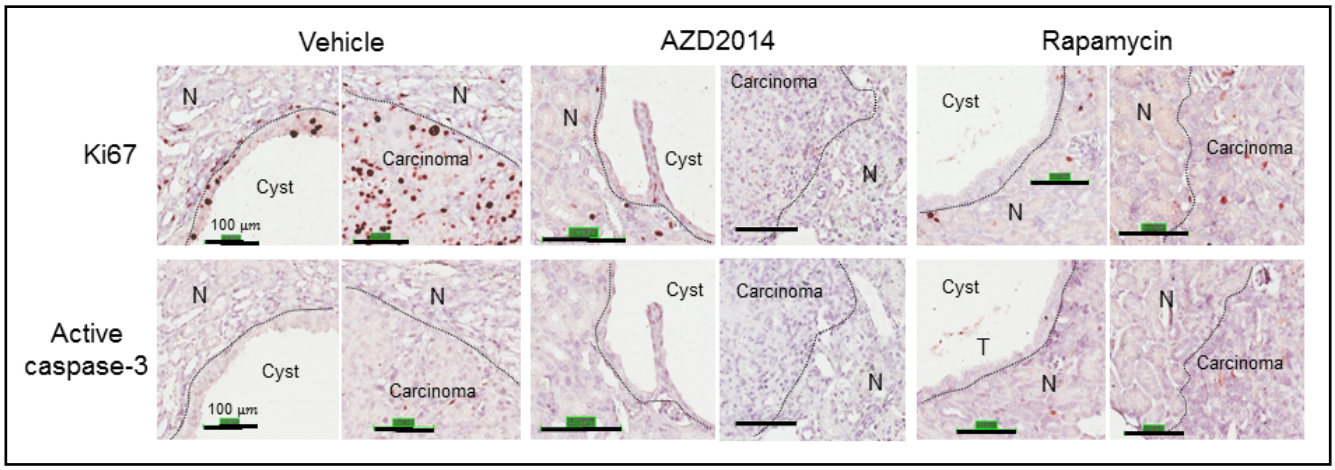

Figure 3.9 Effect of AZD2014 and rapamycin on cell proliferation and apoptosis in renal tumours of *Tsc2*$^{+/-}$ mice by IHC. Kidneys from *Tsc2*$^{+/-}$ mice were dissected after treatment. Kidneys were fixed, processed, sectioned and stained with Ki67 to assess cell proliferation and active caspase-3 to assess apoptosis. Black lines indicate scale bars. Black dotted lines indicate lesion/normal tissue boundary, N = Normal tissue.

3.2.5 Effect of AZD2014 and rapamycin on EMT in renal tumours of *Tsc2*$^{+/-}$ mice

Tsc2$^{+/-}$ mice were treated with vehicle, AZD2014, rapamycin as described above and their effect on EMT in renal tumours was examined by IHC and western analysis. The protein levels of mesenchymal marker vimentin were significantly reduced in AZD2014 and rapamycin treated cysts and papillary adenomas compared to vehicle (Figure 3.10A and B). Twelve point five per cent and 17.5% of cystic/papillary adenomas analysed had one or more cells positive for vimentin after treatment with AZD2014 (P=0.0001) and rapamycin (P=0.0010), respectively, whereas 60% of cystic/papillary adenomas analysed had one or more cells positive for vimentin after vehicle treatment. (Figure 3.10A and Table 3.5). Similar results were obtained by investigating FSP1 protein expression in cystic/papillary adenomas. Five per cent of cystic/papillary adenomas analysed had one or more cells positive for FSP1 after AZD2014 (P=0.0476) or rapamycin (P=0.0476) treatment whereas 22.5% of cystic/papillary adenomas analysed had one or more cells positive for FSP1 after vehicle treatment (Figure 3.10B and Table 3.6). In addition, the expression of vimentin and FSP1 were consistently decreased in solid carcinomas after treatment with AZD2014 and rapamycin compared to vehicle (Figure 3.10C and D). In contrast, E-cadherin showed variable expressions after AZD2014 and rapamycin treatment (Figure 3.10C). Protein samples prepared from solid renal carcinomas of *Tsc2*$^{+/-}$ mice were used for western analysis. AZD2014 and rapamycin clearly reduced vimentin expression and had a variable effect on E-cadherin expression (Figure 3.10D). These results suggest that AZD2014 and rapamycin can inhibit EMT in renal tumours of *Tsc2*$^{+/-}$ mice. However, in one large solid tumour from a *Tsc2*$^{+/-}$ mouse treated with AZD2014, protein levels of vimentin and FSP1 were not significantly affected, which was consistent with phosphorylation levels of S6 and Akt (Figure 3.11), suggesting resistance to AZD2014 and EMT regulation by mTOR.

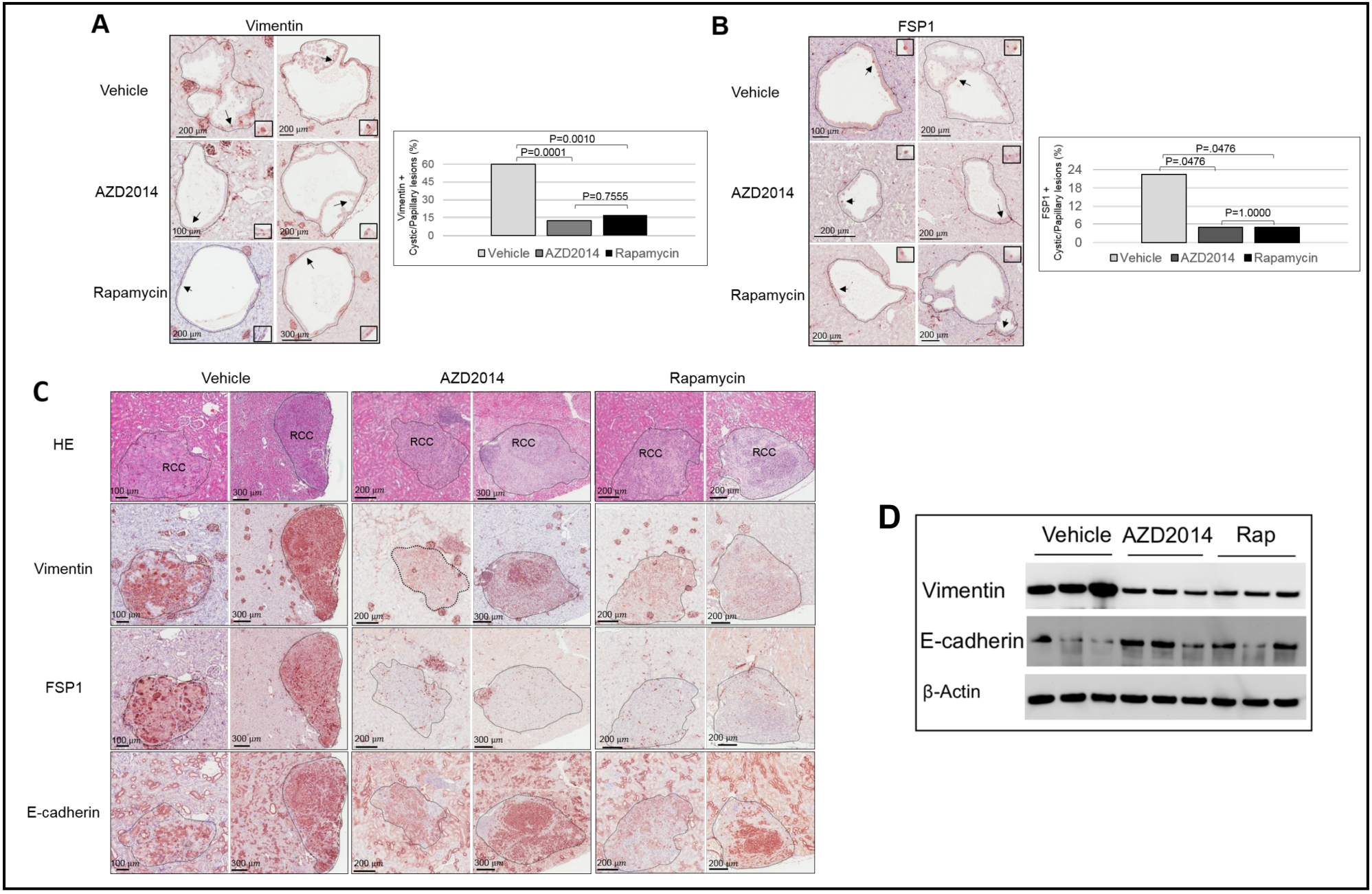
A
Vimentin
Vehicle
AZD2014
Rapamycin
Vimentin + Cystic/Papillary lesions (%)
P=0.0010
P=0.0001
P=0.7555
Vehicle AZD2014 Rapamycin
B
FSP1
FSP1 + Cystic/Papillary lesions (%)
P=.0476
P=.0476
P=1.0000
C
Vehicle
AZD2014
Rapamycin
HE
Vimentin
FSP1
E-cadherin
RCC
D
Vehicle AZD2014 Rap
Vimentin
E-cadherin
β-Actin

Figure 3.10 Effect of AZD2014 and rapamycin on EMT in renal lesions of *Tsc2*$^{+/-}$ mice. Kidneys from 14 months old *Tsc2*$^{+/-}$ mice after 2 months treatment with either AZD2014, rapamycin or vehicle were dissected for IHC and proteins prepare for western analysis. Kidneys were fixed, processed, sectioned and stained to assess EMT status after treatment. **(A)** Protein levels of vimentin were used to assess EMT in cystic/papillary adenomas after treatment. Black arrows indicate tumour cells positive for vimentin, as seen in the black boxes. Solid black lines indicate scale bars. Graph represents the proportion of cystic/papillary adenomas with cells positive for vimentin after each treatment. **(B)** Protein levels of FSP1 were used to assess EMT in cystic/papillary adenomas after treatment. Black arrows indicate tumour cells positive for FSP1, as seen in the black boxes. Solid black lines indicate scale bars. Graph represents the proportion of cystic/papillary adenomas with cells positive for FSP1 after each treatment. **(C)** EMT status of solid carcinomas after treatment. Protein levels of vimentin, FSP1 and E-cadherin are shown in solid carcinomas after treatment. Solid black lines indicate scale bars. RCC = renal cell carcinoma **(D)** Effect of treatment on EMT in solid renal tumours by Western blotting. E-Cadherin was used as an epithelial marker and vimentin was used a mesenchymal marker. β-actin was used as a loading control. $P<0.05$ is considered significant.

Table 3.5 Comparison of vimentin expression in cystic/papillary adenomas in *Tsc2*$^{+/-}$ mice by IHC (Two-tailed Fishers exact test)

Treatment	Number of vimentin + lesions	Number of vimentin- lesions	Total	vimentin + lesions (%)	P value (compared to Vehicle)	P value (compared to AZD2014)
Vehicle	22	18	40	60		
AZD2014	5	35	40	12.5	0.0001	
Rapamycin	7	33	40	17.5	0.001	0.7555

IHC was performed to stain Vimentin as described in the Materails and Methods. Five cystic/papillary lesions per animal were randomly selected and analysed.

Table 3.6 Comparison of FSP1 expression in cystic/papillary adenomas in *Tsc2*$^{+/-}$ mice by IHC (Two-tailed Fishers exact test)

Treatment	Number of FSP1 + lesions	Number of FSP1- lesions	Total	FSP1 + lesions (%)	P value (compared to Vehicle)	P value (compared to AZD2014)
Vehicle	9	31	40	22.5		
AZD2014	2	38	40	5	0.0476	
Rapamycin	2	38	40	5	0.0476	1.0000

IHC was performed to stain FSP1 as described in the Materails and Methods. Five cystic/papillary lesions per animal were randomly selected and analysed.

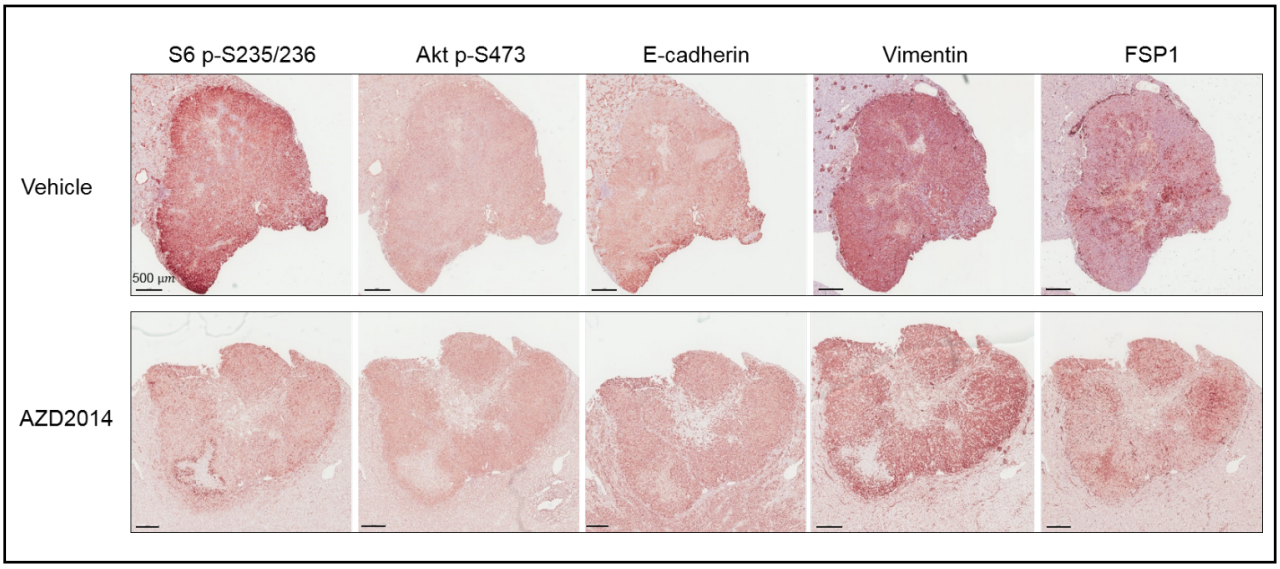

Figure 3.11 mTOR signalling and EMT status in an AZD2014 treated large solid tumour. Kidneys from 16 months old *Tsc2*$^{+/-}$ mice after 2 months treatment with either AZD2014 or vehicle were dissected for IHC. Kidneys were fixed, processed, sectioned and stained to assess mTOR signalling and EMT. Phosphorylation of S6 at S235/236 and Akt at S473 were used to assess mTORC1 and mTORC2 signalling, respectively. Protein levels of E-cadherin, vimentin and FSP1 were used to assess EMT. Solid black lines indicate scale bars.

3.3 Discussion

Tsc1$^{+/-}$ or *Tsc2*$^{+/-}$ mice spontaneously develop renal tumours including cysts, papillary adenomas and solid carcinomas (Onda et al. 1999; Wilson et al. 2005). These mice provide an invaluable model for investigating the efficacy of therapeutic agents for treating TSC-associated tumours and the mechanisms underlying tumorigenesis. In this study, mTOR signalling and EMT status were first examined in renal tumours of *Tsc2*$^{+/-}$ mice and TSC patients. As reported previously, both mTORC1 and mTORC2 were activated in mouse renal tumours (Yang et al. 2015; Narov *et al.* 2017). In human TSC-associated AML and RCC, mTORC1 and mTORC2 were also activated. Increased expression of mesenchymal markers was observed in solid renal tumours from *Tsc2*$^{+/-}$ mice and TSC-associated AML and RCC from TSC patients. Data obtained from this study support the notion that the aberrant activation of mTOR promotes EMT in tumours (Jacinto et al. 2004; Lamouille and Derynck 2007; Gulhati et al. 2011). The results presented here are also consistent with previous findings in AML and LAM of TSC patients (Barnes et al. 2010; Bi et al. 2017). AML and LAM are believed to be mesenchymal tumours, although the origin of these tumours remains unknown. (Barnes et al. 2010; Bi et al. 2017). In a previous study,TSC2 was found to be required for the normal localisation of E-cadherin on the cytoplasmic membrane in epithelial cells and loss of *Tsc2* might lead to EMT associated with the mis-localisation of E-cadherin via activation of the mTOR pathway (Barnes et al. 2010).Taken together, these results indicate that EMT occurs in TSC-associated AML and LAM, despite previous suggestions of their mesenchymal origin.

In this study, partial EMT, not complete EMT, was found to be a dominant feature in TSC-associated tumours shared between mouse and human. Partial EMT represents an intermediate stage of EMT in a cell showing both epithelial and mesenchymal characteristics or leading to hybrid cells with an epithelial and mesenchymal phenotype (Grigore *et al.* 2016; Jolly *et al.* 2016a; Nieto et al. 2016). Partial EMT could facilitate the reverse process of mesenchymal-epithelial transition (MET) for metastatic colonisation (Lecharpentier et al. 2011). It may also make tumour cells more prone to acting like cancer-stem cells. Hybrid cells of partial EMT have been observed in clusters of circulating tumour cells of cancer patients and may give these cells a migratory advantage whilst retaining some degree of cell-cell-adhesion (Lecharpentier et al. 2011; Rhim *et al.* 2012; Jolly et al. 2016a).

Thus far, the majority of research investigating EMT has been explored in cultured cancer cell lines or xenograft models of cancer. Grosse-Wilde *et al* showed the co-expression of epithelial surface marker CD24 and mesenchymal stem cell marker CD44 on a HMLER breast cancer cell line and that these cells co-express epithelial and mesenchymal genes (Grosse-Wilde *et al.* 2015). Co-expression of epithelial and mesenchymal genes have also been observed in lung cancer and brain tumours (Jeevan *et al.* 2016; Jolly et al. 2016a). Studies have more recently used lineage tracking to determine EMT status and assess the function of EMT-inducing transcription factors in tumour progression and metastasis in transgenic mouse models. A transgenic model of pancreatic cancer was used for lineage-tracking through a Pdx-Cre;$Rosa^{YFP}$ system in premalignant lesions to determine the epithelial-mesenchymal states (Rhim et al. 2012). In the current study, MS-IHC, a simple technique, was used to directly characterize individual tumour cells that co-expressed epithelial and mesenchymal markers during tumour progression from cystic lesions to papillary adenomas and solid carcinomas in the kidneys of *Tsc2*$^{+/-}$ mice and proposed a new model of EMT activation during tumour progression. Further studies are, however, required to confirm and refine the roles of partial EMT in tumour progression in these mice, and could be undertaken by generating a series of conditional deletions of EMT-inducing transcription factors. Most tumours in TSC patients are benign (often classified as hamartomas) and there is little evidence of metastatic disease from renal tumours in *Tsc2*$^{+/-}$ mice. Nonetheless, a metastatic mechanism appears to be operating in the *TSC2*-associated lung disease lymphangioleiomyomatosis (LAM) (Henske and McCormack 2012) that is common in females affected by TSC, and lung metastasis occurs from renal cancers in *Tsc1*$^{+/-}$ mice (Wilson et al. 2005). It may be interesting to explore the relationship of EMT to LAM and to tumour progression and lung metastasis in *Tsc1*$^{+/-}$ mice.

ATP-competitive inhibitors of mTOR have been developed to overcome the limitations of rapalogs. ATP-competitive inhibitors such as NVP-BEZ235 and GSK2126458 (dual inhibitors of PI3K and mTOR) have demonstrated anti-tumour efficacy in renal tumours in *Tsc2*$^{+/-}$ mice (Pollizzi et al. 2009b; Narov et al. 2017). In this study, AZD2014 and rapamycin were compared for their anti-tumour efficacy for renal lesions in *Tsc2*$^{+/-}$ mice and both successfully reduced tumour burden. AZD2014 has previously shown anti-tumour efficacy in various cancer cell lines and xenograft models (Pike et al. 2013; Guichard et al. 2015). Importantly, AZD2014 could overcome resistance of tumour cells to rapalogs (Vandamme *et al.* 2016; Kim *et al.* 2017). AZD2014 was reported to have superior anti-tumour efficacy to rapamycin in xenograft models of RCC and

hepatocellular carcinoma (Liao et al. 2014; Zheng et al. 2015). In contrast, AZD2014 in the current study was observed to have similar anti-tumour efficacy to that of rapamycin. The discrepancy between this study and previous ones, possibly reflects differences between studies in tumour types and model systems. A first-in-human pharmacokinetic and pharmacodynamic study observed limited responses to AZD2014 in a patient with breast cancer and a patient with pancreatic cancer (Basu *et al.* 2015). However, a recent randomised phase 2 clinical trial in patients with VEGF-refractory metastatic clear cell renal cancer reported that AZD2014 was less effective than everolimus (a rapamycin derivative) (Powles *et al.* 2015). Combination of AZD2014 and other anti-tumour agents may improve therapeutic efficacy as described in preclinical models of various malignancies (Harada *et al.* 2015; Singleton *et al.* 2015; Li and Cui 2016). AZD2014 has been initiated in over 20 clinical trials, as a single treatment or as a combinational treatment with other chemotherapeutic agents, in the past year (https://clinicaltrials.gov/ct2/results?cond=azd2014&term=&cntry1=&state1=&recrs=). Treatment of patients with TSC using ATP-competitive PI3K/mTOR inhibitors has not been documented although a clinical trial has recently been planned to treat patients with *TSC1/2* mutated refractory solid cancer using AZD2014 (https://www.findmecure.com/clinicaltrials/show/nct03166176). Considering the encouraging but limited response of TSC-associated tumours to rapamycin or its derivatives (Bissler et al. 2008; Davies et al. 2011; Bissler et al. 2013; Kim et al. 2014), further studies comparing the therapeutic efficacy of AZD2014 with rapamycin or its derivatives in clinical settings may be are warranted.

AZD2014 was found to consistently inhibit mTORC1 and mTORC2 signalling pathways *in vitro* and *in vivo* whilst rapamycin was found to strongly inhibit mTORC1 but only to partially inhibit mTORC2 in this study (Liao et al. 2014; Guichard et al. 2015; Yang et al. 2015). The limited efficacy of rapalogs is suggested to be due to the loss of negative feedback on PI3K/Akt signalling and inability to effectively inhibit phosphorylation of 4E-BP1 (O'Reilly et al. 2006; Thoreen et al. 2009). No increased phosphorylation of Akt at S473 and 4E-BP1 at T37/46 was observed following rapamycin treatment in solid carcinomas of this study although some cystic lesions exhibited increased phosphorylation of Akt at S473. In addition, AZD2014 was not more efficacious than rapamycin for these TSC-associated tumours, suggesting that other unidentified mechanisms may contribute to the limited efficacy of rapalogs, and that mTORC2 inhibition may not be required for treating these tumours.

Both AZD2014 and rapamycin were found to suppress EMT while reducing the burden of all types of renal tumours in *Tsc2*$^{+/-}$ mice. Only one single large solid tumour was resistant to AZD2014. EMT suppression may, therefore, contribute to the anti-tumour efficacy of mTOR inhibitors. AZD2014 and rapamycin have also shown inhibition of EMT in cultured hepatoma cells, with AZD2014 having greater effects (Liao et al. 2014). The ATP-competitive mTOR inhibitor, Torin 1, and rapamycin suppress EMT in cultured glioblastoma cells (Catalano *et al.* 2015). EMT is activated and controlled through multiple complex regulatory networks in tumours (Kalluri and Weinberg 2009; Thiery *et al.* 2009). Targeting these networks in combination with mTOR inhibition may deliver alternative opportunities for therapy of refractory tumour types and eradiation of cancer stem cells (Davis *et al.* 2014; Deng *et al.* 2016; Marcucci *et al.* 2016). Further studies are necessary to fully understand the signalling pathways involved in EMT in TSC-associated tumours, such as the transforming growth factor β (TGFβ) signalling pathway, a potent driver of EMT and tumour progression (Massague 2012).

In conclusion, partial EMT, possibly driven by aberrant activation of mTOR, is a shared feature of TSC-associated renal tumours in humans and mice, and occurs during TSC-associated tumour progression. Both AZD2014 and rapamycin effectively reduced tumour burden and suppressed tumour-associated EMT. EMT-related signalling pathways may represent therapeutic targets for tumours associated with mutations in the TSC genes or the mTOR pathway. EMT is controlled by many complex regulatory signalling pathways to drive the expression or repression of genes. Further investigations are required to fully understand the mechanisms of EMT in these tumours. It is worthwhile to test whether combination of EMT inhibitors with mTOR inhibitors could improve therapy for TSC-associated tumours.

4 CHAPTER FOUR

Dual Inhibition of Glycolysis and Glutaminolysis for Therapy of Renal Lesions in a *Tsc2*$^{+/-}$ Mouse Model

4.1 Introduction

As discussed previously, rapalogs are effective for most TSC-associated tumours but some tumours may show little or no response to treatment. Tumours that show resistance to rapamycin and ATP-competitive inhibitors of mTOR require alternative therapeutic strategies. Aberrant cellular metabolism is considered a hallmark of cancer (Hanahan and Weinberg 2011). Tumour cells reprogram their metabolism to ensure that their bioenergetic, biosynthetic and redox needs are met for rapid proliferation (Vander Heiden et al. 2009). Increased aerobic glycolysis (Warburg effect) and glutaminolysis render these cells addicted to glucose and glutamine (Lu *et al.* 2010). mTOR signalling is a central regulator of cellular metabolism and promotes glycolysis and glutaminolysis through the upregulation of genes such as *HIF1*α and *c-myc* (Cantor and Sabatini 2012; Masui et al. 2013; Zha et al. 2014; Altman et al. 2016). The dependence of mTOR-driven tumours, such as TSC-associated tumours, on cellular metabolism provides a potential target for therapeutic intervention.

Metabolic inhibition for anti-tumour therapy is frequently investigated in pre-clinical cancer models. 3-bromopyruvate (3-BrPA) is an effective glycolysis inhibitor through alkylating glycolytic enzymes, such as hexokinase II and GAPDH (Tang *et al.* 2012; Sun et al. 2015; Lis et al. 2016). 3-BrPA has shown anti-tumour efficacy in cancer models *in vitro* through the depletion of ATP with minimal toxicity to normal cells. 3-BrPA is also very effective for treating liver carcinomas in rabbit and mouse models (Ko *et al.* 2012). CB-839 is an allosteric selective inhibitor of glutaminase (GLS). It has shown promise in early cancer studies in triple negative breast cancer models and RCC *in vitro* and *in vivo* (Gross et al. 2014; Emberley *et al.* 2017). CB-839 has also shown to modulate mTOR signalling in these models and has been reported to show anti-tumour efficacy in combination with mTOR inhibitors (Tanaka et al. 2015; Lampa et al. 2017). CB-839 is currently being investigated in several clinical trials as a single agent or in combination with other therapeutics for various types of cancer (https://clinicaltrials.gov/ct2/results?cond=&term=cb839&cntry=&state=&city=&dist=).

Tsc1 or *Tsc2* null cells are highly dependent on glucose for survival. It has previously been reported that *Tsc1* or *Tsc2* null MEFs with activated mTOR show addiction to glucose (Choo et al. 2010; Jiang et al. 2011). Glycolytic inhibition in a mouse model transplanted with *Tsc2* null rat tumour cells resulted in the suppression of tumour growth (Jiang et al. 2011). Activation of mTORC1 is also associated with glutamine addiction in *Tsc2* null MEFs, as seen by increased glutamine consumption and elevated glutaminolysis (Choo et al. 2010; Csibi et al. 2013). Further investigation is required, however, to explore glutaminolysis *in vivo*. Inhibition of glutamine anaplerosis with glycolytic inhibition can cause significant cell death in $Tsc2^{-/-}$ but not $Tsc2^{+/+}$ MEF cells (Csibi et al. 2013). It remains to be determined whether dual inhibition of glycolysis and glutaminolysis has an anti-tumour efficacy in TSC-associated tumours *in vivo*.

In this study, the metabolic status of TSC-associated renal tumours was determined and the therapeutic efficacy of the dual inhibition of glycolysis and glutaminolysis with 3-BrPA and CB-839 was tested for renal tumours in $Tsc2^{+/-}$ mice. The effects of single or combinational treatment on mTOR signalling were also compared in normal and tumour cells.

4.2 Results

4.2.1 mTOR signalling and expression of proteins associated with glycolysis and glutaminolysis in renal tumours of *Tsc2*$^{+/-}$ mice

Tsc2$^{+/-}$ mice at 14 months of age were culled to investigate mTOR signalling and expression of enzymes associated with glycolysis and glutaminolysis in renal lesions including cysts, papillary adenomas and solid carcinomas by IHC. As seen in chapter 3, mTORC1 and mTORC2 were activated in these lesions indicated by the increased phosphorylation of S6 at S235/236, 4E-BP1 at T37/46, Akt at S473 and PKC at S657 (Figure 4.1A). To analysis the metabolic status of these lesions, enzymes essential to glycolysis and glutaminolysis were examined. Glycolytic enzymes investigated included GAPDH and HKII. Glutaminolytic enzymes investigated included GLS and GDH. As shown in figure 4.1B, GAPDH is highly expressed in papillary adenomas and solid carcinomas whereas HKII was highly expressed in solid carcinomas but less expressed in papillary adenomas. GLS is significantly expressed in solid carcinomas but its expression was variable in papillary adenomas. GDH was highly expressed in both papillary adenomas and solid carcinomas. The expression of MCT1 was also examined as it is required for efficient delivery of 3-BrPA to tumour cells (Birsoy *et al.* 2013). As seen in figure 4.1C, the expression of MCT1 was highly expressed in all types of renal lesion.

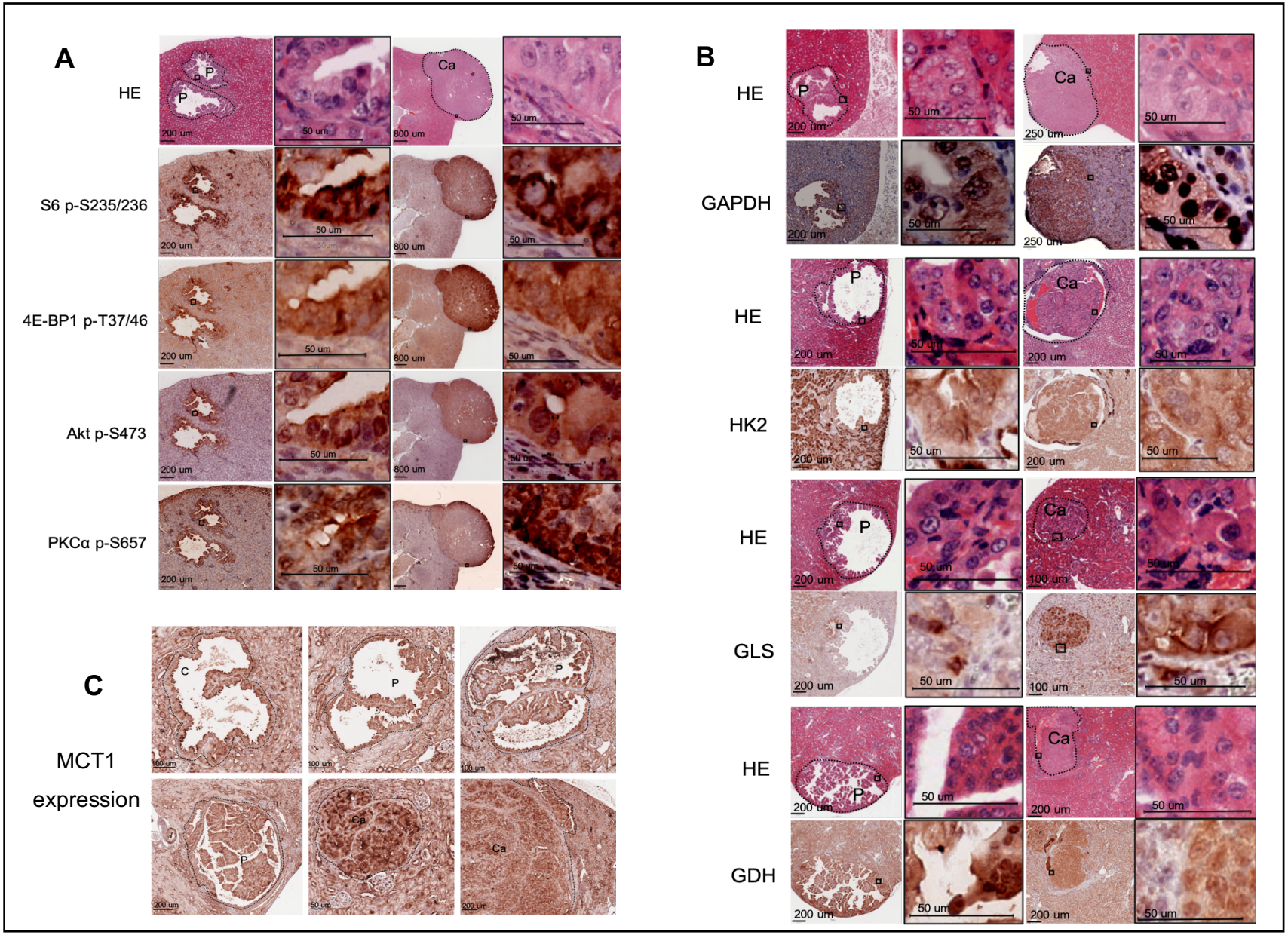
A
HE
S6 p-S235/236
4E-BP1 p-T37/46
Akt p-S473
PKCα p-S657
P
Ca
200 um
50 um
800 um
B
HE
GAPDH
HE
HK2
HE
GLS
HE
GDH
250 um
100 um
C
MCT1
expression
C
P
Ca

Figure 4.1 mTOR signalling and expression of proteins involved in glycolysis and glutaminolysis in renal tumours of *Tsc2*$^{+/-}$ mice. Kidneys from *Tsc2*$^{+/-}$ mice were dissected at 14 months old for IHC. Kidneys were fixed, processed, sectioned and used for IHC. **(A)** mTOR signalling by multiple sequential IHC (MS-IHC). The same kidney section was subjected to 3 rounds of IHC to detect phosphorylation of S6 at S235/236, 4E-BP1 at T37/46 and Akt at S473. Phosphorylation of PKCα at S657 was stained on a separate adjacent section. Black boxes indicate high power views in adjacent image. **(B)** Expression of enzymes crucial for glycolysis and glutaminolysis in renal tumours by IHC. Enzymes analysed include GAPDH, HKII, GLS and GDH. Black boxes indicate high power views in adjacent image **(C)** Detection of MCT1 in renal lesions of *Tsc2*$^{+/-}$ mice. Sections were stained with MCT1 antibody in cystic lesions, papillary adenomas and solid carcinomas. Solid black lines represent scale bar. C: Cystic lesion; P: papillary adenomas; Ca: solid carcinoma. Solid black lines represent scale bar

4.2.2 Therapeutic efficacy of the dual inhibition of glycolysis and glutaminolysis for renal tumours in *Tsc2*$^{+/-}$ mice

Firstly, the maximum tolerated dosage (MTD) of both 3-BrPA and CB-839 were established in a two-week pilot study. All mice used were bred on a balb/c background and genotyped through PCR. Mice were treated at increasing dosages every 2 days until toxicity was observed. Treatment with 3-BrPA showed rapid weight loss at a dosage of 4mg/kg. Treatment with CB-839 showed no signs of toxicity up to the maximum dosage of 200mg/kg. Therefore, it was determined that the lower dosage of 3mg/kg body weight once a day five times a week was the MTD for 3-BrPA via IP and 200mg/kg body weight twice a day, 7 days a week for CB-839 via gavage.

A total of 132 mice were randomly allocated into 7 treatment groups: vehicle (n=17), 3-BrPA (n=19), CB-839 (n=20), rapamycin (n=20), 3-BrPA + rapamycin (n=18), CB-839 + rapamycin (n=20) and 3-BrPA + CB-839 (n=18), as summarised in Table 4.1. Mice were treated for 2 months from 12 months of age. Three mice from the 3-BrPA treatment group, 3 mice from the 3-BrPA + rapamycin group and 4 mice from the 3-BrPA + CB-839 group were culled within the 1st month of treatment and were excluded from analysis due to dramatic weight loss. After treatment, mice were killed and kidneys harvested for tumour burden assessment by histological analysis. To evaluate tumour burden, renal lesions were characterised, counted and measured for their whole area and cellular area (as described in methods 2.2.6.4). The lesion type, total lesion number, total lesion area and total lesion cellular area were documented for each animal and compared between treatment groups (Figure 4.2, 4.3 and 4.4; Table 4.2, 4.3 and 4.4). Tumour burden was compared by analysing all lesions (cystic/papillary/solid), cystic/papillary adenomas only and solid carcinomas only. Combination of 3-BrPA and CB-839 significantly reduced total lesion size (P=0.0209) and total lesion cellular area (P=0.0397). Combination of 3-BrPA and CB-839 also showed a reduction in total lesion number, but the reduction was not statistically significant (P=0.0653) (Figure 4.2, Table 4.2). Rapamycin as a monotherapy and in combination with either 3-BrPA or CB-839 significantly reduced total lesion number (P<0.0001, P<0.0001, P<0.0001), total lesion size (P<0.0001, P<0.0001, P<0.0054) and total lesion cellular area (P<0.0001, P<0.0001, P<0.0001). Rapamycin in combination with 3-BrPA or CB-839, however, did not show any enhanced therapeutic effect compared to rapamycin treatment alone (Table 4.2, Table 4.2). Furthermore, neither 3-BrPA or CB-839 as a monotherapy had any therapeutic effect on total lesion

number (P=0.5033, P=0.9459), total lesion size (P=0.6827, P=0.5168) or total lesion cellular area (P=0.6567, P=0.6191) (Figure 4.2, Table 4.2).

Neither 3-BrPA or CB-839 as a monotherapy or in combination with each other resulted in a significant decrease in total cystic/papillary adenoma number (P=0.3476, P=0.7803, P=0.1456) and total area (P=0.1270, P=0.1248, P=0.4444) (Figure 4.3, Table 4.3). Interestingly, treatment with 3-BrPA showed a significant increase in cystic/papillary cellular area (P=0.0407) but not with CB-339 monotherapy (P=0.0694) or combinational therapy (P=0.4928). Rapamycin alone or in combination with 3-BrPA or CB-839 also significantly reduced cystic/papillary adenoma total number (P<0.0001, P<0.0001, P<0.0001) and lesion cellular area (P<0.0001, P=0.0002, P=0.0009). Rapamycin reduced total size of cystic/papillary adenomas significantly (P=0.0097). Rapamycin in combination with 3-BrPA or CB-839 also reduced total size of cystic/papillary adenomas but the reduction was not statistically significant (P=0.1136, P=0.7980) (Figure 4.3, Table 4.3).

Combination of 3-BrPA and CB-839 significantly reduced total number (P=0.0311), size (P=0.0220) and cellular area (P=0.0226) of solid carcinomas. Rapamycin alone and in combination with 3-BrPA or CB-839 also significantly reduced solid carcinoma number (P<0.0001, P<0.0001, P<0.0001), size (P<0.0001, P<0.0001, P<0.0001) and cellular area (P<0.0001, P<0.0001, P<0.0001). Again, 3-BrPA or CB-839 as monotherapy had no overall effect on solid carcinomas (Figure 4.4, Table 4.4).

Rapamycin alone was consistently more effective at reducing tumour burden of all lesions (cystic/papillary adenomas and solid carcinomas) and solid carcinomas only compared to 3-BrPA, CB-839 or both with respect to lesion number, size and cellular area (Table 4.2, 4.3, 4.4).

Table 4.1 Treatment summary

Treatment Group	Number of *Tsc2*$^{+/-}$ mice	Number of males	Number of females	Treatment start age (months)	Treatment end age (months)	Dosage*	Number of animals killed due to loss of body weight within the first month of treatment**
Vehicle	17	8	9	12	14	10ul/g	0
3-BrPA	19	9	10	12	14	3mg/kg	3
CB-839	20	9	11	12	14	200mg/kg	0
Rapamycin	20	8	12	12	14	4mg/kg	0
3-BrPA+Rapamycin	18	8	10	12	14	3mg/kg + 4mg/kg	3
CB-839+Rapamycin	20	8	12	12	14	200mg/kg + 4mg/kg	0
3-BrPA+CB-839	18	8	10	12	14	3mg/kg + 200mg/kg	4

* *Tsc2*$^{+/-}$ mice were treated twice daily with veihcle or CB-839 via gavage, and 5 times a week with 3-BrPA or rapamycin via intraperitoneal injection.
* *These mice were killed due to significant loss of body weight within the first month of treatment.

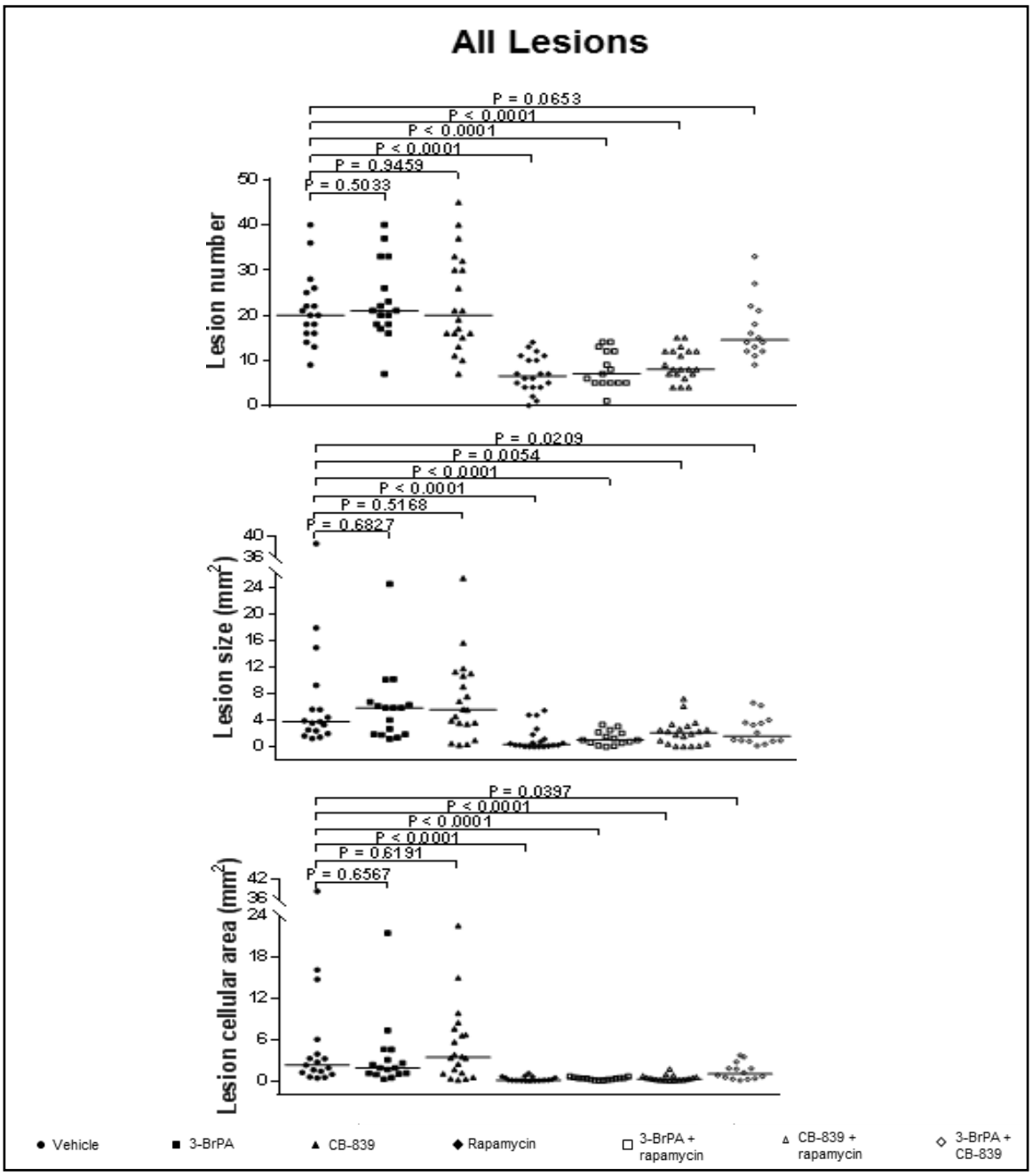

Figure 4.2 Anti-tumour efficacy of dual inhibition of glycolysis and glutaminolysis in all renal lesions of *Tsc2*$^{+/-}$ mice. One hundred and thirty-two *Tsc2*$^{+/-}$ mice were randomly allocated to 7 treatment groups of vehicle (n=17), 3-BrPA (n=19), CB-839 (n=20), rapamycin (n=20), 3-BrPA + rapamycin (n=18), CB-839 + rapamycin (n=20) and 3-BrPA + CB-839 (n=18). Mice were treated from 12 months of age for 2 months. Three mice from the 3-BrPA group, 3 mice from the 3-BrPA+rapamycin group and 4 mice from the 3-BrPA+CB-839 group were euthanized due to significant loss of body weight within the first month of treatment and excluded from further analysis in this study. On treatment end date, mice were culled and kidneys collected for histological analysis. Kidneys were fixed, processed, sectioned and stained with H&E to assess tumour burden. Kidney tumours were located, counted, characterised and measured for comparison of treatment efficacy. Comparison of total lesion number, size and cellular area of all types of lesion (cyst, papillary adenoma and solid carcinoma). Horizontal bars represent the median. P<0.05 is considered significant.

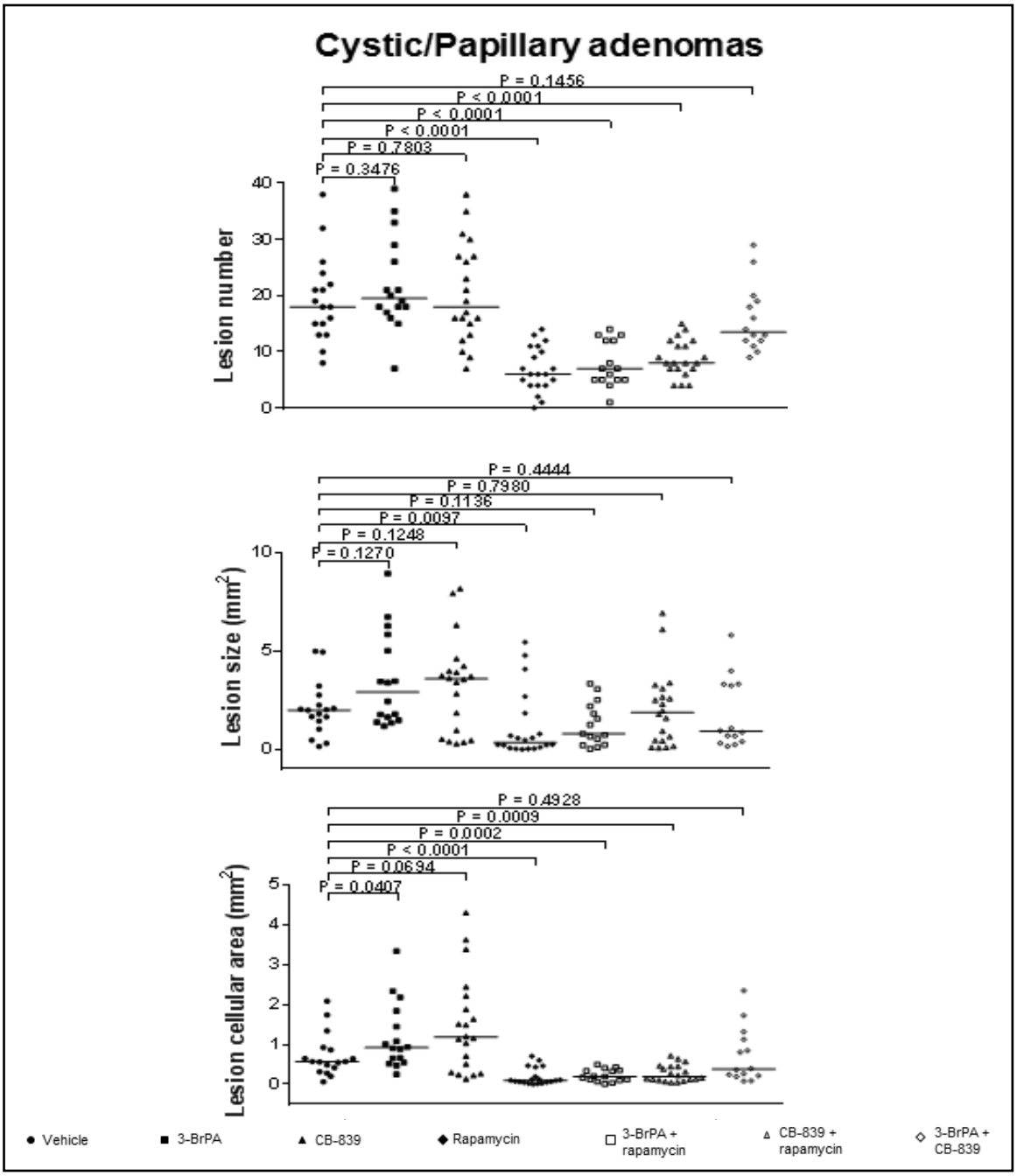

Figure 4.3 Anti-tumour efficacy of dual inhibition of glycolysis and glutaminolysis in cystic/papillary adenomas of *Tsc2*$^{+/-}$ mice. One hundred and thirty-two *Tsc2*$^{+/-}$ mice were randomly allocated to 7 treatment groups of vehicle (n=17), 3-BrPA (n=19), CB-839 (n=20), rapamycin (n=20), 3-BrPA + rapamycin (n=18), CB-839 + rapamycin (n=20) and 3-BrPA + CB-839 (n=18). Mice were treated from 12 months of age for 2 months. Three mice from the 3-BrPA group, 3 mice from the 3-BrPA+rapamycin group and 4 mice from the 3-BrPA+CB-839 group were euthanized due to significant loss of body weight within the first month of treatment and excluded from further analysis in this study. On treatment end date, mice were culled and kidneys collected for histological analysis. Kidneys were fixed, processed, sectioned and stained with H&E to assess tumour burden. Cystic/papillary adenomas from individual mice were located, counted, measured and compared between treatment groups. Horizontal bars represent the median. P<0.05 is considered significant.

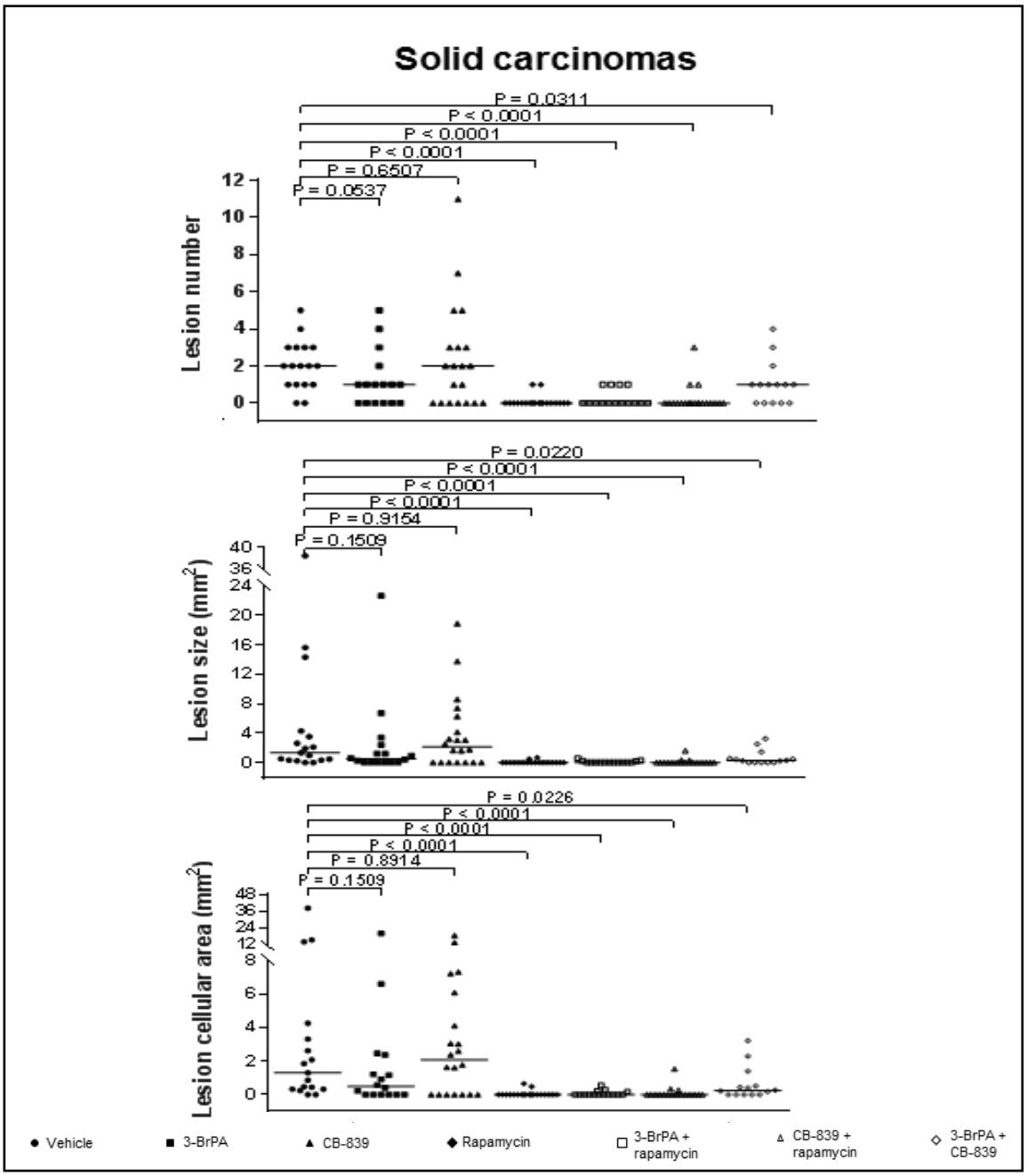

Figure 4.4 Anti-tumour efficacy of dual inhibition of glycolysis and glutaminolysis in solid carcinomas of *Tsc2*$^{+/-}$ mice. One hundred and thirty-two *Tsc2*$^{+/-}$ mice were randomly allocated to 7 treatment groups of vehicle (n=17), 3-BrPA (n=19), CB-839 (n=20), rapamycin (n=20), 3-BrPA + rapamycin (n=18), CB-839 + rapamycin (n=20) and 3-BrPA + CB-839 (n=18). Mice were treated from 12 months of age for 2 months. Three mice from the 3-BrPA group, 3 mice from the 3-BrPA+rapamycin group and 4 mice from the 3-BrPA+CB-839 group were euthanized due to significant loss of body weight within the first month of treatment and excluded from further analysis in this study. On treatment end date, mice were culled and kidneys collected for histological analysis. Kidneys were fixed, processed, sectioned and stained with H&E to assess tumour burden. Solid carcinomas from individual mice were located, counted, measured and compared between treatment groups. Horizontal bars represent the median. P<0.05 is considered significant.

Table 4.2 Comparison of all lesions in *Tsc2*$^{+/-}$mice by histological analysis (Mann Whitney test)

I. Lesion number (all lesions: cystic/papillary adenomas and solid carcinomas)

Treatment	Number of mice	Median	Range	P (compared with Vehicle)	P (compared with Rapamycin)
Vehicle	17	20.0	9-40	-	<0.0001
3-BrPA	16	21	7-40	0.5033	<0.0001
CB-839	20	20	7-45	0.9459	<0.0001
Rapamycin	20	6.5	0-14	<0.0001	-
3-BrPA+Rapamycin	15	7	1-14	<0.0001	0.4028
CB-839+Rapamycin	20	8	4-15	<0.0001	0.0714
3-BrPA+CB-839	14	14.5	9-33	0.0653	<0.0001

II. Lesion size (all lesions: cystic/papillary adenomas and solid carcinomas)

Treatment	Number of mice	Median (mm^2)	Range (mm^2)	P (compared with Vehicle)	P (compared with Rapamycin)
Vehicle	17	3.785335147	1.2727-38.6207	-	<0.0001
3-BrPA	16	5.8634575	1.1981-24.4641	0.6827	<0.0001
CB-839	20	5.616098723	0.2831-25.3557	0.5168	<0.0001
Rapamycin	20	0.359455835	0.000-5.4720	<0.0001	-
3-BrPA+Rapamycin	15	1.030499248	0.0229-3.3532	<0.0001	0.1905
CB-839+Rapamycin	20	2.136923107	0.0733-7.2202	0.0054	0.0524
3-BrPA+CB-839	14	1.603310134	0.1591-6.6137	0.0209	0.0136

III. Lesion cellular area (all lesions: cystic/papillary adenomas and solid carcinomas)

Treatment	Number of mice	Median (mm^2)	Range (mm^2)	P (compared with Vehicle)	P (compared with Rapamycin)
Vehicle	17	2.286726736	0.4163-38.5323	-	<0.0001
3-BrPA	16	1.870045278	0.2487-21.4734	0.6567	<0.0001
CB-839	20	3.430030709	0.1337-22.5655	0.6191	<0.0001
Rapamycin	20	0.094071078	0.0000-1.0937	<0.0001	-
3-BrPA+Rapamycin	15	0.330887242	0.0094-0.6590	<0.0001	0.2022
CB-839+Rapamycin	20	0.245174903	0.0438-1.6907	<0.0001	0.0596
3-BrPA+CB-839	14	1.003887621	0.0808-3.7200	0.0397	0.0001

Table 4.3 Comparison of cystic/papillary adenomas in *Tsc2*$^{+/-}$mice by histological analysis (Mann Whitney test)

I. Lesion number (cystic/papillary adenomas)

Treatment	Number of mice	Median	Range	P (compared with Vehicle)	P (compared with Rapamycin)
Vehicle	17	18.0	8-38	-	<0.0001
3-BrPA	16	19.5	7-39	0.3476	<0.0001
CB-839	20	18	7-38	0.7803	<0.0001
Rapamycin	20	6	0-17	<0.0001	-
3-BrPA+Rapamycin	15	7	1-14	<0.0001	0.4709
CB-839+Rapamycin	20	8	4-15	<0.0001	0.0883
3-BrPA+CB-839	14	13.5	9-29	0.1456	<0.0001

II. Lesion size (cystic/papillary adenomas)

Treatment	Number of mice	Median (mm^2)	Range (mm^2)	P (compared with Vehicle)	P (compared with Rapamycin)
Vehicle	17	1.9954	0.1489-5.0014	-	0.0097
3-BrPA	16	2.924	1.1981-8.9687	0.127	0.0002
CB-839	20	3.5994	0.2831-8.2014	0.1248	0.0016
Rapamycin	20	0.3595	0.0000-5.4719	0.0097	-
3-BrPA+Rapamycin	15	0.7972	0.0229-3.3531	0.1136	0.2680
CB-839+Rapamycin	20	1.8811	0.0733-6.9529	0.798	0.0596
3-BrPA+CB-839	14	0.9182	0.1591-5.8273	0.4444	0.0657

III. Lesion cellular area (cystic/papillary adenomas)

Treatment	Number of mice	Median (mm^2)	Range (mm^2)	P (compared with Vehicle)	P (compared with Rapamycin)
Vehicle	17	0.575	0.0605-2.0908	-	<0.0001
3-BrPA	16	0.9197	0.2487-3.3439	0.0407	<0.0001
CB-839	20	1.1826	0.1337-4.3088	0.0694	<0.0001
Rapamycin	20	0.0941	0.0000-0.7061	<0.0001	-
3-BrPA+Rapamycin	15	0.1952	0.0094-0.4945	0.0002	0.2538
CB-839+Rapamycin	20	0.1944	0.0438-0.7138	0.0009	0.0596
3-BrPA+CB-839	14	0.3805	0.0809-2.3537	0.4928	0.0017

Table 4.4 Comparison of solid carcinomas in *Tsc2*$^{+/-}$mice by histological analysis (Mann Whitney test)

I. Lesion number (solid carcinomas)

Treatment	Number of mice	Median	Range	P (compared with Vehicle)	P (compared with Rapamycin)
Vehicle	17	2	0-5	-	<0.0001
3-BrPA	16	1	0-5	0.0537	0.0007
CB-839	20	2	0-11	0.6507	<0.0001
Rapamycin	20	0	0-1	<0.0001	-
3-BrPA+Rapamycin	15	0	0-1	<0.0001	0.3670
CB-839+Rapamycin	20	0	0-3	<0.0001	0.7367
3-BrPA+CB-839	14	1	0-4	0.0311	0.0007

II. Lesion size (solid carcinomas)

Treatment	Number of mice	Median (mm^2)	Range (mm^2)	P (compared with Vehicle)	P (compared with Rapamycin)
Vehicle	17	1.306566589	0.0000-38.4718	-	<0.0001
3-BrPA	16	0.498485636	0.0000-22.6609	0.1509	0.0004
CB-839	20	2.133097756	0.0000-18.8883	0.9154	<0.0001
Rapamycin	20	0	0.0000-0.6625	<0.0001	-
3-BrPA+Rapamycin	15	0	0.0000-0.5603	<0.0001	0.3564
CB-839+Rapamycin	20	0	0.0000-1.6070	<0.0001	0.8683
3-BrPA+CB-839	14	0.27172263	0.0000-3.2353	0.022	0.0016

III. Lesion cellular area (solid carcinomas)

Treatment	Number of mice	Median (mm^2)	Range (mm^2)	P (compared with Vehicle)	P (compared with Rapamycin)
Vehicle	17	1.306566589	0.0000-38.4718	-	<0.0001
3-BrPA	16	0.496839797	0.0000-20.3648	0.1509	0.0004
CB-839	20	2.083626722	0.0000-18.8102	0.8914	<0.0001
Rapamycin	20	0	0.0000-0.6625	<0.0001	-
3-BrPA+Rapamycin	15	0	0.0000-0.5603	<0.0001	0.3564
CB-839+Rapamycin	20	0	0.0000-1.5417	<0.0001	0.8683
3-BrPA+CB-839	14	0.242979687	0.0000-3.2353	0.0226	0.0016

4.2.3 Treatment effect on mTOR signalling in the kidneys and renal tumours of *Tsc2*$^{+/-}$ mice

Western blotting and IHC were performed to determine the effect of different treatments on mTOR signalling (Figure 4.5). Tissues were harvested from non-tumourous portions of the kidney and solid renal tumours of *Tsc2*$^{+/-}$ mice after final treatment and proteins prepared for Western analysis (Figure 4.5A). Phosphorylation of mTOR at S2448, S6 at S235/236 and 4E-BP1 at T37/46 were used as markers of mTORC1 signalling. Phosphorylation of mTOR at S2481, Akt at S473 and T450, and PKCα at T638 were used as markers of mTORC2 signalling. Rapamycin alone and rapamycin in combination with 3-BrPA or CB-839 significantly decreased the phosphorylation of S6 at S235/236 in the kidneys (Figure 4.5A and 4.5B Table 4.5). Combinational treatment with 3-BrPA and CB-839 also resulted in a significant decrease in phosphorylation of S6 at S235/236 in the kidneys. 3-BrPA treatment alone also significantly reduced phosphorylation of S6 at S235/236 in the kidneys but, CB-839 treatment alone showed a significant increase in the phosphorylation of S6 at S235/236 in the kidneys (Figure 4.5A and 4.5B Table 4.5). Only rapamycin in combination with 3-BrPA showed a clear reduction in the phosphorylation of mTOR at S2448. Rapamycin in combination with 3-BrPA or CB-839 effectively reduced phosphorylation of mTOR at S2481, but rapamycin alone did not show the same effect in the kidneys (Figure 4.5A). 3-BrPA alone and rapamycin in combination with 3-BrPA or CB-836 significantly reduced phosphorylation of Akt at S473 (Figure 4.5A and 4.5C Table 4.6). Rapamycin alone caused a slight increase in phosphorylation of Akt at S473, but this was not significant (Figure 4.5A and 4.5C Table 4.6). Combinational treatment of 3-BrPA and CB-839 decreased phosphorylation of Akt at S473 but the decrease was not significant. No obvious changes were observed in the phosphorylation of PKC at T638 or Akt at T450 following treatment in the kidneys (Figure 4.5A)

Kidney sections of treated 14-month-old *Tsc2*$^{+/-}$ mice were prepared for MS-IHC (Figure 4.6). 3-BrPA or CB-839 exhibited no effect on the phosphorylation of S6 at S235/236 in all types of lesions. Rapamycin alone and rapamycin in combination with 3-BrPA or CB-839 consistently reduced the phosphorylation of S6 at S235/236 in all types of lesions. Combination of 3-BrPA and CB-839 also appeared to slightly reduce phosphorylation of S6 at S235/236 (Figure 4.6). Consistent with western analysis, 3-BrPA alone and rapamycin in combination with 3-BrPA or CB-839 appeared to reduce the

phosphorylation of Akt at S473 in all types of lesions. Combinational treatment with 3-BrPA and CB-839 also reduced phosphorylation of Akt at S473 but to a lesser degree. Rapamycin alone reduced the phosphorylation of Akt at S473 in many solid carcinomas, but a proportion of cystic/papillary adenomas showed an increased phosphorylation at this site, consistent with western analysis.

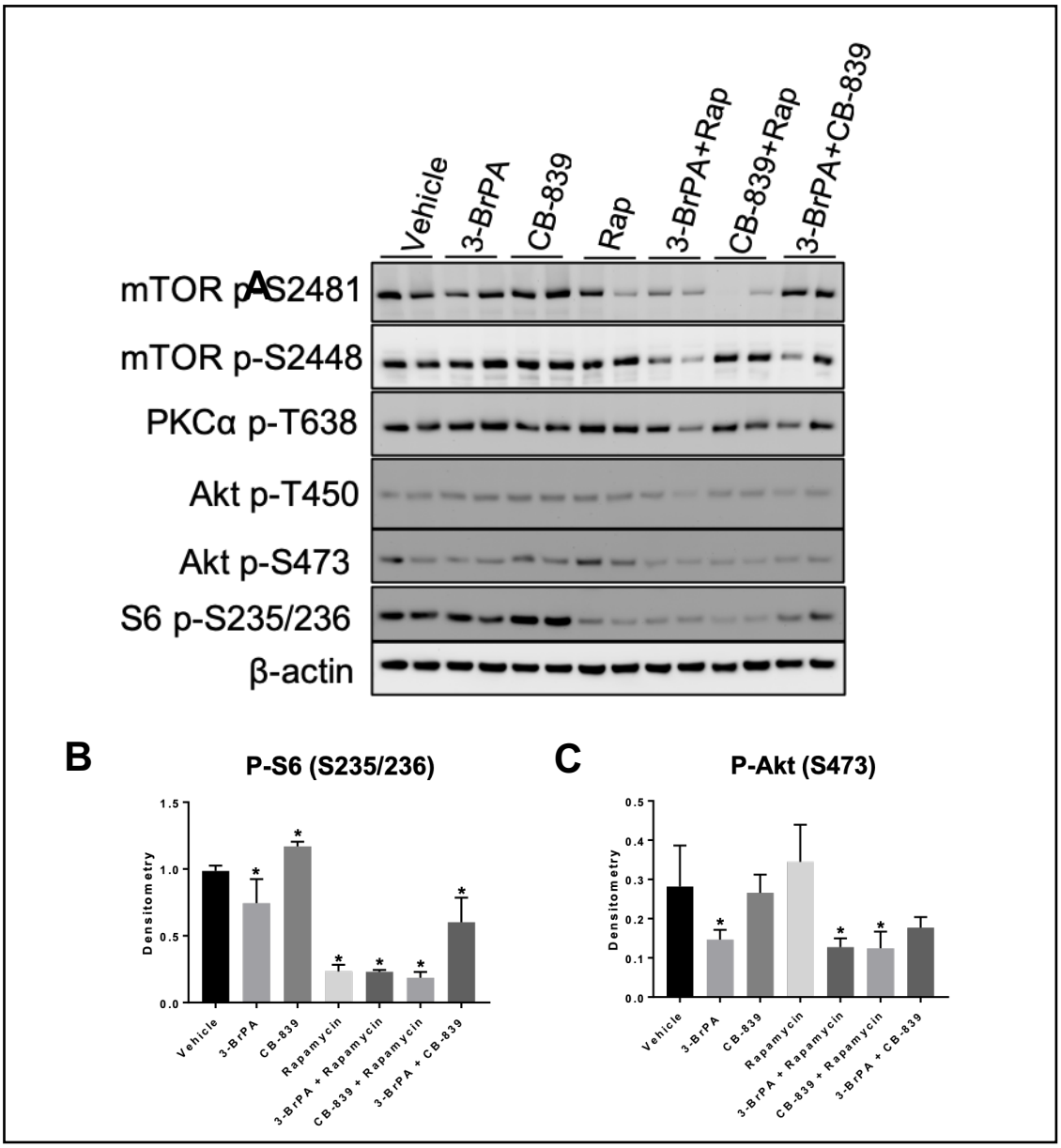

Figure 4.5 Treatment effect on mTOR signalling in the non-tumourous portion of the kidneys and renal tumours of *Tsc2*$^{+/-}$ mice (A) Effect of treatment on mTOR signalling in normal kidney tissue of *Tsc2*$^{+/-}$ mice by Western blotting. Protein samples were prepared from kidney tissue from *Tsc2*$^{+/-}$ mice after 2-months with indicated treatment. Markers used to assess mTORC1 activity include phosphorylation of mTOR at S2448 and S6 at S235/236. Markers used to assess mTORC2 activity include phosphorylation of mTOR at S2481, Akt at S473 and T450 and PKCα at T638 and. β-actin was used as a loading control. **(B)** Relative intensity of the phosphorylation of S6 at S235/236 by western blot. Four samples (n=4) were quantified for their relative intensity by image J and the average relative density was calculated for each treatment group. *: P<0.05 compared to vehicle. Error bars indicate standard deviation. **(C)** Relative intensity of the phosphorylation of Akt at S473 by western blot. Four samples (n=4) were quantified for their relative intensity by image J and the average relative intensity was calculated for each treatment group. *: P<0.05 compared to vehicle. Error bars indicate standard deviation.

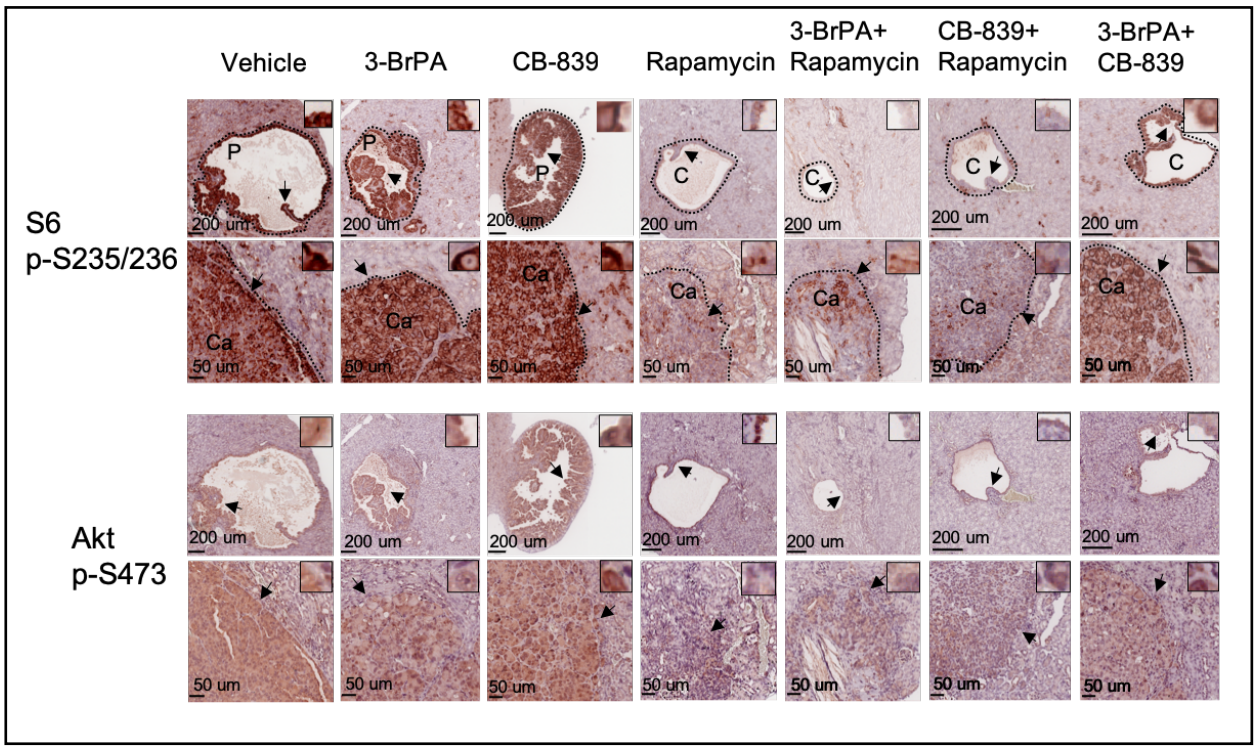

Figure 4.6 Effect of treatment on mTOR signalling in renal lesions of *Tsc2*$^{+/-}$ mice by MS-IHC. Kidneys from *Tsc2*$^{+/-}$ mice were dissected after treatment. Kidneys were fixed, processed, sectioned and stained with antibodies to assess mTOR signalling. Phosphorylation of S6 at S235/236 was used to evaluate mTORC1 activity and phosphorylation of Akt at S473 was used to evaluate mTORC2 activity. Small black boxes indicate high power views of area highlighted by black arrows. Solid black lines indicate scale bars. C: Cystic lesion; P: Papillary adenomas; Ca: Solid carcinomas.

Table 4.5 Relative density of p-S6 (S235/236) by Western blotting as quantified using Image J. (Student t-test)

Treatment	Number of blots analysed	Mean density	P- value compared to vehicle
Vehicle	4	0.98597	-
3-BrPA	4	0.74431	0.0394
CB-839	4	1.169	0.0005
Rapamycin	4	0.23373	<0.0001
3-BrPA+Rapamycin	4	0.23029	<0.0001
CB-839+Rapamycin	4	0.18567	<0.0001
3-BrPA+CB-839	4	0.60146	0.0066

Table 4.6 Relative density of p-S6 (S235/236) by Western blotting as quantified using Image J. (Student t-test)

Treatment	Number of blots analysed	Mean density	P- value compared to vehicle
Vehicle	4	0.2818	-
3-BrPA	4	0.14655	0.0457
CB-839	4	0.26552	0.7859
Rapamycin	4	0.34491	0.4047
3-BrPA+Rapamycin	4	0.12715	0.0278
CB-839+Rapamycin	4	0.12452	0.0318
3-BrPA+CB-839	4	0.17704	0.1008

4.2.4 Treatment effect on cell proliferation and apoptosis in renal tumours of *Tsc2*$^{+/-}$ mice

IHC was used to determine the effect of different treatments on cell proliferation and apoptosis in renal lesions of *Tsc2*$^{+/-}$ mice (Figure 4.7). Ki67 was used as a marker for cell proliferation (Figure 4.7A). Fifteen or more renal tumours were randomly selected per treatment group for proliferation analysis. Ki67 positive cells and total number of cells in these tumours were counted using imageJ and the percentage of Ki67 positive cells per tumour was calculated. Ki67 positive percentage of tumours was used to compare between treatment groups to evaluate its effect on proliferation (Figure 4.7B). Rapamycin alone and rapamycin in combination with either 3-BrPA or CB-839 all significantly reduced the median percentage of Ki67 positive cells from 16.3% in vehicle treated mice to 2.6% ($P<0.0001$), 1.1% ($P<0.0001$) and 0.9% ($P<0.0001$), respectively (Table 4.7). The dual inhibition of glycolysis and glutaminolysis with 3-BrPA and CB-839 also significantly reduced the median percentage of Ki67 positive cells from 16.3% to 13.3% ($P=0.0275$) (Table 4.7).

Active caspase-3 was used as a marker to examine the effect of treatment on apoptosis in renal tumours of *Tsc2*$^{+/-}$ mice by IHC (Figure 4.8). Rapamycin alone and rapamycin in combination with 3-BrPA or CB-839 reduced the protein levels of active caspase-3. Overall, in all treatments, there was no consistent increase in active caspase-3 levels compared to vehicle (Figure 4.8). Interestingly, vehicle treated tumours had a variable expression of active caspase-3 and larger solid carcinomas tend to show more cell death. This may be due to a hypoxic environment inducing cell death in the centre of large tumours.

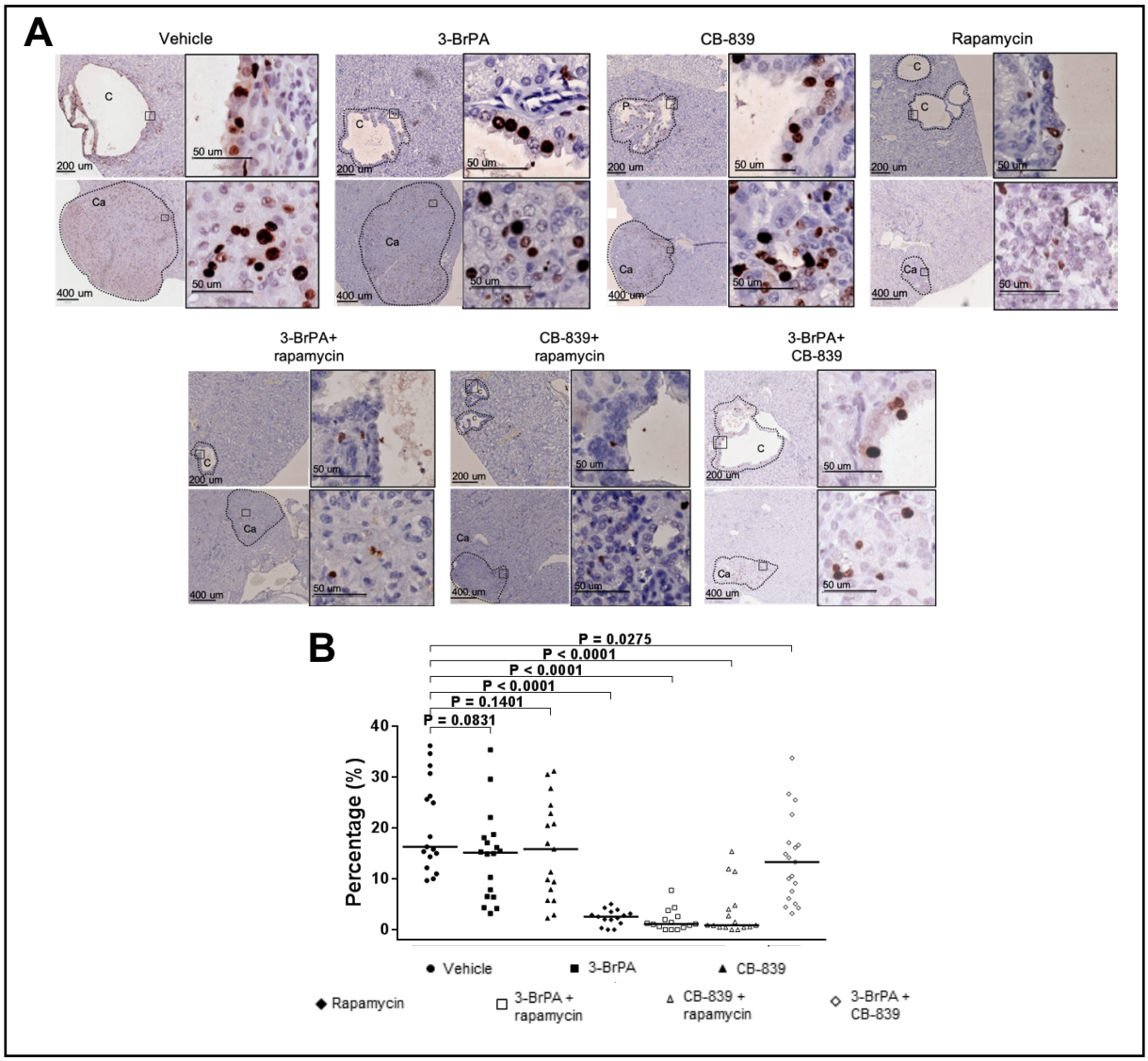

Figure 4.7 Treatment effect on cell proliferation in renal tumours of *Tsc2*$^{+/-}$ mice. **(A)** Effect of treatment on cell proliferation by IHC. Kidneys from *Tsc2*$^{+/-}$ mice were dissected after treatment. Kidneys were fixed, processed, sectioned and stained with Ki67 to assess proliferation of tumour cells. Solid black lines indicate scale bars. C: Cystic lesions; P: Papillary adenomas; Ca: Solid carcinoma **(B)** Percentage of Ki67-positive cells. Fifteen or more renal tumours from each treatment group were randomly selected for proliferation analysis. Positively stained Ki67 cells were identified and counted by imageJ and percentage of Ki67 stained cells per tumour was calculated. P<0.05 is considered significant.

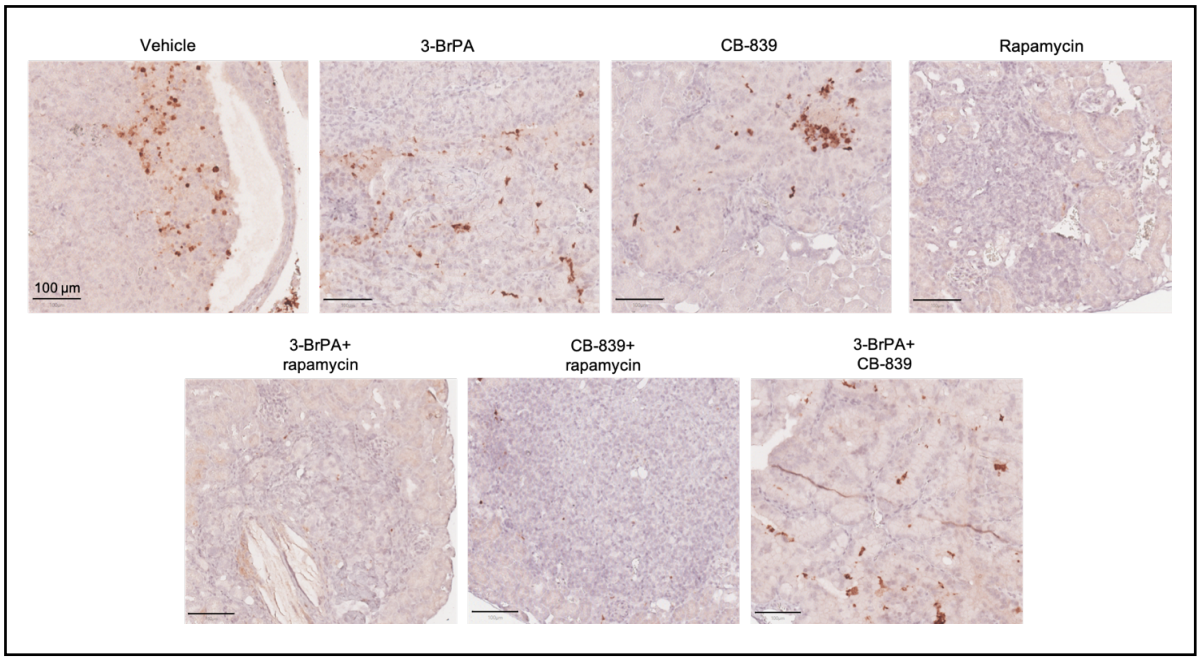

Figure 4.8 Treatment effect on apoptosis in renal tumours of *Tsc2*$^{+/-}$ mice by IHC. Kidneys from *Tsc2*$^{+/-}$ mice were dissected after treatment. Kidneys were fixed, processed, sectioned and stained with active caspase 3 to assess apoptosis of tumour cells. Solid black lines indicate scale bars.

Table 4.7 Effect of treatment on proliferation of renal tumour cells in *Tsc2*$^{+/-}$ mice (Mann Whitney test)

Treatment	Number of tumours examined	Percentage of tumour cells positive for Ki67: Median (%)	Percentage of tumour cells positive for Ki67: Range (%)	P (compared with Vehicle)	P (compared with Rapamycin)
Vehicle	17	16.2901	9.6774-36.1689	-	<0.0001
3-BrPA	18	15.137	3.2019-35.3658	0.0831	<0.0001
CB-839	17	15.849	2.2988-31.1870	0.1401	<0.0001
Rapamycin	15	2.553	0-5.0632	<0.0001	-
3-BrPA+Rapamycin	15	1.1236	0-7.7348	<0.0001	0.1862
CB-839+Rapamycin	16	0.8986	0-15.3846	<0.0001	0.6189
3-BrPA+CB-839	19	13.2979	3.2020-33.7458	0.0275	<0.0001

4.3 Discussion

Rewiring of cellular metabolism is a hallmark of cancer (Hanahan and Weinberg 2011). Reprogramming of glycolysis and glutaminolysis is required for tumour cells to generate sufficient energy and macromolecules for rapid growth and proliferation (Vander Heiden et al. 2009). Targeting glycolysis or glutaminolysis for anti-tumour therapy has been investigated in various types of cancers in pre-clinical and clinical studies (Csibi et al. 2013; Martinez-Outschoorn et al. 2017; Sun *et al.* 2017; Akins *et al.* 2018). Dual inhibition of glycolysis and glutaminolysis with 2-deoxyglucose and aminooxyacetate successfully attenuated proliferation of ovarian cancer cells *in vitro* (Sun et al. 2017). However, dual inhibition of glycolysis and glutaminolysis has not been reported for treating tumours *in viv*o thus far. Dual inhibition of glycolysis and glutaminolysis has previously shown significant cell death in *Tsc2*$^{-/-}$ but not *Tsc2*$^{+/+}$ MEFs (Csibi et al. 2013). In this study, the therapeutic efficacy of dual inhibition of glycolysis and glutaminolysis was tested for treating renal tumours in *Tsc2*$^{+/-}$ mice. Firstly, enzymes associated with glycolysis and glutaminolysis were investigated in TSC-associated renal tumours of these mice. GAPDH, HKII, GLS1 and GDH were highly expressed in solid renal carcinomas. The lactate transporter, MCT1, is an important transporter required for 3-BrPA-mediated inhibition of glycolysis (Birsoy et al. 2013) and was also increased in all types of renal lesions. Combinational treatment with 3-BrPA and CB-839 significantly suppressed tumour burden. These results suggest that dual inhibition of glycolysis and glutaminolysis may offer an alternative therapeutic strategy for treating TSC-associated renal lesions. However, rapamycin alone and rapamycin in combination with 3-BrPA or CB-839 were consistently more effective for treating renal lesions than dual inhibition of glycolysis and glutaminolysis. However, it remains to be investigated whether dual inhibition of glycolysis and glutaminolysis could be effective for TSC-associated tumours that have limited response to rapamycin. Combination of CB-839 and the rapalog everolimus has previously shown an enhanced therapeutic efficacy compared to each agent alone in a RCC xenograft model (Emberley et al. 2017).. Rapamycin in combination with CB-839 did not show any superior therapeutic effect compared to rapamycin alone here. Rapalogs in combination with CB-839 may be a beneficial option for sporadic RCC whereas rapamycin alone remains better for TSC-associated tumours.

In this study, glycolytic inhibition with 3-BrPA resulted in a slight reduction in number of solid carcinomas but this was not statistically significant. However, 3-BrPA has shown

effective anti-tumour activity for hepatocellular carcinoma, bladder cancer, nasopharyngeal carcinoma and renal carcinoma *in vitro* and *in vivo* cancer models (Ko et al. 2004; Ko et al. 2012; Konstantakou *et al.* 2015; Nilsson et al. 2015; Sun et al. 2015; Zou *et al.* 2015). 2-deoxyglucose (2-DG), another glycolysis inhibitor, has been reported to have limited efficacy as a single agent in pre-clinical models but may increase the sensitivity of other chemo preventative agents such as paclitaxel (Maschek *et al.* 2004; Zhang *et al.* 2014). A study using a mouse model transplanted with *Tsc2*-null rat tumour cells, however, has demonstrated anti-tumour efficacy using 2-DG alone (Jiang et al. 2011). Limited response of these tumours to 3-BrPA is unlikely to be caused by inefficient drug delivery since MCT1 is highly expressed in these lesions. In addition, unexpected deaths of mice treated with 3-BrPA suggest a lack of tumour specificity and greater toxicity in TSC-associated tumours.

Inhibition of glutaminolysis with CB-839 had no overall effect on tumour burden in this study. In contrast, CB-839 has shown anti-tumour efficacy in various xenografts models of cancer such as triple negative breast cancer, lung cancer and ovarian cancer (Gross et al. 2014; Xiang *et al.* 2015; Lampa et al. 2017). CB-839 in combination with other therapies was also tested in xenograft mouse models of non-small cell lung cancer and glioblastoma multiforme, and was shown to sensitise tumour cells to chemotherapeutic agents (Tanaka et al. 2015; Guo et al. 2016; Lampa et al. 2017; Momcilovic et al. 2017). CB-839 is currently being tested in phase I clinical trials in patients with solid tumours and haematological cancers (https://clinicaltrials.gov/ct2/results?cond=&term=cb-839&cntry=&state=&city=&dist=).

The limited therapeutic effect of 3-BrPA or lack of therapeutic effect of CB-839 as single agents in this study may be due to differences and unique mechanisms in tumourigenesis between tumour models used, such as in initiating mutations of specific tumour suppressors i.e. *Tsc2*, and in oncogenic signalling i.e. mTOR in *Tsc2*$^{+/-}$ mice. Lack of therapeutic efficacy of glycolysis inhibition may be related to the hyperactivation of mTORC1. Pusaputi *et al*. have suggested a mechanism of tumour cells to bypass glycolytic inhibition through sustained mTORC1 signalling (Pusapati *et al.* 2016). Increased mTORC1 signalling was responsible for shunting glucose into the pentose phosphate pathway and redirect it back into glycolysis, thus avoiding glycolytic block with 2-DG. This mechanism may exist in TSC-associated tumours. Consistent with the present study, glycolytic inhibition in combination with mTORC1 inhibition showed greater anti-tumour efficacy *in vitro* and *in vivo* than glycolytic inhibition alone (Pusapati

et al. 2016),. However, here no significant difference in anti-tumour activity was observed between 3-BrPA in combination with rapamycin and rapamycin alone in *Tsc2*$^{+/-}$ mice. Furthermore, lack of efficacy of 3-BrPA or CB-839 in TSC-associated tumours may be a result of compensatory activation of alternative anabolic or catabolic pathways for glucose and glutamine metabolism. Previous studies have shown increases in glutaminolysis and glycogenesis, following glycolytic inhibition (DeBerardinis and Cheng 2010; Altman et al. 2016; Pusapati et al. 2016) . Glutamine can enter the depleted Krebs cycle following glycolysis inhibition through anaplerosis to sustain high macromolecule synthesis and ATP-generation (DeBerardinis et al. 2007; Mayers and Vander Heiden 2015; Altman et al. 2016). This is consistent with the current observation that dual inhibition of glycolysis and glutaminolysis was more efficacious at reducing tumour burden than either treatment alone.

The treatment effect on mTOR signalling was examined in normal tissue and tumours from the kidneys of *Tsc2*$^{+/-}$ mice. Dual inhibition of glycolysis and glutaminolysis with 3-BrPA and CB-839 suppressed mTORC1 signalling in normal kidney tissue and renal tumours. Rapamycin and rapamycin in combination with 3-BrPA or CB-839 also suppressed mTORC1 signalling in normal kidney tissue and renal tumours but the suppression was much stronger than 3-BrPA and CB-839 together. mTORC1 suppression with these treatments correlated with decrease in cell proliferation in kidney lesions. This suggests that inhibition of mTORC1 signalling contributes to the anti-tumour activity in kidney lesions, with rapamycin alone or rapamycin in combination with 3-BrPA or CB-839 being significantly more effective than 3-BrPA and CB-839 combination for treating renal lesions of *Tsc2*$^{+/-}$ mice. Moreover, rapamycin alone or in combination with 3-BrPA or CB-839 was more effective at reducing lesion number compared to dual inhibition of glycolysis and glutaminolysis, consistent with the role of mTORC1 suppression in blocking tumour formation (Yang et al. 2015). However, treatment with rapamycin showed no increase in cell death highlighting the cytostatic nature of rapalogs. 3-BrPA alone decreased mTORC1 activity possibly explaining its modest anti-tumour effect in solid carcinomas. CB-839 treatment alone has been previously reported to reduce mTORC1 signalling in tumour cells of renal cell carcinoma (Emberley et al. 2017). In contrast to this, CB-839 treatment in *Tsc2*$^{+/-}$ mice did not inhibit mTORC1 signalling in solid tumour cells and, surprisingly, caused a significant increase in mTORC1 signalling in normal kidney tissue. This may explain the lack of anti-tumour activity with CB-839 monotherapy.

Rapamycin in combination 3-BrPA or CB-839 substantially reduced mTORC2 signalling in all renal lesions whereas 3-BrPA alone slightly reduced mTORC2 signalling. Dual inhibition of glycolysis and glutaminolysis also results in a modest decrease in mTORC2 signalling in renal lesions. In contrast, rapamycin alone increased mTORC2 signalling in a proportion of cystic/papillary adenomas but not solid carcinomas. Feedback activation of mTORC2 following mTORC1 inhibition is suggested to contribute to the limited efficacy of rapamycin. However, the role of mTORC2 in tumourigenesis may have various roles on tumorigenesis depending on cellular contexts (Goncharova *et al.* 2011; Liu *et al.* 2014b; Khan *et al.* 2015). It remains to be further investigated whether inhibition of mTORC2 is required for treating TSC-associated tumour, as suggested in Chapter 3.

In summary, this study revealed that the dual inhibition of glycolysis and glutaminolysis significantly reduced tumour burden of TSC-associated renal lesions but was not as effective as rapamycin alone. Inhibition of mTORC1 is likely to account for anti-tumour efficacy of treatments used in this study. However, further studies are required to reveal whether TSC-associated tumours that are resistant to rapalogs respond to dual inhibition of glycolysis and glutaminolysis. CB-839 has recently been granted Fast Track Designation by the US FDA for combination with cabozantinib to treat patients with metastatic renal cell carcinoma. Cabozantinib is a potent VEGFR inhibitor showing anti-tumour efficacy in a xenograft model of colorectal cancer (Song *et al.* 2015; Markowitz and Fancher 2018). Recent clinical trials of cabozantinib in patients with RCC showed a significant improvement in overall and progression free survival (Osanto and van der Hulle 2018). Mechanisms of its anti-tumour activity are suggested to involve its mitigation of angiogenesis and Akt signalling (Song et al. 2015). Increased expression of VEGFR1 and activation of Akt is observed in TSC-associated tumours (Yang et al. 2015; Yang et al. 2017) and may warrant further investigation to compare combination of CB-839 and cabozantinib with rapamycin in renal tumours of *Tsc2*$^{+/-}$ mice.

5 CHAPTER FIVE

Effect of Conditional Deletion of *Pkm2* on Tumourigenesis in the Kidneys of *Tsc2*$^{+/-}$ Mice

5.1 Introduction

Aerobic glycolysis is a hallmark of cancer. The isozyme PKM2 is believed to drive aerobic glycolysis and provide tumour cells with a proliferative advantage by attenuating the final step of glycolysis (Wong *et al.* 2013). This allows the accumulation and shunting of upstream glycolytic intermediates into branching biosynthetic pathways for anabolic growth and proliferation (Cairns et al. 2011; Wong et al. 2013; Hay 2016). PKM2 catalyses the conversion of pyruvate to lactate to further drive aerobic glycolysis (Wong et al. 2015). PKM2 also enhances the Warburg effect through non-glycolytic functions as a protein kinase and a co-transcription factor through its ERK2-mediated translocation to the nucleus (Yang et al. 2012; Wong et al. 2015). The expression of *Pkm2* is increased in many cancer types, such as RCC, and is associated with its metastasis and a poor patient prognosis (Brinck et al. 1994). *Pkm2* is predominantly expressed over the *Pkm1* isoform in many tumours, allowing a greater metabolic plasticity.(Mazurek et al. 2005). Many *in vitro* studies investigating *Pkm2* have shown its requirement for tumour growth and metastasis (Christofk et al. 2008). However, in contrast to these findings, recent *in vivo* studies have demonstrated that *Pkm2* may not be required for tumour growth (Lau et al. 2017) and that deletion of *Pkm2* may even promote tumour formation in some tissue types (Israelsen et al. 2013; Dayton et al. 2016). Tumour formation in a *Brca1*-loss driven mouse model of breast cancer showed an acceleration of tumour growth following a conditional deletion of *Pkm2* (Israelsen et al. 2013). Further investigations are required to fully understand the roles of *Pkm2* in tumourigenesis in the context of different tissue types.

The Cre/loxp technology is widely used to conditionally delete genes for investigation of their roles in tumourigenesis (Stricklett et al. 1999). This technology can be exploited to achieve tissue- and age-specific deletion of genes by tissue-specific promotors via inducible expression of Cre. One of the inducible Cre-mediated conditional gene deletion systems is controlled through tetracycline (Tet system). Tetracycline is required for the binding of reverse tetracycline-dependant trans-activator (rtTA) with a Tet promotor,

resulting in the expression of linked downstream genes, such as Cre-recombinase, enabling time-dependent expression of Cre. (Gossen and Vujard 1992; Gossen *et al.* 1995; St-Onge *et al.* 1996). *Pax8* is highly expressed in the kidneys, thyroid and liver (Poleev *et al.* 1992). *Pax8.rtTA* mice have been generated with high levels of rtTA in the epithelial cells of renal tubules (promoter of *Pax8* was used to drive rtTA in the kidney tubules) (Traykova-Brauch et al. 2008). The combination of TetO.Cre mice and *Pax8.rtTA* mice can result in the tetracycline-dependent deletion of floxed genes within kidney tissue to assess their function.

As discussed previously, mTOR is a master regulator of cell metabolism. TSC-associated tumours have previously been reported to have increased expression of enzymes involved in aerobic glycolysis (Jones *et al.* 2019). mTOR signalling is necessary for *PKM* gene transcription through HIF1α and *Pkm2*-specific mRNA splicing through *c-myc* (David et al. 2010; Sun et al. 2011). Expression of *Pkm2* correlates with mTOR activation and is sensitive to its inhibition (Iqbal and Bamezai 2012). *Tsc2* null MEFs with *Pkm2* deletion have demonstrated a decrease in aerobic glycolysis and lactate production and suppressed mTOR-mediated tumorigenesis in a xenograft mouse model of prostate cancer (Sun et al. 2011). These findings suggest that *Pkm2* may be a potential alternative therapeutic target for TSC-associated tumours. Therefore, in this study, the roles of *Pkm2* in tumourigenesis of renal lesions were investigated by conditionally deleting *Pkm2* in the kidneys of $Tsc2^{+/-}$ mice. The kidney tumour burden of $Tsc2^{+/-}$ mice with or without *Pkm2* was compared. The effect of *Pkm2* deletion on expression of *Pkm1*, mTOR signalling and cell proliferation were also analysed.

5.2 Results

5.2.1 Expression of *Pkm2* in renal lesions of *Tsc2*$^{+/-}$ mice

Tsc2$^{+/-}$ mice at 12 months of age were culled to investigate the expression of *Pkm2* in renal lesions by IHC. As seen in the previous chapters, mTORC1 and mTORC2 are consistently activated in TSC-associated-lesions demonstrated by the increased phosphorylation of S6 at S235/236, 4E-BP1 at T37/46, Akt at S473 and PKC at S657 (Figure 3.1; Figure 4.1A). As shown in figure 5.1, *Pkm2* was highly expressed in the majority of cystic lesions, all papillary adenomas and all solid carcinomas (Figure 5.1A). Around 35.58% (29/81) of small renal cysts from 20 *Tsc2*$^{+/-}$ mice, however, showed little or no expression of *Pkm2* (Figure 5.1B).

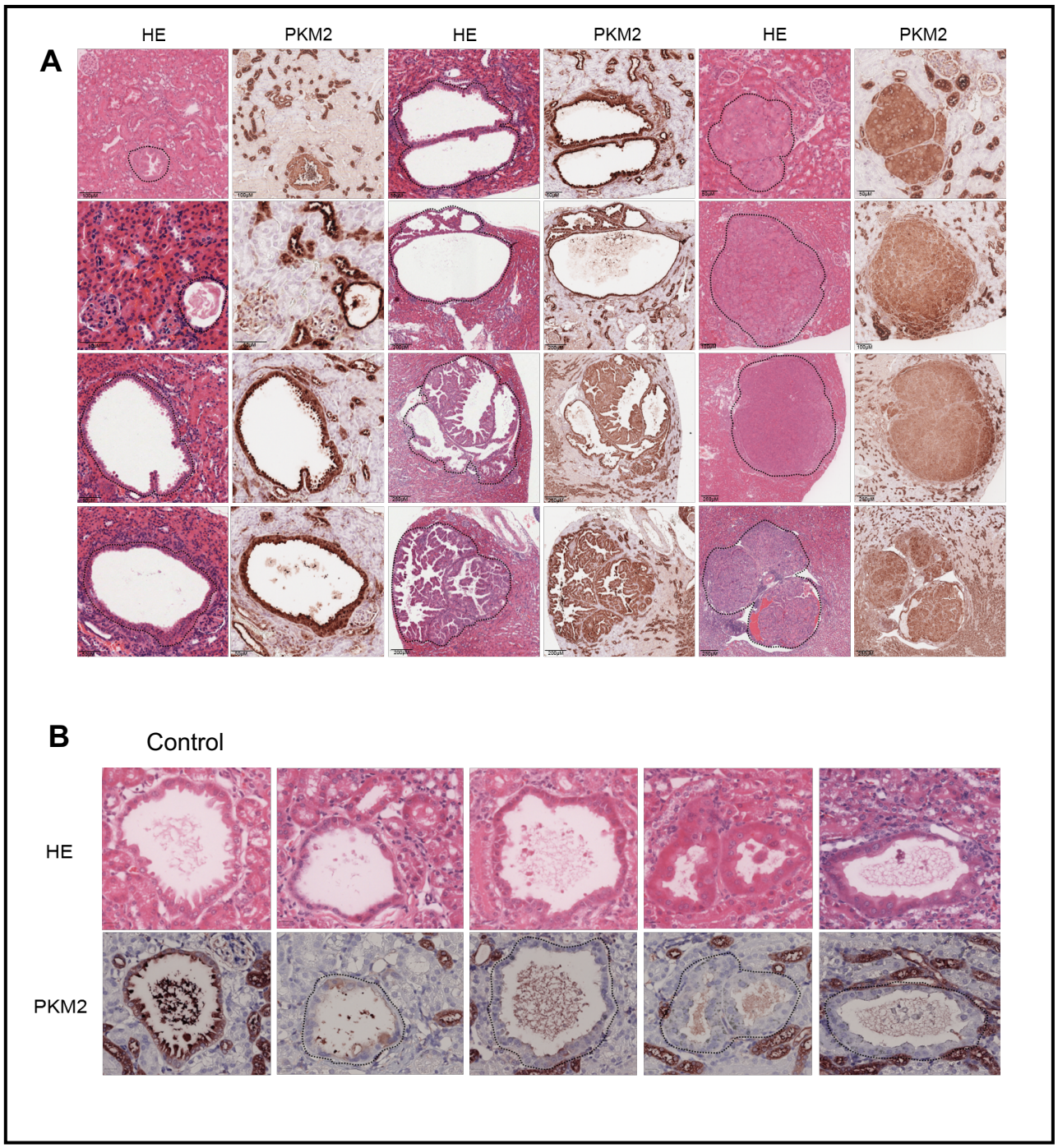

Figure 5.1 Expression of *Pkm2* in renal lesions of *Tsc2*$^{+/-}$ mice. Kidneys from *Tsc2*$^{+/-}$ mice were dissected at 12 months of age to investigate the expression of *Pkm2* by IHC. Kidney sections contained cysts, papillary adenomas and solid carcinomas. Kidneys were fixed, processed, sectioned and stained for *Pkm2* **(A)** *Pkm2* expression in cystic, papillary adenomas and solid carcinomas. Solid black lines represent scale bars **(B)** Expression of *Pkm2* in small cystic lesions. Eighty-one small renal cysts from 20 *Tsc2*$^{+/-}$ mice were investigated for their *Pkm2* expression. Around 35.58% (29/81) of small renal cysts analysed showed little or no expression of *Pkm2*. .

5.2.2 *Pkm2* conditional deletion in the kidneys of *Tsc2*$^{+/-}$ mice

To study roles of *Pkm2* in renal tumorigenesis, series of breedings were performed between *Tsc2*$^{+/-}$ (Onda et al. 1999), B6;129S-*Pkm*$^{tm1.1Mgvh}$/J (Israelsen et al. 2013), B6.Cg-Tg(Pax8-rtTA2S*M2)1Koes/J (Traykova-Brauch et al. 2008) and Tg(tetO-cre)1Jaw/J (Gossen and Vujard 1992) mice to generate mice with a *Pax8.rtTA+/Pkm2*$^{lox/lox}$*/TetO.Cre+/Tsc2*$^{+/-}$ genotype. B6;129S-*Pkm*$^{tm1.1Mgvh}$/J mice (*Pkm2*$^{fl/fl}$) possess *loxP* sites flanking the *Pkm2* specific exon 10 of the *PKM* gene. PCR-based genotyping was carried out to identify *Pax8.rtTA+/Pkm2*$^{lox/lox}$*/TetO.Cre+/Tsc2*$^{+/-}$ mice (Figure 5.2). *Pax8.rtTA+/Pkm2*$^{lox/lox}$*/TetO.Cre+/Tsc2*$^{+/-}$ mice were expected to express Cre recombinase in cells with active *Pax8* promotor following doxycycline treatment, and thereby to induce the deletion of the floxed *Pkm2*-specific exon 10 (Figure 5.3). A total of 10 pairs of mice were randomly allocated into 2 groups: water (n=10) and doxycycline (n=10), as summarised in Table 5.1. To induce expression of Cre and deletion of *Pkm2*, doxycycline of 2mg/ml supplemented with 5% sucrose in drinking water was given for 10 days immediately after weaning (4 weeks of age). After 10 days treatment, mice in the doxycycline treatment group were continued on normal drink water as the control group until 12 months of age. Tissues from the kidney, liver, heart, lung and spleen from mice culled at 12 months were collected and used to determine tissue-specific deletion of *Pkm2* initially by PCR. In the doxycycline treatment group, *Pkm2* was successfully and specifically deleted in the kidney and liver tissues but not in the heart, lung or spleen. (Figure 5.4A). However, *Pkm2* deletion in these tissues was not complete. This may be due to the fact that tissue pieces collected contain other cell types, such as mesenchymal cells, which do not express *Pax8* and therefore have no *Pkm2* deletion. To further investigate the deletion of *Pkm2*, the kidneys of treated and non-treated *Pax8.rtTA+/Pkm2*$^{lox/lox}$*/TetO.Cre+/Tsc2*$^{+/-}$ mice were fixed, processed, sectioned and stained with HE and *Pkm2* by IHC for histological and immunohistochemical analysis. As shown in figure 5.4B, the tubules of the cortex and medulla in non-treated mice had strong expression of *Pkm2*. In the kidneys of the mice treated with doxycycline, the epithelial cells of renal tubules of the cortex and medulla showed specific *Pkm2* deletion whilst surrounding mesenchymal cells were unaffected (Figure 5.4B). Importantly, 92% (33/36) of papillary adenomas and solid carcinomas analysed had no observable expression of *Pkm2* in tumour cells following doxycycline treatment while all tumour cells clearly expressed *Pkm2* in the control group without doxycycline treatment (Figure 5.4C). In contrast, mesenchymal cells within the *Pkm2*

deleted tumours still expressed *Pkm2*, possibly to a higher level compared to *Pkm2* expressing tumours, as described later in section 5.2.5.

These results confirmed the specific deletion of *Pkm2* in the epithelial cells of renal tubules and renal tumour cells of *Pax8.rtTA+/Pkm2*$^{lox/lox}$*/TetO.Cre+/Tsc2*$^{+/-}$ mice following doxycycline treatment.

Table 5.1 Treatment summary

Treatment Group	Number of *Pax8.rtTA+/Pkm2*$^{lox/lox}$*/TetO.Cre+/Tsc2*$^{+/-}$ mice	Number of males	Number of females	Treatment start age (weeks)	Treatment end age (weeks)	Concentration in drink water	Number of animals killed due to sickness before end of treatment
Water	10	5	5	4	6	-	0
Dox	10	5	5	4	6	2 mg/ml with 5% sucrose	0

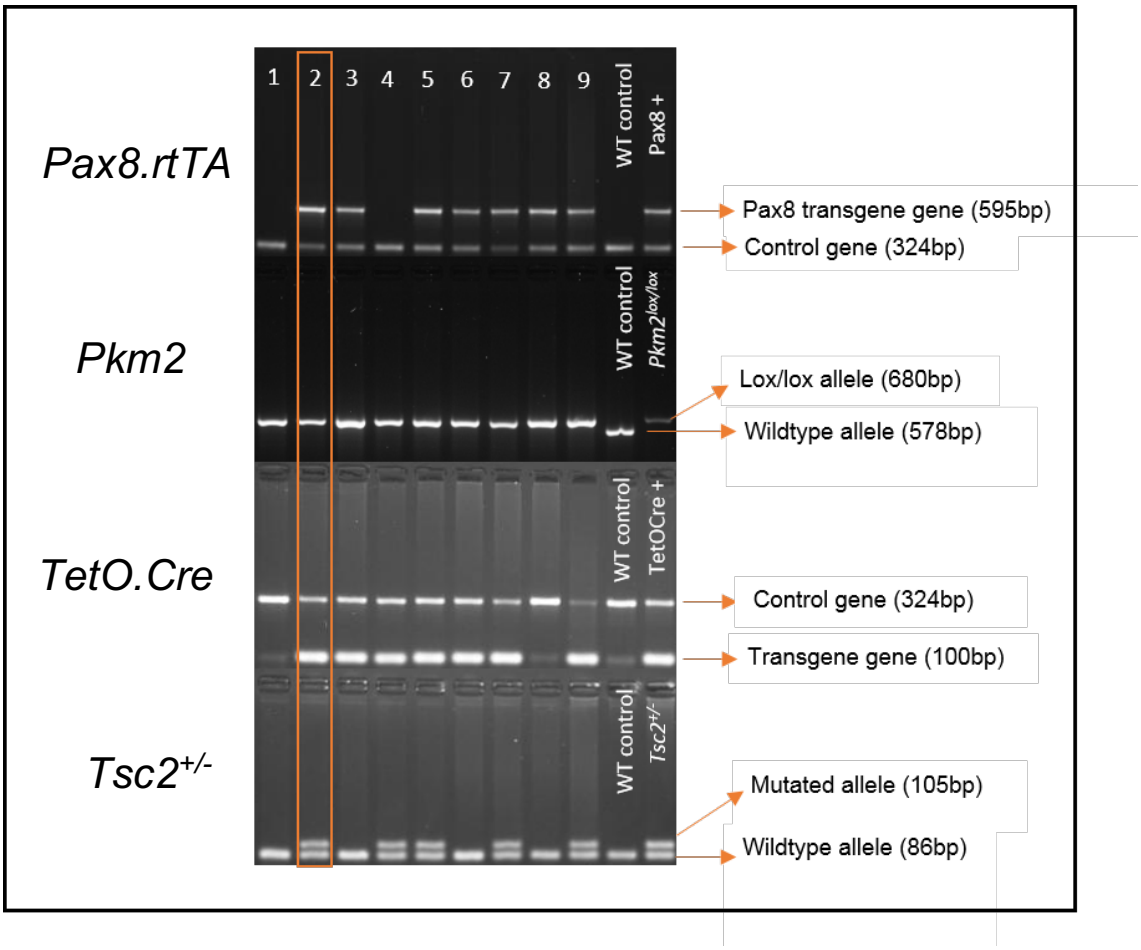

Figure 5.2 Confirmation of *Pax8.rtTA+/Pkm2$^{lox/lox}$/TetO.Cre+/Tsc2$^{+/-}$* mice. DNA was extracted from mouse ear punches and used to identify *Pax8.rtTA+/Pkm2$^{lox/lox}$/TetO.Cre+/Tsc2$^{+/-}$* mice by PCR. Primers and annealing temperatures used for *Pax8.rtTA*, *Pkm2$^{lox/lox}$*, *TetOCre* and *Tsc2* PCR are shown in Table 2.1 (Materials and Methods). PCR products were run on 1.5 or 3% agarose gels and visualised on an UV gel doc. The amplicon size for the *Pax8* transgene was 595bp and the *TetOCre* transgene was 100bp. The *Pkm2$^{lox/lox}$* allele was 680bp. The mutated *Tsc2* allele was 105bp. Mice which were positive for the *Pax8* transgene, *Pkm2$^{lox/lox}$* allele, *TetOCre* transgene and heterozygous for *Tsc2* were selected for study. Lanes 2, 5, 7 and 9 indicate *Pax8.rtTA+/Pkm2$^{lox/lox}$/TetO.Cre+/Tsc2$^{+/-}$* mice.

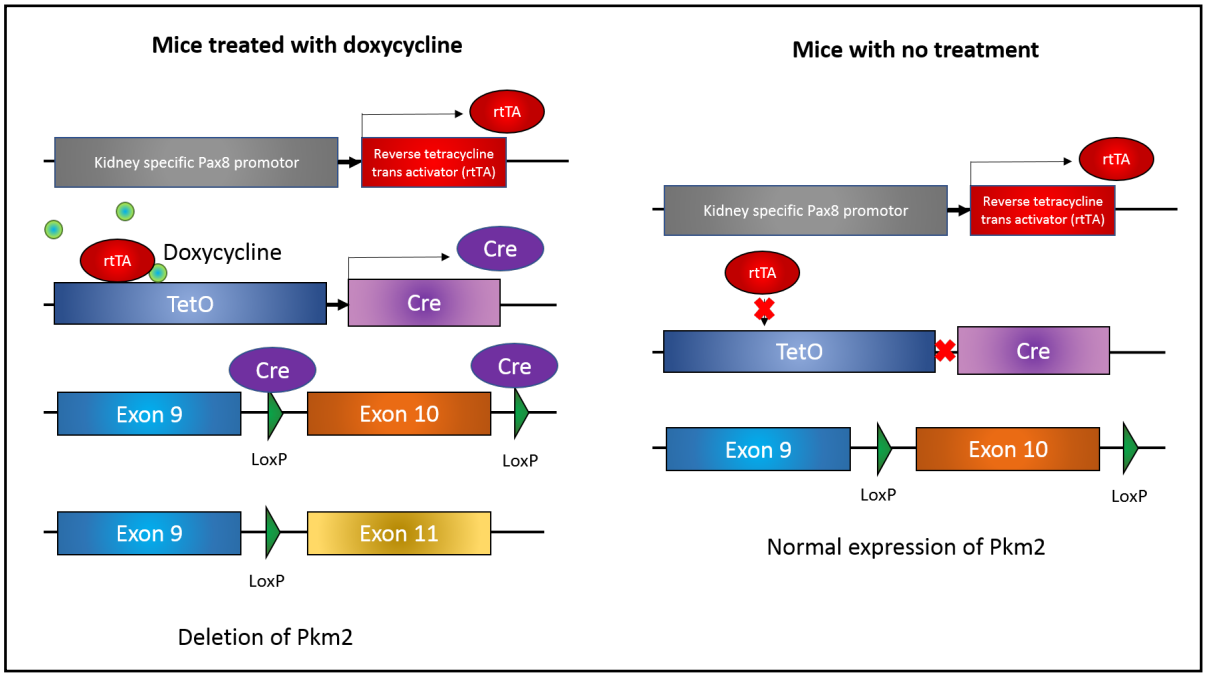

Figure 5.3 Schematic diagram of *Pkm2* conditional deletion. *Pax8.rtTA* mice express rtTA in the epithelial cells of renal tubules. After doxycycline treatment, rtTA-doxycycline complex binds to the TetO transgene, upstream of Cre. This results in the inducible expression of Cre and the cutting of loxp sites either side of exon 10 (*Pkm2* specific-deletion).

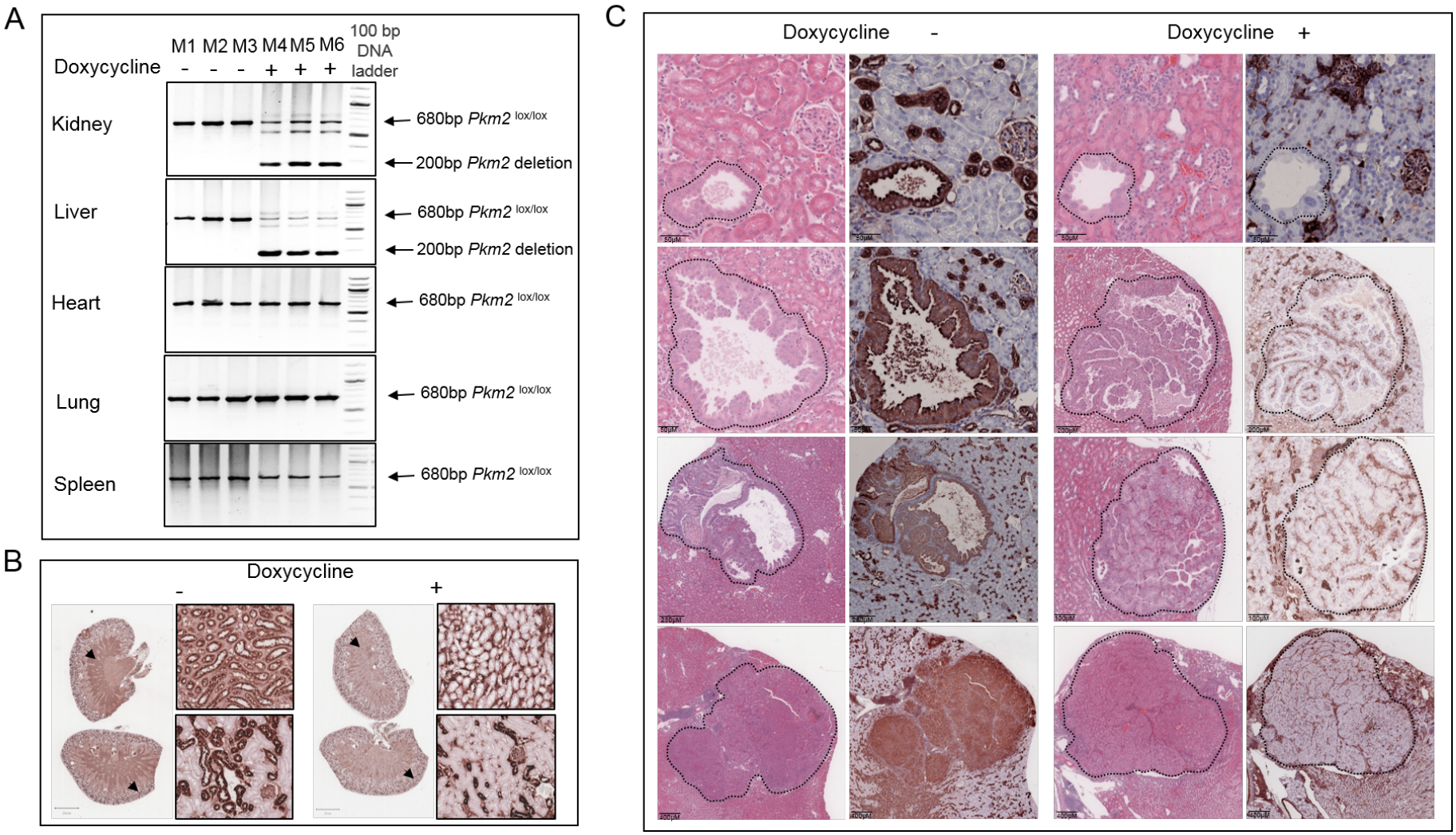
A
M1 M2 M3 M4 M5 M6
100 bp DNA ladder
Doxycycline - - - + + +
Kidney
680bp Pkm2 lox/lox
200bp Pkm2 deletion
Liver
680bp Pkm2 lox/lox
200bp Pkm2 deletion
Heart
680bp Pkm2 lox/lox
Lung
680bp Pkm2 lox/lox
Spleen
680bp Pkm2 lox/lox
B
Doxycycline
-
+
C
Doxycycline -
Doxycycline +

Figure 5.4 Conditional deletion of *Pkm2* in the kidneys and renal tumours of *Pax8.rtTA+/Pkm2$^{lox/lox}$/TetO.Cre+/Tsc2$^{+/-}$* mice treated with doxycycline. (A) Tissue specific *Pkm2* deletion after doxycycline treatment. Mice at 12 months of age were culled and tissues of the kidney, liver, heart, lung and spleen were collected and used for PCR. Primers and annealing temperatures used for *Pkm2$^{lox/lox}$* allele are shown in Table 2.1 (Materials and Methods). PCR products were run on 3% agarose gel and visualised on an UV gel doc. The *Pkm2$^{lox/lox}$* amplicon size was 680bp. The *Pkm2* knockout amplicon size was 200bp. **(B)** Expression of *Pkm2* in the kidneys of *Pax8.rtTA+/Pkm2$^{lox/lox}$/TetO.Cre+/Tsc2$^{+/-}$* mice after treatment with doxycycline. Mice were culled at 12 months of age and kidneys were harvested, fixed, processed, sectioned and stained for *Pkm2*. **(C)** Expression of *Pkm2* in renal lesions of *Pax8.rtTA+/Pkm2$^{lox/lox}$/TetO.Cre+/Tsc2$^{+/-}$* mice after treatment with doxycycline. Mice were culled at 12 months of age and kidneys were harvested, fixed, processed, sectioned and stained for *Pkm2*. Images presented show expression of *Pkm2* in cysts, papillary adenomas and solid carcinomas. Solid black lines indicate scale bars.

5.2.3 Effect of *Pkm2* deletion on renal tumourigenesis in *Tsc2*$^{+/-}$ mice

As doxycycline effectively induced the deletion of *Pkm2* in the epithelial cells of renal tubules and renal tumour cells of *Pax8.rtTA+/Pkm2*$^{lox/lox}$*/TetO.Cre+/Tsc2*$^{+/-}$ mice, it was further investigated whether *Pkm2* deletion had any effect on renal tumourigenesis in *Tsc2*$^{+/-}$ mice (Figure 5.5). Mice were treated as above and culled at 12 months of age. Kidney sections were prepared for tumour burden assessment by histological analysis. To evaluate tumour burden, renal lesions were characterised, counted and measured for their whole area and cellular area (as described in methods 2.2.6.4). The lesion type, total lesion number, total lesion area and total lesion cellular area were documented for each animal and compared between treatment groups (Figure 5.5, Table 5.2, 5.3 and 5.4). Tumour burden was compared by analysing all lesions (cystic/papillary/solid) together, cystic/papillary adenomas only and solid carcinomas only. As shown in Figure 5.5 and Table 5.2, renal tubule specific deletion of *Pkm2* in *Tsc2*$^{+/-}$ mice had no overall effect on total lesion number (P=0.9564) or lesion cellular area (P=0.6842) compared to *Tsc2*$^{+/-}$ mice without treatment of doxycycline. A very small reduction in total lesion size was observed in doxycycline treated mice but this was not significant (P=0.5787) (Figure 5.5; Table 5.2). Similarly, renal tubule specific deletion of *Pkm2* had no effect on number (P=0.9561), size (P=0.9118) cellular area (P=0.8534) of cystic/papillary adenomas (Figure 5.5; Table 5.3). Further, renal tubule specific deletion of *Pkm2* had no effect on number (P=0.9966), size (P=0.9696) or cellular area (P=0.9098) of solid carcinomas. (Figure 5.5; Table 5.4). These results suggested that *Pkm2* deletion had no significant effect on the renal tumourigenesis in *Tsc2*$^{+/-}$ mice

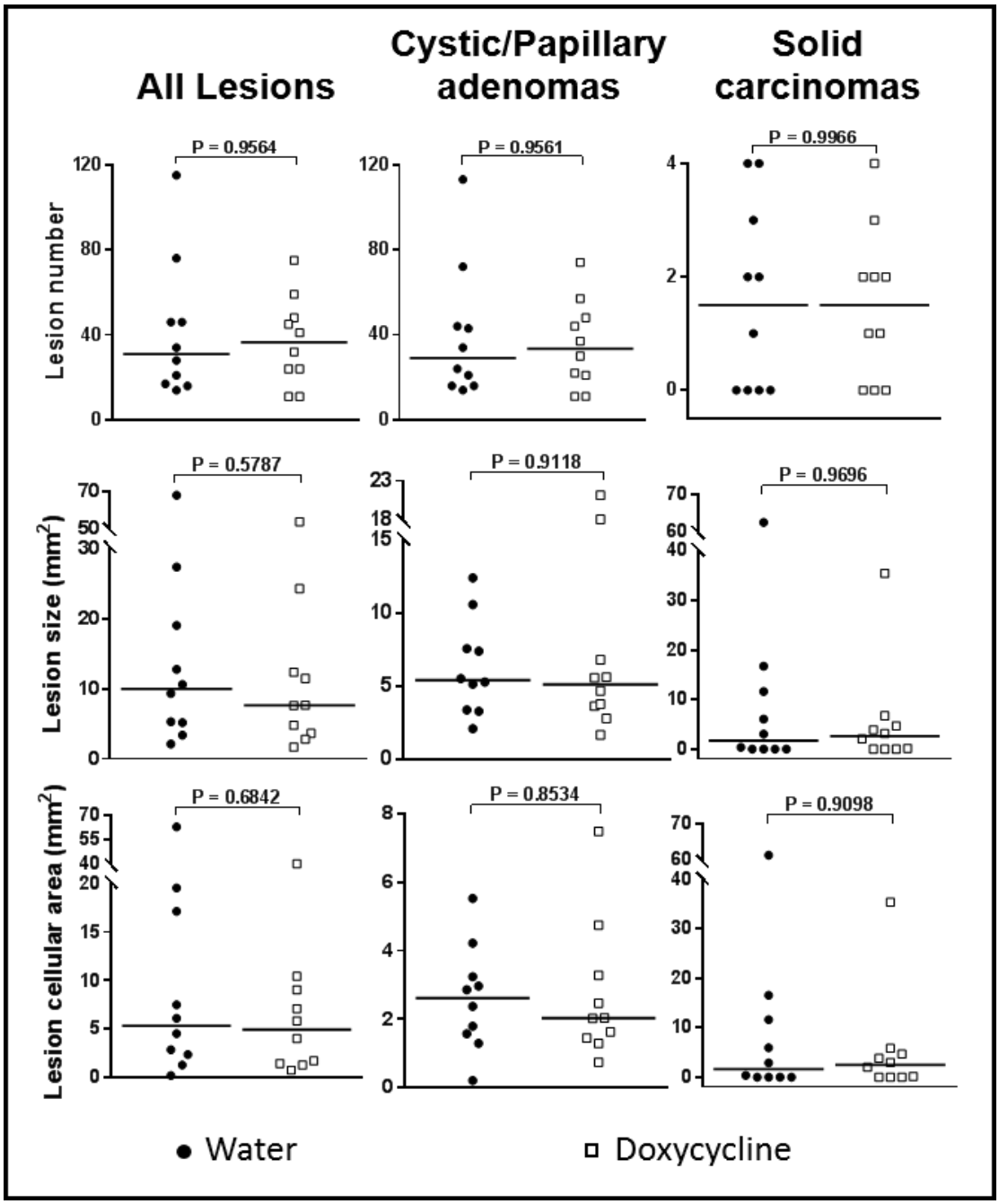

Figure 5.5 Effect of conditional *Pkm2* deletion on tumour burden. Ten pairs of *Pax8.rtTA+/Pkm2*$^{lox/lox}$*/TetO.Cre+/Tsc2*$^{+/-}$ mice were randomly allocated to 2 groups: water (n=10) or doxycycline (n=10). Doxycycline treatment group were given drink water with 2mg/ml doxycycline and 10% sucrose for 10 days at 4 weeks of age. After treatment, mice were continued on normal drink water as control. At 12 months of age, mice from both groups were culled and the kidneys collected for histological analysis. Kidneys were fixed, processed, sectioned and stained with H&E to assess tumour burden. Kidney tumours were located, counted, characterised and measured per animal for comparison between groups. **Left panel:** Comparison of total lesion number, size and cellular area of all types of lesion (cyst, papillary adenomas and solid carcinomas). **Middle panel:** Comparison of total cystic/papillary adenoma number, size, and cellular area. **Right panel:** Comparison of total solid carcinoma number, size and cellular area. Horizontal bars represent the median. P<0.05 is considered significant.

Table 5.2 Comparison of all lesions in *Pax8.rtTA+/Pkm2$^{lox/lox}$/TetO.Cre+/Tsc2$^{+/-}$* mice by histological analysis (Mann Whitney test)

I. Lesion number (all lesions: cystic/papillary adenomas and solid carcinomas)

Treatment	Number of mice	Median	Range (mm^2)	P value (Compared to Water)
Water	10	31	115 - 14	0.9564
Doxycycline	10	36.5	75 - 11	-

II. Lesion size (all lesions: cystic/papillary adenomas and solid carcinomas)

Treatment	Number of mice	Median (mm^2)	Range (mm^2)	P value (Compared to Water)
Water	10	9.965	2.099 - 67.896	0.5787
Doxycycline	10	7.615	1.672 - 53.499	-

III. Lesion cellular area (all lesions: cystic/papillary adenomas and solid carcinomas)

Treatment	Number of mice	Median (mm^2)	Range (mm^2)	P value (Compared to Water)
Water	10	5.324	0.207 - 63.101	0.6842
Doxycycline	10	4.934	0.746 - 40.171	-

Table 5.3 Comparison of all lesions in *Pax8.rtTA+/Pkm2$^{lox/lox}$/TetO.Cre+/Tsc2$^{+/-}$* mice by histological analysis (Mann Whitney test)

I. Lesion number (cystic/papillary adenomas)

Treatment	Number of mice	Median	Range (mm^2)	P value (Compared to Water)
Water	10	29	14 - 113	0.9561
Doxycycline	10	33.5	11 - 74	-

II. Lesion size (cystic/papillary adenomas s)

Treatment	Number of mice	Median (mm^2)	Range (mm^2)	P value (Compared to Water)
Water	10	5.42	2.098 - 12.438	0.9118
Doxycycline	10	5.136	1.672 - 21.160	-

III. Lesion cellular area (cystic/papillary adenomas)

Treatment	Number of mice	Median (mm^2)	Range (mm^2)	P value (Compared to Water)
Water	10	2.6194	0.206 - 5.531	0.8534
Doxycycline	10	2.029	0.7460 - 4.488	-

Table 5.4 Comparison of all lesions in *Pax8.rtTA+/Pkm2$^{lox/lox}$/TetO.Cre+/Tsc2$^{+/-}$* mice by histological analysis (Mann Whitney test)

I. Lesion number (solid carcinomas)

Treatment	Number of mice	Median	Range (mm^2)	P value (Compared to Water)
Water	10	1.5	0 - 4	0.9966
Doxycycline	10	1.5	0 - 4	-

II. Lesion size (solid carcinomas)

Treatment	Number of mice	Median (mm^2)	Range (mm^2)	P value (Compared to Water)
Water	10	1.666	0.0000 - 62.352	0.9696
Doxycycline	10	2.554	0.0000 - 35.473	-

III. Lesion cellular area (solid carcinomas)

Treatment	Number of mice	Median (mm^2)	Range (mm^2)	P value (Compared to Water)
Water	10	1.594	0.0000 - 61.302	0.9098
Doxycycline	10	2.468	0.0000 - 35.421	-

5.2.4 Effect of *Pkm2* deletion on mTOR signalling and cell proliferation of TSC-associated renal tumours

IHC (with consecutive sections) was performed to determine the effect of *Pkm2* deletion on mTOR signalling in renal tumours of *Pax8.rtTA+/Pkm2*$^{lox/lox}$*/TetO.Cre+/Tsc2*$^{+/-}$ mice. *Pkm2* deletion did not significantly change the phosphorylation of S6 at p-S235/236 and Akt at p-S473, as seen by IHC (Figure 5.6). These results suggested that deletion of *Pkm2* has no significant effect on mTORC1 or mTORC2 signalling in renal lesions of *Pax8.rtTA+/Pkm2*$^{lox/lox}$*/TetO.Cre+/Tsc2*$^{+/-}$ mice.

MS-IHC was also used to determine the effect of *Pkm2* deletion on cell proliferation in renal tumours. Ki67 was used as a marker of proliferation (Figure 5.7A). The same kidney section was used by MS-IHC to show the co-localisation of Ki67 and *Pkm2* (Figure 5.7A). Renal tumours were randomly selected per group (n=24 for water group; n=19 for doxycycline group) for proliferation analysis. Ki67 positive cells and total number of cells in these tumours were counted using imageJ and the percentage of Ki67 positive cells per tumour was calculated. Ki67 positive percentage was used to compare between groups to assess *Pkm2* role on cell proliferation. (Figure 5.7B). As seen from Figure 5.7B, *Pkm2* deletion caused a slight reduction in the median percentage of Ki67 positive cells per tumour in doxycycline treated mice (8.586%) compared to mice without doxycycline treatment (10.003%) but this was not significant (P=0.1441) (Table 5.5). These results suggested that *Pkm2* might not be required for cell proliferation of TSC-associated renal tumours.

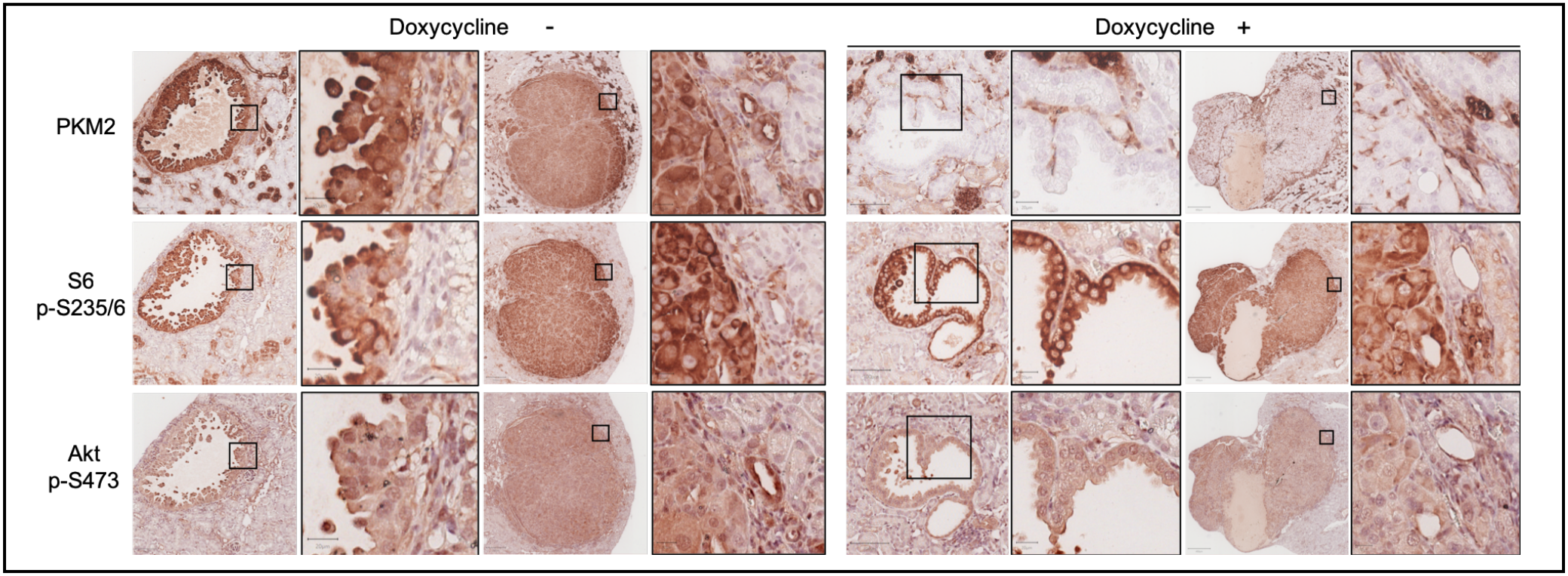

Figure 5.6 Effect of *Pkm2* deletion on mTOR signalling in renal lesions of *Pax8.rtTA+/Pkm2$^{lox/lox}$/TetO.Cre+/Tsc2$^{+/-}$* mice. Kidneys from doxycycline treatment group and water group were dissected at 12 months of age to analyse mTOR signalling by IHC. Kidneys were fixed, processed, sectioned and stained with *Pkm2*, S6 p-S235/236 and Akt p-S473. Phosphorylation of S6 at S235/236 was used to evaluate mTORC1 activity and phosphorylation of Akt at S473 was used to evaluate mTORC2 activity. Black boxes indicate higher power views of adjacent image. Solid black lines indicate scale bars.

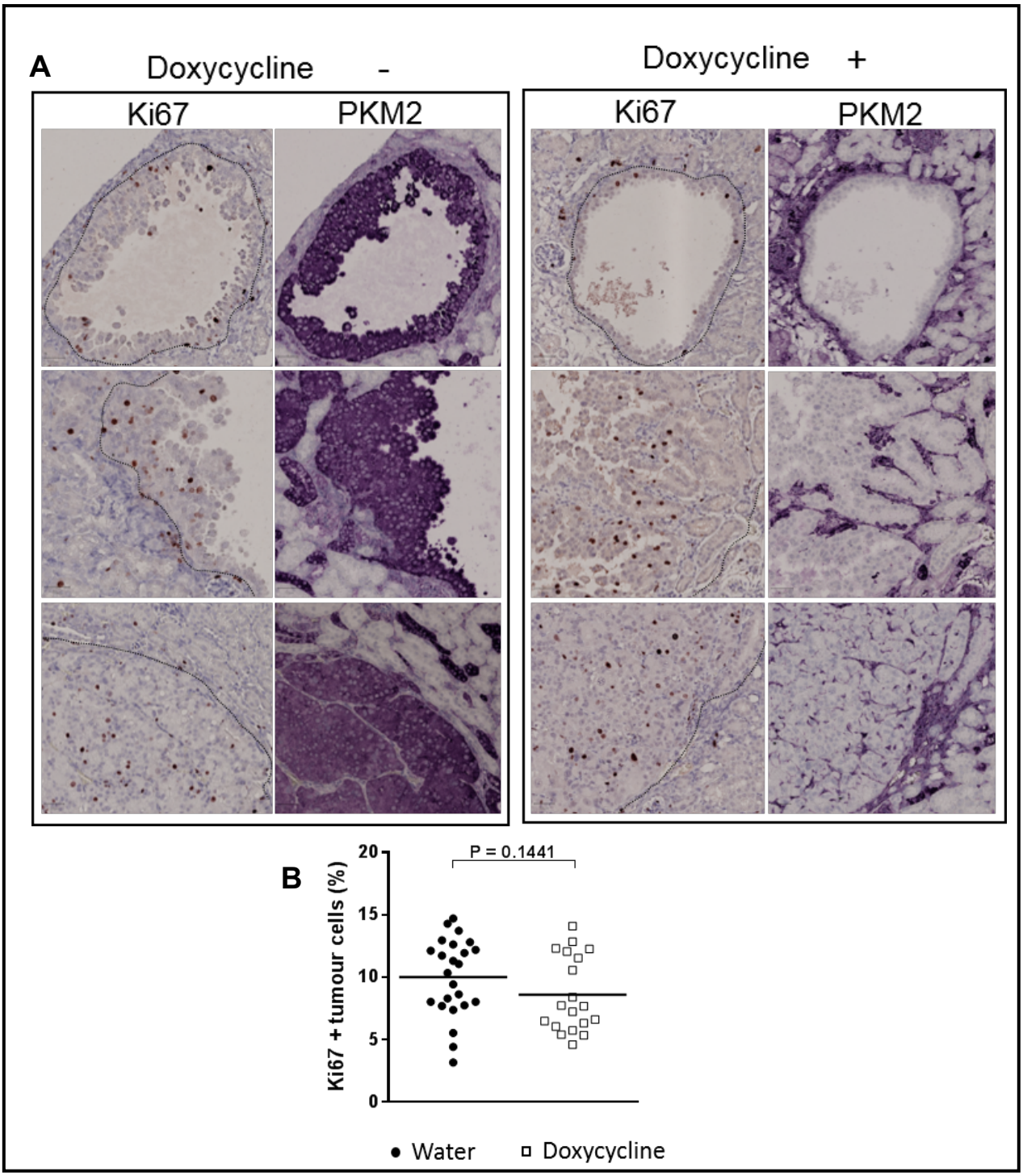

Figure 5.7 Effect of *Pkm2* deletion on cell proliferation in renal lesions of *Pax8.rtTA+/Pkm2$^{lox/lox}$/TetO.Cre+/Tsc2$^{+/-}$* mice. (A) Effect of *Pkm2* deletion on cell proliferation by MS-IHC Kidneys were dissected at 12 months of age, fixed, processed, sectioned and subjected to 2 rounds of staining with Ki67 and *Pkm2,* with complete stripping of each antibody per round. **(B)** Percentage of Ki67-positive cells per renal lesion. Renal tumours from each group (n=24 for water group; n=19 for doxycycline group) were randomly selected for proliferation analysis. Positively stained Ki67 cells were identified and manually counted using imageJ and percentage of Ki67 stained cells per tumour was calculated. Median percentage of Ki67 positive cells in the water group was 10.003% and for the doxycycline treatment group was 8.586% Black horizontal bar indicates mean. P<0.05 is considered significant.

Table 5.5 Effect of treatment on proliferation of renal tumour cells in *Tsc2*$^{+/-}$ mice (Mann Whitney)

Treatment	Number of tumours examined	Percentage of tumour cells positive for Ki67: Median (%)	Percentage of tumour cells positive for Ki67: Range (%)	P (compared with Water)
No treatment (water)	24	10.003	3.151 - 14.701	-
Doxycycline	19	8.586	4.59 - 14.054	0.1441

5.2.5 Expression of *Pkm1* in the kidneys of *Tsc2*$^{+/-}$ mice with *Pkm2* deletion.

The expression of *Pkm1* has previously been reported to be increased after conditional deletion of *Pkm2* in tissues that normally express *Pkm2* in mice (Dayton et al. 2016). Therefore, the expression of *Pkm1* in the kidneys was investigated following *Pkm2* deletion in *Pax8.rtTA+/Pkm2*$^{lox/lox}$*/TetO.Cre+/Tsc2*$^{+/-}$ mice. MS-IHC was performed to assess the expression of *Pkm1* and *Pkm2* on the same kidney sections. As seen in Figure 5.8A, overall expression of *Pkm1* was significantly increased in the kidneys of mice treated with doxycycline while the basal expression of *Pkm1* remained very low in mice not treated with doxycycline. In tumours lacking *Pkm2* expression in mice treated with doxycycline, *Pkm1* was exclusively increased whereas little expression of *Pkm1* was observed in tumours from mice without doxycycline treatment (Figure 5.8B). It was notable that *Pkm1* was not seen in some small cystic lesions that were most likely to be those that initially did not express *Pkm2* as described in Figure 5.1. These results suggest that tumour cells with *Pkm2* deletion had increased expression of *Pkm1.*

Pkm1 expression in *Pkm2* expressing stromal cells was minimal and did not appear to be increased in stromal cells in doxycycline-treated mice. However, the deletion of *Pkm2* in renal tumours enhanced the expression of *Pkm2* in mesenchymal stromal cells within and around tumours (Figure 5.9).

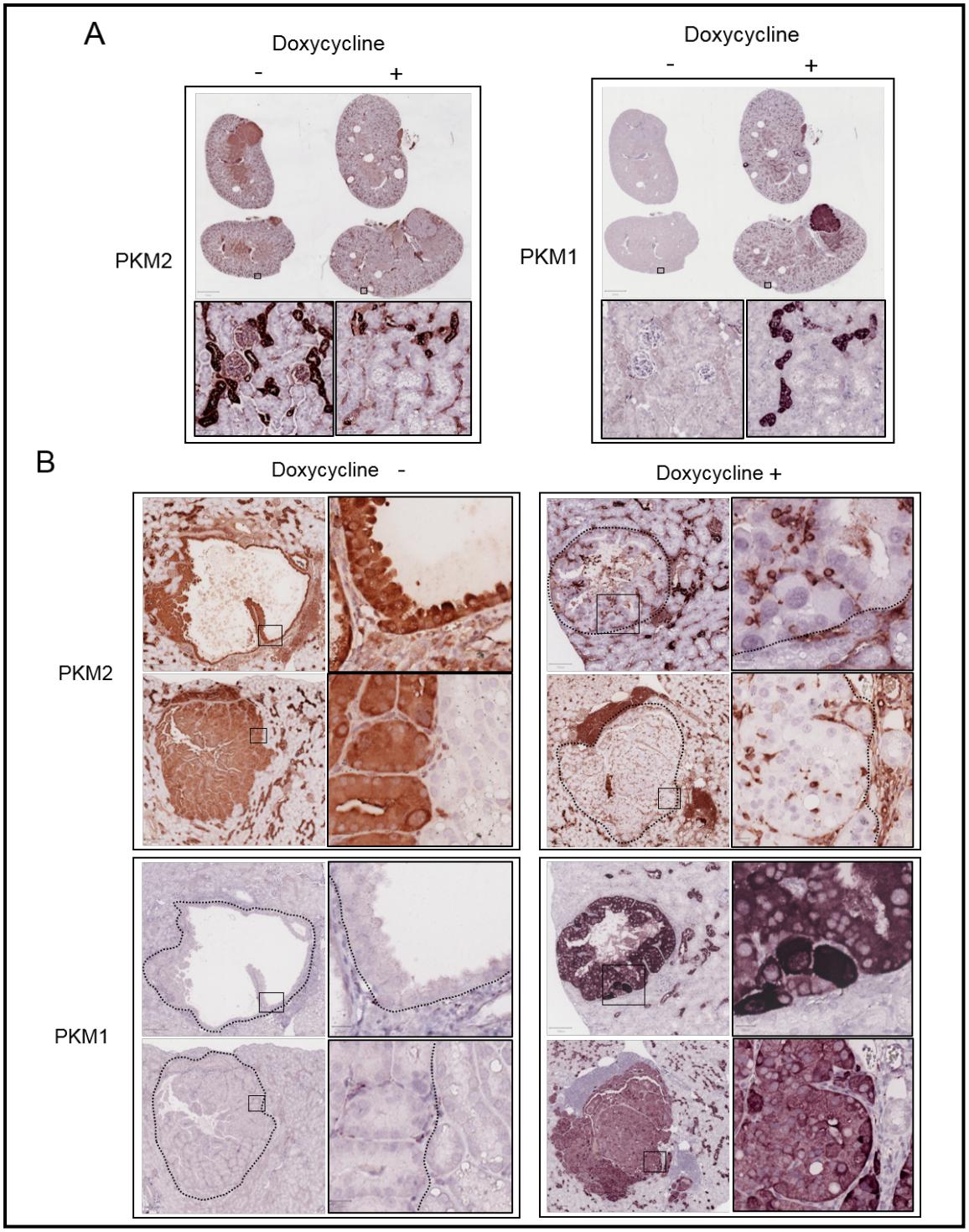

Figure 5.8 Expression of *Pkm1* and *Pkm2* in renal lesions of *Pax8.rtTA+/Pkm2$^{lox/lox}$/TetO.Cre+/Tsc2$^{+/-}$* mice after doxycycline treatment. Kidneys were dissected at 12 months of age for MS-IHC. Kidneys were fixed, processed, sectioned and subjected to 2 rounds of staining with Pkm2 and Pkm1, with complete stripping of each antibody per round. **(A)** *Pkm2* and *Pkm1* expression in the whole kidney by MS-IHC with and without doxycycline treatment. Black boxes indicate higher power views of adjacent image **(B)** *Pkm1* and *Pkm2* expression in renal lesions by MS-IHC with and without doxycycline treatment. Black boxes indicate higher power views of adjacent image

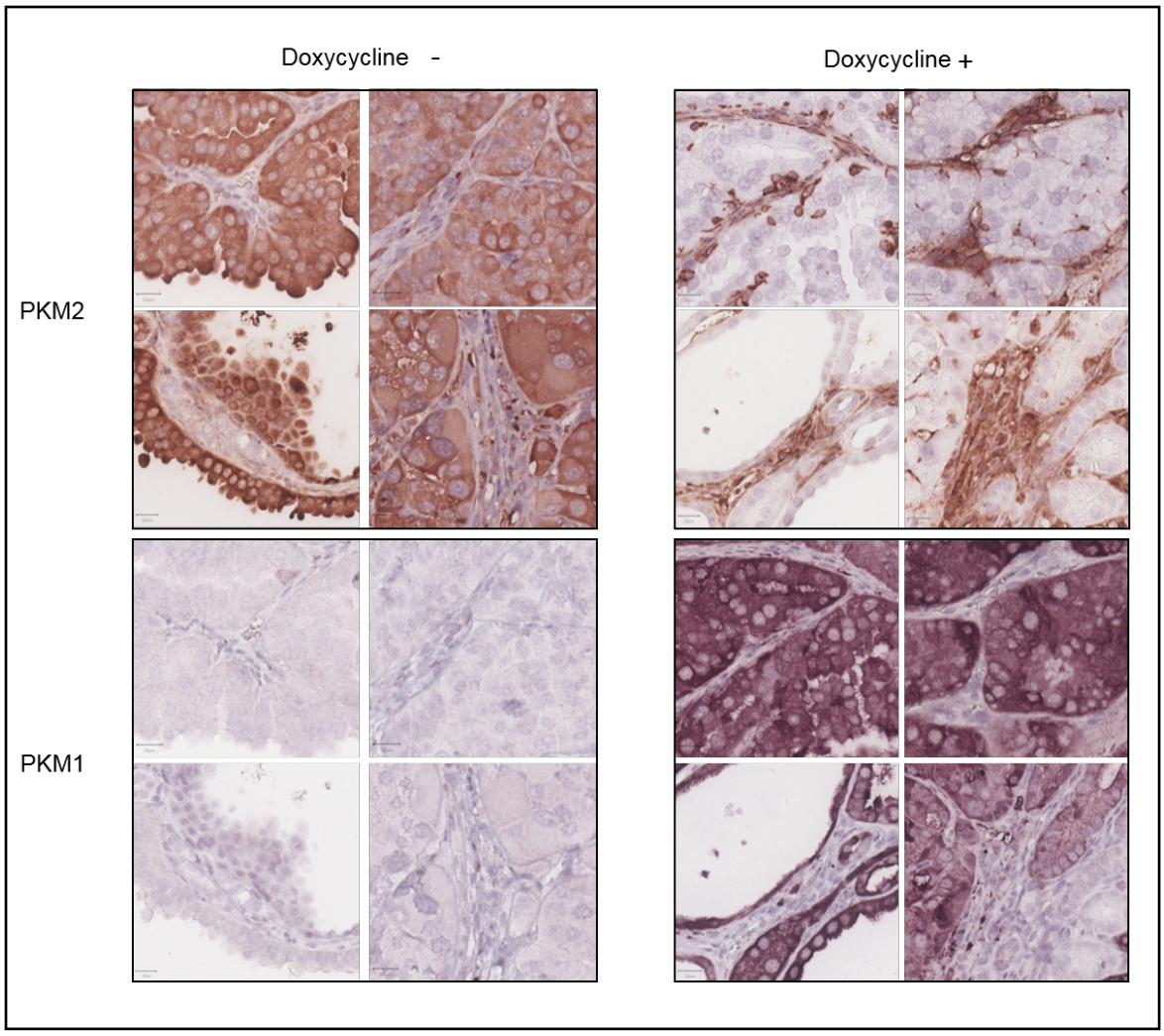

Figure 5.9 Expression of *Pkm1* and *Pkm2* in mesenchymal stromal cells in and around renal lesions of *Pax8.rtTA+/Pkm2$^{lox/lox}$/TetO.Cre+/Tsc2$^{+/-}$* mice treated with doxycycline. Kidneys were dissected at 12 months of age for MS-IHC. Kidneys were fixed, processed, sectioned and subjected to 2 rounds of staining with *Pkm2* and *Pkm1* with complete stripping of each antibody per round. Relative levels of Pkm2 and Pkm1 expression is shown without and with doxycycline treatment.

5.3 Discussion

The exact role of *Pkm2* in tumourigenesis still remains controversial. *Pkm2* is considered to play an important role in tumourigenesis by regulating the Warburg effect (Wong et al. 2013). However, recent studies have shown contradicting effects of *Pkm2* deletion on tumourigenesis in different tissue contexts. The role of *Pkm2* in the tumourigenesis of TSC lesions has never been explored. In the current study, expression of *Pkm2* was first examined in renal tumours. *Pkm2* was vastly increased in all large cystic lesions, papillary adenomas and solid carcinomas in the kidneys of *Tsc2*$^{+/-}$ mice. Renal tumours of *Tsc2*$^{+/-}$ mice have previously shown increased expression of enzymes associated with the Warburg effect, such as HKII and GAPDH (Jones et al. 2019). Elevated *Pkm2* expression has been observed in many advanced cancers, such as renal cell carcinoma and lung cancer, and can be used as a biomarker in these patients (Brinck et al. 1994; Wechsel *et al.* 1999; Schneider *et al.* 2002). The advantage of expressing *Pkm2* in tumour cells rather than attenuating the expression of the constitutively active *Pkm1* is likely to be that *Pkm2* can integrate various metabolic and signalling cues from oncogenes to divert glucose to energy production or biosynthetic synthesis. Unlike *Pkm1*, *Pkm2* can be modulated through a range of signalling effectors to assume greater control of glucose fluxes responsive to cellular needs (van Niekerk and Engelbrecht 2018). *Pkm2* also has the advantage over *Pkm1* to act as a transcriptional regulator when translocated to the nucleus for gene expression (Yang et al. 2012). Interestingly, some smaller cystic lesions showed little or no expression of *Pkm2*. These results suggest that *Pkm2* might be involved in tumour progression from cysts to papillary adenomas and solid carcinomas.

In the current study, *Pkm2* was deleted in the kidneys of *Tsc2*$^{+/-}$ mice to analysis its role in renal tumourigenesis. The deletion of *Pkm2* did not reduce tumour burden and was not required for tumour growth in *Tsc2*$^{+/-}$ mice. These results appear to be consistent with some recent studies. *Pkm2* deletion in an *Apc*-deficient mouse model of colon cancer had no effect on tumour growth (Lau et al. 2017). *Pkm2* deletion in Kras$^{LSL\text{-}G12D}$/p53 driven sarcoma model also exhibited no difference in tumour growth between PKM2$^{+/+}$ and PKM2$^{-/-}$ tumours (Dayton *et al.* 2018). However, some other studies have demonstrated that deletion or inhibition of *Pkm2* reduces tumour burden and blocks tumour progression (Christofk et al. 2008). A previous *in vitro* study using *Tsc*-null MEFs reported that *Pkm2* deletion resulted in a decrease in aerobic glycolysis and lactate production and suppressed mTOR-mediated tumorigenesis in a xenograft mouse model

of prostate cancer (Sun et al. 2011). *Pkm2* deletion in leukaemia has also delayed the onset of leukemogenesis (Wang et al. 2014). Inhibition of *Pkm2* with Shikonin significantly inhibited tumour growth of hypoxic-resistant gastric cell lines and xenograft models (Kitayama *et al.* 2017). In contrast to these findings, some studies also suggest that *Pkm2* deletion promotes tumour formation. A conditional deletion of *Pkm2* in a *Brca1*-loss-driven mouse model of breast cancer showed an accelerated tumour growth (Israelsen et al. 2013). Accelerated tumour growth following *Pkm2* deletion has also been observed in a mouse model of hepatocellular carcinoma (Dayton et al. 2016). These observations suggest potential tumour suppressor functions of *Pkm2* in some tissue types and models. Many factors probably contribute to the different effects of *Pkm2* deletion on tumourigenesis, particularly including different animal models used (xenograft versus transgenic) and different tissue contexts examined. Thus, further investigations are required to clarify the role of *Pkm2* in tumourigenesis in a tissue-dependent manner.

Pkm2 has previously been reported to regulate mTORC1 signalling via the phosphorylation of mTORC1 inhibitor AKT1S1 in cultured human kidney cells (He et al. 2016). The effect of *Pkm2* deletion on mTOR signalling was examined in renal lesions of *Tsc2*$^{+/-}$ mice in this study. *Pkm2* expression was increased with increased mTORC1 and mTORC2 signalling in renal lesions. However, *Pkm2* deletion had no overall effect on mTORC1 or mTORC2 signalling compared to tumours expressing *Pkm2*. This indicates that *Pkm2* is not a major regulator of mTOR activity in these tumours. Moreover, *Pkm2* deletion had no significant effect on cell proliferation. This suggests that, compared to many other studies, *Pkm2* may not be required for cell proliferation in these tumours. The major driver for tumour cell proliferation is likely to be increased mTOR signalling in these tumours. mTOR signalling is aberrantly activated in TSC tumours and its inhibition by mTOR inhibitors effectively attenuates tumour growth (Inoki et al. 2003a; Huang and Manning 2009; Krymskaya and Goncharova 2009; Pollizzi et al. 2009b; Yang et al. 2015; Jones et al. 2019). In addition, the anti-tumour efficacy of metabolic inhibitors was, at least partly, due by inhibiting mTORC1 in *Tsc2*$^{+/-}$ mice (Yang et al. 2015; Yang et al. 2017; Jones et al. 2019). Failure of mTORC1 or mTORC2 inhibition following *Pkm2* deletion here may be responsible for the lack of anti-tumour effectiveness and inhibition of cell proliferation.

Interestingly, expression of *Pkm1* was consistently increased in all *Pkm2*$^{-/-}$ tumour cells while only low levels of basal expression of *Pkm1* was observed in renal tumours and normal tissues with *Pkm2*. However, increased expression of *Pkm1* following *Pkm2*

deletion has been observed in stromal cells but not in tumour cells, and proliferating tumour cells did not express *Pkm1* following *Pkm2* deletion in previous studies (Israelsen et al. 2013). *Pkm1* expression has previously been implicated in cell proliferation attenuation following conditional *Pkm2* deletion in primary cells and *Pkm1* expression, rather than *Pkm2* loss, promotes a metabolic state that is unable to support DNA synthesis (Lunt *et al.* 2015). However, no significant effect of increased *Pkm1* expression after *Pkm2* deletion was found on tumour cell proliferation in the kidneys of *Tsc2*$^{+/-}$ mice in the current study. *Pkm2* activators have previously been used to render *Pkm2* more like *Pkm1* for enhancing flux to the TCA cycle and reduce the build-up of glycolytic precursors for macromolecule biosynthesis. These *Pkm2* activators have successfully inhibited tumour growth in xenografts models bearing non-small-cell lung cancer tumours (Anastasiou *et al.* 2012). In contrast, increased *Pkm1* expression following *Pkm2* deletion in the current study, did not reduce tumour burden. Instead, the expression of *Pkm1* might actually compensate for missing PK activity for tumourigenesis in *Tsc2*$^{+/-}$ mice. Recently, the expression of *Pkm1*, rather than *Pkm2*, has been reported to contribute to tumour growth and proliferation in a mouse model of KRAS^{G12D}-induced non-small cell lung tumours (Morita *et al.* 2018). In this model, PKM1-expressing cells exhibited more active autophagy than PKM2-expressing cells, suggesting that PKM1 drives active glucose metabolism and autophagy in these tumour cells, thus giving these cells a metabolic advantage. These results suggest that increased *Pkm1* expression following *Pkm2* deletion may be required for tumourigenesis TSC-associated renal lesions. However more investigations are needed to test this hypothesis.

In summary, *Pkm2* was specifically deleted in the epithelial cells of renal tubules and renal tumours of *Tsc2*$^{+/-}$ mice. *Pkm2* deletion appeared to have no significant effect on tumour burden, mTOR signalling or proliferation in tumour cells, suggesting that *Pkm2* pharmacological inhibition may not be an effective therapeutic strategy for TSC-associated tumours. In addition, the alternative PKM isoform, *Pkm1*, was highly expressed in tumours with *Pkm2* deletion suggesting a compensatory feedback mechanism for continued pyruvate kinase activity in these tumours. It is still not clear whether *Pkm2* is required or not for tumourigenesis in the kidneys of *Tsc2*$^{+/-}$ mice because it could not be excluded that increased *Pkm1* following *Pkm2* deletion plays a role in tumour initiation and progression in these mice.

6 CHAPTER SIX

General Discussion

This work investigated inhibitors of mTOR and metabolic pathways as anti-tumour therapy for TSC-associated renal tumours and mechanisms of tumourigenesis in the kidneys of *Tsc2*$^{+/-}$ mice. These pre-clinical studies are necessary to improve therapy for TSC-associated renal tumours, and tumours caused by aberrant activation of the mTOR signalling pathway.

6.1 Use of mouse models of TSC-associated tumours in preclinical studies

Mouse models of cancer and tumour syndromes are very useful in cancer research, although complexity of human disease cannot always be exactly recapitulated due to species differences between mouse and human (Frese and Tuveson 2007; Lampreht Tratar *et al.* 2018). They can be used for testing preventive and therapeutic agents before translation into clinical trials, and for studying mechanisms underlying tumourigenesis in ways that cannot be done in humans (van Miltenburg and Jonkers 2012). Although *in vitro* studies are relatively cheap, easier to conduct and flexible to manipulate experimental conditions, mouse models have numerous advantages; they can be utilised to investigate pharmacodynamics and pharmacokinetics of therapeutic agents, assess tumour burden and evaluate toxicity/tolerability. Various mouse models of cancer are available including xenograft, carcinogen-induced and genetically engineered mouse (GEM) models (Lampreht Tratar et al. 2018). Xenograft models are the most widely used animal model and are generated by the implantation of human tumour cells (ectopically or orthotopically) into immunodeficient mice (Becher and Holland 2006). These models can be cheap, reproducible, and produce rapid results. Tumour size in xenograft models can be readily assessed, and treatment effect easily tracked. However, xenograft models use immunosuppressed mice for tumour growth and progression, and therefore mice lack a full immune response to tumours. This becomes particularly problematic for testing immunotherapies (Hou and Ji 2018). Furthermore, implantation of human tumour cells under the skin does not fully represent the natural tumour environment and do not share the genetics and histology seen in human tumours (Becher and Holland 2006).

Carcinogen-induced mouse models have been used for cancer research for many years (Memmott *et al.* 2010; Vikis *et al.* 2013). Some carcinogens can rapidly and reproducibly induce some types of tumour. However, mutations caused by carcinogens could be widespread in the genome, probably with some unwanted phenotypes. GEM models spontaneously develop tumours within the normal architecture of specific tissues to better represent human tumour cell intrinsic and extrinsic mechanisms (Onda et al. 1999; Becher and Holland 2006; Lampreht Tratar et al. 2018). GEM models have one or more genes altered known to induce tumourigenesis. Tumours develop in normal, immunocompetent mice and exact genetic mutations found in human can be induced in these models for tumour formation. However, the development of tumours can be time-consuming and expensive in GEM models (Becher and Holland 2006).

The presented work here used a genetically engineered *Tsc2*$^{+/-}$ mouse model to investigate alternative treatment approaches for renal tumours and to study mechanisms of renal tumourigenesis. *Tsc2*$^{+/-}$ mice were first generated by gene targeting in 1999 and spontaneously develop various types of renal tumours including cystic and papillary adenomas and solid carcinomas during their lifetime (Kobayashi et al. 1999; Onda et al. 1999). *Tsc2*$^{+/-}$ mice have been used to understand roles of mTOR signalling in tumourigenesis. They have also been excellent tumour models for testing anti-tumour efficacy of preventative and therapeutic agents targeting the mTOR pathway and other oncogenic pathways such as tumour metabolism and angiogenesis (Yang et al. 2017; Jones et al. 2019). Pre-clinical studies using *Tsc2*$^{+/-}$ models have demonstrated significant efficacy of rapamycin and rapalogs for treating renal tumours and liver tumours, consistent with clinical studies (Kenerson et al. 2005; Franz et al. 2006; Pollizzi et al. 2009b; Bissler et al. 2013; Guo and Kwiatkowski 2013; Kim et al. 2014). Combination of everolimus with sorafenib was found to be more effective than everolimus alone for treating renal tumours of *Tsc2*$^{+/-}$ mice and it may be worth investigating this combination in clinical settings. ATP-competitive inhibitors of mTOR have been found to be as effective as rapalogs for treating renal tumours in *Tsc2*$^{+/-}$ mice but it may cause more severe side effects (Narov et al. 2017)(to be discussed in more detail later).

Renal tumours are present in 80-90% of TSC patients and is one of the leading causes of morbidity and mortality. Around 2-4% of TSC patients also develop RCCs (Al-Saleem et al. 1998). In contrast, *Tsc2*$^{+/-}$ mice frequently develop RCC and an almost 100% penetrance of RCC is seen in mice at 18 months old (Onda et al. 1999). *Tsc2*$^{+/-}$ mice, therefore, can be recognised as RCC cancer models. Renal cancer cell lines 786-O and

Renca are frequently used to establish xenograft models of RCC to test therapeutic agents (Hirayama *et al.* 2016). However, these xenograft mouse models of RCC do not recapitulate molecular and cellular features of human disease. GEM models have been developed to mimic human RCC (Hou and Ji 2018). These models were generated by simultaneously deleting two or more tumour suppressor genes and/or activating an oncogene following failure to develop RCC in mice with *Vhl* inactivation only (Lonser *et al.* 2003; Sato *et al.* 2013; Bailey *et al.* 2017; Hou and Ji 2018). For example, mouse models with the inactivation of *Vhl* in combination with mutations of other genes such as *trp53* or *pten* deletion or *MYC* amplification have been successfully developed (Frew *et al.* 2008; Albers *et al.* 2013; Shroff et al. 2015; Bailey et al. 2017). These models recapitulate some of the phenotypes of human RCC and together with *Tsc2*$^{+/-}$ mice can be useful to test novel therapies for RCC.

Mechanisms for the progression of TSC renal lesions to RCC in *Tsc2*$^{+/-}$ mice are not well understood. This study provides lines of evidence for a new mechanism underlying tumour progression through the activation of EMT. Partial EMT, possibly driven by mTOR, is a dominant feature during TSC tumour progression in *Tsc2*$^{+/-}$ mice, also shared with human TSC-associated tumours. The co-expression of epithelial and mesenchymal markers was apparent in these tumours as they progressed from cystic to papillary adenomas to solid carcinomas. More thorough investigation revealed that individual tumour cells expressed both epithelial and mesenchymal markers, indicating a transition state of EMT. Partial EMT represents an intermediate stage of EMT where cells confer characteristics of both epithelial and mesenchymal cells (Jolly et al. 2016a; Nieto et al. 2016). This gives cells greater plasticity by obtaining migratory advantages whilst retaining cell-cell adhesion. Partial EMT may also facilitate metastatic colonisation through an easier transition of MET at secondary sites (Lecharpentier et al. 2011). These *Tsc2*$^{+/-}$ mice, therefore, represent a model for RCC research with EMT as a new mechanism for tumour progression.

6.2 ATP-competitive inhibitors of mTOR for treatment of TSC-associated tumours

Rapalogs are effective for treating TSC-associated tumours in both pre-clinical and clinical trials. However, tumour re-growth is apparent upon treatment cessation. In addition, not all patients show a clear anti-tumour effect and not all TSC-associated tumours respond to rapalogs in a patient. One study revealed that around 50% of

patients with TSC-associated LAM treated with rapamycin failed to show any clinical response and showed progressive lung function deterioration (McCormack *et al.* 2011). Long term treatment with rapalogs is normally required and this could cause unacceptable adverse effect such as infection due to immunosuppression (Benjamin et al. 2011). Rapalogs are cytostatic rather than cytotoxic, thus supressing tumour growth rather than killing tumour cells (Bissler et al. 2008). Molecularly, rapalogs are unable to efficiently inhibit phosphorylation 4E-BP1 (Feldman et al. 2009; Thoreen et al. 2009) and believed to have little inhibitory effect on mTORC2 signalling. Furthermore, rapalogs cause the suppression of negative feedback loops (discussed in Introduction), resulting in increased activation of oncogenic signalling pathways such as the PI3K/Akt pathway (Harrington et al. 2004; O'Reilly et al. 2006; Tabernero et al. 2008). These limitations can compromise efficacy of rapalogs for treating TSC-associated tumours. ATP-competitive inhibitors of mTOR are a new generation of inhibitors that have been developed to help overcome some of the limitations of rapalogs. These inhibitors bind the ATP-binding site of mTOR and thus efficiently block both mTORC1 and mTORC2 signalling. ATP-competitive inhibitors have been tested in mTOR-driven cancer models and TSC-associated tumours in *Tsc2*$^{+/-}$ mice. WYE-354, a potent ATP-competitive inhibitor of mTOR, has shown robust antitumor activity in *Pten*-null tumours in a xenograft mouse model (Yu et al. 2009). PP242, another potent ATP-competitive inhibitor of mTOR, has demonstrated superior anti-tumour activity to rapamycin for Akt-driven xenograft tumours (Hsieh *et al.* 2010). Another ATP-competitive inhibitor, AZD8055, has also shown anti-tumour efficacy in a broad range of human tumour xenografts, such as breast, glioma, colon, uterine, prostate and non-small cell lung cancer xenograft models (Chresta *et al.* 2010). Several ATP-competitive inhibitors of mTOR has been tested in *Tsc2*$^{+/-}$ mice mainly for treating renal tumours. The ATP-competitive inhibitor of mTOR, MLN0128, has been compared with rapamycin for its anti-tumour effect on renal cystadenomas in *Tsc2*$^{+/-}$ mice. MLN0128 was well tolerated and as effective at reducing tumour burden as rapamycin. However, when treatment was discontinued with either rapamycin or MLN0128, tumour regrowth was observed (Guo and Kwiatkowski 2013). Other ATP-competitive inhibitors of mTOR such as NVP-BEZ235 and GSK2126458 (dual inhibitors of PI3K and mTOR) have also demonstrated anti-tumour efficacy for renal tumours in *Tsc2*$^{+/-}$ mice (Pollizzi et al. 2009b; Narov et al. 2017). A recently developed ATP competitive inhibitor of mTOR, AZD2014, has shown promising anti-tumour efficacy in various cancer cell lines and xenograft models (Pike et al. 2013; Guichard et al. 2015; Zheng et al. 2015). Importantly, AZD2014 has been shown to overcome rapamycin resistant tumour cells and have a superior therapeutic effect to rapamycin in a xenograft

model of hepatocellular carcinoma (Liao et al. 2014; Vandamme et al. 2016). Zheng et al. also demonstrated superior anti-tumour effects of AZD2014 over rapamycin in a xenograft model of RCC (Zheng et al. 2015). AZD2014 anti-tumour efficacy has never been explored for TSC tumours. The work carried out in chapter 3 investigated the anti-tumour efficacy of AZD2014 in comparison to rapamycin for renal tumours in *Tsc2*$^{+/-}$ mice. AZD2014 in this study effectively reduced tumour burden of all types of renal tumours and potently inhibited both mTORC1 and mTORC2 signalling. Rapamycin also effectively reduced tumour burden and potently inhibited mTORC1 but only partially inhibited mTORC2. The present study did not show any superior anti-tumour effect of AZD2014 over rapamycin. Similar results of an ATP-competitive inhibitor of mTOR compared to rapamycin have been seen previously in *Tsc2*$^{+/-}$ mice (Guo and Kwiatkowski 2013). These results observed in *Tsc2*$^{+/-}$ mice were different from previous findings in xenograft models by Zheng et al. and Liao et al. Yang *et al* have reported that feedback suppression of Akt is lost in *Tsc2*$^{+/-}$ renal tumours with increased Akt signalling (Yang et al. 2015). Since mTORC2 signalling is required for the full activation of Akt, through its phosphorylation of S473, and is involved in many oncogenic downstream signalling pathways associated with cell growth and survival (Jacinto et al. 2004; Sarbassov et al. 2005b), AZD2014 was expected to be more effective for these tumours. The lack of superior efficacy of AZD2014 over rapamycin is surprising and suggests that mTORC2 inhibition might not be required for reduction of tumour burden in these mice. Differences observed between the effects of AZD2014 in this study and others may be due to different models used (xenograft vs transgenic) and the varying mechanisms of tumourigenesis found in *Tsc2*$^{+/-}$ mouse renal tumour (Yang et al. 2015). Moreover, AZD2014 did not show any increased apoptosis compared to rapamycin, suggesting a cytostatic effect rather than cytotoxic. Tumour regrowth would therefore be expected when AZD2014 treatment stops, but this requires further investigation. In clinical settings, AZD2014 has been tested for treating solid tumours. Preliminary results have demonstrated limited tumour responses to AZD2014 in a patient with breast cancer and a patient with pancreatic cancer (Basu et al. 2015). A recent randomised phase 2 clinical trial has shown that AZD2014 was less effective than everolimus in patients with VEGF-refractory metastatic clear cell renal cancer (Powles et al. 2015). However, AZD2014 has not been tested for TSC patients. A clinical trial is currently recruiting patients with *TSC1/2* mutated refractory solid cancer to undergo treatment with AZD2014 (https://www.findmecure.com/clinicaltrials/show/nct03166176).

As discussed above, partial EMT was found to be a mechanism of tumour progression in *Tsc2*$^{+/-}$ mice in this work. Therefore, the effect of AZD2014 and rapamycin on EMT was examined. Indeed, AZD2014 and rapamycin both effectively suppressed EMT in all types of renal tumours. The proportion of mesenchymal markers vimentin and FSP1 in renal tumours after AZD2014 and rapamycin treatment was significantly reduced whereas epithelial marker E-Cadherin was variable. AZD2014 and rapamycin have previously shown inhibition of EMT in cultured hepatoma cells, with AZD2014 having greater effects (Liao et al. 2014). Furthermore, another ATP-competitive mTOR inhibitor, Torin 1, and rapamycin have previously observed to suppress EMT in cultured glioblastoma cells (Catalano et al. 2015). These findings suggest that both rapalogs and ATP-competitive inhibitors of mTOR may exert anti-tumour activity, at least partly, through suppression of partial EMT.

6.3 Targeting metabolic pathways for treatment of TSC-associated renal tumours

ATP-competitive inhibitors of mTOR, thus far, have failed to show a superior anti-tumour efficacy to rapamycin and rapalogs in TSC-associated tumours *in vivo*. This warrants research for alternative therapeutic approaches other than targeting mTOR for treating TSC-associated tumours to improve therapy. Cellular metabolism is highly regulated by the mTOR pathway (Cantor and Sabatini 2012). Aberrant activation of mTOR reprograms metabolic pathways in tumours and leads to increased aerobic glycolysis and glutaminolysis through the upregulation of genes involved in these processes such as *HIF1α* and *c-myc* (Masui et al. 2013; Zha et al. 2014; Altman et al. 2016). Increased flux through glycolysis and glutaminolysis ensures the generation of surplus amounts of ATP and macromolecules to sustain rapid growth and proliferation. Increased mTOR signalling renders tumour cells addiction to glucose and glutamine. Studies have targeted glycolysis and glutaminolysis individually in pre-clinical trials for anti-tumour therapy and have showed promising results both *in vitro* and *in vivo* (Hensley et al. 2013; Altman et al. 2016; Nagarajan et al. 2016; Martinez-Outschoorn et al. 2017). The dual inhibition of glycolysis and glutaminolysis has successfully inhibited proliferation of ovarian cancer cells *in vitro* (Sun et al. 2017) but this combination has never been tested *in vivo* for tumour therapy.

Tsc2 null MEFs with overactivated mTOR are addicted to glucose and glutamine (Choo et al. 2010; Jiang et al. 2011; Csibi et al. 2013). Dual inhibition of glycolysis and

glutaminolysis caused significant cell death in *Tsc2*$^{-/-}$ but not *Tsc2*$^{+/+}$ MEF cells (Csibi et al. 2013). It remains to be tested whether dual inhibition of glycolysis and glutaminolysis is a better therapy than rapalogs for TSC-associated tumours *in vivo*. The work from chapter 4 highlighted that TSC-associated renal tumours from *Tsc2*$^{+/-}$ mice had increased expression of enzymes associated with glycolysis and glutaminolysis including GAPDH, HKII, GLS and GDH. These metabolic enzymes may represent sensible targets for treating these tumours. Therefore, the dual inhibition of glycolysis and glutaminolysis was assessed for anti-tumour therapy of renal lesions in *Tsc2*$^{+/-}$ mice. 3-BrPA, an inhibitor of HKII, was used in combination with CB-839, an inhibitor of GLS (Gross et al. 2014; Sun et al. 2015). Combinational treatment with 3-BrPA and CB-839 significantly suppressed tumour burden in *Tsc2*$^{+/-}$ mice but was not as effective as rapamycin. Individual treatment with 3-BrPA or CB-839 showed no overall effect on renal tumour burden. Glycolytic inhibition with 2-DG has previously been reported to attenuate tumour growth in a mouse model injected with *Tsc2*-null rat tumour cells (Jiang et al. 2011). Glycolytic inhibition with 3-BrPA has shown anti-tumour efficacy in liver carcinomas of rabbit and mouse models (Ko et al. 2012). The lack of therapeutic efficacy in the current study is unlikely to result from inefficient uptake of 3-BrPA as the lactate transporter, MCT1, required for transportation of 3-BrPA (Birsoy et al. 2013) was highly expressed in tumour cells . CB-839 was effective for treating breast cancer and RCC in cultured tumour cells and xenograft mouse models (Gross et al. 2014; Xiang *et al.* 2015; Abu Aboud *et al.* 2017; Lampa et al. 2017). CB-839 is currently being tested in phase I clinical trials in patients with solid and haematological malignancies. Probably several factors may contribute to the limited of efficacy of 3-BrPA or lack of efficacy of CB-839 as a single agent for TSC-associated renal tumours. For example, aberrant activation of mTORC1 has been found to facilitate the bypass of glycolytic block by shunting glucose into the pentose phosphate pathway then back into glycolysis (Pusapati et al. 2016). It has also been reported that inhibition of glycolysis can cause an increase in glutaminolysis and glycogenesis to replace the lost glucose (DeBerardinis and Cheng 2010; Altman et al. 2016). As observed in chapter 3, mTORC1 inhibition was needed for the anti-tumour efficacy by rapamycin or AZD2014 for TSC-associated tumours and, as observed in chapter 4, 3-BrPA or CB-839 had little or no effect on mTORC1. Therefore, the failure of inhibition of mTORC1 with either 3-BrPA or CB-839 may also be partly responsible for lack of efficacy in these tumours. Dual inhibition of glycolysis and glutaminolysis had significant effects on mTORC1 signalling and correspondingly reduced tumour burden significantly.

A major difficulty with targeting cellular metabolism for tumour therapy is the levels of toxicity frequently observed in normal cells. Cellular pathways utilised in tumour cells for rapid growth and proliferation are also normally required for the function of normal cells. HKII has been reported to be expressed in highly proliferative cells and tumours cells (Mathupala *et al.* 2006). Therefore, targeting this enzyme was expected to have low toxicity. However, significant loss of body weight occurred in some mice treated with 3-BrPA alone, combination of 3-BrPA and rapamycin, or combination of 3-BrPA and CB-839, indicating increased toxicity. 3-BrPA has been reported to target other glycolytic enzymes, such as GAPDH and succinate dehydrogenase, and inhibition of these multiple targets could contribute to the increased toxicity seen in these mice. Taken together, these data indicate that inhibition of glycolysis or glutaminolysis or both is unlikely to offer better therapy than rapalogs for treating TSC-associated tumours.

6.4 Conditional gene knockout in the kidneys of *Tsc2*$^{+/-}$ mice for investigation of roles of genes in tumourigenesis

Gene knockout technology has been widely used to produce GEM models carrying single or multiple mutations of oncogenes or tumour suppressor genes to study their functions *in vivo* (Capecchi 2005). Conventional knockout models have germline mutations which could frequently result in embryonic lethality, especially in genes required for development (Wang and Abate-Shen 2014). In addition, whole body gene knockouts do not always replicate human disease and can lead to adverse effects. To overcome these limitations, conditional knockout models utilising the Cre-Loxp system have been developed to allow temporal and spatial deletion of genes. Inducible expression of Cre can be achieved for temporal control of gene deletion mediated through tamoxifen or tetracycline treatment (Gossen and Vujard 1992; Gossen et al. 1995; Feil *et al.* 1997). Inducible Cre expression can be combined with tissue-specific promotors for tissue-specific deletion of genes (Espana-Agusti et al. 2016). These models are well established and are widely used in cancer research (Stricklett et al. 1999; Wang 2009).

As discussed in the introduction, conventional mouse models with homozygous mutation of *Tsc1* and *Tsc2* are embryologically lethal. *Tsc1*$^{+/-}$ or *Tsc2*$^{+/-}$ mice usually require loss of 2nd allele to develop tumours (Onda et al. 1999; Wilson et al. 2005). Conditional knockout models of TSC have been generated to assess the effects of complete gene knockout in specific organs and avoid embryonic lethality. Organs targeted for

conditional deletion of *Tsc1* or *Tsc2* include the kidneys, skin, heart and brain (Uhlmann et al. 2002; Meikle et al. 2005; Prabhakar et al. 2013; Leech et al. 2015; Rozas et al. 2015). For example, *Tsc1* floxed mice crossed with mice carrying Cre under the control of *Darpp32* developed kidney cystadenomas and paw angiosarcomas within 6 weeks, with all other organs unaffected (Leech et al. 2015).

Pkm2 has been considered to drive aerobic glycolysis and is highly expressed in many cancer types including RCC (Brinck et al. 1994; Wong et al. 2013). PKM2 has also been reported to be a selective biomarker for RCC (Wechsel et al. 1999). This study, as described in Chapter 5, sought to investigate the effect of conditional deletion of *Pkm2* on renal tumourigenesis in $Tsc2^{+/-}$ mice. In the current study, tetracycline inducible expression of Cre (*TetO.Cre*) under the control of the *Pax8* promotor (*Pax8.rtTA*) was used to delete *Pkm2* in the tubule epithelial cells of the kidneys in $Tsc2^{+/-}$ mice (Israelsen et al. 2013). *Pax8* is highly expressed in the kidneys, thyroid and liver (Poleev et al. 1992). The promotor of *Pax8* has been previously used to delete genes such as *Vhl* and *Tsc1* in epithelial cells of kidney tubules through inducible expression of Cre by either tamoxifen or tetracycline (Traykova-Brauch et al. 2008; Espana-Agusti et al. 2016). As expected, *Pkm2* was effectively and consistently deleted in the epithelial cells of renal tubules in $Tsc2^{+/-}$ mice. However, no significant difference was observed in tumour burden between mice with or without *Pkm2* in the epithelial cells of renal tubules. These results were consistent with previous findings observed with *Pkm2* conditional deletion in an *Apc*-deficient mouse model of colon cancer and in a $Kras^{LSL\text{-}G12D}$/p53 driven sarcoma model (Lau et al. 2017; Dayton et al. 2018). However, other studies demonstrated that *Pkm2* deletion could either promote or supress tumourigenesis in different mouse models of cancer such as breast and prostate cancer models (Sun et al. 2011; Israelsen et al. 2013), suggesting distinct roles of *Pkm2* within different tissue contexts in tumourigenesis. The results in this study suggest that the pharmacological inhibition of *Pkm2* may not offer an effective treatment approach for TSC-associated renal tumours. It was notable in the current study that *Pkm1* expression was increased in *Pkm2* deleted tumour cells, but previous reports have shown that *Pkm1* was increased in only non-tumour cells after deletion of *Pkm2* (Israelsen et al. 2013). Increased expression of *Pkm1* in TSC-associated tumour cells may functionally compensate for *Pkm2* loss to promote tumourigenesis. This notion is supported by a recent report that the expression of *Pkm1*, rather than *Pkm2*, contributed to tumour growth and proliferation in a mouse model of $KRAS^{G12D}$-induced non-small cell lung tumours (Morita et al. 2018).

Similar strategies could be used to dissect the oncogenic pathways in the kidneys of *Tsc2*$^{+/-}$ mice, particularly the mTORC1, mTORC2 and EMT involvement in tumour formation and progression. As discussed above, ATP-competitive inhibitors of mTOR inhibit both mTORC1 and mTORC2 but do not have greater anti-tumour efficacy than rapalogs. It is important to determine whether it is necessary to inhibit mTORC2 for tumour therapy. *Rictor,* a key component of mTORC2, could be conditionally deleted in the epithelial cells of renal tubules to evaluate its role in renal tumourigenesis in the kidneys of *Tsc2*$^{+/-}$ mice. Many genes are involved in regulation of oncogenic EMT including *TGFβ*, a potent driver of EMT and tumour progression. *TGFβ* could be similarly deleted in the epithelial cells of renal tubules to see whether it promotes or supresses EMT and tumour progression in the kidneys of *Tsc2*$^{+/-}$ mice.

6.5 Conclusions

This work presented a new model of EMT-associated tumour progression in the kidneys of *Tsc2*$^{+/-}$ mice. Both AZD2014 and rapamycin effectively suppressed EMT and significantly reduced renal tumour burden in these mice. This work also demonstrated that the dual inhibition of glycolysis and glutaminolysis significantly reduced renal tumour burden in these mice but was not as efficient as rapamycin. Finally, *Pkm2* was successfully deleted in the epithelial cells of renal tubules in *Tsc2*$^{+/-}$ mice but loss of *Pkm2* did not have significant effect on renal tumourigenesis. However, increased expression of *Pkm1* observed in this study following *Pkm2* deletion in renal tumour cells may functionally compensate for *Pkm2* loss to promote tumourigenesis.

6.6 Future directions

Tsc2$^{+/-}$ mice used in this study provided an invaluable model for testing anti-tumour agents on renal tumours and mechanisms of tumourigenesis. Methods of accelerating RCC formation in *Tsc2*$^{+/-}$ mice could provide more cost-effective approaches for RCC research. Renal tumour progression could be accelerated by inducing multiple genetic mutations, as seen in human disease. Conditional deletion of *Vhl* in renal tumours of *Tsc2*$^{+/-}$ may provide a more aggressive and accelerated model of RCC and is worth investigating further. The use of imaging technologies as non-invasive ways to track tumour size over time could also be beneficial. T2-weighted MRI has been successful at identifying renal tumours of living *Tsc2*$^{+/-}$ mice. However, imaging sensitivity needs improving for identifying solid carcinomas (Kalogerou *et al.* 2012). Other imaging

techniques for assessing treatment effect, such as CT or PET-CT may be worth trying. These imaging techniques may also be useful for investigating tumour regrowth following treatment cessation. The findings in this study highlighted some new areas that could be targeted for anti-tumour therapy of renal tumours. The use of EMT inhibitors in combination with ATP-competitive inhibitors may provide greater therapeutic effects in renal tumours. In addition, third generation inhibitors of mTOR and PI3K currently being developed and tested and may be worth investigating in these tumours although these combinational strategies could have greater toxicity (Rodrik-Outmezguine et al. 2016). Finally, further investigations are also warranted to reveal possible roles of *Pkm1* and EMT-associated genes in renal tumourigenesis of *Tsc2*$^{+/-}$ mice.

7 Publications

First author publications:

Ashley T. Jones, Kalin Narov, Jian Yang, Julian R. Sampson and Ming Hong Shen. 2019. Efficacy of dual inhibition of glycolysis and glutaminolysis for therapy of renal lesions in *Tsc2*$^{+/-}$ mice. *Neoplasia* 21 (2), pp. 230-238.

Ashley T. Jones, Jian Yang, Kalin Narov, Elizabeth P Henske, Julian R. Sampson and Ming Hong Shen. 2018. Allosteric and ATP-competitive inhibitors of mTOR effectively suppress tumour progression associated epithelial-mesenchymal transition in the kidneys of *Tsc2*$^{+/-}$ mice. **Manuscript submitted to *The International Journal of Cancer*.**

Ashley T. Jones, Kalin Narov, Jian Yang, Julian R. Sampson and Ming Hong Shen. The role of *Pkm2* in TSC-associated tumours. 2019. **Manuscript in preparation**.

Other publications during my PhD studies:

Jianling Xie, Kaikai Shen, **Ashley T. Jones**, Jian Yang, Andrew R. Tee, Ming Hong Shen, Mengyuan Yu, Swati Irani, Derick Wong, James Merrett, Roman V. Lenchine, Stuart De Poi, Kirk B. Jensen, Paul J. Trim, Marten F. Snel, Makoto Kamei, Sally Kim Martin, Stephen Fitter, Shuye Tian, Xuemin Wang, Lisa M Butler, Andrew C. W. Zanettino & Christopher G. Proud. mTOR complex 1 (mTORC1) phosphorylates MAP kinase-interacting kinase 2 (MNK2) to signal to cell growth and oncogenesis**. Manuscript submitted to *EMBO J* in March 2019.**

Johnson, Charlotte E., Dunlop, Elaine A., Seifan, Sara, McCann, Henry D., Hay, Trevor, Parfitt, Geraint J., **Jones, Ashley T**., Giles, Peter J., Shen, Ming H., Sampson, Julian R., Errington, Rachel J., Davies, David Mark and Tee, Andrew R. 2018. Loss of tuberous sclerosis complex 2 sensitizes tumors to nelfinavir−bortezomib therapy to intensify endoplasmic reticulum stress-induced cell death. *Oncogene.* 37 (45), pp. 5913-5925

Narov Kalin, Yang Jian, Samsel Paulina, **Jones Ashley**, Sampson Julian R and Shen Ming Hong. 2017. The dual PI3K/mTOR inhibitor GSK2126458 is effective for treating

solid renal tumours in *Tsc2*$^{+/-}$ mice through suppression of cell proliferation and induction of apoptosis. *Oncotarget*. 8 (35), pp. 58504-58512.

Yang Jian, Samsel Paulina A., Narov Kalin, **Jones Ashley**, Gallacher Daniel, Gallacher John, Sampson Julian Roy, and Shen Ming Hong 2017. Combination of everolimus with sorafenib for solid renal tumours in *Tsc2*$^{+/-}$ mice is superior to everolimus alone. *Neoplasia* 19 (2), pp. 112-120.

8 References

Abu Aboud, O., Habib, S. L., Trott, J., Stewart, B., Liang, S., Chaudhari, A. J., Sutcliffe, J. *et al.* (2017). Glutamine Addiction in Kidney Cancer Suppresses Oxidative Stress and Can Be Exploited for Real-Time Imaging. *Cancer Res* **77:**6746-6758.

Adachi, H., Igawa, M., Shiina, H., Urakami, S., Shigeno, K. and Hino, O. (2003). Human bladder tumors with 2-hit mutations of tumor suppressor gene TSC1 and decreased expression of p27. *J Urol* **170:**601-604.

Adler, J., Greweldinger, J. and Litzky, G. (1984). "Macro" aneurysm in renal angiomyolipoma: two cases, with therapeutic embolization in one patient. *Urol Radiol* **6:**201-203.

Adriaensen, M. E., Schaefer-Prokop, C. M., Duyndam, D. A., Zonnenberg, B. A. and Prokop, M. (2011). Radiological evidence of lymphangioleiomyomatosis in female and male patients with tuberous sclerosis complex. *Clin Radiol* **66:**625-628.

Adriaensen, M. E., Schaefer-Prokop, C. M., Stijnen, T., Duyndam, D. A., Zonnenberg, B. A. and Prokop, M. (2009). Prevalence of subependymal giant cell tumors in patients with tuberous sclerosis and a review of the literature. *Eur J Neurol* **16:**691-696.

Akins, N. S., Nielson, T. C. and Le, H. V. (2018). Inhibition of Glycolysis and Glutaminolysis: An Emerging Drug Discovery Approach to Combat Cancer. *Curr Top Med Chem* **18:**494-504.

Al-Saleem, T., Wessner, L., Scheithauer, B., Patterson, K., Roach, E., Dreyer, S., Fujikawa, K. *et al.* (1998). Malignant tumors of the kidney, brain, and soft tissues in children and young adults with the tuberous sclerosis complex. *Cancer* **83:**2208-2216.

Albers, J., Rajski, M., Schonenberger, D., Harlander, S., Schraml, P., von Teichman, A., Georgiev, S. *et al.* (2013). Combined mutation of Vhl and Trp53 causes renal cysts and tumours in mice. *EMBO Mol Med* **5:**949-964.

Altman, B. J., Stine, Z. E. and Dang, C. V. (2016). From Krebs to clinic: glutamine metabolism to cancer therapy. *Nat Rev Cancer*.

Anastasiou, D., Poulogiannis, G., Asara, J. M., Boxer, M. B., Jiang, J. K., Shen, M., Bellinger, G. *et al.* (2011). Inhibition of Pyruvate Kinase M2 by Reactive Oxygen Species Contributes to Cellular Antioxidant Responses. *Science* **334:**1278-1283.

Anastasiou, D., Yu, Y., Israelsen, W. J., Jiang, J. K., Boxer, M. B., Hong, B. S., Tempel, W. *et al.* (2012). Pyruvate kinase M2 activators promote tetramer formation and suppress tumorigenesis. *Nat Chem Biol* **8:**839-847.

Astrinidis, A. and Henske, E. (2004). Aberrant cellular differentiation and migration in renal and pulmonary tuberous sclerosis complex. *J Child Neurol* **19:**710-715.

Astrinidis, A., Senapedis, W., Coleman, T. R. and Henske, E. P. (2003). Cell cycle-regulated phosphorylation of hamartin, the product of the tuberous sclerosis complex 1 gene, by cyclin-dependent kinase 1/cyclin B. *J Biol Chem* **278:**51372-51379.

Au, K., Williams, A., Roach, E., Batchelor, L., Sparagana, S., Delgado, M., Wheless, J. *et al.* (2007). Genotype/phenotype correlation in 325 individuals referred for a diagnosis of tuberous sclerosis complex in the United States. *Genet Med* **9:**88-100.

Au, K. S., Hebert, A. A., Roach, E. S. and Northrup, H. (1999). Complete inactivation of the TSC2 gene leads to formation of hamartomas. *Am J Hum Genet* **65:**1790-1795.

Aubry, M., Myers, J., Ryu, J., Henske, E., Logginidou, H., Jalal, S. and Tazelaar, H. (2000). Pulmonary lymphangioleiomyomatosis in a man. *AM J Respir Crit Care Med* **162:**749-752.

Bader, R. S., Chitayat, D., Kelly, E., Ryan, G., Smallhorn, J. F., Toi, A. and Hornberger, L. K. (2003). Fetal rhabdomyoma: prenatal diagnosis, clinical outcome, and incidence of associated tuberous sclerosis complex. *The Journal of Pediatrics* **143:**620-624.

Bailey, S. T., Smith, A. M., Kardos, J., Wobker, S. E., Wilson, H. L., Krishnan, B., Saito, R. *et al.* (2017). MYC activation cooperates with Vhl and Ink4a/Arf loss to induce clear cell renal cell carcinoma. *Nat Commun* **8:**15770.

Ballif, B. A., Roux, P. P., Gerber, S. A., MacKeigan, J. P., Blenis, J. and Gygi, S. P. (2005). Quantitative phosphorylation profiling of the ERK/p90 ribosomal S6 kinase-signaling cassette and its targets, the tuberous sclerosis tumor suppressors. *Proc Natl Acad Sci U S A* **102:**667-672.

Balzer, F. and Menetrier, P. (1885). Étude sur un cas d'adenomes sebaces de la face et du cuir chevelu. *Arch Physiol Norm Pathol* **6:**564-576.

Bar-Peled, L., Chantranupong, L., Cherniack, A. D., Chen, W. W., Ottina, K. A., Grabiner, B. C., Spear, E. D. *et al.* (2013). A Tumor suppressor complex with GAP activity for the Rag GTPases that signal amino acid sufficiency to mTORC1. *Science* **340:**1100-1106.

Bar-Peled, L. and Sabatini, D. M. (2014). Regulation of mTORC1 by amino acids. *Trends Cell Biol* **24:**400-406.

Bar-Peled, L., Schweitzer, L. D., Zoncu, R. and Sabatini, D. M. (2012). Ragulator is a GEF for the rag GTPases that signal amino acid levels to mTORC1. *Cell* **150:**1196-1208.

Barnes, E. A., Kenerson, H. L., Jiang, X. and Yeung, R. S. (2010). Tuberin regulates E-cadherin localization: implications in epithelial-mesenchymal transition. *Am J Pathol* **177:**1765-1778.

Basu, B., Dean, E., Puglisi, M., Greystoke, A., Ong, M., Burke, W., Cavallin, M. *et al.* (2015). First-in-Human Pharmacokinetic and Pharmacodynamic Study of the Dual m-TORC 1/2 Inhibitor AZD2014. *Clin Cancer Res*.

Becher, O. J. and Holland, E. C. (2006). Genetically engineered models have advantages over xenografts for preclinical studies. *Cancer Res* **66:**3355-3358, discussion 3358-3359.

Becker, A. (2000). Primary heart tumors in the pediatric age group a review of salient pathologic features relevant for clinicians. *Pediatr Cardiol* **21:**317-323.

Benjamin, D., Colombi, M., Moroni, C. and Hall, M. N. (2011). Rapamycin passes the torch: a new generation of mTOR inhibitors. *Nat Rev Drug Discov* **10:**868-880.

Benvenuto, G., Li, S., Brown, S., Braveman, R., Vass, W., Cheadle, J., Halley, D. *et al.* (2000). The tuberous sclerosis-1 (TSC1) gene product hamartin suppresses cell growth and augments the expression of the TSC2 product tuberin by inhibiting its ubiquitination. *Oncogene* **19:**6306-6316.

Bernstein, J. and Robbins, T. (1991). Renal involvement in tuberous sclerosis. *Ann N Y Acad Sci* **615:**36-49.

Bi, X. G., Guo, L., Wang, X. L., Wei, Q., Du, Q., Jiang, W. H., Zheng, G. Y. *et al.* (2017). Distinct subcellular localization of E-cadherin between epithelioid angiomyolipoma and triphasic angiomyolipoma: A preliminary case-control study. *Oncol Lett* **14:**695-704.

Birsoy, K., Wang, T., Possemato, R., Yilmaz, O. H., Koch, C. E., Chen, W. W., Hutchins, A. W. *et al.* (2013). MCT1-mediated transport of a toxic molecule is an effective strategy for targeting glycolytic tumors. *Nat Genet* **45:**104-108.

Bissler, J., McCormack, F., Young, L., Elwing, J., Chuck, G., Leonard, J., Schmithorst, V. *et al.* (2008). Sirolimus for angiomyolipoma in tuberous sclerosis complex or lymphangioleiomyomatosis. *N Engl J Med* **358:**140-151.

Bissler, J. J., Kingswood, J. C., Radzikowska, E., Zonnenberg, B. A., Frost, M., Belousova, E., Sauter, M. *et al.* (2013). Everolimus for angiomyolipoma associated with tuberous sclerosis complex or sporadic lymphangioleiomyomatosis (EXIST-2): a multicentre, randomised, double-blind, placebo-controlled trial. *The Lancet* **381:**817-824.

Bissler, J. J., Racadio, J., Donnelly, L. F. and Johnson, N. D. (2002). Reduction of postembolization syndrome after ablation of renal angiomyolipoma. *Am J Kidney Dis* **39:**966-971.

Bourneville, D. (1880). Sclerose tubereuse des circonvultions cerebrales: idiotie et epilepsie hemiplegique. *Arch Neurol* **1:**81-91.

Bourneville, D. and Brissaud, E. (1881). Encephalite ou sclerose tubereuse descirconvultions cerebrales. *Arch Neurol* **1:**390-410.

Brahimi-Horn, M. C., Chiche, J. and Pouyssegur, J. (2007). Hypoxia signalling controls metabolic demand. *Curr Opin Cell Biol* **19:**223-229.

Brinck, U., Eigenbrodt, E., Oehmke, M., Mazurek, S. and Fischer, G. (1994). L- and M2-pyruvate kinase expression in renal cell carcinomas and their metastases. *Virchows Arch* **424:**177-185.

Brognard, J., Sierecki, E., Gao, T. and Newton, A. C. (2007). PHLPP and a second isoform, PHLPP2, differentially attenuate the amplitude of Akt signaling by regulating distinct Akt isoforms. *Mol Cell* **25:**917-931.

Brown, E., Albers, M., Shin, T., Ichikawa, K., Keith, C., LAne, W. and Schreiber, S. (1994). A mammalian protein targeted by G1-arresting rapamycin-receptor complex. *Nature* **369:**756-758.

Brugarolas, J., Lei, K., Hurley, R. L., Manning, B. D., Reiling, J. H., Hafen, E., Witters, L. A. *et al.* (2004). Regulation of mTOR function in response to hypoxia by REDD1 and the TSC1/TSC2 tumor suppressor complex. *Genes Dev* **18:**2893-2904.

Cafferkey, R., Young, P., McLaughlin, M., Bergsma, D., Koltin, Y., Sathe, G., Faucette, L. *et al.* (1993). Dominant missense mutations in a novel yeast protein related to mammalian phosphatidylinositol 3-kinase and VPS34 abrogate rapamycin cytotoxicity. *Mol Cell Biol* **10:**6012-6023.

Cairns, R. A., Harris, I. S. and Mak, T. W. (2011). Regulation of cancer cell metabolism. *Nature Reviews Cancer* **11:**85-95.

Cantor, J. R. and Sabatini, D. M. (2012). Cancer Cell Metabolism: One Hallmark, Many Faces. *Cancer Discovery* **2:**881-898.

Capecchi, M. (2005). Gene targeting in mice functional analysis of the mammalian genome for the twenty-first century. *Nat Rev Genet* **6:**507-512.

Carroll, B., Maetzel, D., Maddocks, O. D., Otten, G., Ratcliff, M., Smith, G. R., Dunlop, E. A. *et al.* (2016). Control of TSC2-Rheb signaling axis by arginine regulates mTORC1 activity. *Elife* **5**.

Castro, M., Shepherd, C. W., Gomez, M. R., Lie, J. T. and Ryu, J. H. (1995). Pulmonary Tuberous Sclerosis. *Chest* **107:**189-195.

Catalano, M., D'Alessandro, G., Lepore, F., Corazzari, M., Caldarola, S., Valacca, C., Faienza, F. *et al.* (2015). Autophagy induction impairs migration and invasion by reversing EMT in glioblastoma cells. *Mol Oncol* **9:**1612-1625.

Chakraborty, S., Mohiyuddin, S. M., Gopinath, K. S. and Kumar, A. (2008). Involvement of TSC genes and differential expression of other members of the mTOR signaling pathway in oral squamous cell carcinoma. *BMC Cancer* **8:**163.

Chan, J., Zhang, H., Roberts, P., Jozwiak, S., Wielawa, G., Lewin-Kowalik, J., Kotulaka, K. *et al.* (2004). Pathogenesis of tuberous sclerosis subependymal giant cell astrocytomas: biallelic inactivation of TSC1 or TSC2 leads to mTOR activation. *J Neuropathol Exp Neurol* **63:**1236-1242.

Chantranupong, L., Scaria, Sonia M., Saxton, Robert A., Gygi, Melanie P., Shen, K., Wyant, Gregory A., Wang, T. *et al.* (2016). The CASTOR Proteins Are Arginine Sensors for the mTORC1 Pathway. *Cell*.

Chantranupong, L., Wolfson, R. L., Orozco, J. M., Saxton, R. A., Scaria, S. M., Bar-Peled, L., Spooner, E. *et al.* (2014). The Sestrins interact with GATOR2 to negatively regulate the amino-acid-sensing pathway upstream of mTORC1. *Cell Rep* **9:**1-8.

Cheadle, J. P., Reeve, M. P., Sampson, J. R. and Kwiatkowski, D. J. (2000). Molecular genetic advances in tuberous sclerosis. *Human Genetics* **107:**97-114.

Chen, X., Cheng, H., Pan, T., Liu, Y., Su, Y., Ren, C., Huang, D. *et al.* (2015). mTOR regulate EMT through RhoA and Rac1 pathway in prostate cancer. *Mol Carcinog* **54:**1086-1095.

Chen, Z., Zhang, H., Lu, W. and Huang, P. (2009). Role of mitochondria-associated hexokinase II in cancer cell death induced by 3-bromopyruvate. *Biochim Biophys Acta* **1787:**553-560.

Chong-Kopera, H., Inoki, K., Li, Y., Zhu, T., Garcia-Gonzalo, F. R., Rosa, J. L. and Guan, K. L. (2006). TSC1 stabilizes TSC2 by inhibiting the interaction between TSC2 and the HERC1 ubiquitin ligase. *J Biol Chem* **281:**8313-8316.

Choo, A. Y., Kim, S. G., Vander Heiden, M. G., Mahoney, S. J., Vu, H., Yoon, S. O., Cantley, L. C. *et al.* (2010). Glucose addiction of TSC null cells is caused by failed mTORC1-dependent balancing of metabolic demand with supply. *Mol Cell* **38:**487-499.

Chresta, C. M., Davies, B. R., Hickson, I., Harding, T., Cosulich, S., Critchlow, S. E., Vincent, J. P. *et al.* (2010). AZD8055 is a potent, selective, and orally bioavailable ATP-competitive mammalian target of rapamycin kinase inhibitor with in vitro and in vivo antitumor activity. *Cancer Res* **70:**288-298.

Christofk, H. R., Vander Heiden, M. G., Harris, M. H., Ramanathan, A., Gerszten, R. E., Wei, R., Fleming, M. D. *et al.* (2008). The M2 splice isoform of pyruvate kinase is important for cancer metabolism and tumour growth. *Nature* **452:**230-233.

Chu-Shore, C. J., Major, P., Camposano, S., Muzykewicz, D. and Thiele, E. A. (2010). The natural history of epilepsy in tuberous sclerosis complex. *Epilepsia* **51:**1236-1241.

Chung, D., Brown, S., Graeme-Cook, F., Tillotson, L., Warshaw, A., Jensen, R. and Arnold, A. (1998). Localization of putative tumor suppressor loci by genome-wide allelotyping in human pancreatic endocrine tumors. *Cancer Res* **58:**3706-3711.

Cianfanelli, V., Fuoco, C., Lorente, M., Salazar, M., Quondamatteo, F., Gherardini, P. F., De Zio, D. *et al.* (2015). AMBRA1 links autophagy to cell proliferation and tumorigenesis by promoting c-Myc dephosphorylation and degradation. *Nat Cell Biol* **17:**20-30.

Cirstea, D., Hideshima, T., Rodig, S., Santo, L., Pozzi, S., Vallet, S., Ikeda, H. *et al.* (2010). Dual inhibition of akt/mammalian target of rapamycin pathway by

nanoparticle albumin-bound-rapamycin and perifosine induces antitumor activity in multiple myeloma. *Mol Cancer Ther* **9:**963-975.

Clarke, A. R., Hancock, E., Kingswood, C. and Osborne, J. (1999). End-stage renal failure in adults with the tuberous sclerosis complex. *Nephrol Dial Transplant* **14:**988-991.

Conciatori, F., Ciuffreda, L., Bazzichetto, C., Falcone, I., Pilotto, S., Bria, E., Cognetti, F. *et al.* (2018). mTOR Cross-Talk in Cancer and Potential for Combination Therapy. *Cancers (Basel)* **10**.

Connor, J., Pirrit, L., Yates, J., Fryer, A. and Ferguson-Smith, M. (1987). Linkage of the tuberous sclerosis locus to a DNA polymorphism detected by v-abl. *J Med Genet* **24:**544-546.

Consortium, E. C. T. S. (1993). Identification and characterization of the tuberous sclerosis gene on chromosome 16. *Cell* **75:**1305-1315.

Consortium, E. P. K. D. (1994). The polycystic kidney disease 1 gene encodes a 14 kb transcript and lies within a duplicated region on chromosome 16. *Cell* **77:**881-894.

Costello, L., Hartman, T. and Ryu, J. (2000). High frequency of pulmonary lymphangioleiomyomatosis in women with tuberous sclerosis complex. *Mayo Clin Proc* **75:**591-594.

Csibi, A., Fendt, S. M., Li, C., Poulogiannis, G., Choo, A. Y., Chapski, D. J., Jeong, S. M. *et al.* (2013). The mTORC1 pathway stimulates glutamine metabolism and cell proliferation by repressing SIRT4. *Cell* **153:**840-854.

Csibi, A., Lee, G., Yoon, S. O., Tong, H., Ilter, D., Elia, I., Fendt, S. M. *et al.* (2014). The mTORC1/S6K1 pathway regulates glutamine metabolism through the eIF4B-dependent control of c-Myc translation. *Curr Biol* **24:**2274-2280.

Cudzilo, C. J., Szczesniak, R. D., Brody, A. S., Rattan, M. S., Krueger, D. A., Bissler, J. J., Franz, D. N. *et al.* (2013). Lymphangioleiomyomatosis screening in women with tuberous sclerosis. *Chest* **144:**578-585.

Curatolo, P., Moavero, R. and de Vries, P. J. (2015). Neurological and neuropsychiatric aspects of tuberous sclerosis complex. *The Lancet Neurology* **14:**733-745.

Curatolo, P., Napolioni, V. and Moavero, R. (2010). Autism spectrum disorders in tuberous sclerosis: pathogenetic pathways and implications for treatment. *J Child Neurol* **25:**873-880.

Curthoys, N. and Watford, M. (1995). Regulation of glutaminase activity and glutamine metabolism. *Annu Rev Nutr* **15:**133-159.

D'Agati, E., Moavero, R., Caerminara, C. and Curatolo, P. (2009). Attention-deficit hyperactivity disorder (ADHD) and tuberous sclerosis complex. *j Child Neurol* **24:**1282-1287.

Dabora, S. L., Jozwiak, S., Franz, D. N., Roberts, P. S., Nieto, A., Chung, J., Choy, Y. S. *et al.* (2001). Mutational analysis in a cohort of 224 tuberous sclerosis patients indicates increased severity of TSC2, compared with TSC1, disease in multiple organs. *Am J Hum Genet* **68:**64-80.

Dalsgaard-Nielsen, T. (1935). Tuberous sclerosis with unusual roentgen picture *Nord Med* **10:**1541-1548.

Dang, C., Kim, J., Gao, P. and Yustein, J. (2008). The interplay between MYC and HIF in cancer. *Nat Rev Cancer* **8:**51-56.

David, C. J., Chen, M., Assanah, M., Canoll, P. and Manley, J. L. (2010). HnRNP proteins controlled by c-Myc deregulate pyruvate kinase mRNA splicing in cancer. *Nature* **463:**364-368.

Davies, D., De Vries, P., Johnson, S., McCartney, D., Cox, J., Serra, A. and Watson, P. (2011). Sirolimus therapy in tuberous sclerosis or sporadic lymphangioleiomyomatosis. *Clin Cancer Res* **17:**4071-4081.

Davis, F. M., Stewart, T. A., Thompson, E. W. and Monteith, G. R. (2014). Targeting EMT in cancer: opportunities for pharmacological intervention. *Trends Pharmacol Sci* **35:**479-488.

Dayton, T. L., Gocheva, V., Miller, K. M., Bhutkar, A., Lewis, C. A., Bronson, R. T., Vander Heiden, M. G. *et al.* (2018). Isoform-specific deletion of PKM2 constrains tumor initiation in a mouse model of soft tissue sarcoma. *Cancer Metab* **6:**6.

Dayton, T. L., Gocheva, V., Miller, K. M., Israelsen, W. J., Bhutkar, A., Clish, C. B., Davidson, S. M. *et al.* (2016). Germline loss of PKM2 promotes metabolic distress and hepatocellular carcinoma. *Genes Dev* **30:**1020-1033.

de Vries, P. J., Gardiner, J. and Bolton, P. F. (2009). Neuropsychological attention deficits in tuberous sclerosis complex (TSC). *Am J Med Genet A* **149A:**387-395.

de Vries, P. J., Whittemore, V. H., Leclezio, L., Byars, A. W., Dunn, D., Ess, K. C., Hook, D. *et al.* (2015). Tuberous sclerosis associated neuropsychiatric disorders (TAND) and the TAND Checklist. *Pediatr Neurol* **52:**25-35.

De Waele, L., Lagae, L. and Mekahli, D. (2015). Tuberous sclerosis complex: the past and the future. *Pediatr Nephrol* **30:**1771-1780.

DeBerardinis, R. J. and Cheng, T. (2010). Q's next: the diverse functions of glutamine in metabolism, cell biology and cancer. *Oncogene* **29:**313-324.

DeBerardinis, R. J., Lum, J. J., Hatzivassiliou, G. and Thompson, C. B. (2008). The biology of cancer: metabolic reprogramming fuels cell growth and proliferation. *Cell Metab* **7:**11-20.

DeBerardinis, R. J., Mancuso, A., Daikhin, E., Nissim, I., Yudkoff, M., Wehrli, S. and Thompson, C. B. (2007). Beyond aerobic glycolysis: transformed cells can engage in glutamine metabolism that exceeds the requirement for protein and nucleotide synthesis. *Proc Natl Acad Sci U S A* **104:**19345-19350.

Deng, J., Wang, L., Chen, H., Hao, J., Ni, J., Chang, L., Duan, W. *et al.* (2016). Targeting epithelial-mesenchymal transition and cancer stem cells for chemoresistant ovarian cancer. *Oncotarget* **7:**55771-55788.

DeYoung, M. P., Horak, P., Sofer, A., Sgroi, D. and Ellisen, L. W. (2008). Hypoxia regulates TSC1/2-mTOR signaling and tumor suppression through REDD1-mediated 14-3-3 shuttling. *Genes Dev* **22:**239-251.

Dibble, C. C. and Cantley, L. C. (2015). Regulation of mTORC1 by PI3K signaling. *Trends Cell Biol*.

Dibble, C. C., Elis, W., Menon, S., Qin, W., Klekota, J., Asara, J. M., Finan, P. M. *et al.* (2012). TBC1D7 is a third subunit of the TSC1-TSC2 complex upstream of mTORC1. *Mol Cell* **47:**535-546.

Dodd, K. M., Yang, J., Shen, M. H., Sampson, J. R. and Tee, A. R. (2015). mTORC1 drives HIF-1alpha and VEGF-A signalling via multiple mechanisms involving 4E-BP1, S6K1 and STAT3. *Oncogene* **34:**2239-2250.

Dorello, N., Peschiaroli, A., Guardavaccaro, D., Colburn, N., Sherman, N. and Pagano, M. (2006). S6K1- and betaTRCP-mediated degradation of PDCD4 promotes protein translation and cell growth. *Science* **314:**467-471.

Dunlop, E. A., Dodd, K. M., Seymour, L. A. and Tee, A. R. (2009). Mammalian target of rapamycin complex 1-mediated phosphorylation of eukaryotic initiation factor 4E-binding protein 1 requires multiple protein-protein interactions for substrate recognition. *Cell Signal* **21:**1073-1084.

Duran, R. V., Oppliger, W., Robitaille, A. M., Heiserich, L., Skendaj, R., Gottlieb, E. and Hall, M. N. (2012). Glutaminolysis activates Rag-mTORC1 signaling. *Mol Cell* **47:**349-358.

Duvel, K., Yecies, J. L., Menon, S., Raman, P., Lipovsky, A. I., Souza, A. L., Triantafellow, E. *et al.* (2010). Activation of a metabolic gene regulatory network downstream of mTOR complex 1. *Mol Cell* **39:**171-183.

Eagle, H. (1955). Nutrition needs of mammalian cells in tissue culture. *Science* **122:**501-514.

Ebrahimi-Fakhari, D., Meyer, S., Vogt, T., Pfohler, C. and Muller, C. S. L. (2017). Dermatological manifestations of tuberous sclerosis complex (TSC). *J Dtsch Dermatol Ges* **15:**695-700.

Eden, K., de Vries, P. J., Moss, J., Richards, C. and Oliver, C. (2014). Self-injury and aggression in tuberous sclerosis complex cross syndrome comparison and associated risk markers. *Journal of Neurodevelopmental disorders* **6:**-.

Ehninger, D., Han, S., Shilyansky, C., Zhou, Y., Li, W., Kwiatkowski, D. J., Ramesh, V. *et al.* (2008). Reversal of learning deficits in a Tsc2+/- mouse model of tuberous sclerosis. *Nat Med* **14:**843-848.

Eker, R. (1954). Familial renal adenomas in Wistar rats. *Acta Pathol Microbiol Scand* **34:**554-562.

Eker, R., Mossige, J., Johannessen, J. and Aars, H. (1981). Hereditary renal adenomas and adenocarcinomas in rats. *Diagn Histopathol* **4:**99-110.

El Sayed, S. M., Abou El-Magd, R. M., Shishido, Y., Chung, S. P., Sakai, T., Watanabe, H., Kagami, S. *et al.* (2012). D-amino acid oxidase gene therapy sensitizes glioma cells to the antiglycolytic effect of 3-bromopyruvate. *Cancer Gene Ther* **19:**1-18.

Elgadi, K., Meguid, R., Qian, M., Souba, W. and Abcouwer, S. (1999). Cloning and analysis of unique human glutaminase isoforms generated by tissue-specific alternative splicing. *Physiol Genomics* **1:**51-62.

Elstrom, R., Bauer, D., Buzzai, M., Karnauskas, R., Harris, M., Plas, D., Zhuang, H. *et al.* (2004). Akt stimulates aerobic glycolysis in cancer cells. *Cancer Res* **64:**3892-3899.

Emberley, E., Bennett, M., Chen, J., Gross, M., Huang, C., Li, A., Mackinnon, A. *et al.* (2017). CB-839, a selective glutaminase inhibitor, has anti-tumor activity in renal cell carcinoma and synergizes with cabozantinib and everolimus. *Keystone Symposia*.

Eng, C., Sehgal, S. and Vezina, C. (1984). Activity of rapamycin (AY-22,989) against transplanted tumors. *J Antibiot* **37**.

Epstein, T., Xu, L., Gillies, R. and Gatenby, R. (2014). Separation of metabolic supply and demand aerobic glycolysis as a normal physiological response to fluctuating energetic demands in the membrane. *Cancer Metab* **5:**2-7.

Espana-Agusti, J., Zou, X., Wong, K., Fu, B., Yang, F., Tuveson, D. A., Adams, D. J. *et al.* (2016). Generation and Characterisation of a Pax8-CreERT2 Transgenic Line and a Slc22a6-CreERT2 Knock-In Line for Inducible and Specific Genetic Manipulation of Renal Tubular Epithelial Cells. *PLoS One* **11:**e0148055.

Eugene, S. (1998). Lymphangioleiomyomatosis. *Chest* **114:**1689-1703.

Everitt, J., Goldsworthy, T. and Wolf, D. (1992). Hereditary Renal Cell Carcinoma in the Eker Rat: A Rodent Familial Cancer Syndrome. *Journal of Urology* **148:**1932-1936.

Ewalt, D., Sheffield, E., Sparagana, S., Delgado, M. and Roach, E. (1998). Renal lesion growth in children with tuberous sclerosis complex. *J Urol* **160:**141-145.

Feil, R., Wagner, J., Metzger, D. and Chambon, P. (1997). Regulation of Cre recombinase activity by mutated estrogen receptor ligand-binding domains. *Biochem Biophys Res Commun* **237:**752-757.

Feldman, M. E., Apsel, B., Uotila, A., Loewith, R., Knight, Z. A., Ruggero, D. and Shokat, K. M. (2009). Active-site inhibitors of mTOR target rapamycin-resistant outputs of mTORC1 and mTORC2. *PLoS Biol* **7:**e38.

Feng, Z., Zhang, H., Levine, A. J. and Jin, S. (2005). The coordinate regulation of the p53 and mTOR pathways in cells. *Proc Natl Acad Sci U S A* **102:**8204-8209.

Feron, O. (2009). Pyruvate into lactate and back: from the Warburg effect to symbiotic energy fuel exchange in cancer cells. *Radiother Oncol* **92:**329-333.

Fonseca, B. D., Smith, E. M., Lee, V. H., MacKintosh, C. and Proud, C. G. (2007). PRAS40 is a target for mammalian target of rapamycin complex 1 and is required for signaling downstream of this complex. *J Biol Chem* **282:**24514-24524.

Franz, D. (2004). Non-neurologic manifestations of tuberous sclerosis complex. *J Child Neurol* **19:**690-698.

Franz, D., Brody, A., Meyer, C., Leonard, J., Chuck, G., Dabora, S., Sethuraman, G. *et al.* (2001). Mutational and radiographic analysis of pulmonary disease consistent with lymphangioleiomyomatosis and

micronodular pneumocyte hyperplasia in women with tuberous sclerosis. *AM J Respir Crit Care Med* **164:**661-668.

Franz, D. N. and Capal, J. K. (2016). Profile of everolimus in the treatment of tuberous sclerosis complex: an evidence-based review of its place in therapy. *Neuropsychiatr Dis Treat* **12:**2165-2172.

Franz, D. N., Leonard, J., Tudor, C., Chuck, G., Care, M., Sethuraman, G., Dinopoulos, A. *et al.* (2006). Rapamycin causes regression of astrocytomas in tuberous sclerosis complex. *Ann Neurol* **59:**490-498.

Freedom, R. M., Lee, K. J., MacDonald, C. and Taylor, G. (2000). Selected aspects of cardiac tumors in infancy and childhood. *Pediatr Cardiol* **21:**299-316.

Frese, K. K. and Tuveson, D. A. (2007). Maximizing mouse cancer models. *Nat Rev Cancer* **7:**645-658.

Frew, I., Thoma, C., Georgiev, S., Minola, A., Hitz, M., Montani, M., Moch, H. *et al.* (2008). pVHL and PTEN tumour suppressor proteins cooperatively suppress kidney cyst formation. *EMBO* **27:**1747-1757.

Fryer, A., Chalmers, A., Connor, J., Fraser, I., Povey, S., Yates, A. and Osborne, J. (1987). Evidence that the gene for tuberous sclerosis is on chromosome 9. *Lancet* **1:**659-661.

Gabardi, S. and Baroletti, S. (2008). Everolimus: a proliferation signal inhibitor with clinical applications in organ transplantation, oncology, and cardiology. *Pharmacotherapy* **30:**1044-1056.

Ganley, I. G., Lam du, H., Wang, J., Ding, X., Chen, S. and Jiang, X. (2009). ULK1.ATG13.FIP200 complex mediates mTOR signaling and is essential for autophagy. *J Biol Chem* **284:**12297-12305.

Gao, P., Tchernyshyov, I., Chang, T. C., Lee, Y. S., Kita, K., Ochi, T., Zeller, K. I. *et al.* (2009). c-Myc suppression of miR-23a/b enhances mitochondrial glutaminase expression and glutamine metabolism. *Nature* **458:**762-765.

Gao, X., Zhang, Y., Arrazola, P., Hino, O., Kobayashi, T., Yeung, R. S., Ru, B. *et al.* (2002). Tsc tumour suppressor proteins antagonize amino-acid-TOR signalling. *Nat Cell Biol* **4:**699-704.

Garami, A., Zwartkruis, F. J. T., Nobukuni, T., Joaquin, M., Roccio, M., Stocker, H., Kozma, S. C. *et al.* (2003). Insulin Activation of Rheb, a Mediator of mTOR/S6K/4E-BP Signaling, Is Inhibited by TSC1 and 2. *Molecular Cell* **11:**1457-1466.

Garcia-Cao, I., Song, M. S., Hobbs, R. M., Laurent, G., Giorgi, C., de Boer, V. C., Anastasiou, D. *et al.* (2012). Systemic elevation of PTEN induces a tumor-suppressive metabolic state. *Cell* **149:**49-62.

Garcia-Martinez, J. M. and Alessi, D. R. (2008). mTOR complex 2 (mTORC2) controls hydrophobic motif phosphorylation and activation of serum- and glucocorticoid-induced protein kinase 1 (SGK1). *Biochem J* **416:**375-385.

Gatenby, R. A., Gawlinski, E. T., Gmitro, A. F., Kaylor, B. and Gillies, R. J. (2006). Acid-mediated tumor invasion: a multidisciplinary study. *Cancer Res* **66:**5216-5223.

Giudice, F. S. and Squarize, C. H. (2013). The determinants of head and neck cancer: Unmasking the PI3K pathway mutations. *J Carcinog Mutagen* **Suppl 5**.

Gomez, M. (1979). Tuberous Sclerosis. New York: Raven Press.

Gomez, M., Sampson, J. and Whittemore, V. (1999). Tuberous sclerosis complex. UK: Oxford University Press.

Goncharova, E. A., Goncharov, D. A., Li, H., Pimtong, W., Lu, S., Khavin, I. and Krymskaya, V. P. (2011). mTORC2 is required for proliferation and survival of TSC2-null cells. *Mol Cell Biol* **31:**2484-2498.

Gossage, L., Eisen, T. and Maher, E. R. (2015). VHL, the story of a tumour suppressor gene. *Nat Rev Cancer* **15:**55-64.

Gossen, M., Freundlieb, S., Bender, G., Muller, G., Hillen, W. and Bujard, H. (1995). Transcriptional activation by tetracyclines in mammalian cells. *Science* **268:**1766-1769.

Gossen, M. and Vujard, H. (1992). Tight control of gene expression in mammalian cells by tetracycline-responsive promoters. *Proc Natl Acad Sci U S A* **89:**5547-5551.

Grajkowska, W., Kotulaka, K., Jurkiewicz, E. and Matyja, E. (2010). Brain lesions in tuberous sclerosis complex. Review. *Folia Neuropathol* **48:**139-149.

Grewe, M., Gansauge, F., Schmid, R., Adler, G. and Seufferlein, T. (1999). Regulation of cell growth and cyclin D1 expression by the constitutively active FRAP-p70s6K pathway in human pancreatic cancer cells. *Cancer Res* **59:**3581-3587.

Grigore, A. D., Jolly, M. K., Jia, D., Farach-Carson, M. C. and Levine, H. (2016). Tumor Budding: The Name is EMT. Partial EMT. *J Clin Med* **5**.

Gross, M. I., Demo, S. D., Dennison, J. B., Chen, L., Chernov-Rogan, T., Goyal, B., Janes, J. R. *et al.* (2014). Antitumor activity of the glutaminase inhibitor CB-839 in triple-negative breast cancer. *Mol Cancer Ther* **13:**890-901.

Grosse-Wilde, A., Fouquier d'Herouel, A., McIntosh, E., Ertaylan, G., Skupin, A., Kuestner, R. E., del Sol, A. *et al.* (2015). Stemness of the hybrid Epithelial/Mesenchymal State in Breast Cancer and Its Association with Poor Survival. *PLoS One* **10:**e0126522.

Guertin, D. A. and Sabatini, D. M. (2007). Defining the role of mTOR in cancer. *Cancer Cell* **12:**9-22.

Gui, D., Lewis, C. and Vander Heiden, M. G. (2013). Allosteric Regulation of PKM2 Allows Cellular Adaptation to Different Physiological States. *Science* **6**.

Guichard, S. M., Curwen, J., Bihani, T., D'Cruz, C. M., Yates, J. W., Grondine, M., Howard, Z. *et al.* (2015). AZD2014, an inhibitor of mTORC1 and mTORC2, is highly effective in ER+ breast cancer when administered using intermittent or continuous schedules. *Mol Cancer Ther* **14:**2508-2518.

Gulhati, P., Bowen, K. A., Liu, J., Stevens, P. D., Rychahou, P. G., Chen, M., Lee, E. Y. *et al.* (2011). mTORC1 and mTORC2 regulate EMT, motility, and metastasis of colorectal cancer via RhoA and Rac1 signaling pathways. *Cancer Res* **71:**3246-3256.

Guo, L., Zhou, B., Liu, Z., Xu, Y., Lu, H., Xia, M., Guo, E. *et al.* (2016). Blockage of glutaminolysis enhances the sensitivity of ovarian cancer cells to PI3K/mTOR inhibition involvement of STAT3 signaling. *Tumour Biol*.

Guo, Y. and Kwiatkowski, D. J. (2013). Equivalent benefit of rapamycin and a potent mTOR ATP-competitive inhibitor, MLN0128 (INK128), in a mouse model of tuberous sclerosis. *Mol Cancer Res* **11:**467-473.

Gupta, S., Hau, A. M., Al-Ahmadie, H. A., Harwalkar, J., Shoskes, A. C., Elson, P., Beach, J. R. *et al.* (2016). Transforming Growth Factor-beta Is an Upstream Regulator of Mammalian Target of Rapamycin Complex 2-Dependent Bladder Cancer Cell Migration and Invasion. *Am J Pathol* **186:**1351-1360.

Gwinn, D. M., Shackelford, D. B., Egan, D. F., Mihaylova, M. M., Mery, A., Vasquez, D. S., Turk, B. E. *et al.* (2008). AMPK phosphorylation of raptor mediates a metabolic checkpoint. *Mol Cell* **30:**214-226.

Haar, V., Lee, S. I., Bandhakavi, S., Griffin, T. J. and Kim, D. H. (2007). Insulin signalling to mTOR mediated by the Akt/PKB substrate PRAS40. *Nat Cell Biol* **9:**316-323.

Han, S., Santos, T., Puga, A., Roy, J., Thiele, E., McCollin, M., Stemmer-Rachamimov, A. *et al.* (2004). Phosphorylation of tuberin as a novel mechanism for somatic inactivation of the tuberous sclerosis complex proteins in brain lesions. *Cancer Res* **64:**812-816.

Hanahan, D. and Weinberg, Robert A. (2011). Hallmarks of Cancer: The Next Generation. *Cell* **144:**646-674.

Hara, K., MAruki, Y., Long, X., Yoshino, K., Oshiro, N., Hidayat, S. and Tokunaga, C. (2002). Raptor, a binding partner of target of rapamycin (TOR), mediates TOR action. *Cell* **110:**177-189.

Harada, M., Benito, J., Yamamoto, S., Kaur, S., Arslan, D., Ramirez, S., Jacamo, R. *et al.* (2015). The novel combination of dual mTOR inhibitor AZD2014 and pan-PIM inhibitor AZD1208 inhibits growth in acute myeloid leukemia via HSF pathway suppression. *Oncotarget* **6:**37930-37947.

Harrington, L. S., Findlay, G. M., Gray, A., Tolkacheva, T., Wigfield, S., Rebholz, H., Barnett, J. *et al.* (2004). The TSC1-2 tumor suppressor controls insulin-PI3K signaling via regulation of IRS proteins. *J Cell Biol* **166:**213-223.

Hasskarl, J. (2018). Everolimus. *Recent Results Cancer Res* **211:**101-123.

Hawley, S. A., Pan, D. A., Mustard, K. J., Ross, L., Bain, J., Edelman, A. M., Frenguelli, B. G. *et al.* (2005). Calmodulin-dependent protein kinase kinase-beta is an alternative upstream kinase for AMP-activated protein kinase. *Cell Metab* **2:**9-19.

Hay, N. (2016). Reprogramming glucose metabolism in cancer: can it be exploited for cancer therapy? *Nat Rev Cancer*.

He, C. L., Bian, Y. Y., Xue, Y., Liu, Z. X., Zhou, K. Q., Yao, C. F., Lin, Y. *et al.* (2016). Pyruvate Kinase M2 Activates mTORC1 by Phosphorylating AKT1S1. *Sci Rep* **6:**21524.

Henske, E., Scheithauer, B., Short, MP., Wollmann, R., Nahmias, J., NHornigold, N., Van Slegtenhorst, M. *et al.* (1996). Allelic loss is frequent in tuberous sclerosis kidney lesions but rare in brain lesions. *Am J Genet* **59:**400-406.

Henske, E. P. (2005). Tuberous sclerosis and the kidney: from mesenchyme to epithelium, and beyond. *Pediatr Nephrol* **20:**854-857.

Henske, E. P. and McCormack, F. X. (2012). Lymphangioleiomyomatosis - a wolf in sheep's clothing. *J Clin Invest* **122:**3807-3816.

Hensley, C. T., Wasti, A. T. and DeBerardinis, R. J. (2013). Glutamine and cancer: cell biology, physiology, and clinical opportunities. *J Clin Invest* **123:**3678-3684.

Hino, O., Mitani, H., Katsuyama, H. and Kubo, Y. (1994). A novel cancer predisposition syndrome in the Eker rat model. *Cancer Lett* **83:**117-121.

Hirayama, Y., Gi, M., Yamano, S., Tachibana, H., Okuno, T., Tamada, S., Nakatani, T. *et al.* (2016). Anti-PD-L1 treatment enhances antitumor effect of everolimus in a mouse model of renal cell carcinoma. *Cancer Sci* **107:**1736-1744.

Hirschhaeuser, F., Sattler, U. G. and Mueller-Klieser, W. (2011). Lactate: a metabolic key player in cancer. *Cancer Res* **71:**6921-6925.

Holley, D. G., Martin, G. R., Brenner, J. I., Fyfe, D. A., Huhta, J. C., Kleinman, C. S., Ritter, S. B. *et al.* (1995). Diagnosis and management of fetal cardiac

tumors: a multicenter experience and review of published reports. *Journal of the American College of Cardiology* **26:**516-520.

Hosios, A. M., Hecht, V. C., Danai, L. V., Johnson, M. O., Rathmell, J. C., Steinhauser, M. L., Manalis, S. R. *et al.* (2016). Amino Acids Rather than Glucose Account for the Majority of Cell Mass in Proliferating Mammalian Cells. *Dev Cell* **36:**540-549.

Hosoya, M., Naito, H. and Nihei, K. (1999). Neurological prognosis correlated with variations over time in the number of subependymal nodules in tuberous sclerosis. *Brain Dev* **21:**544-547.

Hou, W. and Ji, Z. (2018). Generation of autochthonous mouse models of clear cell renal cell carcinoma: mouse models of renal cell carcinoma. *Exp Mol Med* **50:**30.

Hsieh, A. C., Costa, M., Zollo, O., Davis, C., Feldman, M. E., Testa, J. R., Meyuhas, O. *et al.* (2010). Genetic dissection of the oncogenic mTOR pathway reveals druggable addiction to translational control via 4EBP-eIF4E. *Cancer Cell* **17:**249-261.

Huang, J. and Manning, B. D. (2008). The TSC1-TSC2 complex: a molecular switchboard controlling cell growth. *Biochem J* **412:**179-190.

Huang, J. and Manning, B. D. (2009). A complex interplay between Akt, TSC2 and the two mTOR complexes. *Biochem Soc Trans* **37:**217-222.

Huang, J., Wu, S., Wu, C. L. and Manning, B. D. (2009). Signaling events downstream of mammalian target of rapamycin complex 2 are attenuated in cells and tumors deficient for the tuberous sclerosis complex tumor suppressors. *Cancer Res* **69:**6107-6114.

Huang, S. and Houghton, P. J. (2001). Mechanisms of resistance to rapamycins. *Drug Resist Updat* **4:**378-391.

Huo, H. Z., Zhou, Z. Y., Wang, B., Qin, J., Liu, W. Y. and Gu, Y. (2014). Dramatic suppression of colorectal cancer cell growth by the dual mTORC1 and mTORC2 inhibitor AZD-2014. *Biochem Biophys Res Commun* **443:**406-412.

Ikenoue, T., Inoki, K., Yang, Q., Zhou, X. and Guan, K. L. (2008). Essential function of TORC2 in PKC and Akt turn motif phosphorylation, maturation and signalling. *Embo* **27:**1919-1931.

Ilagan, E. and Manning, B. D. (2016). Emerging Role of mTOR in the Response to Cancer Therapeutics. *Trends in Cancer* **2:**241-251.

Inoki, K., Corradetti, M. N. and Guan, K. L. (2005). Dysregulation of the TSC-mTOR pathway in human disease. *Nature Genetics* **37:**19-24.

Inoki, K., Li, Y., Xu, T. and Guan, K. L. (2003a). Rheb GTPase is a direct target of TSC2 GAP activity and regulates mTOR signaling. *Genes Dev* **17:**1829-1834.

Inoki, K., Li, Y., Zhu, T., Wu, J. and Guan, K. L. (2002). TSC2 is phosphorylated and inhibited by Akt and suppresses mTOR signalling. *Nat Cell Biol* **4:**648-657.

Inoki, K., Ouyang, H., Zhu, T., Lindvall, C., Wang, Y., Zhang, X., Yang, Q. *et al.* (2006). TSC2 integrates Wnt and energy signals via a coordinated phosphorylation by AMPK and GSK3 to regulate cell growth. *Cell* **126:**955-968.

Inoki, K., Zhu, T. Q. and Guan, K. L. (2003b). TSC2 mediates cellular energy response to control cell growth and survival. *Cell* **115:**577-590.

Iqbal, M. A. and Bamezai, R. N. (2012). Resveratrol inhibits cancer cell metabolism by down regulating pyruvate kinase M2 via inhibition of mammalian target of rapamycin. *PLoS One* **7:**e36764.

Israelsen, W. J., Dayton, T. L., Davidson, S. M., Fiske, B. P., Hosios, A. M., Bellinger, G., Li, J. *et al.* (2013). PKM2 isoform-specific deletion reveals a differential requirement for pyruvate kinase in tumor cells. *Cell* **155:**397-409.

Ito, N. and Rubin, G. (1999). Gigas, a Drosophila homolog of tuberous sclerosis gene product-2, regulates the cell cycle. *Cell* **96:**529-539.

Jacinto, E., Facchinetti, V., Liu, D., Soto, N., Wei, S., Jung, S. Y., Huang, Q. *et al.* (2006). SIN1/MIP1 maintains rictor-mTOR complex integrity and regulates Akt phosphorylation and substrate specificity. *Cell* **127:**125-137.

Jacinto, E., Loewith, R., Schmidt, A., Lin, S., Ruegg, M. A., Hall, A. and Hall, M. N. (2004). Mammalian TOR complex 2 controls the actin cytoskeleton and is rapamycin insensitive. *Nat Cell Biol* **6:**1122-1128.

Jacque, N., Ronchetti, A. M., Larrue, C., Meunier, G., Birsen, R., Willems, L., Saland, E. *et al.* (2015). Targeting glutaminolysis has antileukemic activity in acute myeloid leukemia and synergizes with BCL-2 inhibition. *Blood* **126:**1346-1356.

Janssen, L., Sandkuyl, L., Merkens, E., Sampson, J., Flery, P., Hennekam, R., Grosveld, G. *et al.* (1990). Genetic heterogeneity in tuberous sclerosis. *Genomics* **8:**237-242.

Jeevan, D., Cooper, J., Braun, A., Murali, R. and Jhanwar-Uniyal, M. (2016). Molecular Pathways Mediating Metastases to the Brain via Epithelial-to-Mesenchymal Transition: Genes, Proteins, and Functional Analysis. *Anticancer Res* **36:**523-532.

Jiang, W., Sampson, J., Martin, TA., LeeJones, L., Watkins, G., Douglas-Jones, A., Mokbel, K. *et al.* (2005). Tuberin and hamartin are aberrantly expressed and linked to clinical outcome in human breast cancer: the role of promoter methylation of TSC genes. *Eur J Cancer* **41:**1628-1636.

Jiang, X., Kenerson, H. L. and Yeung, R. S. (2011). Glucose deprivation in tuberous sclerosis complex-related tumors. *Cell Biosci* **1:**34.

Jolly, M., Trioathi, S., Jia, D., Mooney, S., Celiktas, M., Hanash, S. M., Mani, S. A. *et al.* (2016a). Stability of the hybrid epithelial/mesenchymal phenotype. *Oncotarget* **7**.

Jolly, M., Tripathi, S., Jia, D., Mooney, S., Celiktas, M., Hanash, S., Mani, S. *et al.* (2016b). Stability of the hybrid epithelialmesenchymal phenotype. *Oncotarget* **7:**27067-27084.

Jones, A., Sampson, J. and Cheadle, J. (2001). Low level mosaicism detectable by DHPLC but not by direct sequencing. *Hum Mutat* **17:**233-234.

Jones, A. T., Narov, K., Yang, J., Sampson, J. R. and Shen, M. H. (2019). Efficacy of Dual Inhibition of Glycolysis and Glutaminolysis for Therapy of Renal Lesions in Tsc2(+/-) Mice. *Neoplasia* **21:**230-238.

Jung, J., Genau, H. M. and Behrends, C. (2015). Amino Acid-Dependent mTORC1 Regulation by the Lysosomal Membrane Protein SLC38A9. *Mol Cell Biol* **35:**2479-2494.

Kahn, J., Hayman, T. J., Jamal, M., Rath, B. H., Kramp, T., Camphausen, K. and Tofilon, P. J. (2014). The mTORC1/mTORC2 inhibitor AZD2014 enhances the radiosensitivity of glioblastoma stem-like cells. *Neuro Oncol* **16:**29-37.

Kaizuka, T., Hara, T., Oshiro, N., Kikkawa, U., Yonezawa, K., Takehana, K., Iemura, S. *et al.* (2010). Tti1 and Tel2 are critical factors in mammalian target of rapamycin complex assembly. *J Biol Chem* **285:**20109-20116.

Kalluri, R. and Weinberg, R. A. (2009). The basics of epithelial-mesenchymal transition. *J Clin Invest* **119:**1420-1428.

Kalogerou, M., Zhang, Y., Yang, J., Garrahan, N., Paisey, S., Tokarczuk, P., Stewart, A. *et al.* (2012). T2 weighted MRI for assessing renal lesions in transgenic mouse models of tuberous sclerosis. *Eur J Radiol* **81:**2069-2074.

Kandt, R., Haines, J., Smith, M., Northrup, H., Gardener, R., Short, M., Dumars, K. *et al.* (1992). Linkage of an important gene locus for tuberous sclerosis to a chromosome 16 marker for polycystic kidney disease. *Nat Genet* **2:**37-41.

Kenerson, H., Dundon, T. A. and Yeung, R. S. (2005). Effects of rapamycin in the Eker rat model of tuberous sclerosis complex. *Pediatr Res* **57:**67-75.

Kessler, O., Gillion, G., Neuman, M., Engelstein, D., Winkler, H. and Baniel, J. (1998). Management of renal angiomyolipoma: analysis of 15 cases. *Eur Urol* **33:**572-575.

Khan, M. W., Biswas, D., Ghosh, M., Mandloi, S., Chakrabarti, S. and Chakrabarti, P. (2015). mTORC2 controls cancer cell survival by modulating gluconeogenesis. *Cell Death Discov* **1:**15016.

Khatri, S., Yepiskoposyan, H., Gallo, C. A., Tandon, P. and Plas, D. R. (2010). FOXO3a regulates glycolysis via transcriptional control of tumor suppressor TSC1. *J Biol Chem* **285:**15960-15965.

Kim, D., Sarbassov, D. D., Ali, S., Latek, R., Guntur, K., Erdjument-Bromage, H. and Sabatini, D. (2003). GbetaL, a positive regulator of the rapamycin-sensitive pathway required for the nutrient-sensitive interaction between raptor and mTOR. *Mol Cell* **11:**895-904.

Kim, E., Goraksha-Hicks, P., Li, L., Neufeld, T. P. and Guan, K. L. (2008). Regulation of TORC1 by Rag GTPases in nutrient response. *Nat Cell Biol* **10:**935-945.

Kim, H., Kim ST, Kang SH, Sung DJ, Kim CH, Shin SW, Kim YH *et al.* (2014). The use of everolimus to target carcinogenic pathways in a patient with renal cell carcinoma and tuberous sclerosis complex- a case report. *J Med Case Rep* **8**.

Kim, J. and Chen, J. (2004). Regulation of peroxisome proliferator-activated receptor-gamma activity by mammalian target of rapamycin and amino acids in adipogenesis. *Diabetes* **53:**2748-2756.

Kim, J. W., Tchernyshyov, I., Semenza, G. L. and Dang, C. V. (2006). HIF-1-mediated expression of pyruvate dehydrogenase kinase: a metabolic switch required for cellular adaptation to hypoxia. *Cell Metab* **3:**177-185.

Kim, M., Soontornniyomkij, V., Ji, B. and Zhou, X. (2012). System-wide immunohistochemical analysis of protein co-localization. *PLoS One* **7:**e32043.

Kim, S., Wang, K., Cho, B., Jung, H., Lee, Y., Chung, Y., Lee, J. *et al.* (2001). Biological behavior and tumorigenesis of subependymal giant cell astrocytomas. *J Neurooncol* **52:**217-225.

Kim, S. T., Kim, S. Y., Klempner, S. J., Yoon, J., Kim, N., Ahn, S., Bang, H. *et al.* (2017). Rapamycin-insensitive companion of mTOR (RICTOR) amplification defines a subset of advanced gastric cancer and is sensitive to AZD2014-mediated mTORC1/2 inhibition. *Ann Oncol* **28:**547-554.

Kitayama, K., Yashiro, M., Morisaki, T., Miki, Y., Okuno, T., Kinoshita, H., Fukuoka, T. *et al.* (2017). Pyruvate kinase isozyme M2 and glutaminase might be promising molecular targets for the treatment of gastric cancer. *Cancer Sci* **108:**2462-2469.

Knight, S. D., Adams, N. D., Burgess, J. L., Chaudhari, A. M., Darcy, M. G., Donatelli, C. A., Luengo, J. I. *et al.* (2010). Discovery of GSK2126458, a Highly Potent Inhibitor of PI3K and the Mammalian Target of Rapamycin. *ACS Med Chem Lett* **1:**39-43.

Knowles, M., Habuchi, T., Kennedy, W. and Cuthbert-Heavens, D. (2003). Mutation spectrum of the 9q34 tuberous sclerosis gene TSC1 in transitional cell carcinoma of the bladder. *Cancer Res* **63:**7652-7656.

Knox, W., Horowitz, M. and Friedell, G. (1969). The proportionality of glutaminase content to growth rate and morphology of rat neoplasms. *Cancer Res* **29:**669-680.

Knudson, A. (1971). Mutation and cancer statistical study of retinoblastoma. *Proc Natl Acad Sci U S A* **68:**820-823.

Ko, Y., Pedersen, P. and Geschwind, J. F. (2001). Glucose catabolism in the rabbit VX2 tumor model for liver cancer characterization and targeting hexokinase. *Cancer Lett* **173:**83-91.

Ko, Y. H., Smith, B. L., Wang, Y., Pomper, M. G., Rini, D. A., Torbenson, M. S., Hullihen, J. *et al.* (2004). Advanced cancers: eradication in all cases using 3-bromopyruvate therapy to deplete ATP. *Biochem Biophys Res Commun* **324:**269-275.

Ko, Y. H., Verhoeven, H. A., Lee, M. J., Corbin, D. J., Vogl, T. J. and Pedersen, P. L. (2012). A translational study "case report" on the small molecule "energy blocker" 3-bromopyruvate (3BP) as a potent anticancer agent: from bench side to bedside. *J Bioenerg Biomembr* **44:**163-170.

Kobayashi, T., Hirayama, Y., Kobayashi, E., Kubo, Y. and Hino, O. (1995). A germline insertion in the tuberous sclerosis (Tsc2) gene gives rise to the Eker rat model of dominantly inherited cancer.

. *Nat Genet* **9:**70-74.

Kobayashi, T., Minowa, O., Kuno, J., Mitani, H., Hino, O. and Noda, T. (1999). Renal carcinogenesis, hepatic hemangiomatosis, and embryonic lethality caused by a germ-line Tsc2 mutation in mice. *Cancer Res* **59:**1206-1211.

Kobayashi, T., Minowa, O., Sugitani, Y., Takai, S., Mitani, H., Kobayashi, E., Noda, T. *et al.* (2001). A germ-line Tsc1 mutation causes tumor development and embryonic lethality that are similar, but not identical to, those caused by Tsc2 mutation in mice. *Proc Natl Acad Sci U S A* **98:**8762-8767.

Kobayashi, T., Mitani, H., Takahashi, R., Hirabayashi, M., Ueda, M., Tamura, H. and Hino, O. (1997a). Transgenic rescue from embryonic lethality and renal carcinogenesis in the Eker rat model by introduction of a wild-type Tsc2 gene. *proc Natl Acad Sci U S A* **94:**3990-3993.

Kobayashi, T., Urakami, S., Cheadle, J., Aspinwall, R., Harris, P. C., Sampson, J. and Hino, O. (1997b). Identification of a leader exon and a core promoter for the rat tuberous sclerosis 2 (Tsc2) gene and structural comparison with the human homolog. *Mamm Genome* **8:**554-558.

Konstantakou, E. G., Voutsinas, G. E., Velentzas, A. D., Basogianni, A. S., Paronis, E., Balafas, E., Kostomitsopoulos, N. *et al.* (2015). 3-BrPA eliminates human bladder cancer cells with highly oncogenic signatures via engagement of specific death programs and perturbation of multiple signaling and metabolic determinants. *Mol Cancer* **14:**135.

Kotulska, K., Larysz-Brysz, M., Grajkowska, W., Jozwiak, J., Wlodarski, P., Sahin, M., Lewin-Kowalik, J. *et al.* (2009). Cardiac rhabdomyomas in tuberous sclerosis complex show apoptosis regulation and mTOR pathway abnormalities. *Pediatr Dev Pathol* **12:**89-95.

Kovacevic, Z. and McGivan, J. (1983). Mitochondrial metabolism of glutamine and glutamate and its physiological significance. *Physiol Rev* **63:**547-605.

Kozlowski, P., Roberts, P., Dabora, S., Franz, D., Bissler, J., Northrup, H., Au, K. S. *et al.* (2007). Identification of 54 large deletions/duplications in TSC1 and TSC2 using MLPA, and genotype-phenotype correlations. *Hum Genet* **121:**389-400.

Krueger, D. A., Wilfong, A. A., Holland-Bouley, K., Anderson, A. E., Agricola, K., Tudor, C., Mays, M. *et al.* (2013). Everolimus treatment of refractory epilepsy in tuberous sclerosis complex. *Ann Neurol* **74:**679-687.

Krymskaya, V. P. and Goncharova, E. A. (2009). PI3K/mTORC1 activation in hamartoma syndromes. *Cell Cycle* **8:**403-413.

Kwiatkowska, J., Wigowska-Sowinska, J., Napierala, D., Slomski, R. and Kwiatkowski, D. (1999). Mosaicism in tuberous sclerosis as a potential cause of the failure of molecular diagnosis. *N Engl J Med* **340:**703-707.

Kwiatkowski, D., Armour, J., Bale, A., Fountain, J., Goudie, D., Haines, J., Knowles, M. *et al.* (1993). Report and abstracts of the Second International Workshop on Human Chromosome 9 Mapping 1993. *Cytogenet Cell Genet* **64:**93-121.

Kwiatkowski, D., Whittemore, V. H. and Thiele, E. A. (2010). Tuberous Sclerosis Complex: genes, clinical features and therapeutics. 1st Edition ed. Germany: Wiley-Blackwell.

Kwiatkowski, D. J., Zhang, H. B., Bandura, J. L., Heiberger, K. M., Glogauer, M., el-Hashemite, N. and Onda, H. (2002). A mouse model of TSC1 reveals sex-dependent lethality from liver hemangiomas, and up-regulation of p70S6 kinase activity in Tsc1 null cells. *Human Molecular Genetics* **11:**525-534.

Lagos, J. and Gomez, M. (1967). Tuberous sclerosis: reappraisal of a clinical entity. *Mayo Clin Proc* **42:**26-49.

Lamouille, S. and Derynck, R. (2007). Cell size and invasion in TGF-beta-induced epithelial to mesenchymal transition is regulated by activation of the mTOR pathway. *J Cell Biol* **178:**437-451.

Lampa, M., Arlt, H., He, T., Ospina, B., Reeves, J., Zhang, B., Murtie, J. *et al.* (2017). Glutaminase is essential for the growth of triple-negative breast cancer

cells with a deregulated glutamine metabolism pathway and its suppression synergizes with mTOR inhibition. *PLoS One* **12:**e0185092.

Lampreht Tratar, U., Horvat, S. and Cemazar, M. (2018). Transgenic Mouse Models in Cancer Research. *Front Oncol* **8:**268.

Laplante, M. and Sabatini, D. M. (2012). mTOR signaling in growth control and disease. *Cell* **149:**274-293.

Laplante, M. and Sabatini, D. M. (2013). Regulation of mTORC1 and its impact on gene expression at a glance. *J Cell Sci* **126:**1713-1719.

Lau, A. N., Israelsen, W. J., Roper, J., Sinnamon, M. J., Georgeon, L., Dayton, T. L., Hillis, A. L. *et al.* (2017). PKM2 is not required for colon cancer initiated by APC loss. *Cancer Metab* **5:**10.

Lecharpentier, A., Vielh, P., Perez-Moreno, P., Planchard, D., Soria, J. C. and Farace, F. (2011). Detection of circulating tumour cells with a hybrid (epithelial/mesenchymal) phenotype in patients with metastatic non-small cell lung cancer. *Br J Cancer* **105:**1338-1341.

Leclezio, L. and de Vries, P. J. (2015). Advances in the treatment of tuberous sclerosis complex. *Curr Opin Psychiatry* **28:**113-120.

Lee, L., Sudentas, P., Donohue, B., Asrican, K., Worku, A., Walker, V., Sun, Y. *et al.* (2005). Efficacy of a rapamycin analog (CCI-779) and IFN-gamma in tuberous sclerosis mouse models. *Genes Chromosomes Cancer* **42:**213-227.

Leech, J. D., Lammers, S. H., Goldman, S., Auricchio, N., Bronson, R. T., Kwiatkowski, D. J. and Sahin, M. (2015). A vascular model of Tsc1 deficiency accelerates renal tumor formation with accompanying hemangiosarcomas. *Mol Cancer Res* **13:**548-555.

Leung, E. Y., Askarian-Amiri, M., Finlay, G. J., Rewcastle, G. W. and Baguley, B. C. (2015). Potentiation of Growth Inhibitory Responses of the mTOR Inhibitor Everolimus by Dual mTORC1/2 Inhibitors in Cultured Breast Cancer Cell Lines. *PLoS One* **10:**e0131400.

Li, J., Kim, S. G. and Blenis, J. (2014). Rapamycin: one drug, many effects. *Cell Metab* **19:**373-379.

Li, M., Li, C., Allen, A., Stanley, C. A. and Smith, T. J. (2012). The structure and allosteric regulation of mammalian glutamate dehydrogenase. *Arch Biochem Biophys* **519:**69-80.

Li, Y. and Cui, J. T. (2016). Inhibition of Bcl-2 potentiates AZD-2014-induced anti-head and neck squamous cell carcinoma cell activity. *Biochem Biophys Res Commun* **477:**607-613.

Liao, H., Huang, Y., Guo, B., Liang, B., Liu, X., Ou, H., Jiang, C. C. *et al.* (2014). Dramatic antitumor effects of the dual mTORC1 and mTORC2 inhibitor AZD2014 in hepatocellular carcinoma. *Am J Cancer Res* **5:**125-139.

Lis, P., Dylag, M., Niedzwiecka, K., Ko, Y. H., Pedersen, P. L., Goffeau, A. and Ulaszewski, S. (2016). The HK2 Dependent "Warburg Effect" and Mitochondrial Oxidative Phosphorylation in Cancer: Targets for Effective Therapy with 3-Bromopyruvate. *Molecules* **21**.

Liu, J., Zhang, C., Lin, M. I., Zhu, W., Liang, Y., Hong, X., Zhao, Y. *et al.* (2014a). Glutaminase 2 negatively regulates the PI3KAKT signaling and shows tumor suppression activity in human hepatocellular carcinoma. *Oncotarget* **5:**2635-2647.

Liu, L., Li, F., Cardelli, J. A., Martin, K. A., Blenis, J. and Huang, S. (2006). Rapamycin inhibits cell motility by suppression of mTOR-mediated S6K1 and 4E-BP1 pathways. *Oncogene* **25:**7029-7040.

Liu, L., Luo, Y., Chen, L., Shen, T., Xu, B., Chen, W., Zhou, H. *et al.* (2010). Rapamycin inhibits cytoskeleton reorganization and cell motility by suppressing RhoA expression and activity. *J Biol Chem* **285:**38362-38373.

Liu, M., Poellinger, L. and Walker, C. (2003). Up-Regulation of Hypoxia-inducible Factor 2 in Renal Cell Carcinoma Associated with Loss of Tsc-2 Tumor Suppressor Gene. *Cancer Res* **63:**2675-2680.

Liu, Z., Zhang, Y. Y., Zhang, Q. W., Zhao, S. R., Wu, C. Z., Cheng, X., Jiang, C. C. *et al.* (2014b). 3-Bromopyruvate induces apoptosis in breast cancer cells by downregulating Mcl-1 through the PI3K/Akt signaling pathway. *Anticancer Drugs* **25:**447-455.

Longa, L., Saluto, A., Brusco, A., Polidoro, S., Padovan, S., Allavena, A., Carbonara, C. *et al.* (2001). TSC1 and TSC2 deletions differ in size, preference for recombinatorial sequences, and location within the gene. *Hum Genet* **108:**156-166.

Lonser, R. R., Glenn, G. M., Walther, M., Chew, E. Y., Libutti, S. K., Linehan, W. M. and Oldfield, E. H. (2003). von Hippel-Lindau disease. *The Lancet* **361:**2059-2067.

Love, D. and Hanover, J. (2005). The hexosamine signaling pathway deciphering the O-GlcNAc code. *Sci STKE* **2005:**13.

Lu, H., Dalgard, C. L., Mohyeldin, A., McFate, T., Tait, A. S. and Verma, A. (2005). Reversible inactivation of HIF-1 prolyl hydroxylases allows cell metabolism to control basal HIF-1. *J Biol Chem* **280:**41928-41939.

Lu, K. H., Wu, W., Dave, B., Slomovitz, B. M., Burke, T. W., Munsell, M. F., Broaddus, R. R. *et al.* (2008). Loss of tuberous sclerosis complex-2 function and activation of mammalian target of rapamycin signaling in endometrial carcinoma. *Clin Cancer Res* **14:**2543-2550.

Lu, W., Pelicano, H. and Huang, P. (2010). Cancer metabolism: is glutamine sweeter than glucose? *Cancer Cell* **18:**199-200.

Lunt, S. Y., Muralidhar, V., Hosios, A. M., Israelsen, W. J., Gui, D. Y., Newhouse, L., Ogrodzinski, M. *et al.* (2015). Pyruvate kinase isoform expression alters nucleotide synthesis to impact cell proliferation. *Mol Cell* **57:**95-107.

Luo, W., Hu, H., Chang, R., Zhong, J., Knabel, M., O'Meally, R., Cole, R. N. *et al.* (2011). Pyruvate kinase M2 is a PHD3-stimulated coactivator for hypoxia-inducible factor 1. *Cell* **145:**732-744.

Ma, L., Chen, Z., Erdjument-Bromage, H., Tempst, P. and Pandolfi, P. P. (2005). Phosphorylation and functional inactivation of TSC2 by Erk implications for tuberous sclerosis and cancer pathogenesis. *Cell* **121:**179-193.

Ma, X. M. and Blenis, J. (2009). Molecular mechanisms of mTOR-mediated translational control. *Nat Rev Mol Cell Biol* **10:**307-318.

Maheshwar, M., Cheadle, J., Jones, A., Myring, J., Fryer, A., Harris, P. and Sampson, J. (1997). The GAP-related domain of tuberin, the product of the TSC2 gene, is a target for missense mutations in tuberous sclerosis. *Hum Mol Genet* **6:**1991-1996.

Majkowska-Skrobek, G., Augustyniak, D., Lis, P., Bartkowiak, A., Gonchar, M., Ko, Y. H., Pedersen, P. L. *et al.* (2014). Killing multiple myeloma cells with the small molecule 3-bromopyruvate: implications for therapy. *Anticancer Drugs* **25:**673-682.

Mak, B. C., Kenerson, H. L., Aicher, L. D., Barnes, E. A. and Yeung, R. S. (2005). Aberrant β-Catenin Signaling in Tuberous Sclerosis. *The American Journal of Pathology* **167:**107-116.

Manning, B. D., Logsdon, M. N., Lipovsky, A. I., Abbott, D., Kwiatkowski, D. J. and Cantley, L. C. (2005). Feedback inhibition of Akt signaling limits the growth of tumors lacking Tsc2. *Genes Dev* **19:**1773-1778.

Marcucci, F., Stassi, G. and De Maria, R. (2016). Epithelial-mesenchymal transition: a new target in anticancer drug discovery. *Nat Rev Drug Discov* **15:**311-325.

Markowitz, J. N. and Fancher, K. M. (2018). Cabozantinib: A Multitargeted Oral Tyrosine Kinase Inhibitor. *Pharmacotherapy* **38:**357-369.

Martel, R., Kllicius, J. and Galet, S. (1977). Inhibition of the immune response by rapamycin, a new antifungal antibiotic. *Can J Physiol Pharmacol* **55:**48-51.

Martin, K. and Blenis, J. (2002). Coordinate regulation of translation by the PI 3-kinase and mTOR pathways.

. *Adv Cancer Res* **86:**1-39.

Martina, J. A., Chen, Y., Gucek, M. and Puertollano, R. (2012). MTORC1 functions as a transcriptional regulator of autophagy by preventing nuclear transport of TFEB. *Autophagy* **8:**903-914.

Martinez-Outschoorn, U. E., Peiris-Pages, M., Pestell, R. G., Sotgia, F. and Lisanti, M. P. (2017). Cancer metabolism: a therapeutic perspective. *Nat Rev Clin Oncol* **14:**11-31.

Maschek, G., Savaraj, N., Priebe, W., Braunschweiger, P., Hamilton, K., Tidmarsh, G., De Young, L. *et al.* (2004). 2-deoxy-D-glucose increases the efficacy of adriamycin and paclitaxel in human osteosarcoma and non-small cell lung cancers in vivo. *Cancer Res* **64:**31-34.

Massague, J. (2012). TGFbeta signalling in context. *Nat Rev Mol Cell Biol* **13:**616-630.

Masui, K., Tanaka, K., Akhavan, D., Babic, I., Gini, B., Matsutani, T., Iwanami, A. *et al.* (2013). mTOR complex 2 controls glycolytic metabolism in glioblastoma through FoxO acetylation and upregulation of c-Myc. *Cell Metab* **18:**726-739.

Mathupala, S. P., Ko, Y. H. and Pedersen, P. L. (2006). Hexokinase II: cancer's double-edged sword acting as both facilitator and gatekeeper of malignancy when bound to mitochondria. *Oncogene* **25:**4777-4786.

Mathupala, S. P., Rempel, A. and Pedersen, P. L. (2001). Glucose catabolism in cancer cells: identification and characterization of a marked activation response of the type II hexokinase gene to hypoxic conditions. *J Biol Chem* **276:**43407-43412.

Mayer, C., Zhao, J., Yuan, X. and Grummt, I. (2003). mTOR-dependent activation of the transcription factor TIF-IA links rRNA synthesis to nutrient availability. *Genes Dev* **18:**423-434.

Mayers, J. R. and Vander Heiden, M. G. (2015). Famine versus feast: understanding the metabolism of tumors in vivo. *Trends Biochem Sci* **40:**130-140.

Mazurek, S., Boschek, C. B., Hugo, F. and Eigenbrodt, E. (2005). Pyruvate kinase type M2 and its role in tumor growth and spreading. *Semin Cancer Biol* **15:**300-308.

McCormack, F. X., Inoue, Y., Moss, J., Singer, L., Strange, C., Nakata, K., Barker, A. *et al.* (2011). Efficacy and safety of sirolimus in lymphangioleiomyomatosis. *N Engl J Med* **364:**1595-1606.

Meikle, L., McMullen, J. R., Sherwood, M. C., Lader, A. S., Walker, V., Chan, J. A. and Kwiatkowski, D. J. (2005). A mouse model of cardiac rhabdomyoma generated by loss of Tsc1 in ventricular myocytes. *Hum Mol Genet* **14:**429-435.

Memmott, R. M., Mercado, J. R., Maier, C. R., Kawabata, S., Fox, S. D. and Dennis, P. A. (2010). Metformin prevents tobacco carcinogen--induced lung tumorigenesis. *Cancer Prev Res (Phila)* **3:**1066-1076.

Milella, M., Falcone, I., Conciatori, F., Cesta Incani, U., Del Curatolo, A., Inzerilli, N., Nuzzo, C. M. *et al.* (2015). PTEN: Multiple Functions in Human Malignant Tumors. *Front Oncol* **5:**24.

Miller, I., Gray, E. and Lloyd, D. (1989). Unilateral cystic disease of the neonatal kidney a rare presentation of tuberous sclerosis. *Histopathology* **14:**529-532.

Mita, M., Sankhala, K., Abdel-Karim, I., Mita, A. and Giles, F. J. (2008). Deforolimus (AP23573) a novel mTOR inhibitor in clinical development.

. *Expert Opin Investig Drugs* **17:**1947-1954.

Molina, J. R. and Adjei, A. (2006). The Ras/Raf/MAPK pathway. *J Thorac Oncol* **1:**7-9.

Momcilovic, M., Bailey, S. T., Lee, J. T., Fishbein, M. C., Magyar, C., Braas, D., Graeber, T. *et al.* (2017). Targeted Inhibition of EGFR and Glutaminase Induces Metabolic Crisis in EGFR Mutant Lung Cancer. *Cell Rep* **18:**601-610.

Moolten, S. (1942). Hamartial nature of the tuberous sclerosis complex and its bearing on the tumor problem: report of one case with tumor anomaly of the kidney and adenoma sebaceum. *Arch Intern Med* **69:**589-623.

Mora, A., Komander, D., van Aalten, D. and Alessi, D. R. (2004). PDK1, the master regulator of AGC kinase signal transduction. *Seminars in Cell & Developmental Biology* **15:**161-170.

Moreadith, R. and Lehninger, A. (1984). The pathways of glutamate and glutamine oxidation by tumor cell mitochondria. Role of mitochondrial NAD(P)+-dependent malic enzyme. *J Biol Chem* **259:**6215-6221.

Morita, M., Sato, T., Nomura, M., Sakamoto, Y., Inoue, Y., Tanaka, R., Ito, S. *et al.* (2018). PKM1 Confers Metabolic Advantages and Promotes Cell-Autonomous Tumor Cell Growth. *Cancer Cell* **33:**355-367 e357.

Moss, S. C., Lightell, D. J., Jr., Marx, S. O., Marks, A. R. and Woods, T. C. (2010). Rapamycin regulates endothelial cell migration through regulation of the cyclin-dependent kinase inhibitor p27Kip1. *J Biol Chem* **285:**11991-11997.

Mullarky, E., Mattaini, K. R., Vander Heiden, M. G., Cantley, L. C. and Locasale, J. W. (2011). PHGDH amplification and altered glucose metabolism in human melanoma. *Pigment Cell Melanoma Res* **24:**1112-1115.

Muzykewicz, D. A., Newberry, P., Danforth, N., Halpern, E. F. and Thiele, E. A. (2007). Psychiatric comorbid conditions in a clinic population of 241 patients with tuberous sclerosis complex. *Epilepsy Behav* **11:**506-513.

Nagarajan, A., Malvi, P. and Wajapeyee, N. (2016). Oncogene-Directed Alterations in Cancer Cell Metabolism. *Trends in Cancer* **2:**365-377.

Narov, K., Yang, J., Samsel, P. A., Jones, A., Sampson, J. R. and Shen, M. (2017). The dual PI3KmTOR inhibitor GSK2126458 is effective for treating solid renal tumours in Tsc2+- mice through suppression of cell proliferation and induction of apoptosis. *Oncotarget* **8:**58504-58512.

Nazio, F., Strappazzon, F., Antonioli, M., Bielli, P., Cianfanelli, V., Bordi, M., Gretzmeier, C. *et al.* (2013). mTOR inhibits autophagy by controlling ULK1 ubiquitylation, self-association and function through AMBRA1 and TRAF6. *Nat Cell Biol* **15:**406-416.

Nellist, M., van Slegtenhorst, M., Goedbloed, M., Van den Ouweland, A., Halley, D. and Van der Slujis, P. (1999). Characterization of the cytosolic tuberin-hamartin complex. Tuberin is a cytosolic chaperone for hamartin. *J Biol Chem* **274:**35647-35652.

Nieto, M. A., Huang, R. Y., Jackson, R. A. and Thiery, J. P. (2016). Emt: 2016. *Cell* **166:**21-45.

Niida, Y., Stemmer-Rachamimov, A. O., Logrip, M., Tapon, D., Perez, R., Kwiatkowski, D. J., Sims, K. *et al.* (2001). Survey of somatic mutations in tuberous sclerosis complex (TSC) hamartomas suggests different genetic mechanisms for pathogenesis of TSC lesions. *Am J Hum Genet* **69:**493-503.

Nilsson, H., Lindgren, D., Mandahl Forsberg, A., Mulder, H., Axelson, H. and Johansson, M. E. (2015). Primary clear cell renal carcinoma cells display minimal mitochondrial respiratory capacity resulting in pronounced sensitivity to glycolytic inhibition by 3-Bromopyruvate. *Cell Death Dis* **6:**e1585.

Nir, A., Tajik, A., Freeman, W., Seward, J., Offord, K., Edwards, W., Mair, D. *et al.* (1995). Tuberous sclerosis and cardiac rhabdomyoma. *Am J Cardiol* **76:**419-421.

Noguchi, T., Inoue, H. and Tanaka, T. (1986). The M1- and M2-type isozymes of rat pyruvate kinase are produced from the same gene by alternative RNA splicing. *J Biol Chem* **261:**13807-13812.

Noguchi, T., Yamada, K., Inoue, H., Matsuda, M. and Tanaka, T. (1987). The L- and R-type isozymes of rat pyruvate kinase are produced from a single gene by use of different promoters. *J Biol Chem* **262:**14366-14371.

Northrup, H., Beaudet, A., O'Brien, W., Herman, G., Lewis, R. and Pollack, M. (1987). Linkage of tuberous sclerosis to ABO blood group. *Lancet* **2:**804-805.

Northrup, H., Krueger, D. A. and International Tuberous Sclerosis Complex Consensus, G. (2013). Tuberous sclerosis complex diagnostic criteria update: recommendations of the 2012 Iinternational Tuberous Sclerosis Complex Consensus Conference. *Pediatr Neurol* **49:**243-254.

Northrup, H., Kwaiatkowski, D., Roach, E., Dobyns, W., Lewis, R., Herman, G., Rodriguez, E. *et al.* (1992). Evidence for genetic heterogeneity in tuberous sclerosis one locus on chromosome 9 and at least one locus elsewhere. *Am J Hum Genet* **51:**709-720.

O'Callaghan, F. J., Noakes, M. J., Martyn, C. N. and Osborne, J. P. (2004). An epidemiological study of renal pathology in tuberous sclerosis complex. *BJU Int* **94:**853-857.

O'Reilly, K. E., Rojo, F., She, Q. B., Solit, D., Mills, G. B., Smith, D., Lane, H. *et al.* (2006). mTOR inhibition induces upstream receptor tyrosine kinase signaling and activates Akt. *Cancer Res* **66:**1500-1508.

Oh, W. J. and Jacinto, E. (2011). mTOR complex 2 signaling and functions. *Cell Cycle* **10:**2305-2316.

Onda, H., Lueck, A., Marks, P. W., Warren, H. B. and Kwiatkowski, D. J. (1999). Tsc2(+/-) mice develop tumors in multiple sites that express gelsolin and are influenced by genetic background. *Journal of Clinical Investigation* **104:**687-695.

Orimoto, K., H., T., Kobayashi, T., Matsuda, T. and Hino, O. (1996). Suppression of the neoplastic phenotype by replacement of the Tsc2 gene in Eker rat renal carcinoma cells. *Biochem Biophys Res Commun* **219:**70-75.

Osanto, S. and van der Hulle, T. (2018). Cabozantinib in the treatment of advanced renal cell carcinoma in adults following prior vascular endothelial growth factor targeted therapy: clinical trial evidence and experience. *Ther Adv Urol* **10:**109-123.

Pan, T., Gao, L., Wu, G., Shen, G., Xie, S., Wen, H., Yang, J. *et al.* (2015). Elevated expression of glutaminase confers glucose utilization via glutaminolysis in prostate cancer. *Biochem Biophys Res Commun* **456:**452-458.

Patel, D., Menon, D., Bernfeld, E., Mroz, V., Kalan, S., Loayza, D. and Foster, D. A. (2016). Aspartate Rescues S-phase Arrest Caused by Suppression of Glutamine Utilization in KRas-driven Cancer Cells. *J Biol Chem* **291:**9322-9329.

Patra, K. C. and Hay, N. (2014). The pentose phosphate pathway and cancer. *Trends Biochem Sci* **39:**347-354.

Patra, K. C., Wang, Q., Bhaskar, P. T., Miller, L., Wang, Z., Wheaton, W., Chandel, N. *et al.* (2013). Hexokinase 2 is required for tumor initiation and maintenance and its systemic deletion is therapeutic in mouse models of cancer. *Cancer Cell* **24:**213-228.

Pearce, L. R., Huang, X., Boudeau, J., Pawlowski, R., Wullschleger, S., Deak, M., Ibrahim, A. F. *et al.* (2007). Identification of Protor as a novel Rictor-binding component of mTOR complex-2. *Biochem J* **405:**513-522.

Pearce, L. R., Komander, D. and Alessi, D. R. (2010). The nuts and bolts of AGC protein kinases. *Nat Rev Mol Cell Biol* **11:**9-22.

Pearce, L. R., Sommer, E. M., Sakamoto, K., Wullschleger, S. and Alessi, D. R. (2011). Protor-1 is required for efficient mTORC2-mediated activation of SGK1 in the kidney. *Biochem J* **436:**169-179.

Pelicano, H., Martin, D. S., Xu, R. H. and Huang, P. (2006). Glycolysis inhibition for anticancer treatment. *Oncogene* **25:**4633-4646.

Peterson, T. R., Laplante, M., Thoreen, C. C., Sancak, Y., Kang, S. A., Kuehl, W. M., Gray, N. S. *et al.* (2009). DEPTOR is an mTOR inhibitor frequently overexpressed in multiple myeloma cells and required for their survival. *Cell* **137:**873-886.

Peterson, T. R., Sengupta, S. S., Harris, T. E., Carmack, A. E., Kang, S. A., Balderas, E., Guertin, D. A. *et al.* (2011). mTOR complex 1 regulates lipin 1 localization to control the SREBP pathway. *Cell* **146:**408-420.

Pfeiffer, T., Schuster, S. and Bonhoeffer, S. (2001). Cooperation and competition in the evolution of ATP-producing pathways. *Science* **292:**504-507.

Phung, T. L., Ziv, K., Dabydeen, D., Eyiah-Mensah, G., Riveros, M., Perruzzi, C., Sun, J. *et al.* (2006). Pathological angiogenesis is induced by sustained Akt signaling and inhibited by rapamycin. *Cancer Cell* **10:**159-170.

Pike, K. G., Malagu, K., Hummersone, M. G., Menear, K. A., Duggan, H. M., Gomez, S., Martin, N. M. *et al.* (2013). Optimization of potent and selective dual mTORC1 and mTORC2 inhibitors: the discovery of AZD8055 and AZD2014. *Bioorg Med Chem Lett* **23:**1212-1216.

Pirson, Y. (2013). Tuberous sclerosis complex-associated kidney angiomyolipoma: from contemplation to action. *Nephrol Dial Transplant* **28:**1680-1685.

Piva, F., Giulietti, M., Santoni, M., Occhipinti, G., Scarpelli, M., Lopez-Beltran, A., Cheng, L. *et al.* (2016). Epithelial to Mesenchymal Transition in Renal Cell Carcinoma: Implications for Cancer Therapy. *Mol Diagn Ther* **20:**111-117.

Plank, T., Yeung, R. and Henske, E. (1998). Hamartin, the product of the tuberous sclerosis 1 (TSC1) gene, interacts with tuberin and appears to be localized to cytoplasmic vesicles. *Cancer Res* **58:**4766-4770.

Poleev, A., Fickenscher, H., Mundlos, S., Winterpacht, A., Zabel, B., Fidler, A., Gruss, P. *et al.* (1992). PAX8, a human paired box gene isolation and expression in developing thyroid, kidney and Wilms' tumors. *Development* **166:**611-623.

Pollizzi, K., Malinowska-Kolodziej, I., Doughty, C., Betz, C., Ma, J., Goto, J. and Kwiatkowski, D. J. (2009a). A hypomorphic allele of Tsc2 highlights the role of TSC1/TSC2 in signaling to AKT and models mild human TSC2 alleles. *Hum Mol Genet* **18:**2378-2387.

Pollizzi, K., Malinowska-Kolodziej, I., Stumm, M., Lane, H. and Kwiatkowski, D. (2009b). Equivalent benefit of mTORC1 blockade and combined PI3K-mTOR blockade in a mouse model of tuberous sclerosis. *Mol Cancer* **8:**38.

Portais, J., Voisin, P., Merle, M. and Canioni, P. (1996). Glucose and glutamine metabolism in C6 glioma cells studied by carbon 13 NMR. *Biochimie* **78:**155-164.

Possemato, R., Marks, K. M., Shaul, Y. D., Pacold, M. E., Kim, D., Birsoy, K., Sethumadhavan, S. *et al.* (2011). Functional genomics reveal that the serine synthesis pathway is essential in breast cancer. *Nature* **476:**346-350.

Potter, C. J., Pedraza, L. G. and Xu, T. (2002). Akt regulates growth by directly phosphorylating Tsc2. *Nat Cell Biol* **4:**658-665.

Powles, T., Wheater, M., Din, O., Geldart, T., Boleti, E., Stockdale, A., Sundar, S. *et al.* (2015). A Randomised Phase 2 Study of AZD2014 Versus Everolimus in Patients with VEGF-Refractory Metastatic Clear Cell Renal Cancer. *Eur Urol*.

Prabhakar, S., Goto, J., Zhang, X., Sena-Esteves, M., Bronson, R., Brockmann, J., Gianni, D. *et al.* (2013). Stochastic model of Tsc1 lesions in mouse brain. *PLoS One* **8:**e64224.

Prather, P. and de Vries, P. (2004). Behavioral and Cognitive Aspects of Tuberous Sclerosis Complex. *J Child Neurol* **19:**666-674.

Pusapati, Raju V., Daemen, A., Wilson, C., Sandoval, W., Gao, M., Haley, B., Baudy, Andreas R. *et al.* (2016). mTORC1-Dependent Metabolic Reprogramming Underlies Escape from Glycolysis Addiction in Cancer Cells. *Cancer Cell* **29:**548-562.

Pymar, L. S., Platt, F. M., Askham, J. M., Morrison, E. E. and Knowles, M. A. (2008). Bladder tumour-derived somatic TSC1 missense mutations cause loss of function via distinct mechanisms. *Hum Mol Genet* **17:**2006-2017.

Radimerski, T., Montagne, J., Hemmings-Mieszczak, M. and Thomas, G. (2002). Lethality of Drosophila lacking TSC tumor suppressor function rescued by reducing dS6K signaling. *Genes Dev* **16:**2627-2632.

Rakowski, S. K., Winterkorn, E. B., Paul, E., Steele, D. J., Halpern, E. F. and Thiele, E. A. (2006). Renal manifestations of tuberous sclerosis complex: Incidence, prognosis, and predictive factors. *Kidney Int* **70:**1777-1782.

Rao, P. and Monks, D. A. (2009). A tetracycline-inducible and skeletal muscle-specific Cre recombinase transgenic mouse. *Dev Neurobiol* **69:**401-406.

Rao, R. D., Mladek, A. C., Lamont, J. D., Goble, J. M., Erlichman, C., James, C. D. and Sarkaria, J. N. (2005). Disruption of Parallel and Converging Signaling Pathways Contributes to the Synergistic Antitumor Effects of Simultaneous mTOR and EGFR Inhibition in GBM Cells. *Neoplasia* **7:**921-929.

Rauktys, A., Lee, N., Lee, L. and Dabora, S. L. (2008). Topical rapamycin inhibits tuberous sclerosis tumor growth in a nude mouse model. *BMC Dermatol* **8:**1.

Ravikumar, B., Sarkar, S., Davies, J. E., Futter, M., Garcia-Arencibia, M., Green-Thompson, Z. W., Jimenez-Sanchez, M. *et al.* (2010). Regulation of mammalian autophagy in physiology and pathophysiology. *Physiol Rev* **90:**1383-1435.

Rayer, P. (1835). Traite Theorique et Pratique des Maladies de la Peau,. *JB Bailliere*.

Reiling, J. H. and Hafen, E. (2004). The hypoxia-induced paralogs Scylla and Charybdis inhibit growth by down-regulating S6K activity upstream of TSC in Drosophila. *Genes Dev* **18:**2879-2892.

Reith, R. M., McKenna, J., Wu, H., Hashmi, S. S., Cho, S. H., Dash, P. K. and Gambello, M. J. (2013). Loss of Tsc2 in Purkinje cells is associated with autistic-like behavior in a mouse model of tuberous sclerosis complex. *Neurobiol Dis* **51:**93-103.

Rhim, A. D., Mirek, E. T., Aiello, N. M., Maitra, A., Bailey, J. M., McAllister, F., Reichert, M. *et al.* (2012). EMT and dissemination precede pancreatic tumor formation. *Cell* **148:**349-361.

Rini, B. I. (2008). Temsirolimus, an inhibitor of mammalian target of rapamycin. *Clin Cancer Res* **14:**1286-1290.

Roach, E., Gomez, M. and Northrup, H. (1998). Tuberous sclerosis complex consensus conference: revised clinical diagnostic criteria. *J Child Neurol* **13:**624-628.

Roach, E., Smith, M., Huttenlocher, P., Bhat, M., Alcorn, D. and Hawley, L. (1992). Diagnostic criteria: tuberous sclerosis complex. Report of the Diagnostic Criteria Committee of the National Tuberous Sclerosis Association. *J Child Neurol* **7:**221-224.

Roach, E. and Sparagana, S. (2004). Diagnosis of tuberous sclerosis complex. *J Child Neurol* **19:**643-649.

Robertson, D. (1991). Ophthalmic manifestations of tuberous sclerosis. *Ann N Y Acad Sci* **615:**17-25.

Robertson, F., Cendron, M., Klauber, G. and Harris, B. (1996). Renal cell carcinoma in association with tuberous sclerosis in children. *J Pediatr Surg* **31:**729-730.

Robey, R. B. and Hay, N. (2009). Is Akt the "Warburg kinase"?-Akt-energy metabolism interactions and oncogenesis. *Semin Cancer Biol* **19:**25-31.

Rodrik-Outmezguine, V. S., Okaniwa, M., Yao, Z., Novotny, C. J., McWhirter, C., Banaji, A., Won, H. *et al.* (2016). Overcoming mTOR resistance mutations with a new-generation mTOR inhibitor. *Nature* **534:**272-276.

Rosser, T., Panigrahy, A. and McClintock, W. (2006). The diverse clinical manifestations of tuberous sclerosis complex: a review. *Semin Pediatr Neurol* **13:**27-36.

Roux, P. P., Ballif, B. A., Anjum, R., Gygi, S. P. and Blenis, J. (2004). Tumor-promoting phorbol esters and activated Ras inactivate the tuberous sclerosis tumor suppressor complex via p90 ribosomal S6 kinase. *Proc Natl Acad Sci U S A* **101:**13489-13494.

Rowley, S., O'Callaghan, F. and Osborne, J. (2001). Ophthalmic manifestations of tuberous sclerosis a population based study. *Br J Ophthalmol* **85:**420-423.

Rozas, N. S., Redell, J. B., McKenna, J., 3rd, Moore, A. N., Gambello, M. J. and Dash, P. K. (2015). Prolonging the survival of Tsc2 conditional knockout mice by glutamine supplementation. *Biochem Biophys Res Commun* **457:**635-639.

Ruppe, V., Dilsiz, P., Reiss, C. S., Carlson, C., Devinsky, O., Zagzag, D., Weiner, H. L. *et al.* (2014). Developmental brain abnormalities in tuberous sclerosis complex: a comparative tissue analysis of cortical tubers and perituberal cortex. *Epilepsia* **55:**539-550.

Sabatini, D., Erdjument-Bromage, H., Lui, M., Tempst, P. and Snyder, S. (1994). RAFT1 a mammalian protein that binds to FKBP12 in a rapamycin-dependent fashion and is homologous to yeast TORs. *Cell* **78:**35-43.

Sakre, N., Wildey, G., Behtaj, M., Kresak, A., Yang, M. and Fu, P. D., A. (2017). RICTOR amplification identifies a subgroup in small cell lung cancer and predicts response to drugs targeting mTOR. *Oncotarget* **8:**5992-6002.

Sampson, J., Janssen, L. and Sandkuyl, L. (1992). Linkage investigation of three putative tuberous sclerosis determining loci on chromosomes 9q, 11q, and 12q. The Tuberous Sclerosis Collaborative Group. *J Med Genet* **29:**861-866.

Sampson, J., Yates, J., Pirrit, L., Fleury, P., Winship, I., Beighton, P. and Connor, J. (1989). Evidence for genetic heterogeneity in tuberous sclerosis. *J Med Genet* **26:**511-516.

Sampson, J. R., Maheshwar, M. M., Aspinwall, R., Thompson, P., Cheadle, J. P., Ravine, D., Roy, S. *et al.* (1997). Renal cystic disease in tuberous sclerosis: role of the polycystic kidney disease 1 gene. *Am J Hum Genet* **61:**843-851.

Samuels, Y., Wang, Z., Bardelli, A., Silliman, N., Ptak, J., Szabo, S., Vogelstein, B. *et al.* (2004). High frequency of mutations of the PIK3CA gene in human cancers. *Science* **304**.

Sancak, O., Nellist, M., Goedbloed, M., Elfferich, P., Wouters, C., Maat-Kievit, A., Zonnenberg, B. *et al.* (2005). Mutational analysis of the TSC1 and TSC2 genes in a diagnostic setting: genotype--phenotype correlations and comparison of diagnostic DNA techniques in Tuberous Sclerosis Complex. *Eur J Hum Genet* **13:**731-741.

Sancak, Y., Bar-Peled, L., Zoncu, R., Markhard, A. L., Nada, S. and Sabatini, D. M. (2010). Ragulator-Rag complex targets mTORC1 to the lysosomal surface and is necessary for its activation by amino acids. *Cell* **141:**290-303.

Sancak, Y., Peterson, B., Shaul, T., Lindguist, R., Thoreen, C., Bar-Peled, L. and Sabatini, D. (2008). The Rag GTPases bind raptor and mediate amino acid signaling to mTORC1. *Science* **320:**1496-1501.

Sancak, Y., Thoreen, C. C., Peterson, T. R., Lindquist, R. A., Kang, S. A., Spooner, E., Carr, S. A. *et al.* (2007). PRAS40 is an insulin-regulated inhibitor of the mTORC1 protein kinase. *Mol Cell* **25:**903-915.

Sarbassov, D. D., Ali, S. M., Kim, D. H., Guertin, D. A., Latek, R. R., Erdjument-Bromage, H., Tempst, P. *et al.* (2004). Rictor, a novel binding partner of mTOR, defines a rapamycin-insensitive and raptor-independent pathway that regulates the cytoskeleton. *Curr Biol* **14:**1296-1302.

Sarbassov, D. D., Ali, S. M. and Sabatini, D. M. (2005a). Growing roles for the mTOR pathway. *Curr Opin Cell Biol* **17:**596-603.

Sarbassov, D. D., Ali, S. M., Sengupta, S., Sheen, J. H., Hsu, P. P., Bagley, A. F., Markhard, A. L. *et al.* (2006). Prolonged rapamycin treatment inhibits mTORC2 assembly and Akt/PKB. *Mol Cell* **22:**159-168.

Sarbassov, D. D., Guertin, D. A., Ali, S. M. and Sabatini, D. (2005b). Phosphorylation and Regulation of AktPKB by the Rictor-mTOR Complex. *Science* **307:**1098-1101.

Sato, Y., Yoshizato, T., Shiraishi, Y., Maekawa, S., Okuno, Y., Kamura, T., Shimamura, T. *et al.* (2013). Integrated molecular analysis of clear-cell renal cell carcinoma. *Nat Genet* **45:**860-867.

Schenone, S., Brullo, C., Musumeci, F., Radi, M. and Botta, M. (2011). ATP-Competitive Inhibitors of mTOR An Update. *Curr Med Chem* **18:**2995-3014.

Schneider, J., Neu, K., Grimm, H., Velcovsky, H., Weisse, G. and Eigenbrodt, E. (2002). Tumor M2-pyruvate kinase in lung cancer patients Immunohistochemical detection and disease monitoring. *Anticancer Res* **22:**311-318.

Scott, R. C., Juhasz, G. and Neufeld, T. P. (2007). Direct induction of autophagy by Atg1 inhibits cell growth and induces apoptotic cell death. *Curr Biol* **17:**1-11.

Sehgal, S. (1998). Rapamune (RAPA, rapamycin, sirolimus) mechanism of action immunosuppressive effect results from blockade of signal transduction and inhibition of cell cycle progression. *Clin Biochem* **31:**335-340.

Sengupta, S., Peterson, T. R. and Sabatini, D. M. (2010). Regulation of the mTOR complex 1 pathway by nutrients, growth factors, and stress. *Mol Cell* **40:**310-322.

Seufferlein, T. and Rozengurt, E. (1996). Rapamycin inhibits constitutive p70s6k phosphorylation, cell proliferation, and colony formation in small cell lung cancer cells. *Cancer Res* **56:**3895-3897.

Shepherd, C., Gomez, M., Lie, J. and Crpwson, C. (1991). Causes of death in patients with tuberous sclerosis. *Mayo Clin Proc* **66:**792-796.

Shim, H., Dolde, C., Lewis, B., Wu, C., Dang, G., Jungmann, R., Dalla-Favera, R. *et al.* (1997). c-Myc transactivation of LDH-A implications for tumor metabolism and growth. *Proc Natl Acad Sci U S A* **94:**6658-6663.

Shor, B., Wu, J., Shakey, Q., Toral-Barza, L., Shi, C., Follettie, M. and Yu, K. (2010). Requirement of the mTOR kinase for the regulation of Maf1 phosphorylation and control of RNA polymerase III-dependent transcription in cancer cells. *J Biol Chem* **285:**15380-15392.

Shroff, E. H., Eberlin, L. S., Dang, V. M., Gouw, A. M., Gabay, M., Adam, S. J., Bellovin, D. I. *et al.* (2015). MYC oncogene overexpression drives renal cell carcinoma in a mouse model through glutamine metabolism. *Proc Natl Acad Sci U S A* **112:**6539-6544.

Singleton, K. R., Hinz, T. K., Kleczko, E. K., Marek, L. A., Kwak, J., Harp, T., Kim, J. *et al.* (2015). Kinome RNAi Screens Reveal Synergistic Targeting of MTOR and FGFR1 Pathways for Treatment of Lung Cancer and HNSCC. *Cancer Res* **75:**4398-4406.

Siracusano, S., Zanon, M., D'Aloia, G., Plaino, F., Trombetta, C. and Bussani, R. (1998). Rare association of renal angiomyolipoma and oncocytoma. *Urology* **51:**837-839.

Smolarek, T. A., Wessner, L. L., McCormack, F. X., Mylet, J. C., Menon, A. G. and Henske, E. P. (1998). Evidence that lymphangiomyomatosis is caused by TSC2 mutations: chromosome 16p13 loss of heterozygosity in angiomyolipomas and lymph nodes from women with lymphangiomyomatosis. *Am J Hum Genet* **62:**810-815.

Song, E. K., Tai, W. M., Messersmith, W. A., Bagby, S., Purkey, A., Quackenbush, K. S., Pitts, T. M. *et al.* (2015). Potent antitumor activity of cabozantinib, a c-MET and VEGFR2 inhibitor, in a colorectal cancer patient-derived tumor explant model. *Int J Cancer* **136:**1967-1975.

Sonveaux, P., Vegran, F., Schroeder, T., Wergin, M. C., Verrax, J., Rabbani, Z. N., De Saedeleer, C. J. *et al.* (2008). Targeting lactate-fueled respiration selectively kills hypoxic tumor cells in mice. *J Clin Invest* **118:**3930-3942.

St-Onge, L., Furth, P. and Gruss, P. (1996). Temporal control of the Cre recombinase in transgenic mice by a tetracycline respomsive promoter. *Nucleic Acids Research* **24:**3875-3877.

Stine, Z. E., Walton, Z. E., Altman, B. J., Hsieh, A. L. and Dang, C. V. (2015). MYC, Metabolism, and Cancer. *Cancer Discov* **5:**1024-1039.

Stricklett, P., Nelson, R. and Kohan, D. (1999). The Cre-loxP system and gene targeting in the kidney, 1999. *Am J Pathol* **276:**651-657.

Sun, L., Yin, Y., Clark, L., Sun, W., Sullivan, S., Tran, A., Han, J. *et al.* (2017). Dual inhibition of glycolysis and glutaminolysis as a therapeutic strategy in the treatment of ovarian cancer. *Oncotarget* **8:**63551-63561.

Sun, Q., Chen, X., Ma, J., Peng, H., Wang, F., Zha, X., Wang, Y. *et al.* (2011). Mammalian target of rapamycin up-regulation of pyruvate kinase isoenzyme type M2 is critical for aerobic glycolysis and tumor growth. *Proc Natl Acad Sci U S A* **108:**4129-4134.

Sun, Y., Liu, Z., Zou, X., Lan, Y., Sun, X., Wang, X., Zhao, S. *et al.* (2015). Mechanisms underlying 3-bromopyruvate-induced cell death in colon cancer. *J Bioenerg Biomembr* **47:**319-329.

Szablewski, L. (2013). Expression of glucose transporters in cancers. *Biochim Biophys Acta* **1835:**164-169.

Tabernero, J., Rojo, F., Calvo, E., Burris, H., Judson, I., Hazell, K., Martinelli, E. *et al.* (2008). Dose- and schedule-dependent inhibition of the mammalian target of rapamycin pathway with everolimus: a phase I tumor pharmacodynamic study in patients with advanced solid tumors. *J Clin Oncol* **26:**1603-1610.

Takamochi, K., Ogura, T., Suzuki, K., Kawasaki, H., Kurashima, Y., Yokose, T., Ochiai, A. *et al.* (2001). Loss of heterozygosity on chromosomes 9q and 16p in atypical adenomatous hyperplasia concomitant with adenocarcinoma of the lung. *Am J Pathol* **159:**1941-7948.

Tanaka, K., Sasayama, T., Irino, Y., Takata, K., Nagashima, H., Satoh, N., Kyotani, K. *et al.* (2015). Compensatory glutamine metabolism promotes glioblastoma resistance to mTOR inhibitor treatment. *J Clin Invest* **125:**1591-1602.

Tang, H., Hornstein, E., Stolovich, M., Levy, G., Livingstone, M., Templeton, D., Avruch, J. *et al.* (2001). Amino acid-induced translation of TOP mRNAs is fully dependent on phosphatidylinositol 3-kinase-mediated signaling, is partially inhibited by rapamycin, and is independent of S6K1 and rpS6 phosphorylation. *Mol Cell Biol* **21:**8671-8683.

Tang, Z., Yuan, S., Hu, Y., Zhang, H., Wu, W., Zeng, Z., Yang, J. *et al.* (2012). Over-expression of GAPDH in human colorectal carcinoma as a preferred target of 3-bromopyruvate propyl ester. *J Bioenerg Biomembr* **44:**117-125.

Tapon, N., Ito, N., Dickson, B., Treisman, J. and Hariharan, I. (2001). The Drosophila tuberous sclerosis complex gene homologs restrict cell growth and cell proliferation. *Cell* **105:**345-355.

Tee, A., Manning, B., Roux, P., Cantley, L. and Blenis, J. (2003). Tuberous Sclerosis Complex Gene Products, Tuberin and Hamartin, Control mTOR Signaling by Acting as a GTPase-Activating Protein Complex toward Rheb. *Current Biology* **13:**1259-1268.

Teng, J. M., Cowen, E. W., Wataya-Kaneda, M., Gosnell, E. S., Witman, P. M., Hebert, A. A., Mlynarczyk, G. *et al.* (2014). Dermatologic and dental aspects of the 2012 International Tuberous Sclerosis Complex Consensus Statements. *JAMA Dermatol* **150:**1095-1101.

Thiery, J. P., Acloque, H., Huang, R. Y. and Nieto, M. A. (2009). Epithelial-mesenchymal transitions in development and disease. *Cell* **139:**871-890.

Thoreen, C. C., Kang, S. A., Chang, J. W., Liu, Q., Zhang, J., Gao, Y., Reichling, L. J. *et al.* (2009). An ATP-competitive mammalian target of rapamycin inhibitor reveals rapamycin-resistant functions of mTORC1. *J Biol Chem* **284:**8023-8032.

Thorpe, L. M., Yuzugullu, H. and Zhao, J. J. (2015). PI3K in cancer: divergent roles of isoforms, modes of activation and therapeutic targeting. *Nat Rev Cancer* **15:**7-24.

Traykova-Brauch, M., Schonig, K., Greiner, O., Miloud, T., Jauch, A., Bode, M., Felsher, D. W. *et al.* (2008). An efficient and versatile system for acute and chronic modulation of renal tubular function in transgenic mice. *Nat Med* **14:**979-984.

Tsai, P. T., Hull, C., Chu, Y., Greene-Colozzi, E., Sadowski, A. R., Leech, J. M., Steinberg, J. *et al.* (2012). Autistic-like behaviour and cerebellar dysfunction in Purkinje cell Tsc1 mutant mice. *Nature* **488:**647-651.

Tsun, Z. Y., Bar-Peled, L., Chantranupong, L., Zoncu, R., Wang, T., Kim, C., Spooner, E. *et al.* (2013). The folliculin tumor suppressor is a GAP for the RagC/D GTPases that signal amino acid levels to mTORC1. *Mol Cell* **52:**495-505.

Tucker, T. and Friedman, J. (2002). Pathogenesis of hereditary tumors beyond the two-hit hypothesis. *Clin Genet* **62:**345-357.

Tyburczy, M. E., Wang, J. A., Li, S., Thangapazham, R., Chekaluk, Y., Moss, J., Kwiatkowski, D. J. *et al.* (2014). Sun exposure causes somatic second-hit mutations and angiofibroma development in tuberous sclerosis complex. *Hum Mol Genet* **23:**2023-2029.

Uhlmann, E. J., Wong, M., Baldwin, R. L., Bajenaru, M. L., Onda, H., Kwiatkowski, D. J., Yamada, K. *et al.* (2002). Astrocyte-specific TSC1 conditional knockout mice exhibit abnormal neuronal organization and seizures. *Ann Neurol* **52:**285-296.

Um, S., Frigerio, F., Watanabe, M., Picard, F., Joaquin, M., Sticker, M. and Thomas, G. (2004). Absence of S6K1 protects against age- and diet-induced obesity while enhancing insulin sensitivity. *Nature* **431:**200-205.

Valenti, D., Vacca, R. A. and de Bari, L. (2015). 3-Bromopyruvate induces rapid human prostate cancer cell death by affecting cell energy metabolism, GSH pool and the glyoxalase system. *J Bioenerg Biomembr* **47:**493-506.

van den Heuvel, A. P., Jing, J., Wooster, R. F. and Bachman, K. E. (2012). Analysis of glutamine dependency in non-small cell lung cancer: GLS1 splice variant GAC is essential for cancer cell growth. *Cancer Biol Ther* **13:**1185-1194.

van Miltenburg, M. H. and Jonkers, J. (2012). Using genetically engineered mouse models to validate candidate cancer genes and test new therapeutic approaches. *Curr Opin Genet Dev* **22:**21-27.

van Niekerk, G. and Engelbrecht, A. M. (2018). Role of PKM2 in directing the metabolic fate of glucose in cancer: a potential therapeutic target. *Cell Oncol (Dordr)* **41:**343-351.

van Slegtenhorst, M., de Hoogt, R., Hermans, C., Nellist, M., Janssen, B., BVerhoef, S., Lindhout, D. *et al.* (1997). Identification of the tuberous sclerosis gene TSC1 on chromosome 9q34. *Science* **277:**805-808.

Van Slegtenhorst, M., Nellist, M., Nagelkerken, B., Cheadle, J. P., Snell, R., Van den Ouweland, A., Reuser, A. *et al.* (1998). Interaction between hamartin and tuberin, the TSC1 and TSC2 gene products. *Hum Mol Genet* **7:**1053-1057.

Vandamme, T., Beyens, M., de Beeck, K. O., Dogan, F., van Koetsveld, P. M., Pauwels, P., Mortier, G. *et al.* (2016). Long-term acquired everolimus resistance in pancreatic neuroendocrine tumours can be overcome with novel PI3K-AKT-mTOR inhibitors. *Br J Cancer* **114:**650-658.

Vander Heiden, M. G., Cantley, L. C. and Thompson, C. B. (2009). Understanding the Warburg effect: the metabolic requirements of cell proliferation. *Science* **324:**1029-1033.

Vanhaesebroeck, B., Stephens, L. and Hawkins, P. (2012). PI3K signalling: the path to discovery and understanding. *Nat Rev Mol Cell Biol* **13:**195-203.

Verhoef, S., Bakker, L., Tempelaars, A. M., Hesseling-Janssen, A. L., Mazurczak, T., Jozwiak, S., Fois, A. *et al.* (1999). High rate of mosaicism in tuberous sclerosis complex. *Am J Hum Genet* **64:**1632-1637.

Vezina, C., Kudelski, A. and Sehgal, S. (1975). Rapamycin (AY-22,989), a new antifungal antibiotic. I. Taxonomy of the producing streptomycete and isolation of the active principle. *J Antibiot* **28:**721-726.

Vikis, H., Rymaszewski, A. and Tichelaar, J. (2013). Mouse models of chemically-induced lung carcinogenesis. *Front Biol* **1:**939-946.

Vogt, H. (1908). Zur Pathologie und pathologishcen Anatomie der verschiedenen Idiotieform. *Monatsschr Psychiatr Neurol* **24:**106-150.

von Recklinghausen, F. (1862). Ein Herz von einem Neugeborene welches mehrere theils nach aussen, theils nach den H€ohlen prominirende Tumoren. *Monatschr Geburtsheklkd* **20:**1-2.

Wander, S. A., Hennessy, B. T. and Slingerland, J. M. (2011). Next-generation mTOR inhibitors in clinical oncology: how pathway complexity informs therapeutic strategy. *J Clin Invest* **121:**1231-1241.

Wang, J. and Abate-Shen, C. (2014). Analyses of tumor-suppressor genes in germline mouse models of cancer. *Cold Spring Harb Protoc* **8:**807-812.

Wang, L., Harris, T. E. and Lawrence, J. C., Jr. (2008). Regulation of proline-rich Akt substrate of 40 kDa (PRAS40) function by mammalian target of rapamycin complex 1 (mTORC1)-mediated phosphorylation. *J Biol Chem* **283:**15619-15627.

Wang, X. (2009). Cre transgenic mouse lines. *Methods Mol Biol* **561:**265-273.

Wang, Y. H., Israelsen, W. J., Lee, D., Yu, V. W. C., Jeanson, N. T., Clish, C. B., Cantley, L. C. *et al.* (2014). Cell-state-specific metabolic dependency in hematopoiesis and leukemogenesis. *Cell* **158:**1309-1323.

Warburg, O. (1927). THE METABOLISM OF TUMORS IN THE BODY. *The Journal of General Physiology* **8:**519-530.

Warburg, O. (1956). On the origin of cancer cells. *Science* **123:**309-314.

Wechsel, H., Petri, E., Bichler, K. and Feil, G. (1999). Marker for renal cell carcinoma (RCC): the dimeric form of pyruvate kinase type M2 (Tu M2-PK). *Anticancer Res* **19:**2583-2590.

Wei, F., Zhang, Y., Geng, L., Zhang, P., Wang, G. and Liu, Y. (2015). mTOR inhibition induces EGFR feedback activation in association with its resistance to human pancreatic cancer. *Int J Mol Sci* **16:**3267-3282.

Willems, L., Tamburini, J., Chapuis, N., Lacombe, C., Mayeux, P. and Bouscary, D. (2012). PI3K and mTOR signaling pathways in cancer: new data on targeted therapies. *Curr Oncol Rep* **14:**129-138.

Wilson, C., Idziaszczyk, S., Parry, L., Guy, C., Griffiths, D. F., Lazda, E., Bayne, R. A. *et al.* (2005). A mouse model of tuberous sclerosis 1 showing background specific early post-natal mortality and metastatic renal cell carcinoma. *Hum Mol Genet* **14:**1839-1850.

Wilson, J. E. (2003). Isozymes of mammalian hexokinase: structure, subcellular localization and metabolic function. *Journal of Experimental Biology* **206:**2049-2057.

Wise, D. R., DeBerardinis, R. J., Mancuso, A., Sayed, N., Zhang, X. Y., Pfeiffer, H. K., Nissim, I. *et al.* (2008). Myc regulates a transcriptional program that stimulates mitochondrial glutaminolysis and leads to glutamine addiction. *Proc Natl Acad Sci U S A* **105:**18782-18787.

Wise, D. R., Ward, P. S., Shay, J. E., Cross, J. R., Gruber, J. J., Sachdeva, U. M., Platt, J. M. *et al.* (2011). Hypoxia promotes isocitrate dehydrogenase-

dependent carboxylation of alpha-ketoglutarate to citrate to support cell growth and viability. *Proc Natl Acad Sci U S A* **108:**19611-19616.

Wolf, D., Whiteley, H. and Everitt, J. (1995). Preneoplastic and neoplastic lesions of rat hereditary renal cell tumors express markers of proximal and distal nephron. *Vet Pathol* **32:**379-386.

Wong, N., De Melo, J. and Tang, D. (2013). PKM2, a Central Point of Regulation in Cancer Metabolism. *Int J Cell Biol* **2013:**242513.

Wong, N., Ojo, D., Yan, J. and Tang, D. (2015). PKM2 contributes to cancer metabolism. *Cancer Lett* **356:**184-191.

Xian, S. L., Cao, W., Zhang, X. D. and Lu, Y. F. (2015). 3-Bromopyruvate inhibits human gastric cancer tumor growth in nude mice via the inhibition of glycolysis. *Oncol Lett* **9:**739-744.

Xiang, Y., Stine, Z. E., Xia, J., Lu, Y., O'Connor, R. S., Altman, B. J., Hsieh, A. L. *et al.* (2015). Targeted inhibition of tumor-specific glutaminase diminishes cell-autonomous tumorigenesis. *J Clin Invest* **125:**2293-2306.

Yamakado, K., Tanaka, N., Nakagawa, T., Kobayashi, E., Yanagawa, M. and Takeda, K. (2002). Renal angiomyolipoma: relationships between tumor size, aneurysm formation, and rupture. *Radiology* **225:**78-82.

Yang, J., Kalogerou, M., Gallacher, J., Sampson, J. R. and Shen, M. H. (2013). Renal tumours in a Tsc1+/- mouse model show epigenetic suppression of organic cation transporters Slc22a1, Slc22a2 and Slc22a3, and do not respond to metformin. *Eur J Cancer* **49:**1479-1490.

Yang, J., Kalogerou, M., Samsel, P. A., Zhang, Y., Griffiths, D. F., Gallacher, J., Sampson, J. R. *et al.* (2015). Renal tumours in a Tsc2(+/-) mouse model do not show feedback inhibition of Akt and are effectively prevented by rapamycin. *Oncogene* **34:**922-931.

Yang, J., Samsel, P. A., Narov, K., Jones, A., Gallacher, D., Gallacher, J., Sampson, J. R. *et al.* (2017). Combination of Everolimus with Sorafenib for Solid Renal Tumors in Tsc2(+/-) Mice Is Superior to Everolimus Alone. *Neoplasia* **19:**112-120.

Yang, M. and Vousden, K. H. (2016). Serine and one-carbon metabolism in cancer. *Nat Rev Cancer*.

Yang, P., Cornejo, K. M., Sadow, P. M., Cheng, L., Wang, M., Xiao, Y., Jiang, Z. *et al.* (2014). Renal cell carcinoma in tuberous sclerosis complex. *Am J Surg Pathol* **38:**895-909.

Yang, W., Zheng, Y., Xia, Y., Ji, H., Chen, X., Guo, F., Lyssiotis, C. A. *et al.* (2012). ERK1/2-dependent phosphorylation and nuclear translocation of PKM2 promotes the Warburg effect. *Nat Cell Biol* **14:**1295-1304.

Yeung, R., Buetow, K., Testa, J. and Knudson, A. (1993). Susceptibility to renal carcinoma in the Eker rat involves a tumor suppressor gene on chromosome 10. *Proc Natl Acad Sci U S A* **90:**8038-8042.

Yeung, R., Katsetos, C. and Klein-Szanto, A. (1997). Subependymal astrocytic hamartomas in the Eker rat model of tuberous sclerosis. *Am J Pathol* **151:**1477-1486.

Yeung, R., Xiao, G., Jin, F., Lee, W., Testa, J. and Knudson, A. (1994). Predisposition to renal carcinoma in the Eker rat is determined by germ-line mutation of the tuberous sclerosis 2 (TSC2) gene.

. *Proc Natl Acad Sci U S A* **91:**11413-11416.

Yu, C. C., Huang, H. B., Hung, S. K., Liao, H. F., Lee, C. C., Lin, H. Y., Li, S. C. *et al.* (2016). AZD2014 Radiosensitizes Oral Squamous Cell Carcinoma by Inhibiting AKT/mTOR Axis and Inducing G1/G2/M Cell Cycle Arrest. *PLoS One* **11:**e0151942.

Yu, K., Toral-Barza, L., Discafani, C., Zhang, W., Skotnicki, J., Frost, P. and Gibbons, J. (2001). mTOR, a novel target in breast cancer the effect of CCI-779, an mTOR inhibitor, in preclinical models of breast cancer. *Endocr Relat Cancer* **8:**249-258.

Yu, K., Toral-Barza, L., Shi, C., Zhang, W. G., Lucas, J., Shor, B., Kim, J. *et al.* (2009). Biochemical, cellular, and in vivo activity of novel ATP-competitive and selective inhibitors of the mammalian target of rapamycin. *Cancer Res* **69:**6232-6240.

Yu, Y., Yoon, S., Poulogiannis, G., Yang, Q., Ma, X., Villen, J., Kubica, N. *et al.* (2011). Phosphoproteomic analysis identifies Grb10 as an mTORC1 substrate that negatively regulates insulin signaling. *Science* **332:**1322-1326.

Yuneva, M., Zamboni, N., Oefner, P., Sachidanandam, R. and Lazebnik, Y. (2007). Deficiency in glutamine but not glucose induces MYC-dependent apoptosis in human cells. *J Cell Biol* **178:**93-105.

Zerban, H., Noqueira, E., Riedasch, G. and Bannasch, P. (1987). Renal oncocytoma: origin from the collecting duct. *Virchows Arch B Cell Pathol Incl Mol Pathol* **52:**375-387.

Zha, X., Sun, Q. and Zhang, H. (2014). mTOR upregulation of glycolytic enzymes promotes tumor development. *Cell Cycle* **10:**1015-1016.

Zhang, D., Li, J., Wang, F., Hu, J., Wang, S. and Sun, Y. (2014). 2-Deoxy-D-glucose targeting of glucose metabolism in cancer cells as a potential therapy. *Cancer Lett* **355:**176-183.

Zhang, H., Bajraszewski, N., Wu, E., Wang, H., Moseman, A. P., Dabora, S. L., Griffin, J. D. *et al.* (2007). PDGFRs are critical for PI3K/Akt activation and negatively regulated by mTOR. *J Clin Invest* **117:**730-738.

Zhang, H., Cicchetti, G., Onda, H., Koon, H. B., Asrican, K., Bajraszewski, N., Vazquez, F. *et al.* (2003a). Loss of Tsc1/Tsc2 activates mTOR and disrupts PI3K-Akt signaling through downregulation of PDGFR. *J Clin Invest* **112:**1223-1233.

Zhang, H., Stallock, J., Ng, J., Reinhard, C. and Neufeld, T. (2000). Regulation of cellular growth by the Drosophila target of rapamycin dTOR. *Genes Dev* **14:**12*-24.

Zhang, J., Wang, C., Chen, M., Cao, J., Zhong, Y., Chen, L., Shen, H. *et al.* (2013). Epigenetic silencing of glutaminase 2 in human liver and colon cancers. *BMC Cancer* **13:**1471-1480.

Zhang, Q., Pan, J., Lubet, R. A., Komas, S. M., Kalyanaraman, B., Wang, Y. and You, M. (2015). Enhanced antitumor activity of 3-bromopyruvate in combination with rapamycin in vivo and in vitro. *Cancer Prev Res (Phila)* **8:**318-326.

Zhang, Y., Gao, X., Saucedo, L., Ru, B., Edgar, B. and Pan, D. (2003b). Rheb is a direct target of the tuberous sclerosis tumour suppressor proteins. *Nat Cell Biol* **5:**478-581.

Zheng, B., Mao, J. H., Qian, L., Zhu, H., Gu, D. H., Pan, X. D., Yi, F. *et al.* (2015). Pre-clinical evaluation of AZD-2014, a novel mTORC1/2 dual inhibitor, against renal cell carcinoma. *Cancer Lett* **357:**468-475.

Zinzalla, V., Stracka, D., Oppliger, W. and Hall, M. N. (2011). Activation of mTORC2 by association with the ribosome. *Cell* **144:**757-768.

Zoncu, R., Bar-Peled, L., Efeyan, A., Wang, S., Sancak, Y. and Sabatini, D. M. (2011). mTORC1 senses lysosomal amino acids through an inside-out mechanism that requires the vacuolar H(+)-ATPase. *Science* **334:**678-683.

Zong, H., Yin, B., Zhou, H., Cai, D., Ma, B. and Xiang, Y. (2014). Inhibition of mTOR pathway attenuates migration and invasion of gallbladder cancer via EMT inhibition. *Mol Biol Rep* **41:**4507-4512.

Zou, X., Zhang, M., Sun, Y., Zhao, S., Wei, Y., Zhang, X., Jiang, C. *et al.* (2015). Inhibitory effects of 3-bromopyruvate in human nasopharyngeal carcinoma cells. *Oncol Rep* **34:**1895-1904